MAGNETOM Flash

Issue Number 96 · 1/2026
SCMR Edition

magnetomworld.siemens-healthineers.com

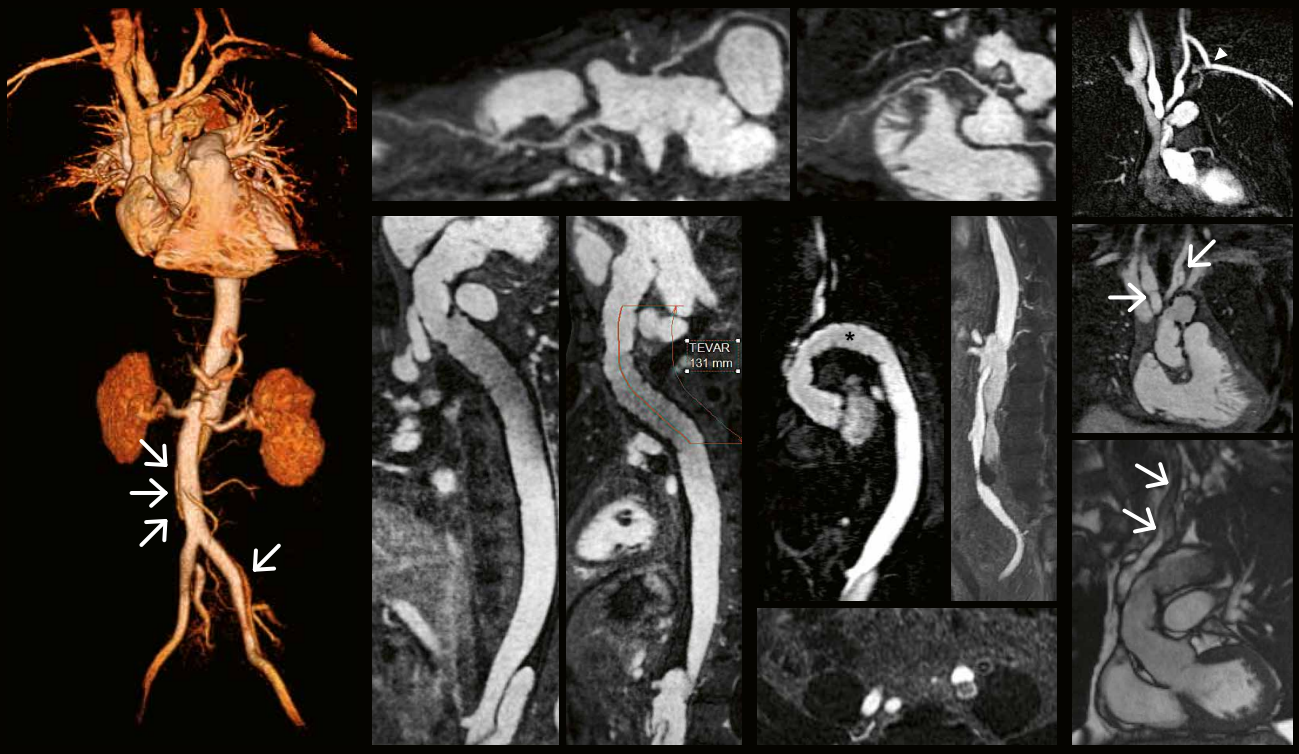

SIEMENS Healthineers

Editorial Comment

Cardiomyopathies

Cardiac Arrhythmias

Microstructural Imaging

Valvular Heart Disease

Angiography

Cover images from *Contrast-Enhanced iNAV MRA[1] for Whole-Chest, Whole-Heart, and Whole-Aortic Imaging* by Jason Craft, et al. (DeMatteis Cardiovascular Institute, St. Francis Hospital & Heart Center, Roslyn, NY, USA)

Congenital / Pediatric CMR

Workflow Optimization / AI in CMR

Implants

Product News

Meet Siemens Healthineers

[1]Work in progress. The application is currently under development and is not for sale in the U.S. and in other countries. Its future availability cannot be ensured.
[2]MR scanning has not been established as safe for imaging fetuses and infants less than two years of age. The responsible physician must evaluate the benefits of the MR examination compared to those of other imaging procedures.
[3]The MRI restrictions (if any) of the metal implant must be considered prior to patient undergoing MRI exam. MR imaging of patients with metallic implants brings specific risks. However, certain implants are approved by the governing regulatory bodies to be MR conditionally safe. For such implants, the previously mentioned warning may not be applicable. Please contact the implant manufacturer for the specific conditional information. The conditions for MR safety are the responsibility of the implant manufacturer, not of Siemens Healthineers.

Carlos Rochitte, M.D., Ph.D., FSCMR, is an Associate Professor of cardiology at Heart Institute (InCor), University of São Paulo Medical School, Brazil. He is also director of cardiovascular MR and CT at Heart Hospital (HCor) in São Paulo, and works at Dasa/Alta, also in São Paulo. He is academic coordinator of the two-year post-doctoral cardiovascular MR and CT fellowship programs, and has trained over 100 cardiologists and radiologists in both institutions.

He received his medical degree from São Paulo State University School of Medicine (UNESP), in 1990 and completed his cardiology clinical fellowship in 1993. He earned his Ph.D. in medicine in 2001 at InCor. He was a post-doctoral fellow in cardiovascular MRI at Johns Hopkins Hospital, Baltimore, MD, USA from 1995 to 1999. He is an established researcher in Brazil and has over 350 scientific publications indexed in PubMed, including research papers on myocardial infarctions/microvascular obstruction myocardial sodium-23 CMR studies in animals and humans. He has also pioneered the use of late gadolinium enhancement in four specific non-ischemic cardiomyopathies: Chagas disease, muscular dystrophy, aortic valve disease, and endomyocardial fibrosis. Dr. Rochitte is a founder and the former president (2020–2021) of the Cardiovascular Imaging Department (DIC) of the Brazilian Society of Cardiology (SBC), a founding member and the current President of SCMR and he has been actively participating in SCMR meetings since 1996. He was chair of the Latin American chapter of SCMR, member of the Editorial Board of the Journal of Cardiovascular Magnetic Resonance, member of the Scientific Program Committee, and member of the SCMR Board of Trustees from 2013 to 2017.

Artificial Intelligence in Cardiovascular Magnetic Resonance: From Precision Imaging to Global Accessibility

Cardiovascular magnetic resonance (CMR) is the non-invasive gold standard for assessing cardiac morphology, function, and tissue composition. Yet its clinical dissemination has historically been constrained by technical complexity, long acquisition times, and dependence on expert manual analyses. Segmenting cardiac chambers manually, for instance, may take up to 20 minutes for only two cardiac phases – a limitation that hinders scalability and accessibility, particularly in resource-limited settings.

Beyond these operational challenges, cardiovascular disease (CVD) remains the leading cause of morbidity and mortality worldwide. In Brazil, despite decades of decline, recent data show a subtle reversal of mortality trends among adults aged 20–54 (Fig. 1), signaling a persistent burden of premature cardiovascular events. This reinforces the urgency of making precision diagnostics – such as CMR – accessible, efficient, and globally deployable as tools for early detection and improved disease management. This need for scalable precision imaging aligns with SCMR's mission and strategic plan to democratize CMR and expand its availability across diverse healthcare settings.

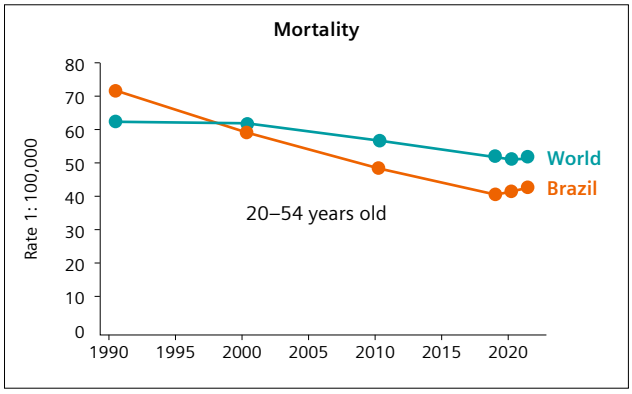

1 Trends in cardiovascular disease mortality (in people aged 20–54) in Brazil and worldwide, 1990–2020. While global mortality rates have shown a consistent decline, Brazil experienced a sustained reduction followed by a slight increase in recent years, suggesting a potential reversal of this trend.
Data sources: WHO Mortality Database (2022); Global Burden of Disease Study 1990–2021 (Seattle: IHME, 2022); Saloni Dattani, Veronika Samborska, Hannah Ritchie, and Max Roser, 2023. Courtesy of Dr. Gláucia Moraes, UFRJ.

From visualization to quantification: The power of objective imaging

CMR is rapidly evolving from qualitative visualization toward quantitative precision, a shift that redefines its prognostic and diagnostic role. Quantitative perfusion (QP) CMR exemplifies this transformation. By measuring absolute myocardial blood flow (MBF) and myocardial perfusion reserve (MPR), it provides objective, reproducible insights into ischemic burden – overcoming the subjectivity of visual interpretation.

Artificial intelligence (AI)-based corrections for the arterial input function (AIF) now allow accurate single-bolus quantification, eliminating complex dual-bolus protocols and facilitating workflow integration (Fig. 2). Beyond ischemia, tissue characterization techniques – including late gadolinium enhancement (LGE), T1 mapping, and extracellular volume (ECV) quantification – provide deep insight into myocardial remodeling and risk stratification (Fig. 3). Together, these quantitative biomarkers expand CMR's potential as a foundation for precision and predictive cardiology. SCMR consensus documents have been instrumental in harmonizing quantitative acquisition and interpretation, enabling reproducibility across centers internationally.

CMR growth worldwide and in Brazil: A shift toward intelligent imaging

Over the past decade, the utilization of CMR has expanded substantially across healthcare systems worldwide. Data from North America and the United Kingdom show a steady rise in clinical adoption, while the MR/CT Registry in Europe reported a 3.8-fold increase between 2011 and 2023, totaling nearly 400,000 studies (Fig. 3). This consistent global expansion highlights the consolidation of CMR as a pivotal tool in cardiovascular diagnosis and management.

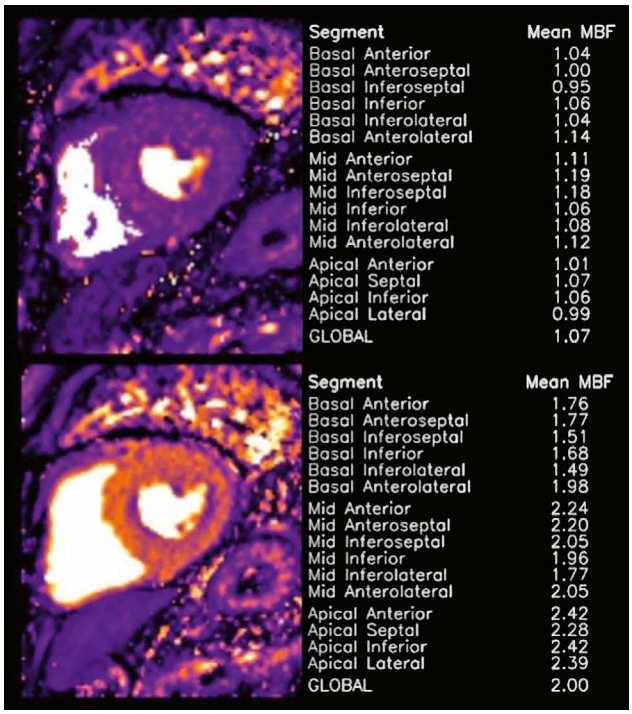

2 Representative quantitative perfusion maps acquired at rest (top) and during pharmacologic stress (bottom), illustrating absolute myocardial blood flow (MBF, mL/min/g) across all left ventricular segments. Segmental MBF values are automatically calculated. Images were acquired using a work-in-progress quantitative perfusion sequence[1] developed at King's College London. It enables high-resolution pixel-wise quantification of myocardial perfusion.

[1] *Work in progress. The application is currently under development and is not for sale in the U.S. and in other countries. Its future availability cannot be ensured.*

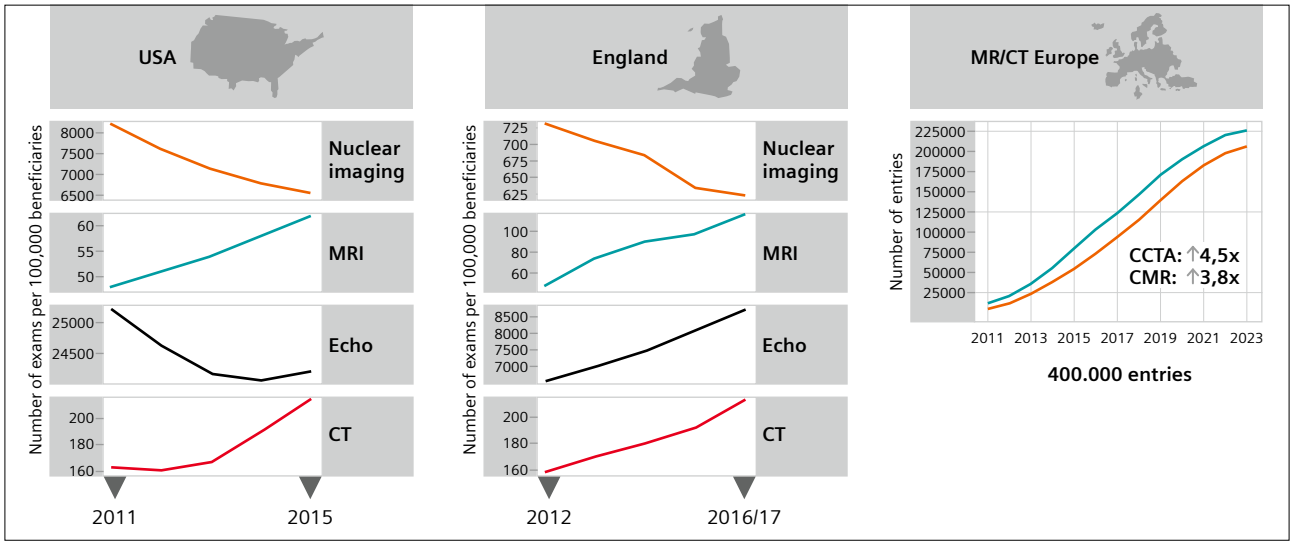

3 Increasing global use of CMR across healthcare systems, with a decline in molecular imaging. Data from the MR/CT Registry show a 3.8-fold rise in CMR and 400,000 recorded studies in Europe (2011–2023).

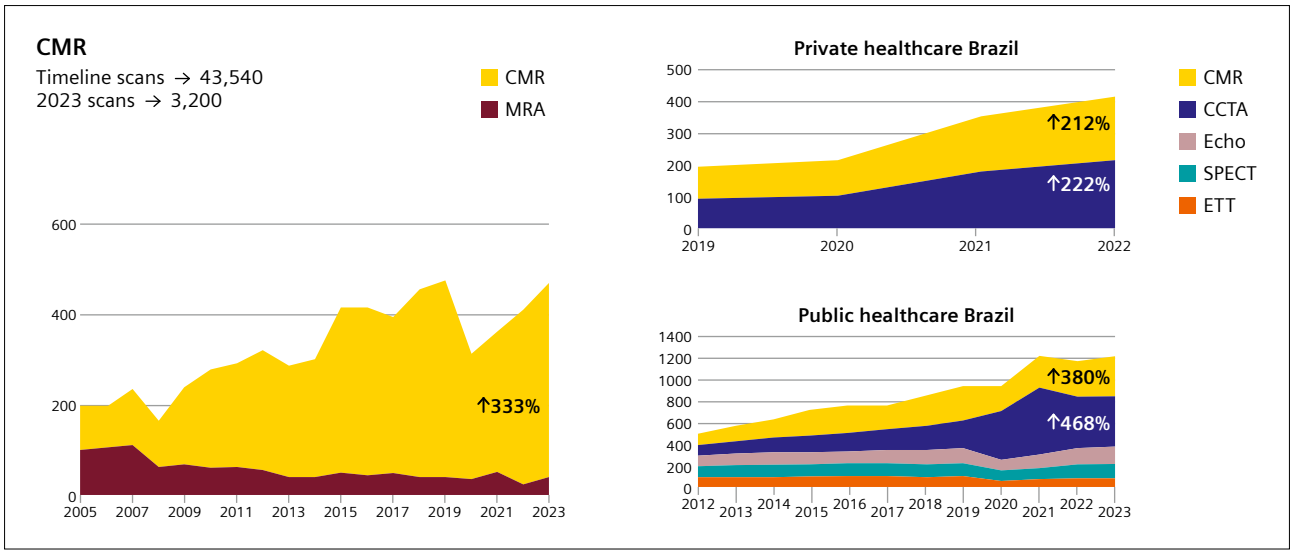

4 Significant growth in CMR utilization across Brazil over the past decade. Data from InCor show a 333% increase in CMR scans, while national trends indicate rises of 380% in the public health system (SUS) and 212% in the supplementary health sector.

In Brazil, the growth has been even more striking. Within the public healthcare system (SUS), CMR utilization has increased by nearly 380% nationwide. In the private health sector, the rise reached 212% across Brazil. Data from the Heart Institute (InCor) at the University of São Paulo show a 333% increase in examinations (Fig. 4). This trajectory reflects both clinical maturity and technological evolution, reinforced by the integration of AI, which is redefining efficiency, accessibility, and precision in modern cardiovascular imaging. Moreover, these trends reflect not only technological progress but also the global outreach and educational programs promoted by SCMR, which have supported CMR adoption in both high- and middle-income regions.

Artificial intelligence: Efficiency, automation, and reproducibility

AI has become an intrinsic component of the CMR workflow, driving efficiency, standardization, and diagnostic reliability. From acquisition to reconstruction, deep learning (DL) models accelerate and simplify processes that were once dependent on highly specialized expertise.

AI-assisted planning and motion correction reduce scan times by up to 30%, while DL-based reconstruction and compressed sensing enable high-resolution cine imaging under free-breathing conditions. In post-processing, convolutional networks achieve near-expert accuracy for automated segmentation of cine (Fig. 5) and LGE datasets, with frameworks such as nnU-Net adapting seamlessly across centers. These advances collectively transform CMR from an expert-dependent modality into an intelligent, scalable, and reproducible diagnostic tool.

New frontiers: Multiparametric and contrast-free imaging

Emerging techniques such as cardiac MR Fingerprinting (cMRF) integrate multiparametric quantification within a single, short acquisition. Simultaneous mapping of T1 and T2 in one breath-hold enhances patient comfort and reproducibility. DL-driven reconstruction reduces computation times to under two minutes while preserving quantitative accuracy.

Virtual native enhancement (VNE) further redefines tissue characterization by generating gadolinium-free "virtual" LGE images from native cine and mapping data. With diagnostic equivalence to conventional LGE and faster acquisition, these methods move CMR toward sustainable, contrast-free imaging that is safer for patients and more environmentally responsible.

Education, equity, and global workforce development

As the leading global society in CMR, SCMR has been pivotal in advancing education and capacity-building. Technology alone cannot democratize access; education remains fundamental. The InCor School of Cardiovascular Magnetic Resonance and Computed Tomography exemplifies this integration of innovation and capacity-building. To date, 250 residents and fellows have been trained in advanced CMR techniques, forming a distributed network of specialists now active in Brazil, Latin America, the United States, Europe, and Oceania (Fig. 6).

This global educational model, grounded in inclusion, diversity, and equity (IDE), ensures that technological advancement translates into equitable clinical benefit. The InCor experience demonstrates how innovation and human development must progress hand in hand to

achieve true scalability and sustainability in precision imaging.

Responsible innovation: The path forward

AI-enabled CMR is no longer aspirational; it is a living reality transforming how we acquire, reconstruct, and interpret cardiac data. Yet progress demands responsibility. Ensuring data diversity, compliance with FAIR (findable, accessible, interoperable, reusable) principles and with the Checklist for Artificial Intelligence in Medical Imaging (CLAIM), and transparent model validation are essential for equitable adoption.

Ultimately, the success of AI in CMR will not be measured by speed or automation alone, but also by its impact on patient outcomes and access. When technology, education, and ethics converge, precision medicine becomes a collective achievement – one that bridges innovation with inclusion and transforms cardiovascular health across all regions.

Conclusion: A transformative opportunity requiring responsible stewardship

AI-enabled CMR is no longer a vision of the future; it is an evolving reality that is redefining how we acquire, process, and interpret cardiac data. From accelerating acquisitions and reconstructing images in near real-time to enabling contrast-free tissue characterization and fully automated quantification, AI is transforming CMR into a faster, more accessible, and more predictive tool for patient care. Yet this transformation demands more than algorithms; it requires stewardship, collaboration, and ethical responsibility.

The democratization of high-precision cardiovascular imaging depends on ensuring that innovation is coupled with inclusivity. Initiatives such as those led by InCor

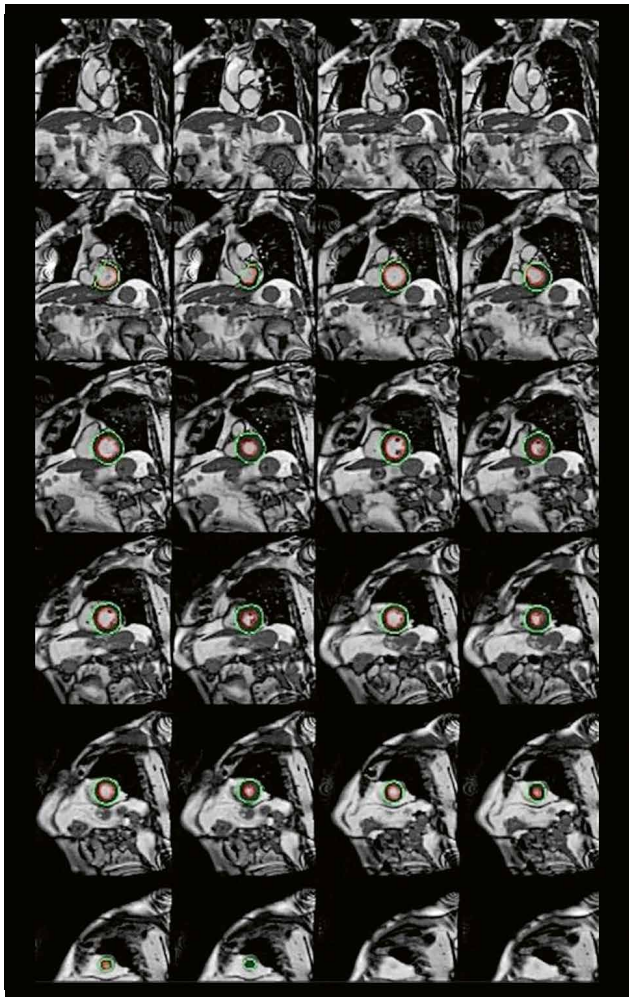

5 Automated segmentation and quantification of left ventricular function using fully convolutional networks (FCNs), demonstrating accurate contouring and volumetric analysis comparable to expert manual assessment.

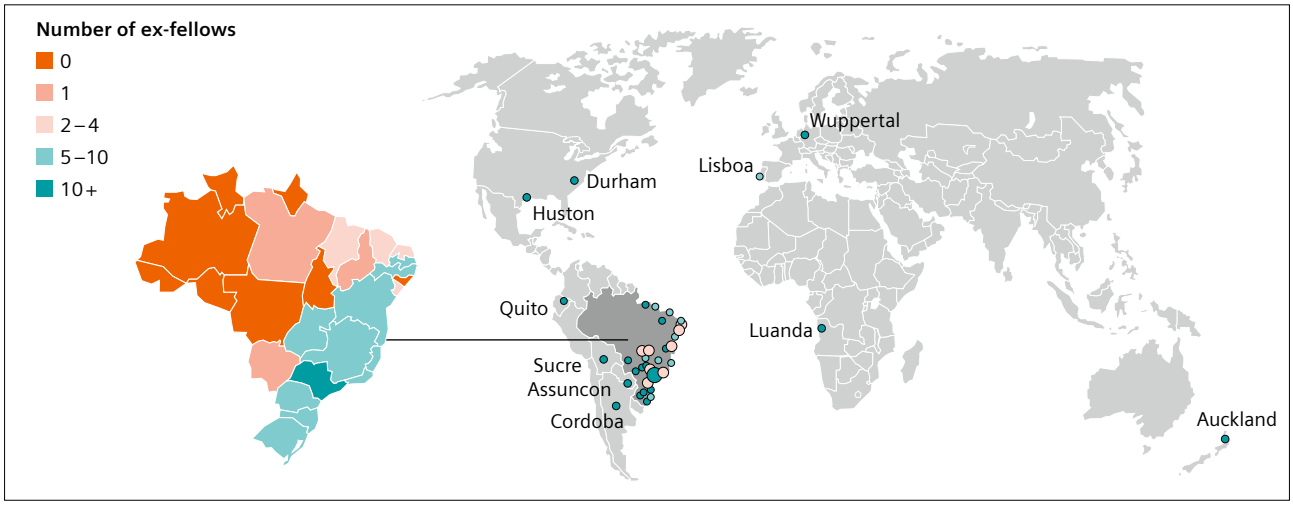

6 Global distribution of InCor-trained fellows in cardiovascular imaging, showing their presence across Brazil and internationally.

exemplify how technological advancement and education can move in parallel – empowering clinicians, expanding regional expertise, and building sustainable models of care that transcend geographic and socioeconomic barriers. Through its guidelines, registry efforts, and global training initiatives, SCMR continues to play a central role in guiding responsible innovation and equitable dissemination of CMR.

As CMR enters the era of intelligent automation, its greatest promise lies not merely in speed or efficiency, but also in its capacity to humanize precision medicine – to deliver data-driven insights that improve outcomes for all, not just for those with privileged access. Achieving this future will depend on global collaboration among clinicians, scientists, and policymakers who share a common goal: transforming cardiovascular imaging into a truly equitable, data-driven discipline that serves the world's diverse populations with excellence and compassion.

Carlos E. Rochitte

References

1 LeCun Y, Bengio Y, Hinton G. Deep learning. Nature. 2015;521(7553):436–44.
2 Litjens G, Kooi T, Bejnordi BE, Setio AAA, Ciompi F, Ghafoorian M, et al. A survey on deep learning in medical image analysis. Med Image Anal. 2017;42: 60–88.
3 Akçakaya M, Basha TA, Chan RH, Manning WJ, Nezafat R. Accelerated isotropic sub-millimeter whole-heart coronary MRI: compressed sensing versus parallel imaging. Magn Reson Med. 2014;71(2):815–22.
4 Basha TA, Akçakaya M, Liew C, Tsao CW, Delling FN, Addae G, et al. Clinical performance of high-resolution late gadolinium enhancement imaging with compressed sensing. J Magn Reson Imaging. 2017;46(6):1829–1838.
5 Ronneberger O, Fischer P, Brox T. U-net: Convolutional Networks for Biomedical Image Segmentation. In: Navab N, Hornegger J, Wells W, Frangi A, Editors. Medical Image Computing and Computer-Assisted Intervention – MICCAI 2015. Proceedings, Part III. 18th International Conference Munich, Germany, October 5–9, 2015. Cham, Switzerland: Springer; 2015. 234–241.
6 Ambale-Venkatesh B, Yang X, Wu CO, Liu K, Hundley WG, McClelland R, et al. Cardiovascular Event Prediction by Machine Learning: The Multi-Ethnic Study of Atherosclerosis. Circ Res. 2017;121(9):1092–1101.
7 Ambale-Venkatesh B, Yoneyama K, Sharma RK, Ohyama Y, Wu CO, Burke GL, et al. Left ventricular shape predicts different types of cardiovascular events in the general population. Heart. 2017;103(7):499–507.
8 Zhang X, Ambale-Venkatesh B, Bluemke DA, Cowan BR, Finn JP, Kadish AH, et al. Information maximizing component analysis of left ventricular remodeling due to myocardial infarction. J Transl Med. 2015;13:343.
9 Biffi C, de Marvao A, Attard MI, Dawes TJW, Whiffin N, Bai W, et al. Three-dimensional cardiovascular imaging-genetics: a mass univariate framework. Bioinformatics 2018;34(1):97–103.
10 Bai W, Sinclair M, Tarroni G, Oktay O, Rajchl M, Vaillant G, et al. Automated cardiovascular magnetic resonance image analysis with fully convolutional networks. J Cardiovasc Magn Reson. 2018;20(1):65.
11 Ripley DP, Musa TA, Dobson LE, Plein S, Greenwood JP. Cardiovascular magnetic resonance imaging: what the general cardiologist should know. Heart. 2016;102(19):1589–603.
12 Petersen SE, Matthews PM, Francis JM, Robson MD, Zemrak F, Boubertakh R, et al. UK Biobank's cardiovascular magnetic resonance protocol. J Cardiovasc Magn Reson. 2016;18:8.
13 Isensee F, Jaeger PF, Kohl SAA, Petersen J, Maier-Hein KH. nnU-Net: a self-configuring method for deep learning-based biomedical image segmentation. Nat Methods 2021;18:203–211.
14 Zhang Q, Burrage MK, Lukaschuk E, Shanmuganathan M, Popescu IA, Nikolaidou C, et al. Toward Replacing Late Gadolinium Enhancement With Artificial Intelligence Virtual Native Enhancement for Gadolinium-Free Cardiovascular Magnetic Resonance Tissue Characterization in Hypertrophic Cardiomyopathy. Circulation. 2021;144(8):589–599.
15 Kellman P, Arai AE, McVeigh ER, Aletras AH. Phase-sensitive inversion recovery for detecting myocardial infarction using gadolinium-delayed hyperenhancement. Magn Reson Med. 2002;47(2):372–83.
16 Ma D, Gulani V, Seiberlich N, Liu K, Sunshine JL, Duerk JL, et al. Magnetic resonance fingerprinting. Nature. 2013;495(7440):187–92.
17 Kim RJ, Wu E, Rafael A, Chen EL, Parker MA, Simonetti O, et al. The use of contrast-enhanced magnetic resonance imaging to identify reversible myocardial dysfunction. N Engl J Med. 2000;343(20):1445–53.

CMR in Light of the 2025 ESC Guidelines on Myocarditis and Pericarditis: Opportunities and Challenges

Andreas Schuster[1]; Jan Gröschel[2]; Johannes Kowallick[3]; Valentino Collini[4]; Massimo Imazio[4]; Jeanette Schulz-Menger[2]

[1]FORUM Medizin, Kardiologie, Rosdorf, Germany
[2]Charité – Universitätsmedizin Berlin, corporate member of Freie Universität Berlin and Humboldt-Universität zu Berlin; ECRC (Experimental and Clinical Research Center), Berlin, Germany; DZHK (German Centre for Cardiovascular Research), partner site Berlin, Berlin, Germany; Deutsches Herzzentrum der Charité Berlin, Germany; Cardiology and Nephrology, HELIOS Hospital Berlin-Buch, Berlin, Germany
[3]FORUM Medizin, Radiologie, Rosdorf, Germany
[4]Department of Medicine, University of Udine, and Cardiothoracic Department, University Hospital Santa Maria della Misericordia, ASUFC, Udine, Italy

Clinical impact of the 2025 ESC Guidelines on routine management of patients with myocarditis

The release of the 2025 European Society of Cardiology (ESC) Guidelines for the management of myocarditis and pericarditis signals a watershed moment in cardiac imaging. These guidelines fundamentally reshape the diagnostic landscape, placing cardiovascular magnetic resonance (CMR) at the forefront of routine clinical practice [1]. This paradigm shift necessitates a comprehensive understanding of the updated guidelines and a critical reassessment of current practices for clinicians.

The core message is clear: Non-invasive evaluation of myocardial inflammation has reached a new level of sophistication and importance (Fig. 1). The guidelines champion a holistic approach to inflammatory heart disease, moving beyond the limitations of solely relying on invasive procedures. There are essential changes affecting clinicians, particularly imaging specialists, that need to be considered to ensure that patient care fully benefits from these advancements.

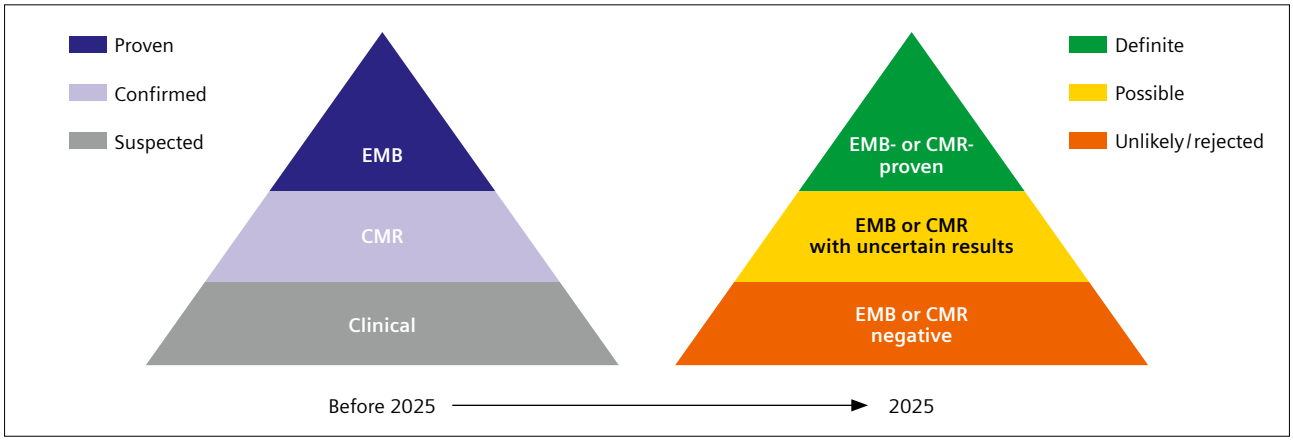

1 Visualization of the diagnostic criteria for myocarditis according to the current ESC guidelines [1]. A paradigm shift has occurred in the clinical diagnosis of myocarditis: Both cardiovascular magnetic resonance (CMR) and endomyocardial biopsy (EMB) can establish a definitive diagnosis, but are applied in different clinical contexts.

The shifting diagnostic paradigm: Embracing "IMPS" and updated imaging criteria

The 2025 guidelines introduce the term "inflammatory myopericardial syndrome" (IMPS) [1]. This recognizes the clinical spectrum of disease, ranging from simple myocarditis, through mixed forms, to simple pericarditis. IMPS serves as a framework for initiating a diagnostic workup that considers both myocardial and pericardial involvement, and urges clinicians to be aware of the overlapping nature of these conditions (Table 1).

This approach directly impacts imaging protocols and interpretation. Instead of narrowly focusing on fulfilling specific criteria for myocarditis *or* pericarditis, imaging specialists should now consider the possibility of both, and tailor imaging acquisitions and analyses accordingly. This necessitates incorporating specific imaging sequences that can detect both myocardial and pericardial inflammation, including sequences to assess edema and tissue characterization [2, 3].

Moreover, the guidelines solidify the importance of the Lake Louise criteria (LLC) for the CMR diagnosis of myocarditis [4, 5]. It is imperative for imaging specialists to thoroughly familiarize themselves with the updated LLC and understand the nuances. Furthermore, since myocardial inflammation can arise from various causes, imaging results must also be weighed in the relevant clinical context rather than solely relying on abnormal imaging parameters [6]. This not only involves acquiring high-quality images, but also recognizing the patterns and distribution of myocardial edema, assessing non-ischemic scar distribution, and accurately evaluating ventricular function to aid in the non-invasive diagnosis of myocarditis.

Inflammatory Myopericardial Syndrome

If diagnostic criteria for myocarditis and/or pericarditis are fulfilled

	Myocarditis	Pericarditis
Definite	Clinical presentation and CMR- or EMB-proven	Clinical presentation with >1 additional criterion
Possible	Clinical presentation with at least 1 additional criterion CMR- or EMB-uncertain or not available	Clinical presentation with 1 additional criterion
Unlikely/rejected	Only clinical presentation without additional criteria	Only clinical presentation without additional criteria

Additional criteria beyond clinical presentations

	Myocarditis	Pericarditis
Clinical	Non-specific findings	Pericardial rubs
ECG	ST-T changes	PR depression, widespread ST-segment elevation
Biomarkers	Troponin elevation	C-reactive protein elevation
Imaging	Abnormal strain, wall motion, reduced EF Myocardial oedema and/or LGE (CMR findings)	New or worsening pericardial effusion Percardial oedema and/or LGE (CMR findings)

Table 1: Diagnostic criteria and classification for inflammatory myopericardial syndrome.
CMR, cardiovascular magnetic resonance; ECG, electrocardiogram; EF, ejection fraction; EMB, endomyocardial biopsy; IMPS, inflammatory myopericardial syndrome; LGE, late gadolinium enhancement; LLC, Lake Louise criteria
Clinical presentations include chest pain or infarct-like symptoms, arrhythmias, heart failure, aborted sudden cardiac death.
Cardiovascular magnetic resonance categories:
proven = 2 out of 2 updated LLC fulfilled; uncertain = only 1 out of 2 updated LLC fulfilled; rejected = negative CMR.

From biopsy-driven to CMR-centric: A new diagnostic era

The most significant change is the transition from endomyocardial biopsy (EMB) as a primary diagnostic tool to CMR as the leading modality for initial assessment in appropriate cases.

Traditionally, EMB played a central role in confirming the diagnosis of myocarditis [7]. Although EMB remains crucial for specific scenarios and when tissue analysis is required, it is no longer the first step for the vast majority of patients with suspected myocarditis. EMB is now reserved for cases in which its findings would specifically alter management strategies, such as directing targeted therapies or identifying the underlying cause of the myocardial disease. Imaging specialists should therefore proactively guide clinical decision-making by emphasizing the strengths and limitations of CMR in identifying myocardial inflammation, assessing the extent and severity of disease, and excluding other potential causes of cardiac dysfunction. Skillful application of these insights will enable more informed patient management, allowing clinical cardiologists to make appropriate referral decisions for EMB if required.

These scenarios may include high-risk myocarditis (e.g., with hemodynamic or arrhythmic instability) or when specific histopathologic diagnoses (e.g., giant cell myocarditis) are needed to guide targeted therapy. EMB is also appropriate in moderate-risk cases that do not respond to conventional treatments when a viral or specific cause is suspected and impacts decision-making. It is important to note that the relative fraction of these scenarios is relatively small given the large number of myocarditis patients that can be sufficiently managed based on non-invasive imaging only.

Unmasking inherited risks: The interplay of genetics and inflammatory heart disease

A further significant advancement of the guidelines is the recognition of the influence of genetics on inflammatory heart conditions. The guidelines now recommend obtaining a detailed family history in cases of recurrent IMPS to uncover potential inherited causes, assess inheritance patterns, and identify at-risk relatives. Genetic testing should be considered, especially with a family history of IMPS, inherited cardiomyopathy, or unexplained sudden cardiac death, as certain genetic variants can increase susceptibility to IMPS or influence disease severity. Notably, there is an overlap between genes associated with inherited cardiomyopathies, such as arrhythmogenic right ventricular cardiomyopathy (ARVC) and dilated cardiomyopathy (DCM), and those that may predispose a person to myocardial inflammation. This highlights the need to consider genetic testing in cases where IMPS presents atypically or with a strong family history, potentially unveiling an underlying inherited risk [8, 9].

Risk stratification and return-to-activity: Guiding a safe resumption

CMR plays a crucial role in risk stratification, identifying those at higher risk for adverse events and guiding recommendations for a safe return to physical activity and work. By characterizing myocardial damage and assessing potential arrhythmogenic substrates (e.g., using late gadolinium enhancement, LGE), CMR provides clinicians with essential information for evaluating prognoses and guiding management decisions. Imaging specialists should proactively communicate the presence of concerning CMR findings – such as extensive LGE, significant ventricular dysfunction, or evidence of ongoing inflammation – in their reports. These findings should be carefully considered in the context of other clinical data to determine the appropriate level of monitoring, treatment, and activity restrictions for each patient.

In general, the guidelines recommend surveillance including imaging. Specifically, they provide a detailed follow-up schedule for patients diagnosed with IMPS, differentiating between myocarditis and pericarditis cases. Clinical evaluations, alongside specific testing, are consistently recommended at each follow-up interval – within one month, at three to six months, at 12 months, and beyond. Detailed recommendations regarding CMR for myocarditis include a one-month scan or within three to six months, then a second CMR at six to 12 months, and a long-term follow-up if required depending on the results of the initial scans [1, 10].

One of the less-discussed but equally important roles of CMR is its ability to definitively exclude both myocarditis and pericarditis in patients with suspected symptoms. A negative CMR scan, when combined with a thorough clinical evaluation, can provide significant reassurance to patients and clinicians, ruling out myocardial and/or pericardial inflammation as a cause of their symptoms.

For imaging specialists, this requires clear and confident communication of negative CMR findings in their reports. This will minimize unnecessary anxiety and enable prompt investigation for other potential causes of chest pain, dyspnea, or arrhythmias [11]. It is also important to identify and rule out other potential causes of symptoms, including acute coronary syndrome (ACS), as appropriate.

The updated Lake Louise criteria in clinical practice: Application, technical challenges, and confounding factors

The ESC guidelines emphasize the use of the updated LLC for the detection of myocarditis [1]. While the original LLC were based on T2-weighted sequences, early gadolinium enhancement sequences, and LGE [12], the updated LLC incorporate parametric mapping [4] (Fig. 2). With this refinement, sensitivity is greatly increased [13]. Currently, the diagnosis of acute myocarditis can be made when a T1 criterion (T1 mapping, LGE, or extracellular volume) and a T2 criterion (T2-weighted imaging or T2 mapping) are fulfilled (Figs. 3 and 4). It should be noted that even in the absence of one criterion, the diagnosis of myocarditis is still possible in the proper clinical scenario. If not all criteria are fulfilled, diagnostic accuracy is lower but remains above 75%. Importantly, T2-based criteria specifically reflect the current activity of the disease. Although parametric mapping has revolutionized the approach to IMPS in CMR, certain issues remain. Consensus statements from the Society for Cardiovascular Magnetic Resonance (SCMR) provide guidance regarding acquisition and analysis [14], yet inter-scanner and inter-vendor differences remain [15]. Promising research has been published regarding post-hoc standardization, but further prospective approaches should aim to overcome the need for additional post-processing steps [16]. In addition to standardization across sequences, scanners, and vendors, other patient- and acquisition-related factors must also be considered. Artifacts, such as those caused by motion or metallic objects, can impair image quality. Therefore, careful quality assurance is essential to identify and exclude non-diagnostic images [17].

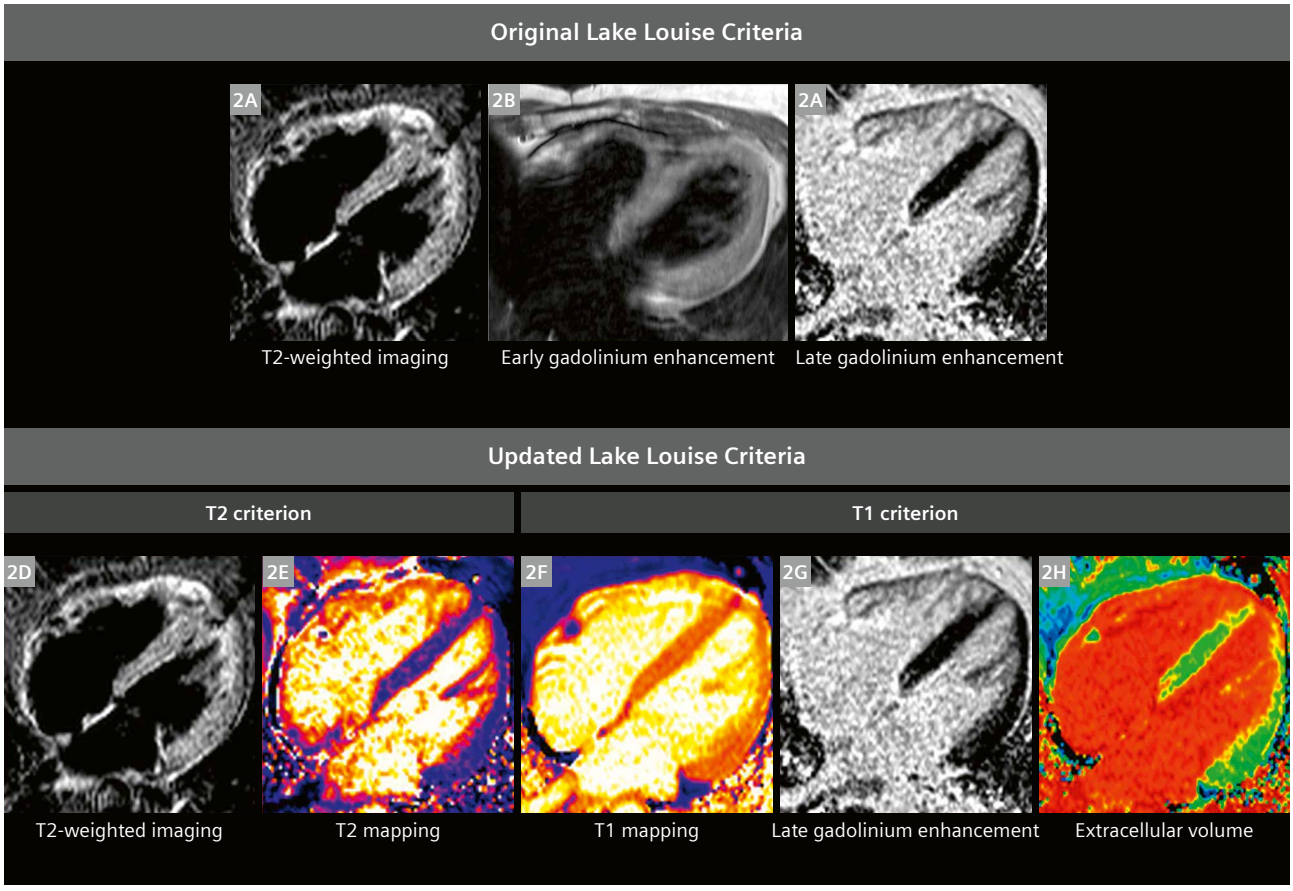

2 Example images comparing the former Lake Louise criteria (top row) with the updated Lake Louise criteria (bottom row). Top row: **(2A)** T2-weighted imaging based on a TIRM sequence, **(2B)** early gadolinium enhancement based on a T1-weighted gradient echo sequence, **(2C)** late gadolinium based on a PSIR sequence. Botton row: **(2D)** T2-weighted imaging based on a TIRM sequence, **(2E)** T2 mapping based on a bSSFP sequence, **(2F)** T1 mapping based on a MOLLI sequence, **(2G)** late gadolinium enhancement based on a PSIR sequence, **(2H)** extracellular volume map based on pre- and post-contrast MOLLI-based T1 mapping sequences.
Images acquired on a 1.5T MAGNETOM Avanto Fit at Charité Campus Berlin-Buch.

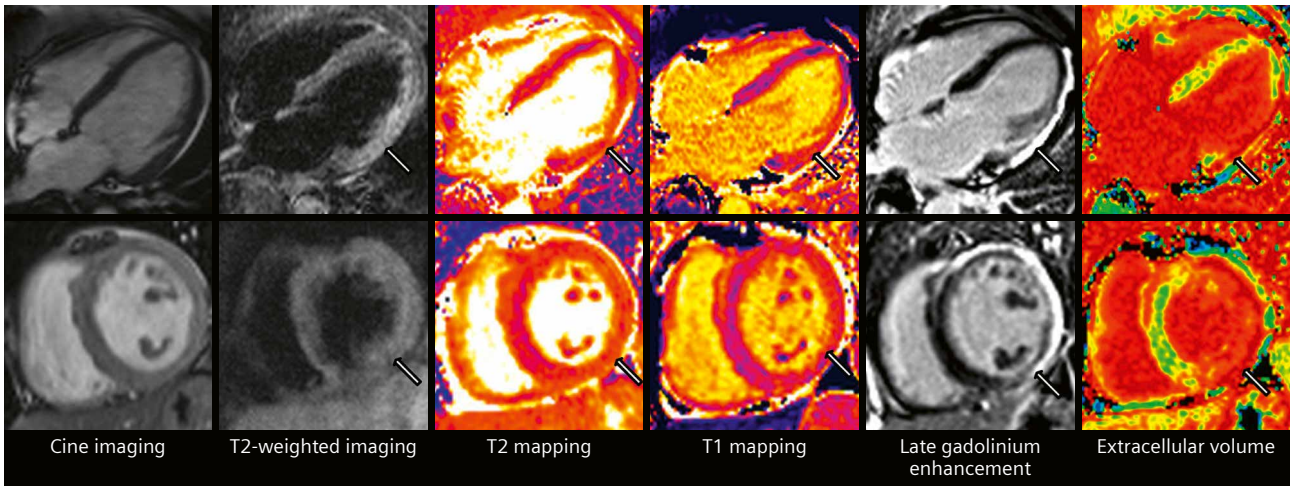

3 Cardiovascular magnetic resonance (CMR) findings in a 56-year-old woman presenting with dyspnea and elevated NT-proBNP. CMR demonstrates features consistent with acute myocarditis. Cine imaging showed reduced left ventricular systolic function with global hypokinesia. T2-weighted imaging and T2 mapping revealed increased myocardial signal and elevated T2 values, indicating myocardial edema (arrows). Native T1 mapping showed diffusely increased relaxation times. Late gadolinium enhancement imaging demonstrated extensive subepicardial enhancement of the lateral wall extending into the anteroseptal region, confirming active myocardial injury. PET-CT was unremarkable and genetic testing is pending.
Images acquired on a 1.5T MAGNETOM Avanto Fit at Charité Campus Berlin-Buch.

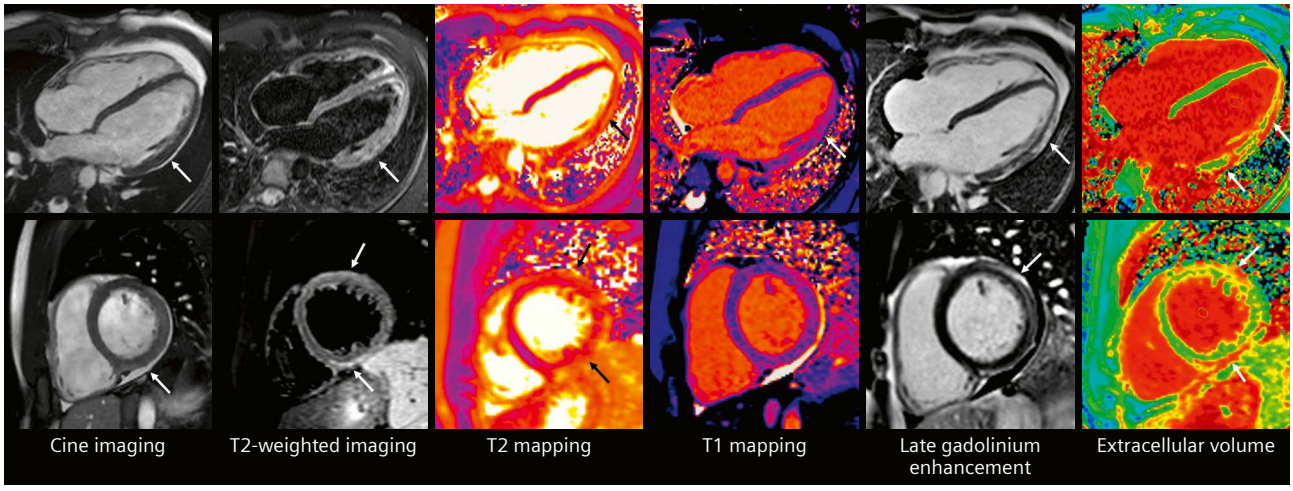

4 Cardiovascular magnetic resonance findings in a 28-year-old man presenting with chest pain and dyspnea. Elevated troponin levels were detected. CMR findings are characteristic of acute myocarditis. There was preserved left ventricular systolic function on Compressed Sensing cine imaging (LV EF: 55%; GLS: 15.9%) in the presence of a small pericardial effusion (arrows). STIR T2-weighted imaging and T2 mapping revealed increased myocardial signal and elevated T2 values indicative of myocardial edema (arrows). Native T1 mapping showed diffusely increased relaxation times. Free-breathing LGE imaging demonstrated characteristic subepicardial enhancement of the lateral wall and extending into the anterolateral and inferolateral region, confirming active myocardial injury.
Images acquired on a 1.5T MAGNETOM Sola at FORUM Medizin, Rosdorf, Germany.

Future perspectives

In the 2025 ESC Guidelines for the management of myocarditis and pericarditis, a considerable number of recommendations are classified as Class I, but are supported only by Level C evidence. This reflects strong agreement within the writing group, as the voting on recommendations is a secret process. However, a high level of evidence is missing, since prospective and outcome-oriented multicenter studies are lacking. This can be an opportunity for our community to generate the data, as this may define the next stage of evidence-based management for IMPS.

Our community generally agrees that efficient and reproducible CMR examinations are essential, and that the updated LLC provide a corresponding consensus protocol [4]. At the same time, CMR protocols should be tailored to the clinical question. In follow-up studies that focus primarily on disease activity, it may be reasonable to reconsider the routine use of contrast agents, as parametric mapping, T2 imaging, and cine techniques can provide reliable information. Such an approach emphasizes both clinical relevance and resource efficiency.

Innovation has always been a hallmark of the CMR community. Novel pulse sequences and AI-based analytic tools are constantly being developed, opening new doors in cardiac imaging. Yet every new technique must undergo systematic validation. This requires coordinated efforts and robust tools, including quality assurance pipelines and possibly a gold-standard dataset driven by SCMR. While we can be proud of what we have achieved with CMR so far, even greater progress is possible by pooling our efforts.

References

1 Schulz-Menger J, Collini V, Gröschel J, Adler Y, Brucato A, Christian V, et al. ESC Guidelines for the management of myocarditis and pericarditis. Eur Heart J. 2025;46(40):3952–4041.

Contact

Professor Jeanette Schulz-Menger, M.D.
University Medicine Berlin
Charité Campus Buch, ECRC
HELIOS Clinics Berlin-Buch
Department of Cardiology and Nephrology
Lindenberger Weg 80
13125 Berlin, Germany
Tel.: +49 30 040153536
jeanette.schulz-menger@charite.de

Professor Andreas Schuster, M.D., Ph.D.
Forum Medizin GbR
An der Ziegelei 1
37124 Rosdorf
Germany
Tel.: +49 551 89069840
andreas.schuster@forum-medizin-goettingen.de
https://forum-medizin-goettingen.de/

2 Kramer CM, Barkhausen J, Bucciarelli-Ducci C, Flamm SD, Kim RJ, Nagel E. Standardized cardiovascular magnetic resonance imaging (CMR) protocols: 2020 update. J Cardiovasc Magn Reson. 2020;22(1):17.
3 Schulz-Menger J, Bluemke DA, Bremerich J, Flamm SD, Fogel MA, Friedrich MG, et al. Standardized image interpretation and post-processing in cardiovascular magnetic resonance 2020 update: Society for Cardiovascular Magnetic Resonance (SCMR): Board of Trustees Task Force on Standardized Post-Processing. J Cardiovasc Magn Reson. 2020;22(1):19.
4 Ferreira VM, Schulz-Menger J, Holmvang G, Kramer CM, Carbone I, Sechtem U, et al. Cardiovascular Magnetic Resonance in Nonischemic Myocardial Inflammation: Expert Recommendations. J Am Coll Cardiol. 2018;72(24):3158–3176.
5 Writing Committee, Drazner MH, Bozkurt B, Cooper LT, Aggarwal NR, Basso C, et al. 2024 ACC Expert Consensus Decision Pathway on Strategies and Criteria for the Diagnosis and Management of Myocarditis: A Report of the American College of Cardiology Solution Set Oversight Committee. J Am Coll Cardiol. 2025;85(4):391–431.
6 Hua A, Domenech-Ximenos B, Lopez B, Sanna G, Chiribiri A, Rajani R, et al. Diagnostic utility of the revised Lake Louise criteria in myocarditis associated with active autoimmune rheumatic disease. J Cardiovasc Magn Reson. 2025;27(2):101916.
7 Schultheiss HP, Kühl U, Cooper LT. The management of myocarditis. Eur Heart J. 2011;32(21):2616–25.
8 Gasperetti A, Muller SA, Peretto G, Asatryan B, Protonotarios A, Laredo M, et al. Prognostic Role of Myocarditis-Like Episodes and Their Treatment in Patients With Pathogenic Desmoplakin Variants. Circulation. 2025;152(14):978–989.
9 Piriou N, Marteau L, Kyndt F, Serfaty JM, Toquet C, Le Gloan L, et al. Familial screening in case of acute myocarditis reveals inherited arrhythmogenic left ventricular cardiomyopathies. ESC Heart Fail. 2020;7(4):1520–1533.
10 Aquaro GD, Ghebru Habtemicael Y, Camastra G, Monti L, Dellegrottaglie S, Moro C, et al. Prognostic Value of Repeating Cardiac Magnetic Resonance in Patients With Acute Myocarditis. J Am Coll Cardiol. 2019;74(20):2439–2448.
11 Writing Committee Members, Gulati M, Levy PD, Mukherjee D, Amsterdam E, Bhatt DL, et al. 2021 AHA/ACC/ASE/CHEST/SAEM/SCCT/SCMR Guideline for the Evaluation and Diagnosis of Chest Pain: A Report of the American College of Cardiology/American Heart Association Joint Committee on Clinical Practice Guidelines. J Am Coll Cardiol. 2021;78(22):e187–e285.
12 Friedrich MG, Sechtem U, Schulz-Menger J, Holmvang G, Alakija P, Cooper LT, et al. Cardiovascular magnetic resonance in myocarditis: A JACC White Paper. J Am Coll Cardiol. 2009;53(17):1475–87.
13 Luetkens JA, Faron A, Isaak A, Dabir D, Kuetting D, Feisst A, et al. Comparison of Original and 2018 Lake Louise Criteria for Diagnosis of Acute Myocarditis: Results of a Validation Cohort. Radiol Cardiothorac Imaging. 2019;1(3):e190010.
14 Messroghli DR, Moon JC, Ferreira VM, Grosse-Wortmann L, He T, Kellman P, et al. Clinical recommendations for cardiovascular magnetic resonance mapping of T1, T2, T2* and extracellular volume: A consensus statement by the Society for Cardiovascular Magnetic Resonance (SCMR) endorsed by the European Association for Cardiovascular Imaging (EACVI). J Cardiovasc Magn Reson. 2017;19(1):75.
15 Gröschel J, Trauzeddel RF, Müller M, von Knobelsdorff-Brenkenhoff F, Viezzer D, Hadler T, et al. Multi-site comparison of parametric T1 and T2 mapping: healthy travelling volunteers in the Berlin research network for cardiovascular magnetic resonance (BER-CMR). J Cardiovasc Magn Reson. 2023;25(1):47.
16 Viezzer D, Hadler T, Gröschel J, Ammann C, Blaszczyk E, Kolbitsch C, et al. Post-hoc standardisation of parametric T1 maps in cardiovascular magnetic resonance imaging: a proof-of-concept. EBioMedicine. 2024;102:105055.
17 Fenski M, Gröschel J, Gatehouse P, Kolbitsch C, Schulz-Menger J. Artifacts in cardiac T1 and T2 mapping techniques – Influence on reliable quantification. J Cardiovasc Magn Reson. 2025;101934

Myocardial Tuberculosis: A Curable Form of Cardiomyopathy in Endemic Countries. Know This Great Masquerader

Priya Chudgar, FSCMR; Nitin Burkule, FSCMR

Jupiter Hospital, Thane, Mumbai, India

Abstract

Pericardial affection in tuberculosis has been widely described in the literature. Myocardial involvement is considered a rare manifestation, but is associated with high mortality. Variations in clinical and imaging presentations can often cause diagnostic dilemmas and further delay appropriate management. We share our experience of myocardial involvement in histopathologically proven cases of tuberculosis. The main intention is to create awareness about this rare but curable form of cardiomyopathy.

Introduction

Tuberculous infection is widespread in tropical countries. It occurs due to the spread of mycobacterium tuberculosis. The lungs are primarily involved. However, extrapulmonary involvement (lymph node, central nervous system, bone, cutaneous, abdominal) is also not uncommon (10%–15%) [1].

Cardiovascular involvement is rare and accounts for 1%–2% of extrapulmonary tuberculosis [2]. It is often associated with high mortality and morbidity. Pericardium is most commonly involved [3]. This can present as pericardial effusion, constrictive pericarditis, and pericardial calcification.

Myocardial tuberculosis is a rare but potentially life-threatening form of tuberculosis. A high index of suspicion and multimodality imaging workup is needed for evaluation. Confirmation of diagnosis with histopathology workup is essential to improve outcomes with prompt anti-tubercular treatment.

Tuberculosis can reach the myocardium through:

1. Hematogenous spread from primary infection or reactivation of latent focus.
2. Direct extension from adjacent infected structures like the pericardium and mediastinal lymph nodes.
3. Lymphatic spread through infected lymph nodes.

Clinical presentation is highly variable depending on the severity and location of myocardial involvement. Systemic symptoms like fever or weight loss may not be present. Patients can manifest with rhythm disturbances, cardiac failure, dilated cardiomyopathy, or (rarely) sudden cardiac death.

This article describes interesting cases of myocardial involvement in tuberculosis. Images were acquired using our 3T MAGNETOM Verio and 1.5T MAGNETOM Altea scanners (Siemens Healthineers, Erlangen, Germany).

Case 1

A 12-year-old female patient presented with dyspnea on exertion, giddiness, and palpitations. She had a history of loss of appetite and weight loss with low-grade fever and abdominal pain in the recent past. Multiple tests and hematological workup failed to reveal significant abnormalities.

She was admitted to the hospital with a syncopal episode. 2D echocardiography during this hospital admission revealed reduced ejection fraction and global hypokinesia. Her serum troponin levels were also elevated, so further workup was performed with cardiac MRI.

The results revealed global hypokinesia and severely reduced systolic function of the left ventricle. Multiple small patchy foci of late gadolinium enhancement were seen in the septum (Fig. 1), and on the inferior and lateral walls. These were non-coronary territorial in distribution and showed elevated values on T1 and T2 mapping. Multiple conglomerated necrotic mediastinal lymph nodes were also demonstrated.

Further workup with tracheobronchial lymph node biopsy was performed. It revealed non-necrotizing epithelioid cell granulomas of mycobacterial etiology. The patient was started on antitubercular medications and heart failure management. The follow-up study showed significant clinical improvement and increase in ejection fraction.

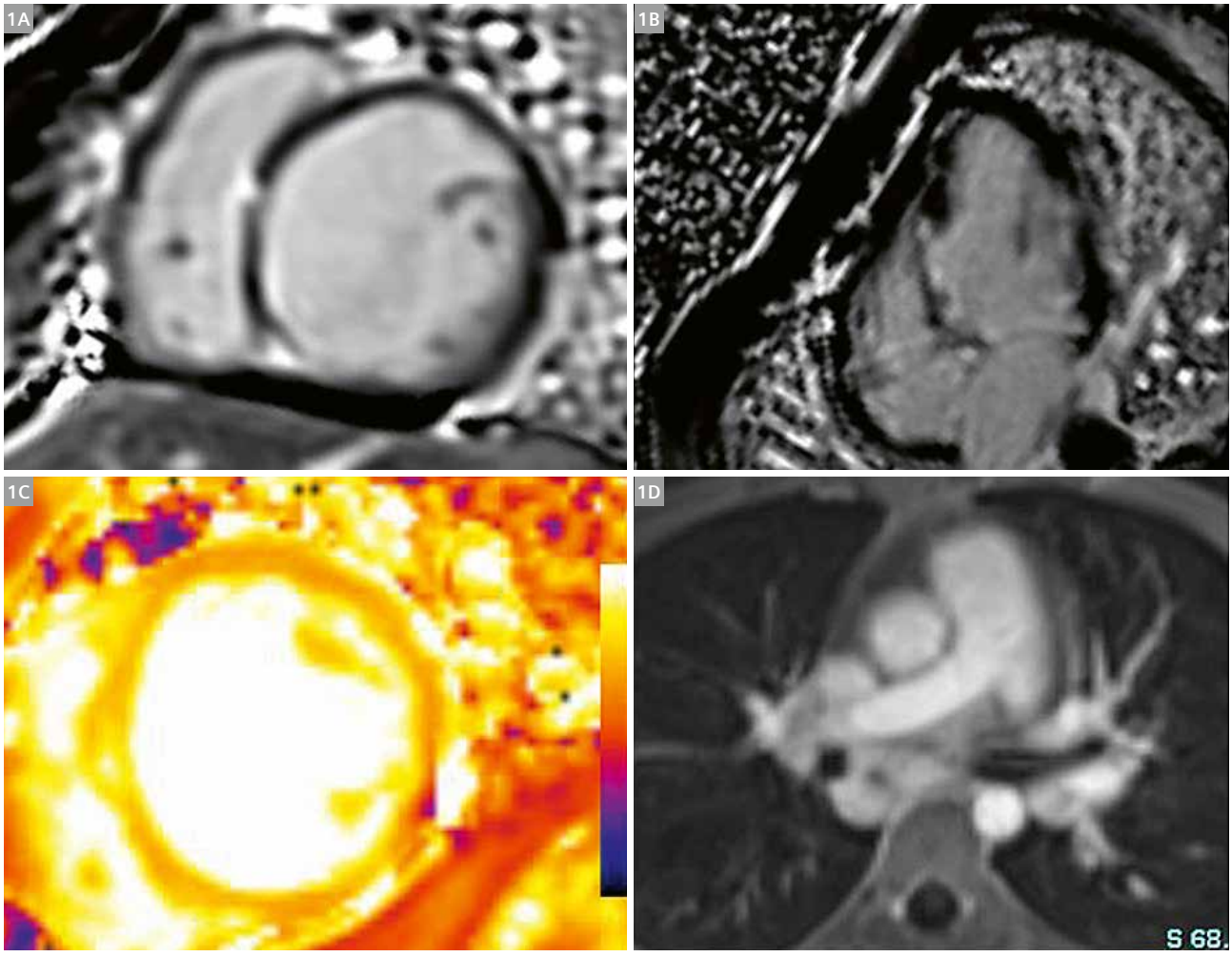

1 Patchy areas of late gadolinium enhancement are seen on phase-sensitive inversion recovery (PSIR) images **(1A** and **1B)** with elevated values on T1 mapping **(1C)**. This non coronary territorial distribution and the necrotic mediastinal lymph nodes **(1D)** raised the possibility of tuberculosis, which was confirmed with lymph node biopsy.

Case 2

A 38-year-old female patient presented to the emergency department with cardiogenic shock. She was stabilized with DC cardioversion. Her serum troponins were significantly elevated, so cardiac MRI was performed for further workup. This revealed preserved function and extensive mid-myocardial and epicardial late gadolinium enhancement. This involved the anterior wall, septum, and the lateral and inferior walls. These segments revealed elevated values on T1 and T2 mapping. No mediastinal lymph nodes were present. However, fibrotic changes were observed in the right upper lobe of the lung (Fig. 2).

After insertion of an implantable cardioverter defibrillator (ICD), a PET-CT exam was performed to evaluate the inflammatory cardiomyopathy. It showed multiple lymph nodes in the abdomen with high uptake in the right Ileocecal region. A biopsy of these abdominal lymph nodes confirmed tuberculosis, and the patient was started on antitubercular therapy.

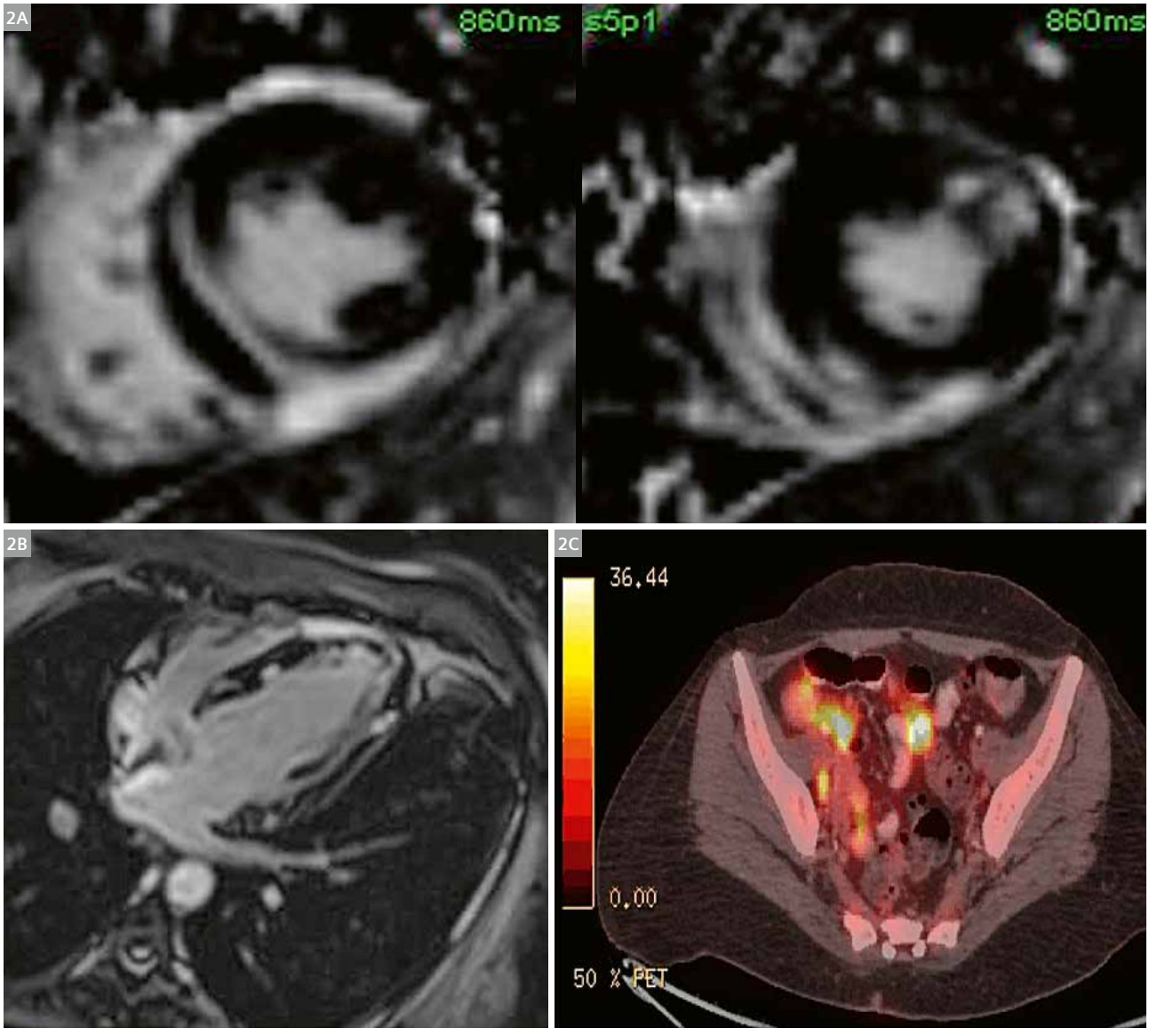

2 Multifocal patchy areas of mid-myocardial and epicardial late gadolinium enhancement were visualized on short-axis **(2A)** and 4-chamber-view **(2B)** images. PET imaging showing increased uptake in the right iliac fossa **(2C)** and abdominal lymph nodes. Biopsy confirmed tuberculous pathology.

Case 3

A 30-year-old male patient with massive tuberculous pleural effusion was evaluated using CT imaging. An incidental note of soft-tissue abnormality along the free wall of the right ventricle was made, so further workup with cardiac MRI was performed. This revealed soft-tissue thickening along the free wall of the right atrium and right ventricle with vascularity on perfusion images, and heterogeneous post-contrast enhancement. An incidental note of focal osteolytic lesion in the dorsal vertebra was also made (Fig. 3). The patient was not willing to undergo an invasive procedure like endomyocardial biopsy. However, aggressive treatment with second-line antitubercular therapy was started in view of the tuberculous pleural effusion.
A follow-up study revealed significant regression of the right ventricular abnormality. Clinical improvement was observed, along with an increase in ejection fraction.

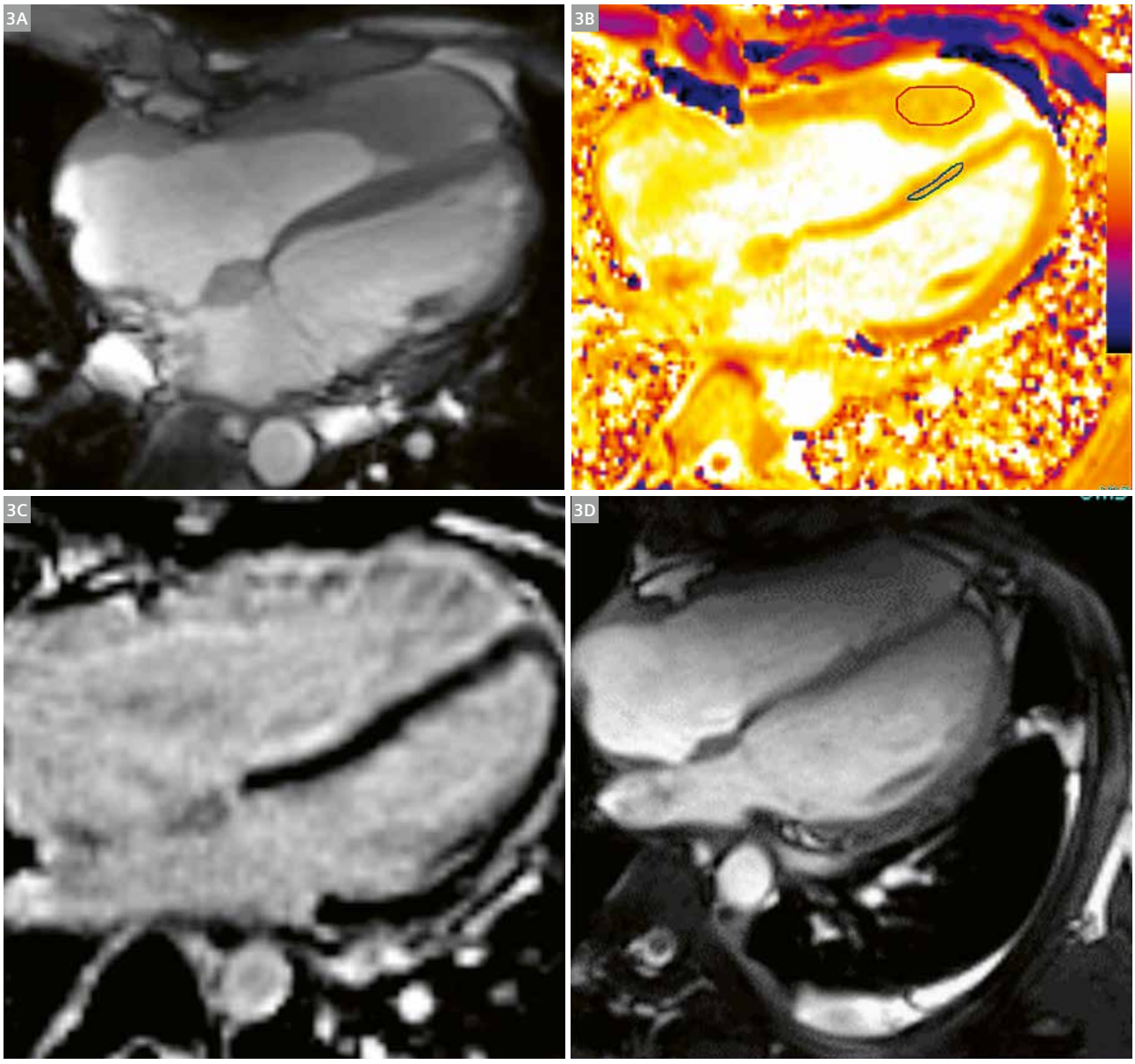

3 Soft-tissue thickening along the free wall of the right atrium and ventricle **(3A)**, which showed increased values on T1 mapping **(3B)**, and late gadolinium enhancement on PSIR images **(3C)**. A follow-up study after antitubercular treatment showed significant resolution **(3D)**. Note the residual pleural effusion.

Comments

Myocardial involvement with tuberculosis is rare, and potentially treatable. Prompt recognition of this entity is crucial to prevent sudden cardiac death. High clinical suspicion and relevant investigations are necessary, along with cardiac MRI workup. Antitubercular therapy can result in successful regression of the disease and termination of malignant arrhythmia. More research is required to study this rare disease.

References

1 Baykan AH, Sayiner HS, Aydin E, Koc M, Inan I, Erturk SM. Extrapulmonary tuberculosis: an old but resurgent problem. Insights Into Imaging. 2022; 13(1):1–21.

2 Shabil M, Bushi G, Beig MA, Rais MA, Ahmed M, Padhi BK. Cardiovascular Manifestation in Tuberculosis Cases: A Systematic Review and Meta-Analysis. Curr Probl Cardiol. 2023; 48(7):101666.

3 Lucero OD, Bustos MM, Ariza Rodríguez DJ, Perez JC. Tuberculous pericarditis-a silent and challenging disease: A case report. World J Clin Cases. 2022;10(6):1869–1875.

Contact

Dr Priya Chudgar, FSCMR
Consultant Radiologist
Jupiter Hospital
Service Rd, Eastern Express Hwy,
next to Viviana Mall
Thane, Maharashtra 400601
India
Tel: +91 22 6297 5555
priyachudgar@gmail.com

Normal Global and Segmental Myocardial T1 and T2 Mapping Values in Two Different Scanner Models

Gabriela Meléndez-Ramírez, Yuridiana Aguilera-Gutiérrez, Melissa Jessi Inquilla-Coyla, Miguel Angel Cruz-Marmolejo, Aloha Meave-Gonzalez, Omar Antonio Gamboa-Abundis, Karen De-Icaza-Benet, Sergio Alfonso Patron-Chi, Pablo Andrés Hernández-Soto

Instituto Nacional de Cardiología Ignacio Chávez, Ciudad de México, México

Introduction

Magnetic resonance imaging (MRI) is a valuable non-invasive modality for the evaluation of a wide range of cardiac pathologies. Late gadolinium enhancement (LGE) is a well-established MRI technique used to detect myocardial fibrosis and/or necrosis. However, it requires the administration of contrast agents and the presence of normal reference myocardium to identify abnormalities. Myocardial mapping enables tissue characterization without the need for contrast administration, even in cases of diffuse disease. Each tissue type exhibits specific T1 values (characterizing longitudinal relaxation) and T2 values (reflecting transverse relaxation).

Normal mapping values are affected by multiple factors, including magnetic field strength, sequence type

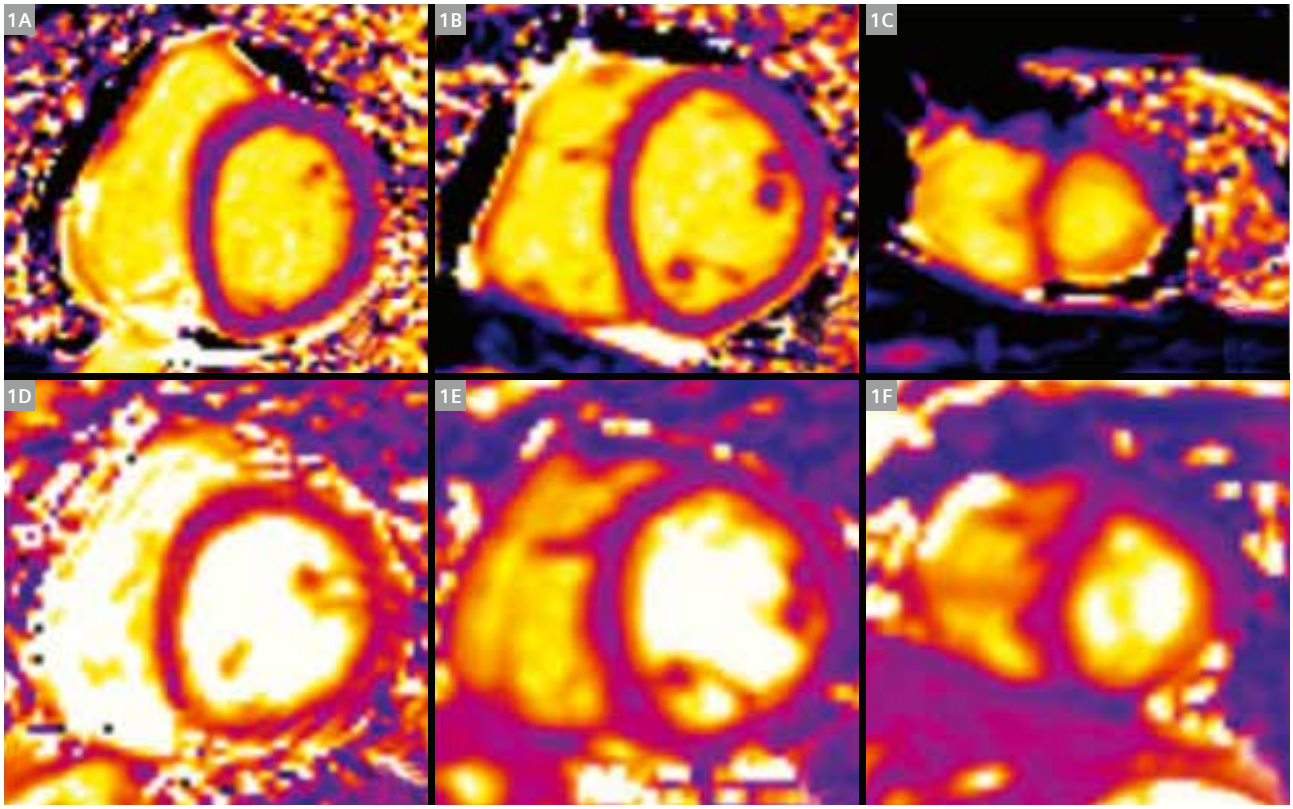

1 T1 and T2 mapping in short-axis basal **(1A, 1D)**, mid-cavity **(1B, 1E)**, and apical **(1C, 1F)**.

(MOLLI, ShMOLLI, or SASHA), [1] sex, age, [2] hematocrit [3] and patient temperature [4]. Because of this variability, the Society for Cardiovascular Magnetic Resonance (SCMR) recommends that each center establish its own local reference values [5]. Few studies to date have included Mexican or Latin American populations. Therefore, the primary objective of this study was to establish and compare normal segmental myocardial values in healthy Mexican individuals separated by sex at our two 1.5T scanners, a MAGNETOM Avanto and a MAGNETOM Sola (Siemens Healthineers, Erlangen, Germany), and compare them.

Methods

This was an observational, descriptive, cross-sectional, single-center study conducted over two different time periods.

Inclusion criteria were adults of either sex, aged 18–65 years, with low cardiovascular risk.

Exclusion criteria were abnormal findings on cardiovascular clinical evaluation or evidence of pathology on cardiac MRI.

Written informed consent was obtained from all participants. The study protocol was approved by the institutional research ethics committee and conforms to the ethical principles of the 1975 Declaration of Helsinki.

Cardiac MRI was performed on the 1.5T MAGNETOM Avanto and the 1.5T MAGNETOM Sola using the standard phased-array cardiac coils. The protocol included ECG-triggered, breath-hold, segmented steady-state free precession cine images in long-axis, short-axis, and four-chamber views. Quantitative T1 and T2 mapping were acquired using MyoMaps sequences in the short axis with a multi-beat mapping sequence. Using the AHA segmentation [6] each segment was manually measured and the average of each one of the 3 thirds was reported.

For the **MAGNETOM Avanto**, T1 mapping parameters included: resolution matrix 256 × 145, FOV read 380 mm, FOV phase 75%, slice thickness 10 mm, and flip angle 35°. T2 mapping parameters included: resolution matrix 192 × 109, FOV read 380 mm, FOV phase 75%, slice thickness 10 mm, and flip angle 70°.

For the **MAGNETOM Sola**, T1 mapping parameters included: resolution matrix 265 × 144, FOV read 360 mm, FOV phase 85%, slice thickness 8 mm, repetition time 395 ms, and flip angle 35°. T2 mapping parameters included: resolution matrix 192 × 116, FOV read 360 mm, FOV phase 80%, slice thickness 8 mm, repetition time 273 ms, and flip angle 70°.

	Total (n = 51)	Male (n = 25)	Female (n = 26)	p
Basal	1002 ± 36	982 ± 32	1026 ± 24	< 0.001
Mid-cavity	1005 ± 27	988 ± 13	1024 ± 25	< 0.001
Apical	1022 ± 48	997 ± 28	1049 ± 51	< 0.001
Global	1008 ± 28	986 ± 19	1028 ± 17	< 0.001

Table 1: MAGNETOM Avanto T1 mapping (ms)

	Total (n = 51)	Male (n = 25)	Female (n = 26)	p
Basal	49.4 ± 3.3	47.7 ± 2.4	51.1 ± 3.3	< 0.001
Mid-cavity	48.6 ± 3.2	47.3 ± 2.5	50 ± 3.2	0.003
Apical	50.4 ± 3.5	49.1 ± 3.1	53 ± 5.9	0.008
Global	49.2 ± 2.7	47.7 ± 2.1	50.1 ± 2.7	< 0.001

Table 2: MAGNETOM Avanto T2 mapping (ms)

Results

Using the **MAGNETOM Avanto**, we evaluated 51 healthy individuals: 25 (49%) male and 26 (51%) female. The median age was 30 years (IQR 28–31). Mean body mass index (BMI) was 25 ± 3.1 kg/m^2 and mean body surface area (BSA) was 1.76 ± 0.15 m^2.

Starting in 2024, we used the **MAGNETOM Sola** to scan 27 subjects: 14 (51.8%) male and 13 (48.2%) female. The median age was 32 years (IQR 28–34). Mean BMI was 25.7 ± 3.9 kg/m^2 and mean BSA was 1.83 ± 0.21 m^2. Tables 1–4 show the T1 and T2 values obtained from both scanners, and Table 5 shows the comparative analysis.

With the Avanto scanner, T1 and T2 values were significantly higher in women. With the Sola scanner, although the values were also higher in females, statistical significance was only observed for T1 at the mid-cavity level and for T2 at the apical level.

Importantly, the comparisons were not performed with the same acquisition parameters; in particular, the different slice thicknesses and matrix sizes will influence the T1 and T2 values. The comparison between scanners demonstrated significantly higher T2 values with the MAGNETOM Avanto, while T1 values were higher only among women.

	Total (n = 27)	Male (n = 14)	Female (n = 13)	p
Basal	1000 ± 17.7	993.9 ± 19.4	1007.2 ± 12.9	0.055
Mid-cavity	995.1 ± 24	985.6 ± 22.6	1005.4 ± 21.8	**0.029**
Apical	1021.4 (1005.9–1021.4)	1011.3 (972.6–1040)	1030 (1010.1–1047.9)	0.18
Global	1006.8 ± 32.3	1002.3 ± 43.2	1011.6 ± 13.8	0.46

Table 3: MAGNETOM Sola T1 mapping (ms)

	Total (n = 27)	Male (n = 14)	Female (n = 13)	p
Basal	46 ± 2.26	45.3 ± 2.6	46.9 ± 1.3	0.06
Mid-cavity	46.2 ± 2.7	45.9 ± 2.2	46.6 ± 2.3	0.40
Apical	49.2 ± 3.9	47.8 ± 4.1	50.9 ± 2.9	**0.036**
Global	46.8 ± 2.2	46.1 ± 2.5	47.6 ± 1.5	0.085

Table 4: MAGNETOM Sola T2 mapping (ms)

	MAGNETOM Avanto	MAGNETOM Sola	p
T1 global	1008 ± 28	1006.8 ± 32.3	0.86
T1 female	1028 ± 17	1011.6 ± 13.8	**0.004**
T1 male	986 ± 19	1002.3 ± 43.2	0.11
T2 global	49.2 ± 2.7	46.8 ± 2.2	**0.0002**
T2 female	50.1 ± 2.7	47.6 ± 1.5	**0.0037**
T2 male	47.7 ± 2.1	46.1 ± 2.5	**0.039**

Table 5: MAGNETOM Avanto vs. MAGNETOM Sola T1 and T2 mapping (ms)

Discussion

Cardiac T1 and T2 mapping enables the detection of subtle myocardial abnormalities at early disease stages when only minimal extracellular and/or intracellular changes are present and conventional techniques are insufficient. These methods are useful for diagnosing disease, monitoring therapeutic response, evaluating short- and long-term adverse effects of medications (such as chemotherapeutics), and guiding invasive procedures (biopsies, ablations).

Because multiple factors influence T1 and T2 values, expert consensus recommends that each center performing mapping sequences establish its own reference ranges. We found slight but significant differences in average T1 in females between the two installations. In addition, our results are consistent with the slightly increased T1 values reported in the literature for females [3].

References

1 Gottbrecht M, Kramer CM, Salerno M. Native T1 and Extracellular Volume Measurements by Cardiac MRI in Healthy Adults: A Meta-Analysis. Radiology. 2019;290(2):317–326.

2 Rosmini S, Bulluck H, Captur G, Treibel TA, Abdel-Gadir A, Bhuva AN, et al. Myocardial native T1 and extracellular volume with healthy ageing and gender. Eur Heart J Cardiovasc Imaging. 2018;19(6):615–621.

3 Rosmini S, Bulluck H, Abdel-Gadir A, Treibel TA, Culotta V, Thompson R, et al. The Effect of Blood Composition on T1 Mapping. JACC Cardiovasc Imaging. 2019;12(9):1888–1890.

4 Vassiliou VS, Heng EL, Gatehouse PD, Donovan J, Raphael CE, Giri S, et al. Magnetic resonance imaging phantoms for quality-control of myocardial T1 and ECV mapping: specific formulation, long-term stability and variation with heart rate and temperature. J Cardiovasc Magn Reson. 2016;18(1):62.

5 Messroghli DR, Moon JC, Ferreira VM, Grosse-Wortmann L, He T, Kellman P, et al. Clinical recommendations for cardiovascular magnetic resonance mapping of T1, T2, T2* and extracellular volume: A consensus statement by the Society for Cardiovascular Magnetic Resonance (SCMR) endorsed by the European Association for Cardiovascular Imaging (EACVI). J Cardiovasc Magn Reson. 2017;19(1):75.

6 Cerqueira MD, Weissman NJ, Dilsizian V, Jacobs AK, Kaul S, Laskey WK, et al. Standardized myocardial segmentation and nomenclature for tomographic imaging of the heart. A statement for healthcare professionals from the Cardiac Imaging Committee of the Council on Clinical Cardiology of the American Heart Association. Int J Cardiovasc Imaging. 2002;18(1):539–542.

Contact

Gabriela Meléndez-Ramírez, M.D.
Instituto Nacional de Cardiología Ignacio Chávez
Calle Juan Badiano 1
Col. Sección XVI, C.P. 14080
Tlalpan, Ciudad de México
Mexico
gabrielamelram@yahoo.com.mx.

Cardiac Amyloidosis Through the Lens of Cardiac MRI

José Martín Alanís-Naranjo, M.D.; Miguel Ángel Cruz-Marmolejo, M.D.; Diego Artemio Valadez-Villegas, M.D.

Instituto Nacional de Cardiología Ignacio Chávez, Ciudad de México, CDMX, Mexico

Cardiac magnetic resonance (CMR) is central to evaluating heart failure because it clarifies etiology and prognosis [1, 2]. Among its most relevant applications is the assessment of cardiac amyloidosis (CA), a progressive and underdiagnosed disease caused by the accumulation of amyloid fibrils in the extracellular space of the myocardium, altering contractility, impairing relaxation, and causing restrictive physiology associated with high morbidity and mortality [3, 4, 5].

CA is most commonly due to either light-chain (AL) amyloidosis, derived from clonal plasma cell dyscrasia and associated with poor outcomes, or transthyretin (ATTR) amyloidosis, related to misfolded transthyretin protein synthesized in the liver. ATTR manifests as wild-type (ATTRwt), linked to age-related misfolding, or as hereditary (ATTRv/ATTRm) associated with TTR gene mutations [2, 5, 6]. Median survival ranges from less than six months in untreated AL to three to five years in ATTR, although novel therapeutic approaches for transthyretin disease are changing this prognosis [2, 7]. Disease progression results not only from diffuse extracellular amyloid deposition but also from the direct toxic effects of prefibrillar oligomers, particularly in AL, which exacerbate organ dysfunction [8].

Until recently, diagnosis relied on biopsy, but this approach is invasive, less sensitive in ATTR, and limited in early disease [2]. CMR has therefore emerged as a non-invasive, reproducible, whole-heart technique capable of characterizing myocardial composition and distinguishing CA from other cardiomyopathies [2, 3]. With gadolinium, CMR identifies extracellular expansion with high spatial resolution, and late gadolinium enhancement (LGE) provides excellent diagnostic accuracy compared with biopsy while serving as an independent predictor of mortality [9]. Beyond LGE, advanced mapping techniques, such as native T1 and T2 mapping and extracellular volume (ECV) quantification, offer quantitative and reproducible assessments of infiltration [10, 11]. Indirect consequences of amyloid deposition, including matrix remodeling, capillary rarefaction, edema, and increased ventricular mass, can also be visualized [2].

Increasing recognition of ATTRwt has driven broader adoption of imaging and has coincided with new therapeutic strategies, making early detection and accurate characterization of amyloid fibrils essential [1]. Imaging not only stratifies risk, but also guides treatment decisions, from optimizing chemotherapy in AL to enabling early initiation of disease-modifying therapies in ATTR gene carriers or patients with heart failure with preserved ejection fraction (HFpEF) [2]. Today, amyloid cardiomyopathy is increasingly recognized as a significant cause of HFpEF worldwide, and CMR provides a sensitive, non-ionizing, and comprehensive tool for diagnosis, monitoring, and prognostic assessment [12].

Morphological features

Morphological evaluation by CMR plays a central role in CA characterization. As in echocardiography, left ventricular hypertrophy (LVH) is the hallmark finding, regardless of amyloid subtype [1, 6]. Compared with healthy volunteers, patients with CA show higher left ventricular mass index (LVMI), lower left ventricle end-diastolic volume index (LVEDVI), and reduced left ventricular ejection fraction (LVEF) [6].

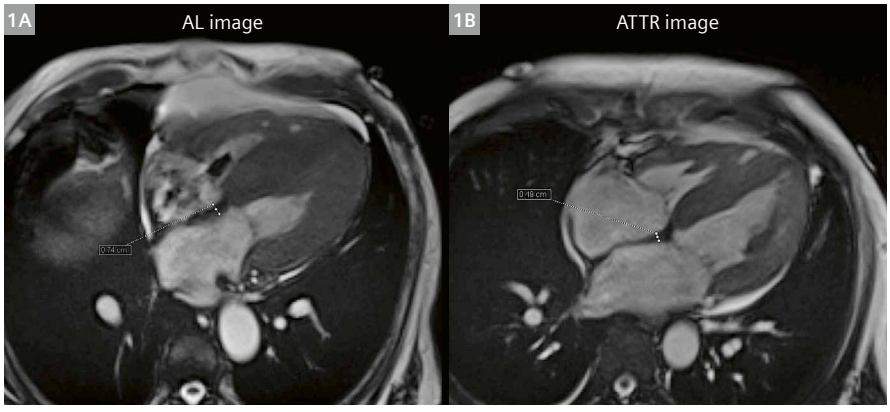

1 4-chamber views of AL **(1A)** and ATTR **(1B)** amyloidosis showing increased thickness of the interatrial septum.

CMR outperforms echocardiography in assessing atrial abnormalities. Early reports suggested interatrial septal thickening > 5–6 mm as a specific marker of CA, more frequently observed in ATTRwt, although this finding appears less common in contemporary cohorts, likely due to earlier diagnosis. CA patients frequently show biatrial enlargement, atrial septal thickening, and impaired atrial function [4, 6].

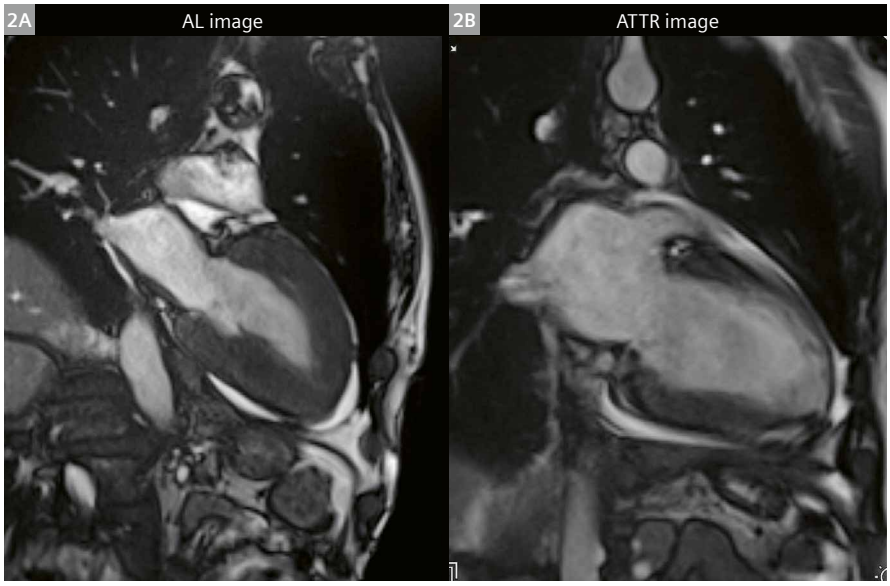

2 2-chamber views of AL **(2A)** and ATTR **(2B)** amyloidosis.

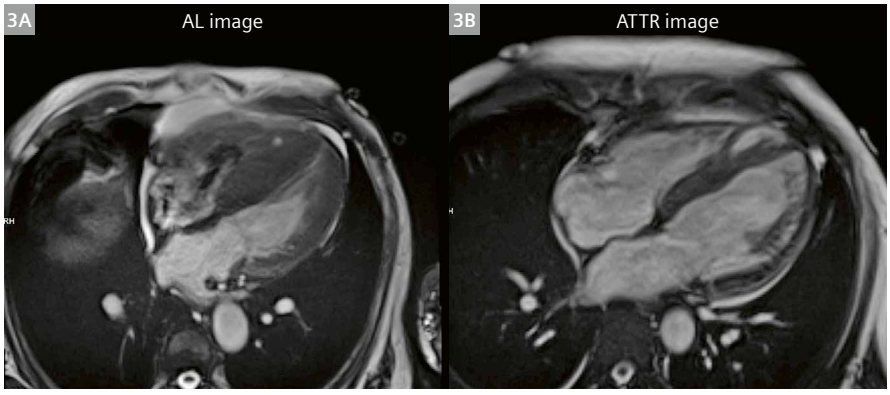

3 4-chamber views of AL **(3A)** and ATTR **(3B)** amyloidosis showing left ventricular hypertrophy.

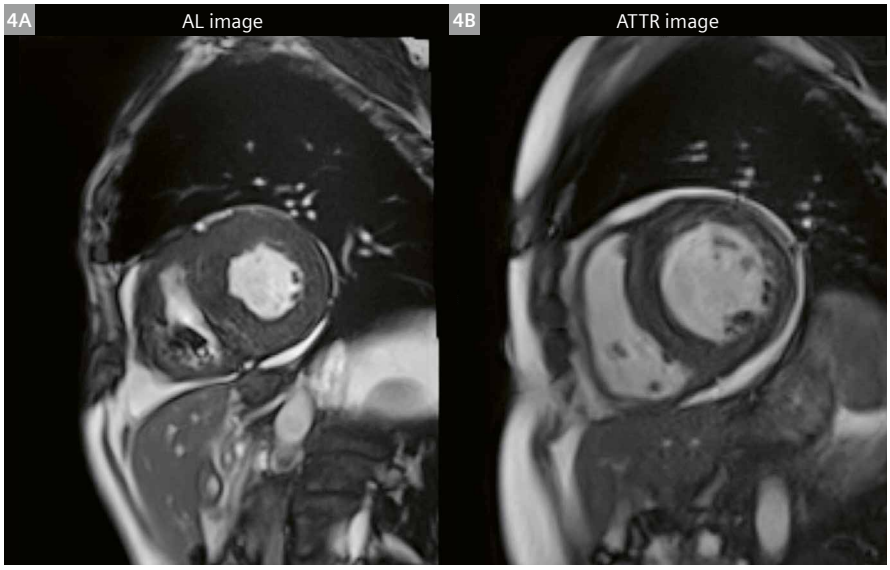

4 Short-axis views showing left ventricular hypertrophy in AL **(4A)** and ATTR **(4B)**.

Cine CMR consistently demonstrates concentric and symmetric LV thickening, although asymmetric patterns can occur, particularly in ATTR, and may mimic hypertrophic cardiomyopathy with a risk of misdiagnosis [2, 4]. Morphological subtypes such as sigmoid septum and reverse septal contour are described, and concentric thickening may involve both ventricles as well as the atria. In advanced disease, ventricles are thick with small cavity size, reduced stroke volume, and fixed cardiac output [2].

T1 mapping

The key advantage of CMR in CA is myocardial tissue characterization, and among its novel tools, T1 mapping has emerged as a powerful technique [1]. T1 mapping is a quantitative technique that measures myocardial T1 relaxation time on a voxel basis, reflecting both intracellular and extracellular components. Native T1 values rise with fibrosis, infiltrative processes, or edema, and are markedly elevated in amyloid infiltration [13].

Elevated native T1 is a sensitive marker of early amyloid infiltration, often increasing even before LGE develops, and has been reported in ATTRv gene carriers without enhancement [2, 3]. Native T1 is markedly elevated in CA and correlates with markers of systolic and diastolic dysfunction, with reported sensitivity and specificity above 90% [2, 3]. AL-CA has been associated with higher native T1 and longitudinal reductions after chemotherapy, which correlate with favorable hematologic responses, while increasing predicted worse survival [1].

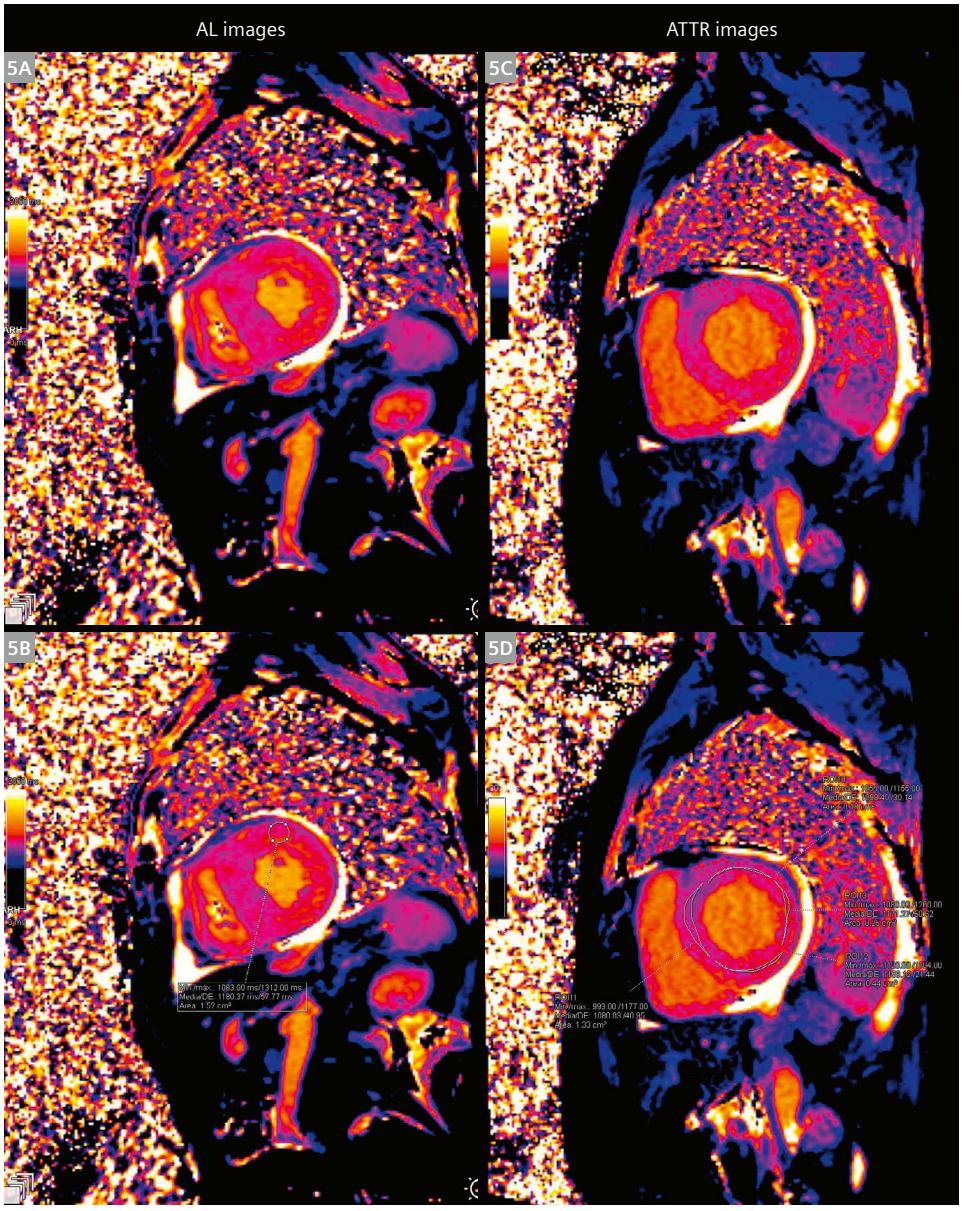

5 Native T1 mapping **(5A, 5C)** and increased native T1 mapping measurements **(5B, 5D)**.

In CA, global T1 is consistently increased, with higher values in basal than apical segments, paralleling the base-to-apex gradients observed with strain and ECV [4, 6, 14]. Regional distribution correlates with segmental dysfunction, LGE, and higher mortality [6].

Importantly, native T1 is valuable in patients with renal dysfunction, a frequent comorbidity in CA, where gadolinium may be contraindicated. Approximately one third of patients with AL or ATTR present with impaired renal function, and non-contrast T1 mapping provides reliable diagnostic accuracy even in advanced kidney disease or nephrotic syndrome, without the confounding effects of proteinuria or anemia [2, 5]. Native T1 is substantially elevated in both AL and ATTR, without consistent differences between subtypes [15]. Unlike ECV, which is specific to interstitial expansion, T1 values capture changes in both myocytes and the extracellular matrix, suggesting that additional factors, including myocardial edema from light-chain toxicity, could contribute to higher AL values [4].

Beyond diagnosis, T1 mapping shows prognostic relevance. Studies and meta-analyses have demonstrated a continuous relationship between high T1 and adverse outcomes, as elevated values represent greater amyloid burden and interstitial expansion [12]. However, its independent prognostic role remains less well established than LGE or ECV, partly due to technical variability. T1 values differ across scanners, field strengths, and mapping sequences. Inversion recovery sequences based on the Look-Locker protocol, such as Modified Look-Locker inversion recovery (MOLLI) and Shortened Modified Look-Locker

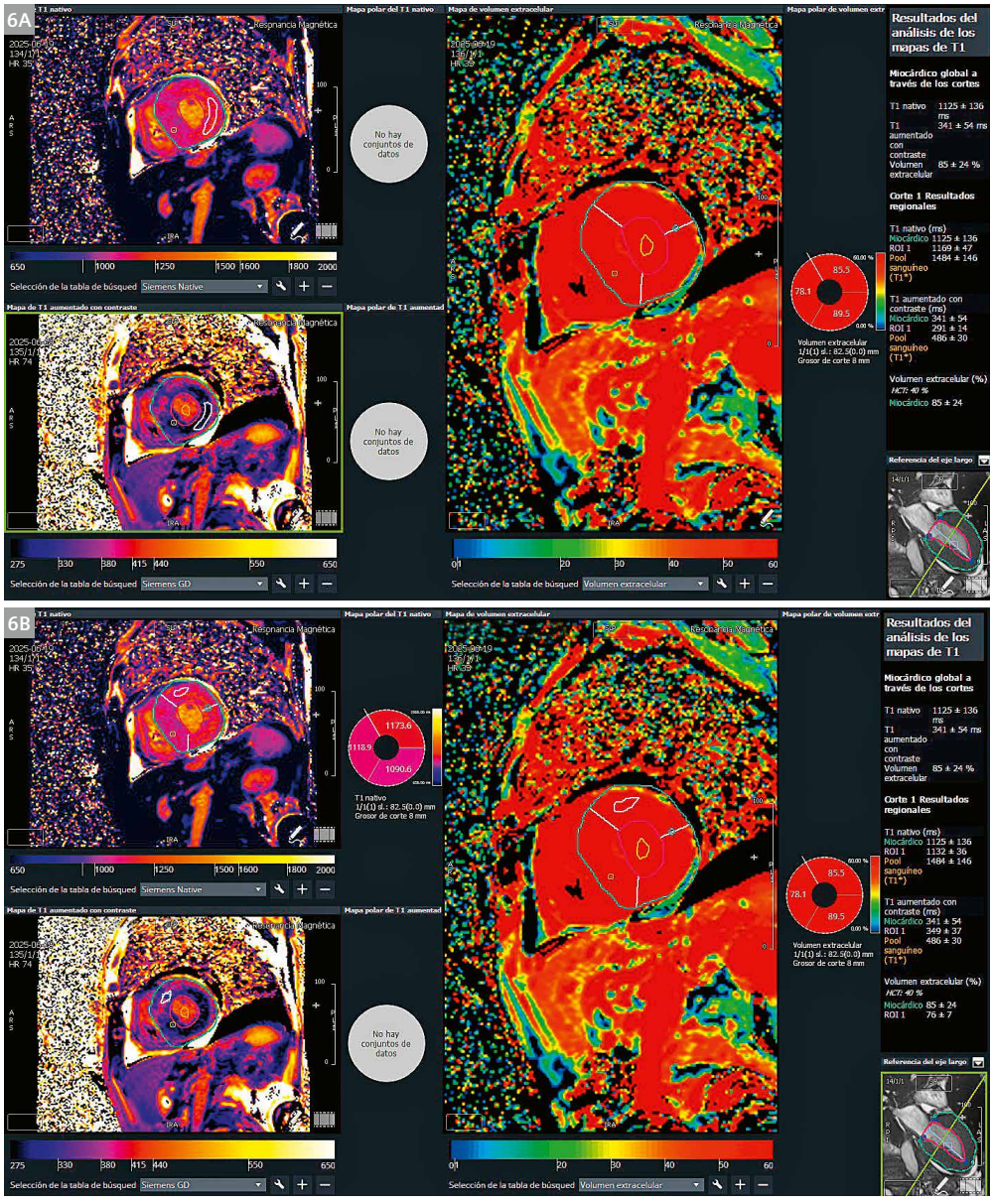

6 Velocity encoding.

inversion recovery (ShMOLLI), generate similar results, while SAturation recovery single-SHot Acquisition (SASHA) produces higher absolute T1 values, underscoring the need for center-specific reference ranges [2, 8, 12].

In practice, combining morphological features such as concentric hypertrophy, atrial wall thickening, and pericardial effusion with diffuse elevation of native T1 strengthens diagnostic confidence, even without LGE [1]. Non-contrast T1 mapping thus provides a safe, reproducible alternative in CA patients unable to receive gadolinium. This enables early diagnosis and risk stratification, and can potentially guide therapeutic monitoring [5, 9, 13].

Extracellular volume

ECV – derived from post-contrast T1 mapping – is markedly elevated in CA and is more reproducible than absolute T1 values [2]. ECV correlates with markers of disease severity, tracks amyloid burden, and outperforms native or post-contrast T1 mapping alone as a prognostic marker [2, 11]. Reported myocardial ECV values range from 44% to 61% in CA compared with 25%–27% in healthy patients [4], with average levels of 54% in ATTR and 51% in AL, substantially higher than diffuse fibrotic conditions, where values rarely exceed 40% [9]. ATTR-CA has been consistently associated with greater ECV than AL-CA [1].

ECV measurement reflects extracellular amyloid fibril accumulation and provides a surrogate of interstitial expansion independent of necrosis. Elevated ECV correlates with systolic and diastolic dysfunction but also with all-cause mortality, heart failure hospitalizations, and major adverse cardiac events, outperforming native T1 in predicting outcomes [7, 11, 12]. Prognostic studies confirm a continuous relationship between higher ECV and worse survival, with incremental increases associated with increased mortality [12]. In AL cohorts, reductions in ECV after chemotherapy correlated with hematologic response and improved prognosis, suggesting a role for monitoring treatment response [1].

The diagnostic accuracy of ECV is excellent, with sensitivity and specificity approaching 86% and 97%, respectively, for identifying ATTR-CA [1]. In comparative studies, ECV shows higher diagnostic performance than LGE, capturing both early infiltration and diffuse burden even when LGE is absent [3, 9]. Base-to-apex ECV gradients parallel those of native T1, with basal segments typically showing elevated values [6, 14]. Patients with diffuse transmural LGE demonstrate markedly higher ECV, while those with subendocardial or heterogeneous LGE still exhibit globally elevated values compared with healthy controls, indicating diffuse involvement at different stages [6].

Technical limitations of ECV include accurate registration of pre- and post-contrast T1 maps and hematocrit measurements. Alternative surrogate indices, such as the myocardium-to-lumen R1 ratio or the post-contrast myocardial–luminal T1 difference, have demonstrated high diagnostic performance comparable to ECV. In large cohorts, both ECV and myocardium-to-lumen ratios showed excellent accuracy, superior to native T1 [16].

Meta-analyses confirm that elevated ECV is the strongest imaging biomarker for prognosis in CA, with higher reproducibility and clinical utility than native T1, and incremental increases in ECV provide a continuous risk relationship for mortality [11, 12]. Cutoff values between 30%–47% have been proposed to differentiate CA from other causes of LVH [15]. Ultimately, ECV represents the most robust quantitative CMR parameter for detecting CA, assessing disease burden, guiding treatment monitoring, and predicting outcomes across both AL and ATTR subtypes [2, 9, 12].

T2 mapping

T2 mapping has not been as extensively evaluated in CA as native T1 or ECV, but it provides additional insights into myocardial involvement [2]. T2 mapping reflects myocardial water content and serves as a surrogate marker of edema. It has been traditionally used in inflammatory diseases such as myocarditis but is being increasingly applied to CA, where elevated values have been associated with mortality and may track treatment response [3, 11]. Histological evidence confirms that myocardial edema is present in CA, suggesting mechanisms beyond amyloid deposition that contribute to disease progression and adverse outcomes [11].

Studies demonstrated significantly increased T2 values in CA compared with controls, with mean values ranging from 56.6–63.2 ms in AL, 54.2–56.2 ms in ATTR, and 48.9–51.1 ms in healthy subjects [4]. Both the ATTR and AL groups show increased T2 relative to hypertensive LVH, consistent with fibril deposition leading to altered fluid retention and myocardial edema [15]. However, the results are not fully consistent: Some reports found no significant differences between AL and ATTR [8, 14], while others showed higher mean T2 in AL, possibly reflecting light-chain-induced cytotoxicity and increased interstitial fluid accumulation [15].

T2 mapping offers complementary diagnostic and prognostic information. Elevated myocardial T2 values in CA support the concept that the disease is not purely infiltrative but also involves an edematous component, which may influence injury mechanisms and therapeutic response [8]. The presence of abnormal T2 values, in combination with T1 or ECV changes, provides a more comprehensive characterization of CA and may help assess disease stage, risk, and treatment monitoring [3, 8].

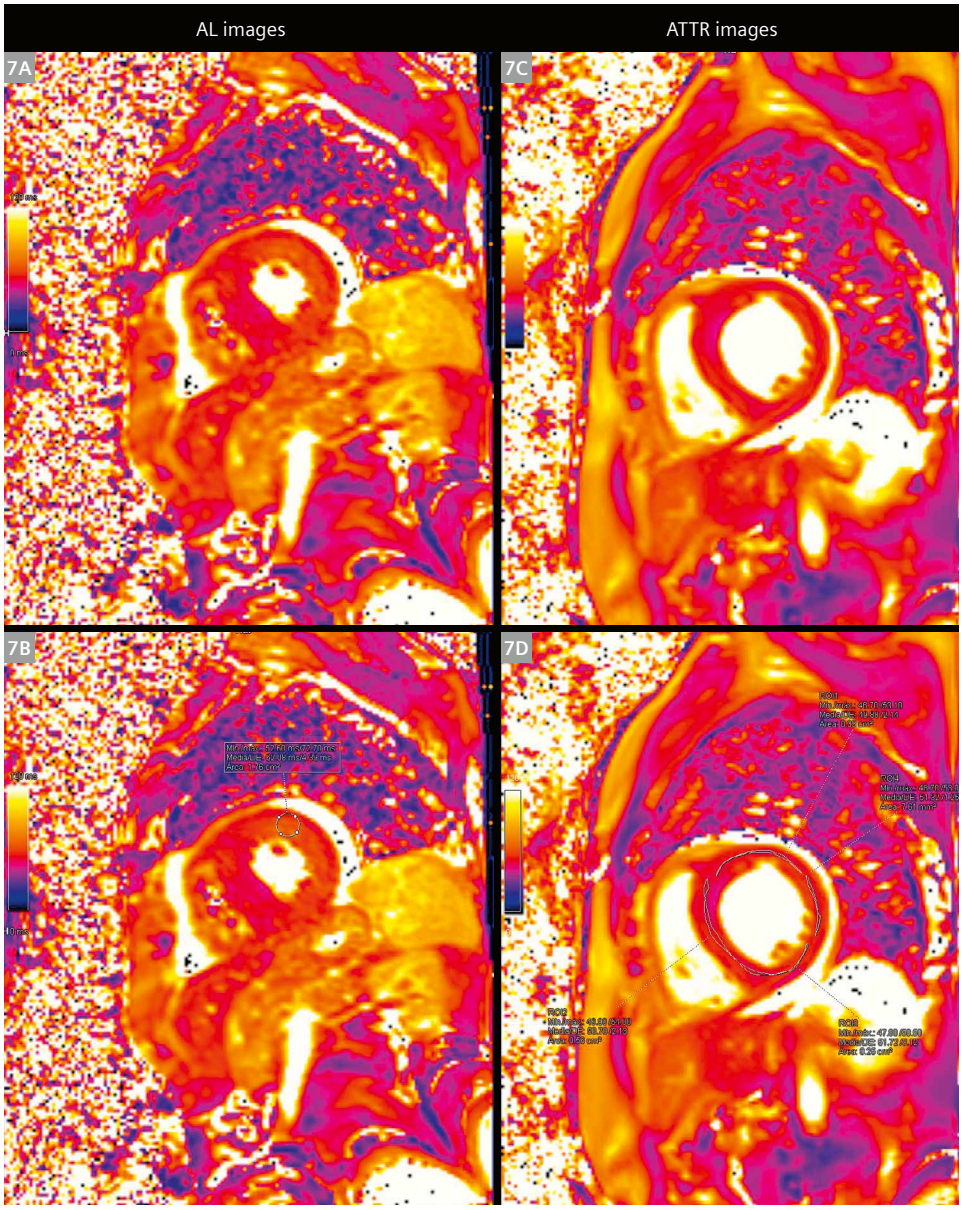

7 **(7A, 7C)** T2 mapping; **(7B, 7D)** T2 mapping increased in AL amyloidosis.

Late gadolinium enhancement

LGE is the cornerstone CMR technique for diagnosing CA, as gadolinium accumulates in the abnormally expanded extracellular space [2, 3]. To achieve optimal contrast between normal and abnormal myocardium, gadolinium-based contrast material must be administered intravenously, and imaging must be delayed for at least 10 minutes following the injection [4].

The characteristic finding is diffuse, circumferential subendocardial enhancement, often progressing to transmural involvement, with additional atrial or right ventricular (RV) LGE frequently observed [1, 9, 13]. LGE is highly prevalent, occurring in nearly all CA patients, with greater transmural and RV involvement in ATTR compared with AL, although CMR alone cannot definitively distinguish amyloid subtypes [1, 15]. Patterns differ by stage and type: AL more often shows subendocardial or patchy mid-wall enhancement, while ATTR is associated with extensive transmural and RV LGE, and atrial LGE is more common in ATTR [1, 6, 15].

Traditional LGE relies on operator-determined nulling of normal myocardium, which is often difficult in CA because the entire myocardium is infiltrated, sometimes nulling before the blood pool. The difficulty in nulling myocardium or in myocardial nulling before blood pool on the TI scout is highly suggestive of CA, with a sensitivity

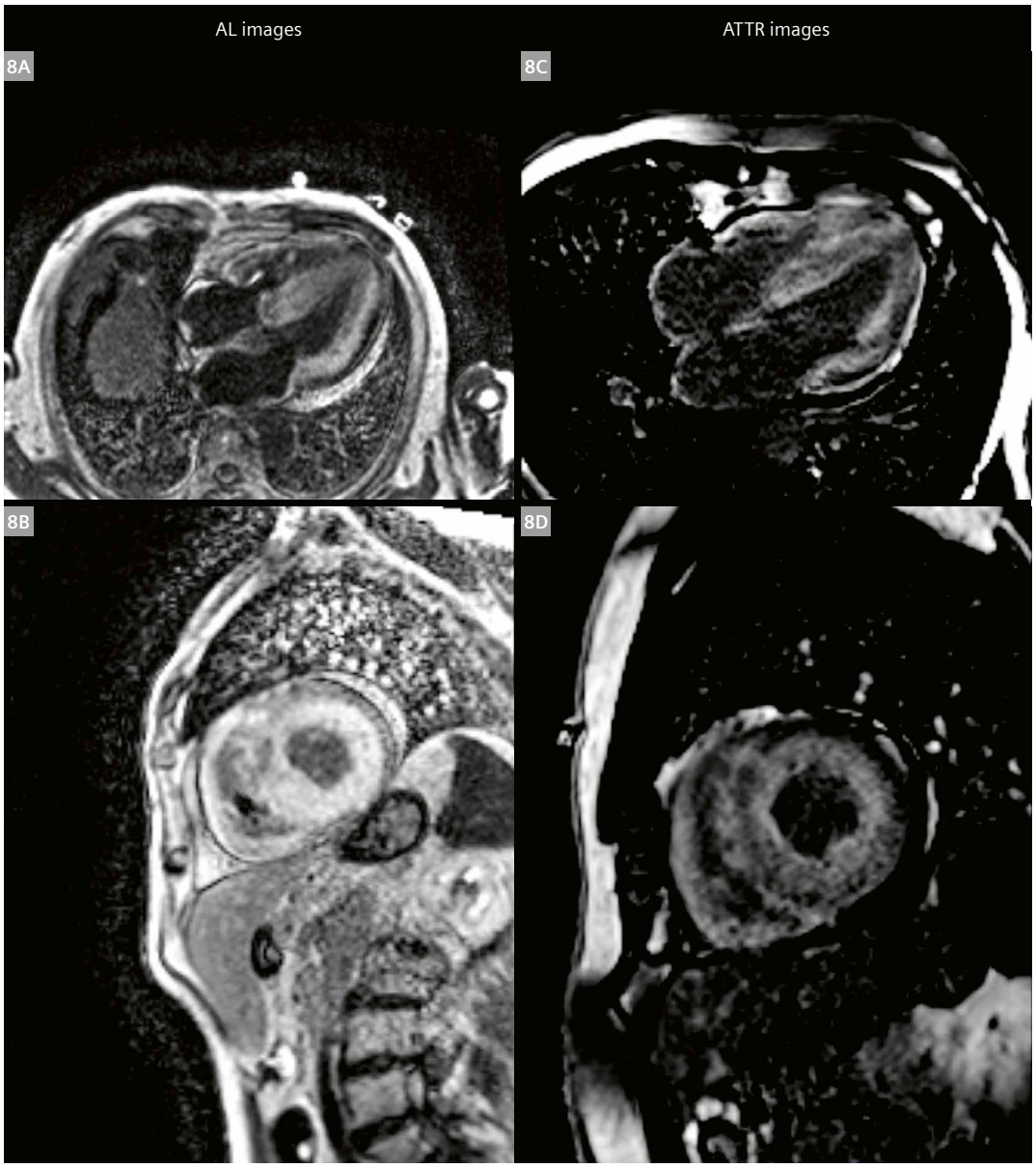

8 Diffuse intramyocardial and subendocardial LGE of AL **(8A, 8B)** and of ATTR **(8C, 8D)**.

approaching 100% [1, 2]. Phase-sensitive inversion recovery (PSIR) reduces operator dependence and increases reproducibility, with strong concordance with T1 mapping [6].

The prognostic value of LGE is well established. Transmural involvement is associated with poor survival regardless of amyloid subtype, while subendocardial LGE indicates intermediate risk. Studies show 24-month survival rates of 92% in patients without LGE, 81% with subendocardial LGE, and 61% with transmural involvement [6, 9]. RV LGE is consistently linked to a worse prognosis [6]. Although prevalence and extent are greater in ATTR, mortality is higher in AL when transmural LGE is present [2].

LGE remains the most widely established CMR method for identifying cardiac amyloid infiltration, with sensitivity and specificity around 85%–90% [4]. Its characteristic patterns, especially diffuse subendocardial or transmural enhancement combined with abnormal gadolinium kinetics, provide strong diagnostic confidence and important prognostic information, despite the need for complementary mapping techniques to overcome its inherent limitations [8, 15].

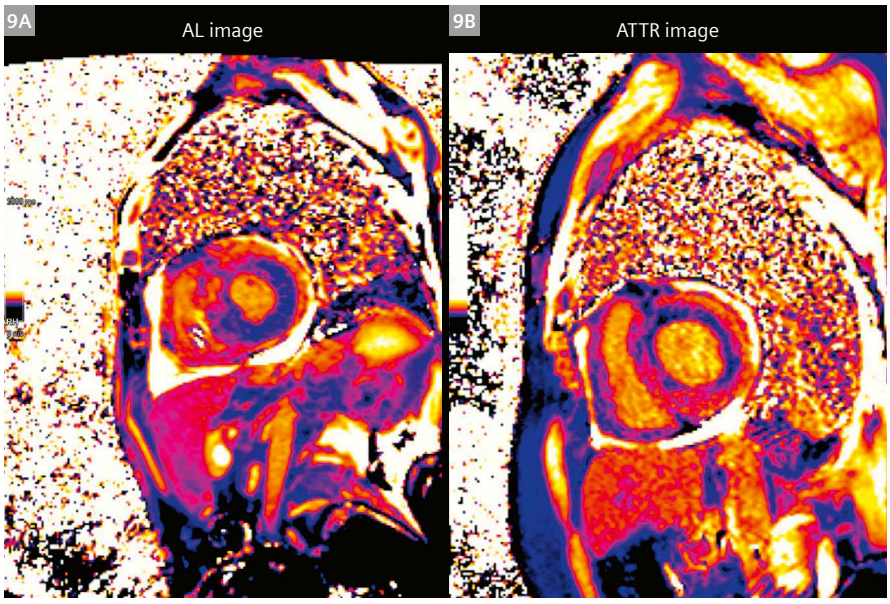

9 Post-contrast T1 mapping of AL **(9A)** and ATTR **(9B)**.

Strain analysis

Strain analysis with CMR feature tracking (FT) parallels speckle-tracking echocardiography and typically shows reduced global longitudinal strain (GLS) with a base-to-apex gradient and relative apical sparing in CA [1]. Cine-derived FT allows the quantification of longitudinal, circumferential, and radial strains. In CA, FT-GLS and FT-global circumferential strain (GCS) are reduced, while FT-global radial strain (GRS) is lower than non-amyloid hypertrophy, with marked base-to-apex differences across strain components. These structural and functional alterations correlate with clinical and imaging parameters: GCS shows moderate correlations with T1 and ECV, and strain measures correlate strongly with LVEF. Diagnostic performance is improved when combining basal T1 with apical-to-basal strain ratios, approaching ECV accuracy [14].

Conclusion

Cardiac amyloidosis is a progressive and underdiagnosed cause of heart failure. Cardiac magnetic resonance has become a key imaging tool, combining detailed morphology with advanced tissue characterization. Late gadolinium enhancement identifies typical infiltration patterns and predicts outcome. Native T1 detects early disease and is particularly valuable in renal dysfunction patients. Extracellular volume is the strongest quantitative marker of amyloid burden and treatment response. T2 mapping reveals myocardial edema, adding insight into disease mechanisms. Strain analysis detects subtle functional impairments and carries prognostic value, especially for right ventricular involvement. Combined, these techniques provide a comprehensive, noninvasive approach to diagnosis, risk stratification, and monitoring, placing CMR at the forefront of contemporary care in cardiac amyloidosis.

Take-home

- Cardiac magnetic resonance is the noninvasive cornerstone for the diagnosis, risk stratification, and follow-up of cardiac amyloidosis.
- TI-scout evidence of difficult myocardial nulling is highly suggestive of cardiac amyloidosis, and phase-sensitive inversion recovery improves reliability.
- Late gadolinium enhancement patterns stratify prognosis: Absence indicates the most favorable outcomes, subendocardial involvement indicates intermediate risk, and transmural or right-ventricular involvement indicates the highest risk.
- Quantitative mapping provides complementary information: Native T1 detects early disease and is valuable when contrast is contraindicated; extracellular volume quantifies amyloid burden and supports serial assessment; T2 mapping identifies myocardial edema.
- CMR feature tracking typically shows reduced global longitudinal strain with a base-to-apex gradient and relative apical sparing; combining basal native T1 with apical-to-basal strain ratios enhances diagnostic performance and approaches that of extracellular volume.
- Integrated interpretation of late gadolinium enhancement, T1/ECV, T2, and strain yields high diagnostic confidence and robust prognostic assessment.

References

1 Hosadurg N, Rodriguez Lozano P, Patel AR, Kramer CM. Cardiac Magnetic Resonance in the Evaluation and Management of Nonischemic Cardiomyopathies. JACC Heart Fail. 2025;13(9):102525.
2 Dorbala S, Cuddy S, Falk RH. How to Image Cardiac Amyloidosis: A Practical Approach. JACC Cardiovasc Imaging. 2020;13(6):1368–1383.
3 Ioannou A, Patel R, Gillmore JD, Fontana M. Imaging Guided Treatment for Cardiac Amyloidosis. Curr Cardiol Rep. 2022;24(7):839–850.
4 Oda S, Kidoh M, Nagayama Y, Takashio S, Usuku H, Ueda M, et al. Trends in Diagnostic Imaging of Cardiac Amyloidosis: Emerging Knowledge and Concepts. Radiographics. 2020;40(4):961–981.
5 Baggiano A, Boldrini M, Martinez-Naharro A, Kotecha T, Petrie A, Rezk T, et al. Noncontrast Magnetic Resonance for the Diagnosis of Cardiac Amyloidosis. JACC Cardiovasc Imaging. 2020;13(1 Pt 1):69–80.
6 Scheel PJ 3rd, Mukherjee M, Hays AG, Vaishnav J. Multimodality Imaging in the Evaluation and Prognostication of Cardiac Amyloidosis. Front Cardiovasc Med. 2022;9:787618.
7 Boretto P, Patel NH, Patel K, Rana M, Saglietto A, Soni M, et al. Prognosis prediction in cardiac amyloidosis by cardiac magnetic resonance imaging: a systematic review with meta-analysis. Eur Heart J Open. 2023;3(5):oead092.
8 Grazzini G, Pradella S, Bani R, Fornaciari C, Cappelli F, Perfetto F, et al. The Role of T2 Mapping in Cardiac Amyloidosis. Diagnostics (Basel). 2024;14(10):1048.
9 Pan JA, Kerwin MJ, Salerno M. Native T1 Mapping, Extracellular Volume Mapping, and Late Gadolinium Enhancement in Cardiac Amyloidosis: A Meta-Analysis. JACC Cardiovasc Imaging. 2020;13(6):1299–1310.
10 Yilmaz A. Interpretation of CMR-Based Mapping Findings in Cardiac Amyloidosis: Please Act With Caution! JACC Cardiovasc Imaging. 2022;15(4):604–606.
11 Forouzannia SA, Rafiei Alavi SR, Forouzannia SM, Abdulla J, Ioannou A, Francese G, et al. Prognostic value of CMR parametric mapping in cardiac amyloidosis: an updated systematic review and meta-analysis. Open Heart. 2025;12(2):e003551.
12 Cai S, Haghbayan H, Chan KKW, Deva DP, Jimenez-Juan L, Connelly KA, et al. Tissue mapping by cardiac magnetic resonance imaging for the prognostication of cardiac amyloidosis: A systematic review and meta-analysis. Int J Cardiol. 2024;403:131892.
13 Aquaro GD, Monastero S, Todiere G, Barison A, De Gori C, Grigoratos C, et al. Diagnostic Role of Native T1 Mapping Compared to Conventional Magnetic Resonance Techniques in Cardiac Disease in a Real-Life Cohort. Diagnostics (Basel). 2023;13(14):2461.
14 Zaarour Y, Sifaoui I, Remili H, Kharoubi M, Zaroui A, Damy T, et al. Diagnostic performance and relationships of structural parameters and strain components for the diagnosis of cardiac amyloidosis with MRI. Diagn Interv Imaging. 2024;105(12):489–497.
15 Kravchenko D, Isaak A, Zimmer S, Öztürk C, Mesropyan N, Bischoff LM, et al. Parametric mapping using cardiovascular magnetic resonance for the differentiation of light chain amyloidosis and transthyretin-related amyloidosis. Eur Heart J Cardiovasc Imaging. 2024;25(10):1451–1461.
16 Kidoh M, Oda S, Takashio S, Kawano Y, Hayashi H, Morita K, et al. Cardiac MRI-derived Extracellular Volume Fraction versus Myocardium-to-Lumen R1 Ratio at Postcontrast T1 Mapping for Detecting Cardiac Amyloidosis. Radiol Cardiothorac Imaging. 2023;5(2): e220327.

Contact

Diego Artemio Valadez-Villegas, M.D.
Instituto Nacional de Cardiología Ignacio Chávez
Juan Badiano 1, Belisario Domínguez Secc 16,
Tlalpan, 14080 Ciudad de México, CDMX, Mexico
Tel.: +52 55 5573 2911
dr.diegovaladez@gmail.com

Advanced Imaging in Cardio-Oncology: Cardiac Magnetic Resonance for Cardiotoxicity Assessment

Federica Brilli, M.D.; Costanza Lisi, M.D.; Stefano Figliozzi, M.D.; Federica Catapano, M.D.; Marco Francone, M.D., Ph.D.

Department of Biomedical Sciences, Humanitas University, Milan, Italy
IRCCS Humanitas Research Hospital, Milan, Italy

Cardiotoxicity: Background and definition

In recent decades, advancements in cancer therapies have significantly improved survival rates, leading to a growing number of cancer survivors. However, these successes highlight the need to address therapy-related side effects, particularly those affecting cardiovascular health, which can arise both acutely and chronically [1]. This recognition has fostered the development of cardio-oncology, a field dedicated to the cardiovascular implications of cancer treatments. Cardio-oncology employs integrated strategies for the prevention and management of associated risks, ultimately aiming to enhance cancer patients' quality of life [2].

The field adopts a multidisciplinary approach, with collaboration among various healthcare professionals to tackle the unique challenges faced by patients. Radiology plays a crucial role, providing essential diagnostic and monitoring tools that facilitate the early detection and characterization of cardiotoxicity. Advanced imaging modalities enable clinicians to identify subtle changes in cardiac function and structure, allowing for timely interventions that can prevent irreversible cardiac damage.

Historically, confusion has existed regarding the definitions of cardiotoxicity. This is due to the varied terminology used to describe the cardiovascular impacts of cancer treatments. Until 2022, the only widely accepted definition of treatment-induced cardiac dysfunction was from the American Society of Echocardiography, which defined it as a reduction in left ventricular ejection fraction (LVEF) of more than 10%, falling below 53% [3]. This definition has since broadened to encompass a wider array of cardiac issues stemming from cancer therapies.

In 2022, the International Cardio-Oncology Society (IC-OS) introduced a consensus definition for cancer therapy-related cardiac dysfunction (CTRCD), which includes conditions such as cardiomyopathy, heart failure (HF), myocarditis, vascular toxicity, hypertension (HTN), arrhythmias, and QT interval prolongation associated with anticancer treatments [4]. This comprehensive framework aims to address long-standing issues of misclassification and misdiagnosis in the field. In August 2022, the European Society of Cardiology (ESC) published its first guidelines on cardio-oncology, establishing international standards for the diagnosis and management of cancer therapy-related cardiovascular toxicity (CTR-CVT). This initiative involved collaboration with the European Hematology Association (EHA), the European Society for Therapeutic Radiology and Oncology (ESTRO), and the International Cardio-Oncology Society, highlighting the need for a systematic approach to managing cardiovascular toxicities in cancer patients [5]. The guidelines stress the importance of early detection, risk assessment, and preventive measures to improve outcomes for this at-risk population.

Pathophysiology of cardiotoxicity

Cardiotoxicity arises from complex, multifactorial mechanisms that include direct myocardial injury, vascular endothelial damage, and inflammation, leading to structural and functional cardiac impairment [6].

Oxidative stress and mitochondrial dysfunction
Anthracyclines induce oxidative stress, generating reactive oxygen species (ROS) that damage cardiac myocytes. The heart's reliance on mitochondria makes it vulnerable. ROS accumulation leads to mitochondrial dysfunction, impaired adenosine triphosphate (ATP) synthesis, cardiomyocyte apoptosis, myocardial atrophy, fibrosis, contractile dysfunction, and heart failure [7].

Inflammatory pathways and immune activation
Immunotherapy, like checkpoint inhibitors (ICI), improves outcomes in malignancies but can cause immune-related adverse events (IrAEs), including cardiotoxicity in up to 1% of patients. Symptoms include hypotension, arrhythmias, and left ventricular dysfunction linked to cytokine release syndrome. Acute myocarditis occurs in 0.04% to 1.14% of cases, with risks ranging from fatal outcomes to transient edema within one to two months of treatment [8]. Mechanisms involve T cells targeting shared antigens in tumors and heart tissues, pericardial inflammation, myocardial ischemia affecting coronary plaques, and coronary spasms post PD-1 inhibitor treatment [9]. Imaging, especially cardiac magnetic resonance (CMR), aids in diagnosing cardiovascular adverse reactions as per the 2022 ESC guidelines, and offers advantages in identifying myocarditis.

Microvascular injury
Tyrosine kinase inhibitors (TKIs) induce endothelial dysfunction and microvascular damage, reducing coronary flow reserve and causing vasospasm, increased vascular permeability, and myocardial ischemia [10].

The role of imaging in cardio-oncology

Advanced cardiovascular imaging plays a major role in detecting subclinical cardiovascular diseases and directly influences clinical decisions. The guidelines advocate for transthoracic echocardiography (TTE) as the primary imaging technique for baseline evaluations of heart structure and function before chemotherapy [11]. TTE quantitatively assesses left and right ventricular function, chamber dilation, hypertrophy, regional wall motion abnormalities, diastolic function, valvular heart disease, and pulmonary arterial pressure – all of which can guide therapeutic strategies.

The guidelines highlight the need for consistent imaging modalities throughout the treatment process to facilitate accurate comparisons over time. While TTE is crucial for assessing left ventricular function and global longitudinal strain (GLS) [12], CMR should be used when TTE yields poor quality images or non-diagnostic results [13].

In circumstances where TTE fails to identify specific conditions like hypertrophic cardiomyopathy, CMR becomes essential for thorough risk assessment. Both cardiac computed tomography angiography (CCTA) and CMR are indicated for detecting subclinical coronary artery disease (CAD) through coronary calcium scoring and identifying

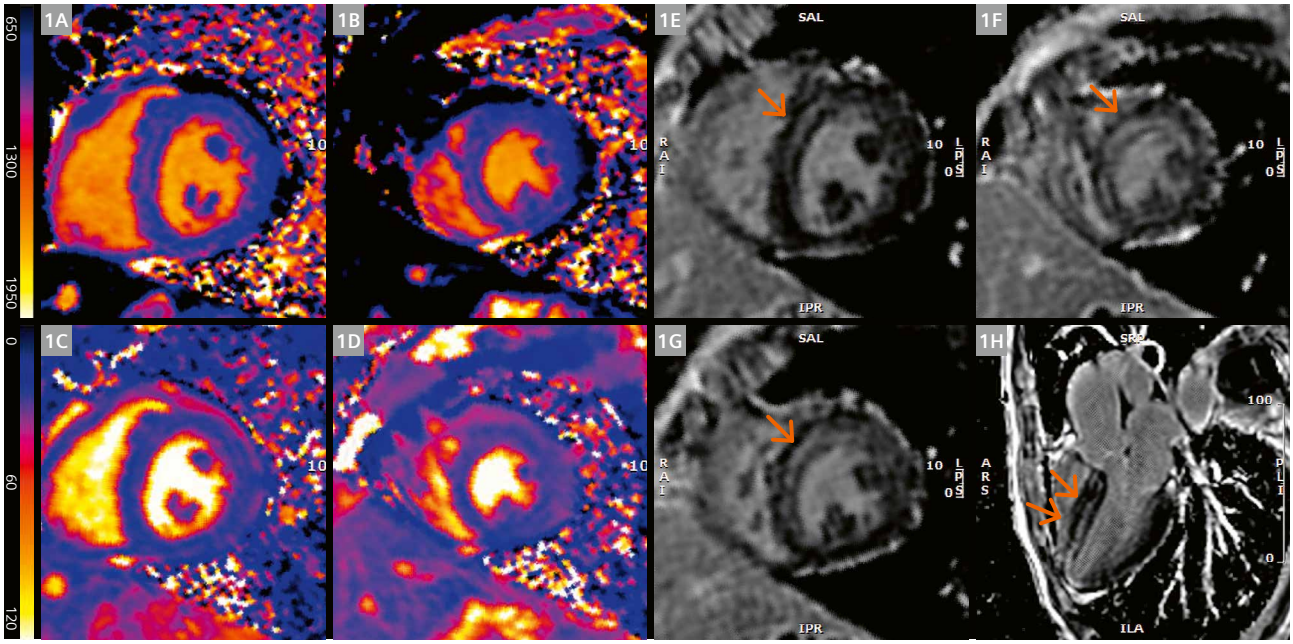

1 A 65-year-old woman with Stage IV clear cell renal carcinoma developing immuno-checkpoint-inhibitor-related myocarditis. The CMR shows focally increased T1 values (1090 msec; normal value < 1059 msec; **1A, 1B**) and T2 values (55 msec; normal value < 51 msec; **1C, 1D**) at midventricular anteroseptal and apical septal wall. Late gadolinium enhancement (LGE) sequences show mid-myocardial wall LGE at the same level, as seen in the midventricular and apical short-axis view (orange arrows in **1E–1G**) and three-chamber view (orange arrows in **1H**).

intracardiac masses [14]. For symptomatic CAD, functional imaging techniques such as stress CMR are warranted, while CCTA serves as the standard test to exclude coronary obstructions in patients at low to intermediate risk of CAD [15].

Role of CMR in tissue characterization and functional evaluation

Thanks to its spatial and temporal resolution, CMR is an invaluable tool for assessing cardiac structure and function without reliance on geometric assumptions – unlike other imaging modalities. It excels in characterizing myocardial tissue abnormalities stemming from chemotherapy, which can range from edema and necrosis to more chronic changes such as fibrosis. The use of advanced multiparametric CMR imaging allows clinicians to explore various aspects of cardiotoxicity through a combination of conventional and innovative T1/T2 mapping techniques [16–20]. Quantitative T1 and T2 mapping techniques in CMR have proven useful in reflecting subclinical histopathological changes in anthracycline-induced cardiotoxicity, aiding in early detection and management [21].

As well as providing critical insights into myocardial edema and inflammation, the mapping techniques also quantify extracellular volume (ECV), which serves as an indirect biomarker for tissue fibrosis and interstitial expansion. This quantitative approach is vital for comprehensively evaluating the extent of myocardial damage, particularly in cases of diffuse myocardial disease, where regional changes may escape detection with standard imaging techniques like late gadolinium enhancement (LGE). Generally, an increase in pre-contrast T1 values indicates myocardial edema inflammation, and fibrosis, while prolonged T2 relaxation time correlates with acute edema. In several cases, cardiotoxic drug exposure has been associated with an increase in both native T1 and T2 relaxation times. Tissue characterization in cardiac imaging also employs qualitative and semi-quantitative methods that involve the use of gadolinium contrast agents. Early gadolinium enhancement (EGE) and late gadolinium enhancement are critical indicators of underlying pathological processes such as inflammation, edema, and myocardial fibrosis, all of which are associated with cardiotoxic chemotherapy [22]. Research has shown that EGE can predict a decline in left ventricular ejection fraction within the first month of anthracycline therapy. Additionally, the LGE pattern seen in trastuzumab- and anthracycline-induced myocardial fibrosis is characterized as non-ischemic subepicardial contrast enhancement [23].

Another significant factor in tissue assessment is extracellular volume, which effectively detects diffuse

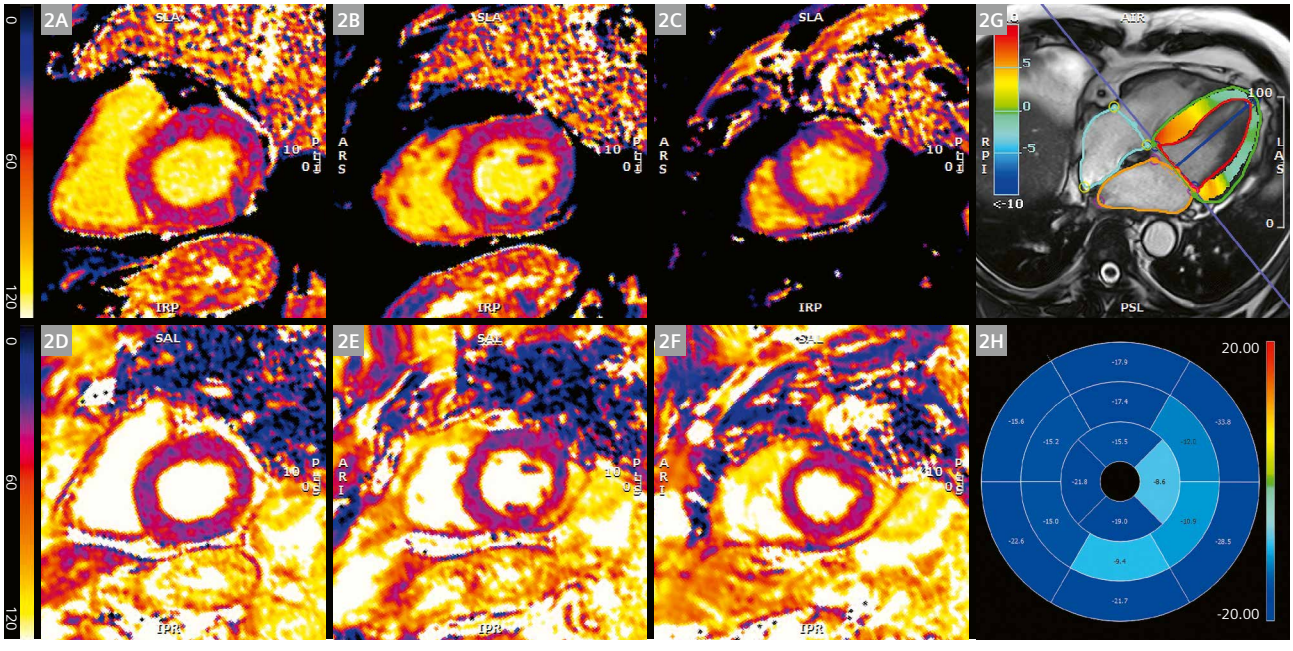

2 A 45-year-old woman with breast cancer undergoing anthracycline chemotherapy. The CMR shows diffusely increased global T1 value (1045 msec; normal value < 1031 msec; **2A–2C**), with normal global T2 value **(2D–2F)** and mildly reduced global longitudinal strain (GLS = –17%; **2G and 2H**).

myocardial fibrosis that may not be easily identified using LGE alone. Studies indicate a strong correlation between ECV measurements and histological specimens, highlighting its reliability [24]. In the acute phase, an increase in ECV may result from inflammation and interstitial edema [25]. Over time, persistently elevated ECV values are likely due to the progression of edema into interstitial fibrosis, providing crucial insights into myocardial health and the long-term effects of treatment.

Value of tracking CMR features

Subtle early tissue changes following chemotherapy can result in regional wall motion abnormalities, which can be detected using advanced cardiac magnetic resonance (CMR) strain imaging. Global longitudinal strain (GLS) is increasingly recognized as a more accurate measure of left ventricular dysfunction compared to traditional left ventricular ejection fraction assessments [26]. Several studies have shown that both GLS and global circumferential strain (GCS) are critical for identifying early signs of cardiotoxicity, particularly in patients treated with anthracyclines and trastuzumab, where reductions in GLS and GCS may occur alongside minor decreases in LVEF [27]. The assessment of deformation parameters like GLS is essential for risk stratification of cancer therapy-related cardiovascular toxicity prior to the initiation of cardiotoxic treatments. GLS and GCS are preferred over global radial strain (GRS), as they have fewer technical limitations [28]. In patients undergoing anthracycline therapy, declines in LVEF and strain values have been associated with atrophic remodeling of the myocardium resulting from oxidative damage. Significant decreases in left ventricular mass have been observed after anthracycline therapy, indicating an increased risk of cardiac events and heart failure symptoms, which may be more pronounced than the changes seen in LVEF alone [29, 30].

The financial, operational, and clinical benefits of CMR in detecting chemotherapy-induced cardiotoxicity

CMR has become an essential tool in the early detection and management of chemotherapy-induced cardiotoxicity, offering significant financial, operational, and clinical advantages. By providing precise, non-invasive, and highly accurate cardiac assessments, CMR enhances patient care while reducing healthcare costs and improving operational efficiency in oncology and cardiology settings.

The integration of CMR into routine monitoring protocols for patients undergoing potentially cardiotoxic chemotherapy can lead to substantial healthcare cost savings. By accurately identifying early signs of cardiac dysfunction, CMR enables timely interventions that may prevent progression to severe cardiotoxicity, thereby reducing the need for expensive treatments associated with advanced heart failure [31]. Moreover, the precision of CMR decreases the reliance on multiple diagnostic tests, streamlining patient care and reducing expenses.

Operationally, CMR enhances diagnostic efficiency in the oncology setting. Its comprehensive imaging capabilities allow for the simultaneous assessment of cardiac structure, function, and tissue characterization in a single session, reducing the need for multiple imaging modalities. This efficiency optimizes workflow and resource utilization within healthcare facilities. Additionally, the non-invasive nature of CMR minimizes patient discomfort and risk, facilitating smoother operational processes.

Clinically, CMR offers unparalleled accuracy in detecting subclinical myocardial changes before the onset of overt cardiac dysfunction. Advanced techniques, such as myocardial strain analysis and tissue mapping, have demonstrated high sensitivity in identifying early myocardial injury. For instance, a cohort study highlighted the clinical usefulness of CMR-based tissue characterization for cardiotoxicity assessment, emphasizing its role in early detection and improved patient outcomes [32]. Early detection through CMR facilitates prompt cardioprotective interventions, potentially reversing myocardial damage and enhancing patient prognosis [33].

In summary, the integration of CMR into the diagnostic pathway for chemotherapy-induced cardiotoxicity offers comprehensive benefits. Its ability to provide early and accurate detection not only enhances patient care, but also contributes to the financial sustainability and operational efficiency of healthcare systems.

References

1 Zamorano JL, Lancellotti P, Rodriguez Muñoz D, Aboyans V, Asteggiano R, Galderisi M, et al. 2016 ESC Position Paper on cancer treatments and cardiovascular toxicity developed under the auspices of the ESC Committee for Practice Guidelines: The Task Force for cancer treatments and cardiovascular toxicity of the European Society of Cardiology (ESC). Eur Heart J. 2016;37(36):2768–2801.

2 Lancellotti P, Suter TM, López-Fernández T, Galderisi M, Lyon AR, Van der Meer P, et al. Cardio-Oncology Services: rationale, organization, and implementation. Eur Heart J. 2019;40(22):1756–1763.

3 Plana JC, Galderisi M, Barac A, Ewer MS, Ky B, Scherrer-Crosbie M, et al. Expert consensus for multimodality imaging evaluation of adult patients during and after cancer therapy: a report from the American Society of Echocardiography and the European Association of Cardiovascular Imaging. J Am Soc Echocardiogr. 2014;27(9):911–39.

4 Burashnikov A, Abbate A, Booz GW. Cardiovascular Complications of Anticancer Therapy: A Developing Storm in Medicine. J Cardiovasc Pharmacol. 2022;80(4):491–492.

5 Lyon AR, López-Fernández T, Couch LS, Asteggiano R, Aznar MC, Bergler-Klein J, et al. 2022 ESC Guidelines on cardio-oncology developed in collaboration with the European Hematology Association (EHA), the European Society for Therapeutic Radiology and Oncology (ESTRO) and the International Cardio-Oncology Society (IC-OS). Eur Heart J. 2022;43(41):4229–4361.

6 Dempke WCM, Zielinski R, Winkler C, Silberman S, Reuther S, Priebe W. Anthracycline-induced cardiotoxicity - are we about to clear this hurdle? Eur J Cancer. 2023;185:94–104.
7 Herrmann J. Adverse cardiac effects of cancer therapies: cardiotoxicity and arrhythmia. Nat Rev Cardiol. 2020;17(8):474–502.
8 Lorente-Ros Á, Rajjoub-Al-Mahdi EA, Monteagudo Ruiz JM, Rivas García S, Ortega Pérez R, Fernández Golfín C, et al. Checkpoint Immunotherapy-Induced Myocarditis and Encephalitis Complicated with Complete AV Block: Not All Hope Is Lost. JACC Case Rep. 2022;4(16):1032–1036.
9 Shiravand Y, Khodadadi F, Kashani SMA, Hosseini-Fard SR, Hosseini S, Sadeghirad H, et al. Immune Checkpoint Inhibitors in Cancer Therapy. Curr Oncol. 2022;29(5):3044–3060.
10 Herrmann J, Yang EH, Iliescu CA, Cilingiroglu M, Charitakis K, Hakeem A, et al. Vascular Toxicities of Cancer Therapies: The Old and the New--An Evolving Avenue. Circulation. 2016;133(13):1272–89.
11 Curigliano G, Lenihan D, Fradley M, Ganatra S, Barac A, Blaes A, et al. Management of cardiac disease in cancer patients throughout oncological treatment: ESMO consensus recommendations. Ann Oncol. 2020;31(2):171–190.
12 Thavendiranathan P, Negishi T, Somerset E, Negishi K, Penicka M, Lemieux J, et al. Strain-Guided Management of Potentially Cardiotoxic Cancer Therapy. J Am Coll Cardiol. 2021;77(4):392–401.
13 Korosoglou G, Giusca S, Montenbruck M, Patel AR, Lapinskas T, Götze C, et al. Fast Strain-Encoded Cardiac Magnetic Resonance for Diagnostic Classification and Risk Stratification of Heart Failure Patients. JACC Cardiovasc Imaging. 2021;14(6):1177–1188.
14 Phillips WJ, Johnson C, Law A, Turek M, Small AR, Dent S, et al. Comparison of Framingham risk score and chest-CT identified coronary artery calcification in breast cancer patients to predict cardiovascular events. Int J Cardiol. 2019;289:138–143.
15 Lopez-Mattei J, Yang EH, Baldassarre LA, Agha A, Blankstein R, Choi AD, et al. Cardiac computed tomographic imaging in cardio-oncology: An expert consensus document of the Society of Cardiovascular Computed Tomography (SCCT). Endorsed by the International Cardio-Oncology Society (ICOS). J Cardiovasc Comput Tomogr. 2023;17(1):66–83.
16 Eschenhagen T, Force T, Ewer MS, de Keulenaer GW, Suter TM, Anker SD, et al. Cardiovascular side effects of cancer therapies: a position statement from the Heart Failure Association of the European Society of Cardiology. Eur J Heart Fail. 2011;13(1):1–10.
17 Lisi C, Catapano F, Rondi P, Figliozzi S, Lo Monaco M, Brilli F, et al. Multimodality imaging in cardio-oncology: the added value of CMR and CCTA. Br J Radiol. 2023;96(1150):20220999.
18 Bottinor W, Trankle CR, Hundley WG. The Role of Cardiovascular MRI in Cardio-Oncology. Heart Fail Clin. 2021;17(1):121–133.
19 Saunderson CED, Plein S, Manisty CH. Role of cardiovascular magnetic resonance imaging in cardio-oncology. Eur Heart J Cardiovasc Imaging. 2021;22(4):383–396.
20 O'Quinn R, Ferrari VA, Daly R, Hundley G, Baldassarre LA, Han Y, et al. Cardiac Magnetic Resonance in Cardio-Oncology: Advantages, Importance of Expediency, and Considerations to Navigate Pre-Authorization. JACC CardioOncol. 2021;3(2):191–200.
21 Park HS, Hong YJ, Han K, Kim PK, An E, Lee JY, et al. Ultrahigh-field cardiovascular magnetic resonance T1 and T2 mapping for the assessment of anthracycline-induced cardiotoxicity in rat models: validation against histopathologic changes. J Cardiovasc Magn Reson. 2021;23(1):76.
22 Messroghli DR, Moon JC, Ferreira VM, Grosse-Wortmann L, He T, Kellman P, et al. Clinical recommendations for cardiovascular magnetic resonance mapping of T1, T2, T2* and extracellular volume: A consensus statement by the Society for Cardiovascular Magnetic Resonance (SCMR) endorsed by the European Association for Cardiovascular Imaging (EACVI). J Cardiovasc Magn Reson. 2016;19(1):75.
23 Fallah-Rad N, Lytwyn M, Fang T, Kirkpatrick I, Jassal DS. Delayed contrast enhancement cardiac magnetic resonance imaging in trastuzumab induced cardiomyopathy. J Cardiovasc Magn Reson. 2008;10(1):5.
24 Armenian SH, Lacchetti C, Barac A, Carver J, Constine LS, Denduluri N, et al. Prevention and Monitoring of Cardiac Dysfunction in Survivors of Adult Cancers: American Society of Clinical Oncology Clinical Practice Guideline. J Clin Oncol. 2017;35(8):893–911.
25 Meléndez GC, Jordan JH, D'Agostino RB, Vasu S, Hamilton CA, Hundley WG. Progressive 3-Month Increase in LV Myocardial ECV After Anthracycline-Based Chemotherapy. JACC Cardiovasc Imaging. 2017;10(6):708–709.
26 Rahman ZU, Sethi P, Murtaza G, Virk HUH, Rai A, Mahmod M, et al. Feature tracking cardiac magnetic resonance imaging: A review of a novel non-invasive cardiac imaging technique. World J Cardiol. 2017;9(4):312–319.
27 Drafts BC, Twomley KM, D'Agostino R, Lawrence J, Avis N, Ellis LR, et al. Low to Moderate Dose Anthracycline-Based Chemotherapy Is Associated With Early Noninvasive Imaging Evidence of Subclinical Cardiovascular Disease. JACC Cardiovasc Imaging. 2013;6(8):877–85.
28 Jordan JH, Sukpraphrute B, Meléndez GC, Jolly MP, D'Agostino RB, Hundley WG. Early Myocardial Strain Changes During Potentially Cardiotoxic Chemotherapy May Occur as a Result of Reductions in Left Ventricular End-Diastolic Volume: The Need to Interpret Left Ventricular Strain With Volumes. Circulation. 2017;135(25):2575–2577.
29 Jordan JH, Castellino SM, Meléndez GC, Klepin HD, Ellis LR, Lamar Z, et al. Left Ventricular Mass Change After Anthracycline Chemotherapy. Circ Heart Fail. 2018;11(7):e004560.
30 Ferreira de Souza T, Quinaglia A.C. Silva T, Osorio Costa F, Shah R, Neilan TG, Velloso L, et al. Anthracycline Therapy Is Associated With Cardiomyocyte Atrophy and Preclinical Manifestations of Heart Disease. JACC Cardiovasc Imaging. 2018;11(8):1045–1055.
31 Burrage MK, Ferreira VM. The use of cardiovascular magnetic resonance as an early non-invasive biomarker for cardiotoxicity in cardio-oncology. Cardiovasc Diagn Ther. 2020;10(3):610–624.
32 Thavendiranathan P, Shalmon T, Fan CPS, Houbois C, Amir E, Thevakumaran Y, et al. Comprehensive Cardiovascular Magnetic Resonance Tissue Characterization and Cardiotoxicity in Women With Breast Cancer. JAMA Cardiol. 2023;8(6):524–534.
33 Cardinale D, Colombo A, Bacchiani G, Tedeschi I, Meroni CA, Veglia F, et al. Early detection of anthracycline cardiotoxicity and improvement with heart failure therapy. Circulation. 2015;131(22):1981–8.

Contact

Federica Brilli, M.D.
Department of Biomedical Sciences
Humanitas University
via Rita Levi Montalcini 4
20072 Pieve Emanuele
Milan
Italy
federica.brilli@humanitas.it

Application of the Arrhythmia Detection Feature to Reduce Image Artifacts in CMR of Patients with Atrial Fibrillation

Suzane Silva Lima[1], Jacqueline Kioko Nishimura Matsumoto[1], Gabriela Nicolini Carvalho[1], João Victor Santana Muslera[2], Michael Silva[2], Cesar Higa Nomura[1]

[1]Department of Diagnostic Imaging, Heart Institute (InCor), Hospital das Clínicas, University of São Paulo Medical School, São Paulo, Brazil
[2]Siemens Healthineers, São Paulo, Brazil

Introduction

The Heart Institute at Hospital das Clínicas (InCor-HCFMUSP) was officially established in 1963, with the objective of creating a center for training and technological development in cardiology in Brazil. Currently, it is internationally recognized as a leading institution in cardiovascular care, ranked as the best hospital in Latin America in the Cardiology category of the "World's Best Specialized Hospitals 2025" list [1, 2]. Cardiac magnetic resonance (CMR) is a high-complexity examination that enables functional assessment of the heart and provides essential diagnostic information, including detection of edema, myocardial perfusion, and fibrosis. The clinical workflow routinely addresses complex cases referred from healthcare units across Brazil.

Currently, we perform an average of 12 CMR studies per day on the 1.5T MAGNETOM Altea system. Although this number may appear modest, it is important to consider the high clinical complexity of patients at InCor-HCFMUSP. Many patients are hospitalized, in critical condition, and receiving continuous intravenous medications (e.g., dobutamine, norepinephrine), which means they require prolonged preparation and scan time. Moreover, patients often struggle to perform adequate breath-holds or maintain optimal positioning due to severe pain, post-surgical status, or deconditioning from prolonged hospitalization. Even outpatients, particularly elderly individuals or those with compromised respiration, may have difficulty completing the exam. These conditions pose additional challenges to the imaging team: They require a thorough understanding of available resources, and the adoption of techniques to optimize scan time and improve image quality, ultimately supporting safer and more accurate diagnosis.

Patients with arrhythmia, and the use of Arrhythmia Detection

At InCor-HCFMUSP, we frequently image patients with various arrhythmias, including atrial fibrillation (AF). Atrial fibrillation is characterized by disorganized atrial electrical activity. It is the most common sustained arrhythmia in clinical practice and affects approximately 3% of the adult population. Risk factors include advanced age, hypertension, diabetes mellitus, heart failure, and valvular disease [3]. Once electrodes are positioned on the patient's chest and the electrocardiogram (ECG) is synchronized, significant variations are observed in waves, intervals, and segments of the cardiac trace. During image acquisition, these variations directly impact image quality, causing blurring and loss of sharpness.

In this context, Siemens Healthineers developed the Arrhythmia Detection feature, which is integrated into the MAGNETOM Altea system. It allows real-time detection of RR interval variability and dynamic adaptation of the acquisition process to minimize artifacts.

1 Step-by-step activation of Arrhythmia Detection: In the Physio tab under Signal, switch Arrhythmia Detection from None to By Time. When set to By Time, the Trigger Window option appears with a default value of 200 ms. This value can remain or be adjusted to match the Target RR value captured during the cardiac cycle acquisition.

Key parameters include Average Cycle (mean RR interval based on the patient's heart rate), Trigger Window (permissible RR interval range), and Target RR (center of the permissible RR interval) [4]. For example, if the system captures an RR interval of 1,000 ms with a ± 60 ms variation, the acquisition window can extend 30 ms before and after the RR interval. With Arrhythmia Detection, this window can be further expanded, increasing the likelihood of accurate cardiac synchronization and rejection of irregular beats, thereby reducing motion artifacts.

A major challenge in severe arrhythmia is the additional time required for the system to align acquisition with the ECG signal, often necessitating prolonged breath-holds that patients may not tolerate. Free-breathing acquisitions combined with an increased number of averages can compensate for respiratory motion while maintaining cardiac synchronization, improving image quality.

The following section presents two clinical cases that illustrate the practical application of Arrhythmia Detection and demonstrate its effectiveness in obtaining high-quality images with fewer artifacts.

Case reports

Two patients with atrial fibrillation underwent CMR examinations using the same imaging protocol. Several parameter configurations were tested, and the optimal results were achieved using the Arrhythmia Detection feature combined with retrospective ECG gating and free-breathing acquisition. The resulting images demonstrated significant improvements in sharpness and myocardial contour definition and a reduction of motion artifacts when compared to acquisitions without the feature.

In both cases, while the Arrhythmia Detection feature did not completely eliminate artifacts, it produced a substantial qualitative enhancement in the diagnostic value of the images. This improvement is especially relevant for patients with persistent arrhythmia, where the ability to obtain reliable functional and structural information is often limited.

Case 1

A 55-year-old male patient with dilated cardiomyopathy, a left ventricular ejection fraction (LVEF) of 38%, and AF was referred to InCor-HCFMUSP for CMR follow-up. At the time of the exam, the patient was asymptomatic. Significant difficulty performing breath-holds was observed, and instructions were provided regarding immobility and proper breath-hold technique. The presence of AF with marked heart-rate variability resulted in relevant motion artifacts. Arrhythmia Detection was activated, with testing of multiple parameters. Optimal results were achieved with a 750 ms trigger window in breath-hold mode, and a 900 ms trigger window with four averages in free-breathing mode. Dynamic adjustment of the trigger window according to the patient's heart rate allowed acquisition of sharper images with reduced arrhythmia-related artifacts.

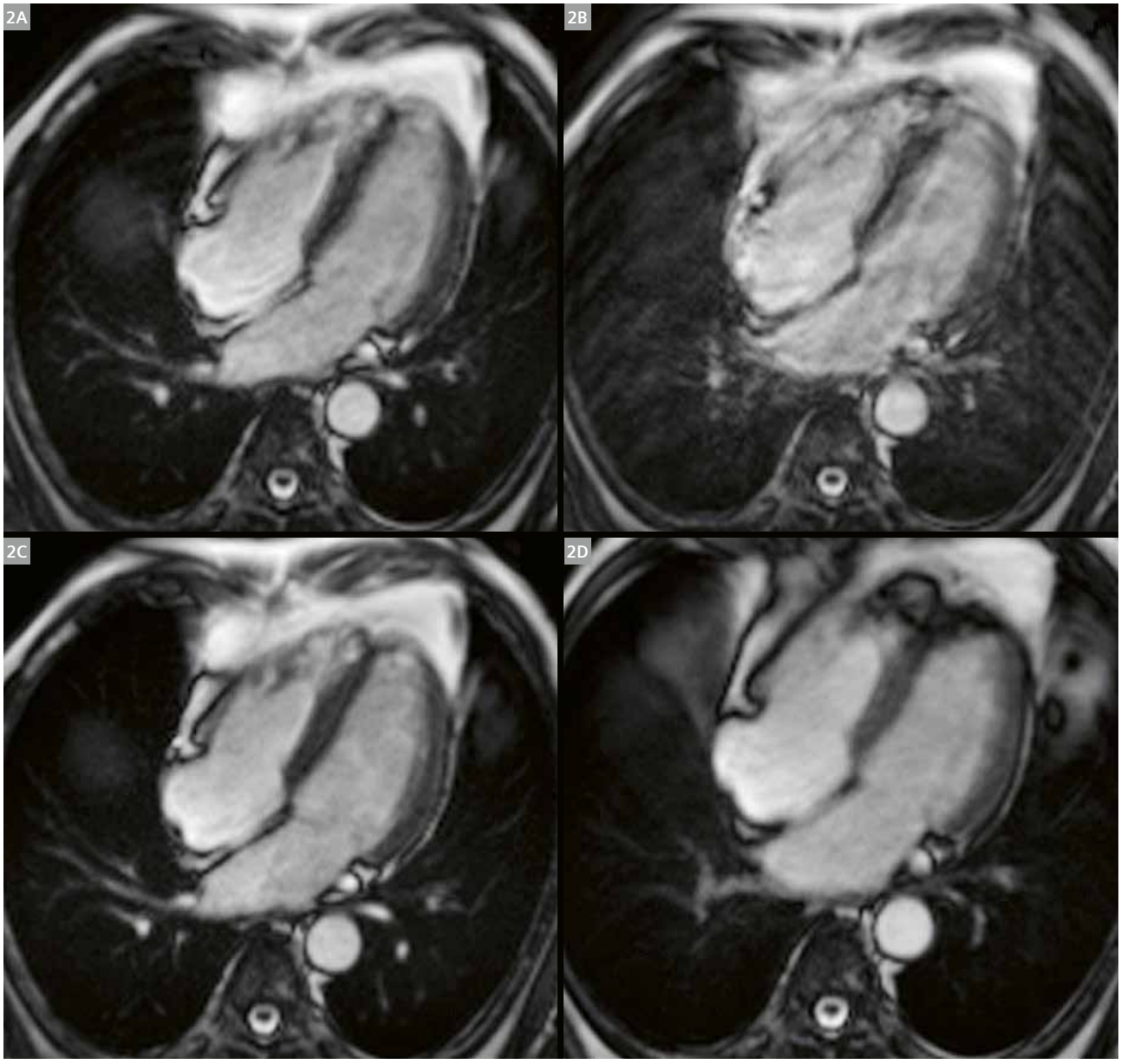

2 **(2A)** 4-chamber breath-hold sequence without Arrhythmia Detection; **(2B)** 4-chamber breath-hold sequence with Arrhythmia Detection and 200 ms increased trigger window; **(2C)** 4-chamber breath-hold sequence with Arrhythmia Detection and 750 ms increased trigger window; **(2D)** 4-chamber free-breathing sequence with four averages and 900 ms increased trigger window.

Case 2

A 59-year-old male patient with ischemic cardiomyopathy, a LVEF of 24%, permanent AF for 10 years, and a history of myocardial infarction in 2013 and 2018 was referred for CMR to assess cardiac function and detect myocardial fibrosis. Due to permanent AF and inability to perform breath-holds, Arrhythmia Detection was employed. Acquisition tests with and without breath-holds were performed using a 600 ms trigger window. Free-breathing acquisition with four averages and dynamic adjustment of the trigger window according to the heart rate enabled improved image quality, reduced arrhythmia-related artifacts, and optimized functional and tissue characterization.

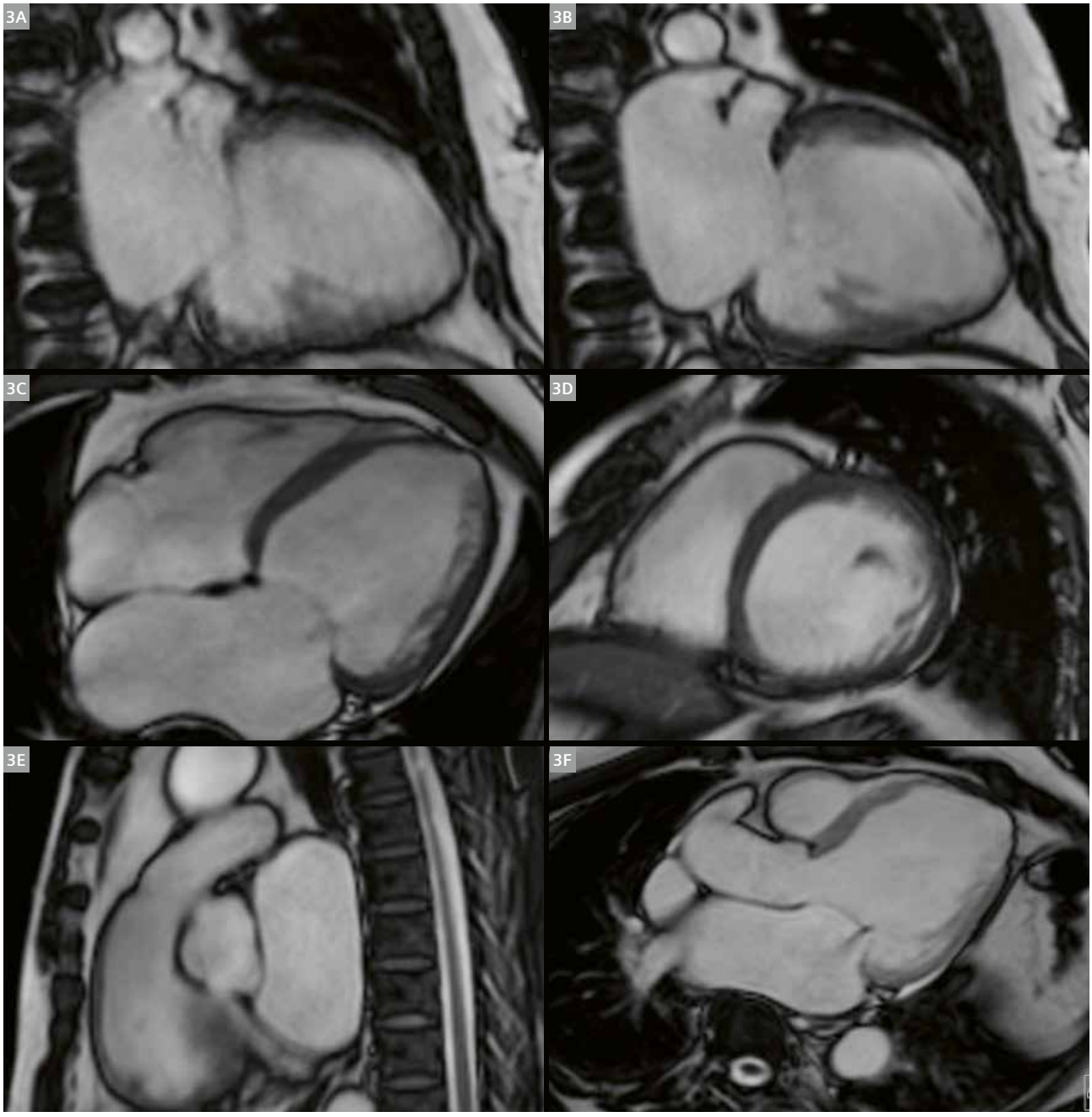

3 **(3A)** 2-chamber breath-hold sequence with 600 ms increased trigger window; **(3B)** 2-chamber free-breathing sequence with four averages and 600 ms trigger window; **(3C)** 4-chamber free-breathing sequence with four averages and 600 ms trigger window; **(3D)** short-axis free-breathing sequence with four averages and 600 ms trigger window; **(3E)** RVOT free-breathing sequence with four averages and 600 ms trigger window; **(3F)** LVOT free-breathing sequence with four averages and 700 ms trigger window.

Conclusion

The integration of advanced features such as Arrhythmia Detection into modern MRI platforms provides radiology teams with greater control over acquisition parameters, allowing effective management of cardiac rhythm irregularities and significantly reducing motion artifacts. These resources directly contribute to improved diagnostic confidence and patient safety, while optimizing workflow efficiency. Ongoing professional training and technical expertise remain fundamental to maximizing the potential of these technologies and ensuring high-quality CMR examinations.

References

1 InCor-HCFMUSP. History. [Internet]. São Paulo, Brazil: InCor-HCFMUSP. 2024 [cited 2025 Sep 2]. Available from: https://www2.incor.usp.br/sites/incor2024/historia.
2 InCor-HCFMUSP. News. [Internet]. São Paulo, Brazil: InCor-HCFMUSP. 2024. [cited 2025 Sep 9]. Available from: https://www2.incor.usp.br/sites/incor2024/noticia/incor-o-melhor-hospital-especializado-em-cardiologia-e-cirurgia-cardiovascular-da-america-latina.
3 Cintra FD, Figueiredo MJO. Atrial Fibrillation (Part 1): Pathophysiology, Risk Factors, and Therapeutic Basis. Arq Bras Cardiol. 2021;116(1):129–139. English, Portuguese.
4 Siemens Healthineers. ECG Heart Trigger Online Training. [Internet]. Malvern, PA, USA: Siemens Medical Solutions USA Inc. [cited 2025 Sep 11]. Available from: ↗ https://pep.siemens-info.com/launch/course/pt-br/disparo-cardiaco-ecg-treinamento-online.

Contact

Suzane Silva Lima
Biomedical Imaging Scientist
Heart Institute (InCor-HCFMUSP)
Av. Dr. Enéas de Carvalho Aguiar, 44 (subsolo)
Cerqueira César
São Paulo – SP, 05403-000
Brazil
suzane.lima@hc.fm.usp.br

João Victor Santana Muslera
MRI Clinical Application Specialist
Siemens Healthineers LAM
joaovictorsantana.muslera@siemens-healthineers.com

Unlocking the Heart's Microstructure: Cardiac Diffusion MRI with Ultra-Strong Gradients

Maryam Afzali, Ph.D.[1,2,3]; Lars Mueller, Ph.D.[1]; Sam Coveney, Ph.D.[1]; Fabrizio Fasano, Ph.D.[4,5]; Filip Szczepankiewicz, Ph.D.[6]; Derek K Jones, Ph.D.[2]; Jürgen E Schneider, Ph.D.[1]

[1]Biomedical Imaging Science Department, Leeds Institute of Cardiovascular and Metabolic Medicine, University of Leeds, Leeds, UK
[2]Cardiff University Brain Research Imaging Centre (CUBRIC), School of Psychology, Cardiff University, Cardiff, UK
[3]Division of Cardiovascular Sciences, College of Life Sciences, University of Leicester, the National Institute for Health Research Leicester Biomedical Research Centre and British Heart Foundation Leicester Centre of Research Excellence, Glenfield Hospital, Leicester, UK
[4]Siemens Healthcare Ltd, Camberley, UK
[5]Siemens Healthineers, Erlangen, Germany
[6]Department of Medical Radiation Physics, Lund University, Lund, Sweden

Abstract

Diffusion MRI of the human heart provides unique insight into myocardial microstructure but has been hampered by cardiac and respiratory motion, short T2 of the heart muscle, and limited gradient strength. Recent advances in ultra-strong gradient technology not only help to overcome these technical challenges but also allow higher diffusion weighting (i.e., b-values) with clinically compatible echo times. Our recent studies demonstrate how this enabled in vivo diffusion kurtosis imaging (DKI) and q-space trajectory imaging (QTI) in the beating human heart, therefore moving beyond the Gaussian assumptions of diffusion tensor imaging (DTI). These advances may pave the way for more sensitive biomarkers of pathological changes of the myocardium and bring microstructural imaging closer to clinical application.

Key points

- Ultra-strong gradients (300 mT/m) make cardiac diffusion MRI feasible at higher b-values.
- In vivo cardiac diffusion kurtosis imaging and q-space trajectory imaging (QTI) were demonstrated with clinically compatible echo times.
- Kurtosis and QTI metrics reveal non-Gaussian diffusion, offering access to new imaging biomarkers of myocardial microstructure.
- Translation to clinical systems is within reach with new 200 mT/m gradient scanners.

Clinical motivation: The unmet need for microstructural cardiac imaging

Cardiovascular disease remains one of the leading causes of death worldwide [1]. While conventional cardiac MRI has revolutionized non-invasive assessment of cardiac anatomy, function, perfusion, and viability, it offers only indirect surrogates of myocardial microstructure [2]. Yet microstructural remodeling – including cardiomyocyte disarray, hypertrophy, fibrosis, and altered cellularity – underpins the pathogenesis of cardiomyopathies, ischemic injury, heart failure, and arrhythmias [3].

Histology provides exquisite microstructural information but is invasive, destructive, and limited to the biopsied region. Clinicians have long sought a "virtual biopsy" tool that could provide microstructural insights non-invasively and reproducibly [4]. Diffusion MRI offers precisely this promise, with sensitivity to water motion at the cellular scale [5]. However, its potential has remained largely unrealized in the heart, where motion, limited gradient performance, and low signal-to-noise ratio (SNR) have posed formidable barriers [6].

Why standard diffusion MRI falls short in the heart

T2 in the brain tissue is about 69 ms in white matter and around 99 ms in gray matter [8] (using a 3T MRI system). T2 in the heart muscle (i.e., myocardium) is ~46 ms at 3T [7], which is about two-thirds to half of the values found

in the brain. It is therefore important to achieve shorter echo times in cardiac imaging compared to brain imaging. In addition, motion-compensated diffusion gradient waveforms are needed for cardiac diffusion-weighted MRI (due to the motion of heart), which adds to the required echo time. Finally, mean diffusivity in the myocardium (~1.5 μm²/ms) [9] is higher than in brain tissue (0.93 μm²/ms in white matter [10, 11]), which causes higher signal attenuation in the heart compared to the brain for the same b-value, and hence puts further constraints on the SNR. Therefore, short TE are essential for the successful application of cardiac diffusion MRI techniques, which in turn require higher gradient performance.

Ultra-strong gradients: A step-change for diffusion encoding

The advent of ultra-strong gradient systems, such as the 3T MAGNETOM Connectom[1] system equipped with a 300 mT/m gradient coil, has transformed what is experimentally possible. By enabling higher b-values at shorter echo times, these systems provide a new window into tissue microstructure. Originally developed for brain imaging, the MAGNETOM Connectom has subsequently become a unique platform for translational "below-the-neck" research, including the heart.

In our recent studies, we leveraged the capability of the MAGNETOM Connectom MR system to push the boundaries of cardiac diffusion MRI. We performed, for the first time, in vivo cardiac diffusion tensor imaging (DTI) on the MAGNETOM Connectom, which enabled higher b-value and higher-order motion compensation (up to third order; diffusion gradient waveforms were designed using the NOW toolbox [12, 13], see Fig. 1) [11] with an echo time comparable to what is commonly used on clinical scanners (such as the 3T MAGNETOM Prisma) for cardiac DTI. Diffusion-weighted imaging was performed with a prototype pulse sequence[2] that enabled diffusion encoding with user-defined gradient waveforms [14, 15]. This work already hinted at non-Gaussian behavior and potentially time-dependent diffusion effects [16], and showed that the myocardium can be probed more deeply and specifically than ever before. It also demonstrated that strong gradients do not merely "improve" existing methods, but also unlock qualitatively new experimental spaces.

Building on this foundation [16], our 2025 *Magnetic Resonance in Medicine* paper [17] reported the first successful implementation of diffusion kurtosis imaging (DKI) in the human heart. DKI extends beyond the Gaussian assumption of DTI, quantifying how water diffusion deviates from it due to microstructural heterogeneity.

We acquired multi-shell diffusion data in healthy volunteers using 300 mT/m gradients, fitted a DKI model, and obtained parametric maps of mean, axial, and radial kurtosis (see Fig. 2). These maps revealed measurable non-Gaussian behavior in the myocardium, consistent with the tissue's known complexity.

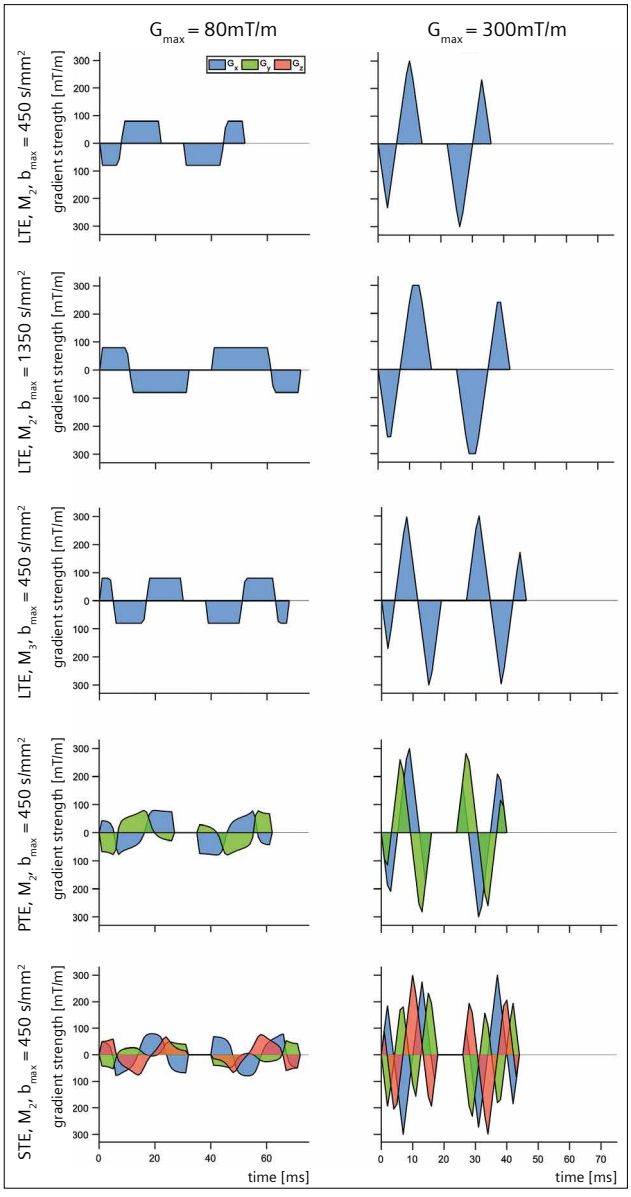

1 Gradient performance comparison. Schematic showing the difference between 80 mT/m and 300 mT/m gradient strength for different b-values, motion compensation order, and encoding schemes (LTE, PTE, STE).

[1] *MAGNETOM Connectom is ongoing research. All data shown are acquired using a non-commercial system under institutional review board permission. Siemens Healthineers does not intend to commercialize the system.*

[2] *Work in progress. The application is currently under development and is not for sale in the U.S. and in other countries. Its future availability cannot be ensured.*

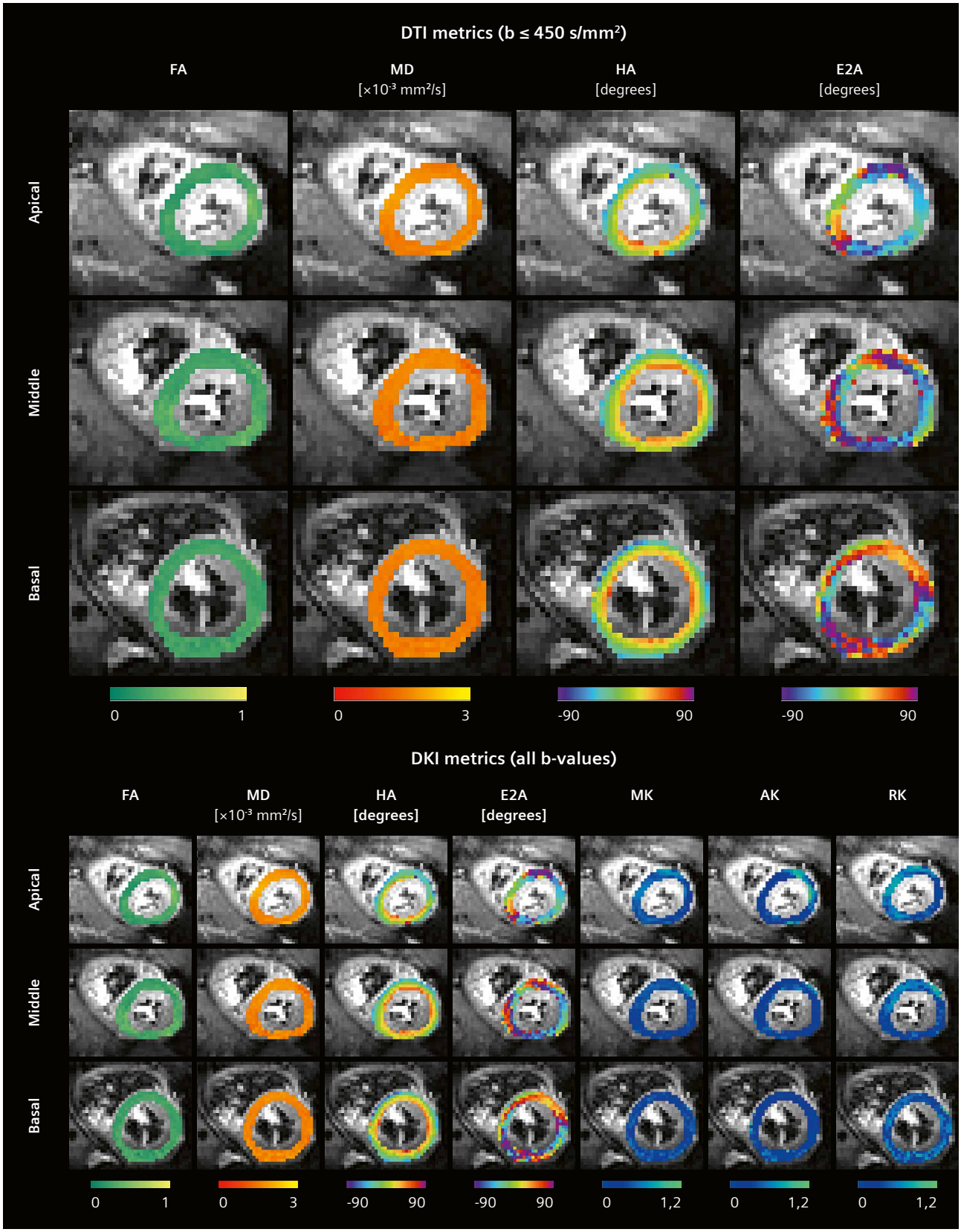

2 Example fractional anisotropy (FA), mean diffusivity (MD), helix angle (HA), and secondary eigenvector angle (E2A) maps using cardiac diffusion tensor imaging and mean, axial, and radial kurtosis maps (MK, AK, RK) using cardiac diffusion kurtosis imaging.

Together, these results provide a new set of imaging biomarkers for characterizing myocardial tissue – potentially sensitive to disease processes such as hypertrophy, fibrosis, and microstructural disarray.

Probing complex microstructure

Q-space trajectory imaging (QTI) represents a paradigm shift in (cardiac) diffusion MRI [16]. Unlike conventional DTI or DKI, which sample diffusion along a single encoding direction at a time (linear tensor encoding (LTE)), QTI explores diffusion along continuous or arbitrarily shaped trajectories in q-space, allowing direct estimation of higher-order diffusion moments and compartment-specific properties [18]. QTI can capture features such as microscopic anisotropy, isotropic and anisotropic kurtosis, heterogeneity, and orientation dispersion, providing a rich description of myocardial microstructure that is inaccessible with lower-order models.

Using an ultra-strong gradient system, we were able to acquire cardiac diffusion weighted images using advanced diffusion encoding schemes such as planar tensor encoding (PTE) and spherical tensor encoding (STE). These enable the quantification of microstructural features of the tissue such as microscopic anisotropy and isotropic and anisotropic kurtosis [19] (see Fig. 3).

Bridging to clinical translation

While the MAGNETOM Connectom system is unique (there are only four scanners of this kind worldwide), its insights are not destined to remain restricted to these highly specialized scanners. The emergence of new clinical systems with significantly improved gradient performance, such as the 3T MAGNETOM Cima.X system equipped with a 200 mT/m gradient coil, brings these advances closer to patients.

The implications could be profound:

- Microstructural biomarkers such as kurtosis could enrich clinical MRI protocols for cardiomyopathies and heart failure.
- Higher b-value DTI may improve sensitivity to remodeling processes, better guide therapies, and benefit prognosis.
- Motion-compensated encoding and novel readouts (e.g., spiral) should allow integration into clinically feasible scan times.

By demonstrating feasibility at the high gradient strengths, our work provides a roadmap for translating cardiac microstructural imaging to the new generation of clinical scanners.

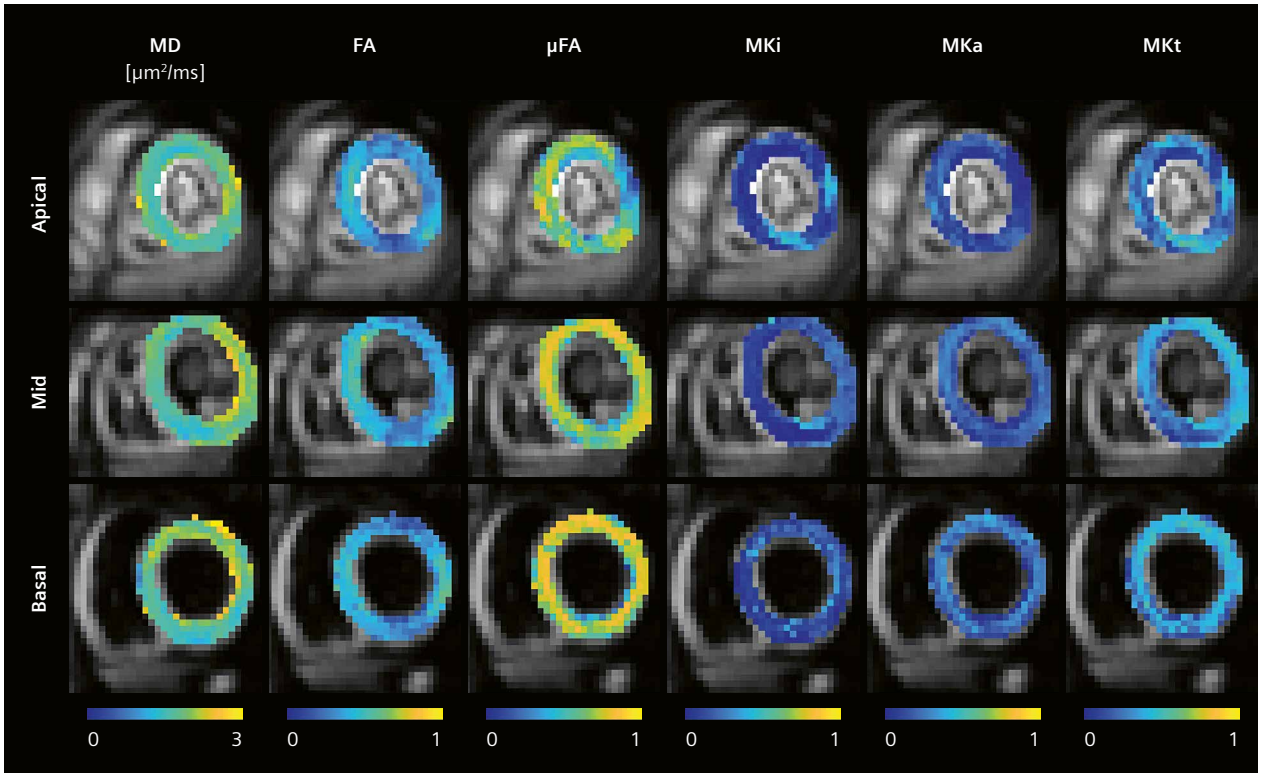

3 Example q-space trajectory imaging (QTI) metrics, microscopic fractional anisotropy (μFA), and isotropic (MKi), anisotropic (MKa), and total mean kurtosis (MKt).

Towards a virtual microscope for the heart

The ability to non-invasively probe myocardial microstructure represents a paradigm shift for cardiovascular imaging. With ultra-strong gradients, cardiac diffusion MRI is evolving from an experimental tool into a powerful research and diagnostic tool.

Future directions may include:

- Extending cardiac diffusion kurtosis imaging to patient populations with hypertrophic and dilated cardiomyopathy, ischemic heart disease, and arrhythmogenic disorders.
- Combining diffusion with relaxation dimensions, creating multidimensional "fingerprints" of cardiac tissue.
- Developing robust, motion-compensated sequences and advanced reconstruction strategies.
- Standardizing acquisition and analysis across centers, paving the way for multi-site clinical studies.

In essence, we are moving closer to a "virtual microscope" for the heart – a tool that could reveal the tissue-level signatures of disease, guide personalized treatment, and reduce reliance on invasive biopsies.

This research was funded by the Wellcome Trust Investigator Award (219536/Z/19/Z).

References

1 Lindstrom M, DeCleene N, Dorsey H, Fuster V, Johnson CO, LeGrand KE, et al. Global Burden of Cardiovascular Diseases and Risks Collaboration, 1990-2021. J Am Coll Cardiol. 2022;80(25):2372–2425.

2 Simkowski J, Eck B, Wilson Tang WH, Nguyen C, Kwon DH. Next-Generation Cardiac Magnetic Resonance Imaging Techniques for Characterization of Myocardial Disease. Curr Treat Options Cardiovasc Med. 2024;26(8):243–254.

3 Ashkir Z, Samat AHA, Ariga R, Finnigan LEM, Jermy S, Akhtar MA, et al. Myocardial disarray and fibrosis across hypertrophic cardiomyopathy stages associate with ECG markers of arrhythmic risk. Eur Heart J Cardiovasc Imaging. 2025;26(2):218–228.

4 Jelescu IO, Palombo M, Bagnato F, Schilling KG. Challenges for biophysical modeling of microstructure. J Neurosci Methods. 2020;344:108861.

5 Basser PJ, Pierpaoli C. Microstructural and physiological features of tissues elucidated by quantitative-diffusion-tensor MRI. 1996. J Magn Reson. 2011;213(2):560–70.

6 Gamper U, Boesiger P, Kozerke S. Diffusion imaging of the in vivo heart using spin echoes--considerations on bulk motion sensitivity. Magn Reson Med. 2007;57(2):331–7.

7 Hanson CA, Kamath A, Gottbrecht M, Ibrahim S, Salerno M. T2 Relaxation Times at Cardiac MRI in Healthy Adults: A Systematic Review and Meta-Analysis. Radiology. 2020;297(2):344–351.

8 Stanisz GJ, Odrobina EE, Pun J, Escaravage M, Graham SJ, Bronskill MJ, et al. T1, T2 relaxation and magnetization transfer in tissue at 3T. Magn Reson Med. 2005;54(3):507–12.

9 Nguyen C, Fan Z, Sharif B, He Y, Dharmakumar R, Berman DS, et al. In vivo three-dimensional high resolution cardiac diffusion-weighted MRI: A motion compensated diffusion-prepared balanced steady-state free precession approach. Magn Reson Med. 2014;72(5):1257–67.

10 Cercignani M, Inglese M, Pagani E, Comi G, Filippi M. Mean diffusivity and fractional anisotropy histograms of patients with multiple sclerosis. AJNR Am J Neuroradiol. 2001;22(5):952–8.

11 Afzali M, Mueller L, Coveney S, Fasano F, Evans CJ, Engel M, et al. In vivo diffusion MRI of the human heart using a 300 mT/m gradient system. Magn Reson Med. 2024;92(3):1022–1034.

12 Sjölund J, Szczepankiewicz F, Nilsson M, Topgaard D, Westin CF, Knutsson H. Constrained optimization of gradient waveforms for generalized diffusion encoding. J Magn Reson. 2015;261:157–68.

13 Szczepankiewicz F, Sjölund J, Dall'Armellina E, Plein S, Schneider JE, Teh I, et al. Motion-compensated gradient waveforms for tensor-valued diffusion encoding by constrained numerical optimization. Magn Reson Med. 2021;85(4):2117–2126.

14 Szczepankiewicz F, Sjölund J, Ståhlberg F, Lätt J, Nilsson M. Tensor-valued diffusion encoding for diffusional variance decomposition (DIVIDE): Technical feasibility in clinical MRI systems. PLoS One. 2019;14(3):e0214238.

15 Mueller L, Afzali M, Coveney S, Doring A, Fasano F, Evans J, et al. ZOOM and enhance: Zonally magnified Oblique Multi-slice for cardiac DTI with ultra-strong gradients. Proc Intl Soc Mag Reson Med. 2024:1269.

16 Teh I, Shelley D, Boyle JH, Zhou F, Poenar AM, Sharrack N, et al. Cardiac q-space trajectory imaging by motion-compensated tensor-valued diffusion encoding in human heart in vivo. Magn Reson Med. 2023;90(1):150–165.

17 Afzali M, Coveney S, Mueller L, Jones S, Fasano F, Evans CJ, et al. Cardiac diffusion kurtosis imaging in the human heart in vivo using 300 mT/m gradients. Magn Reson Med. 2025;94(5):2100–2112.

18 Westin CF, Knutsson H, Pasternak O, Szczepankiewicz F, Özarslan E, van Westen D, et al. Q-space trajectory imaging for multidimensional diffusion MRI of the human brain. Neuroimage. 2016;135:345–62.

19 Afzali M, Mueller L, Coveney S, Jones S, Evans J, Fasano F, et al. Quantifying microscopic anisotropy in the human heart in vivo using ultra-strong gradients. Proc Intl Soc Mag Reson Med. 2024:1267.

Contact

Maryam Afzali, Ph.D.
Lecturer
Division of Cardiovascular Sciences
University of Leicester
Glenfield Hospital, Groby Road,
Leicester, LE39QP
United Kingdom
mad37@leicester.ac.uk

Jürgen E Schneider, Professor
Leeds Institute of Cardiovascular and Metabolic Medicine
University of Leeds
Clarendon Way
Leeds, LS2 9JT
United Kingdom
J.E.Schneider@leeds.ac.uk

The Role of Cardiac Magnetic Resonance Imaging in Valvular Heart Disease

Nikoo Aziminia; Jonathan Bennett; Iain Pierce; George D Thornton; Thomas A Treibel

Institute of Cardiovascular Science, University College London, London, UK
Barts Heart Centre, St. Bartholomew's Hospital, Barts Health, London, UK

Background

Valvular heart disease (VHD) is increasing in prevalence, affecting up to 50% of the population aged over 65 [1]. Echocardiography is the first-line imaging test in VHD, for surveillance and assessment of valve anatomy for pre-procedural planning. Cardiac computed tomography (CT) has also become essential in planning transcatheter interventions. However, cardiovascular magnetic resonance (CMR) provides a comprehensive assessment of the valve morphology, lesion severity, ventricular remodelling, and extracardiac abnormalities such as aortopathy (Figure 1). This review explores the value of CMR in the assessment of VHD.

Why CMR in VHD?

CMR is the gold standard for quantifying ventricular size and function with high reproducibility, which is critical for surveillance, particularly of regurgitant lesions [2]. ...

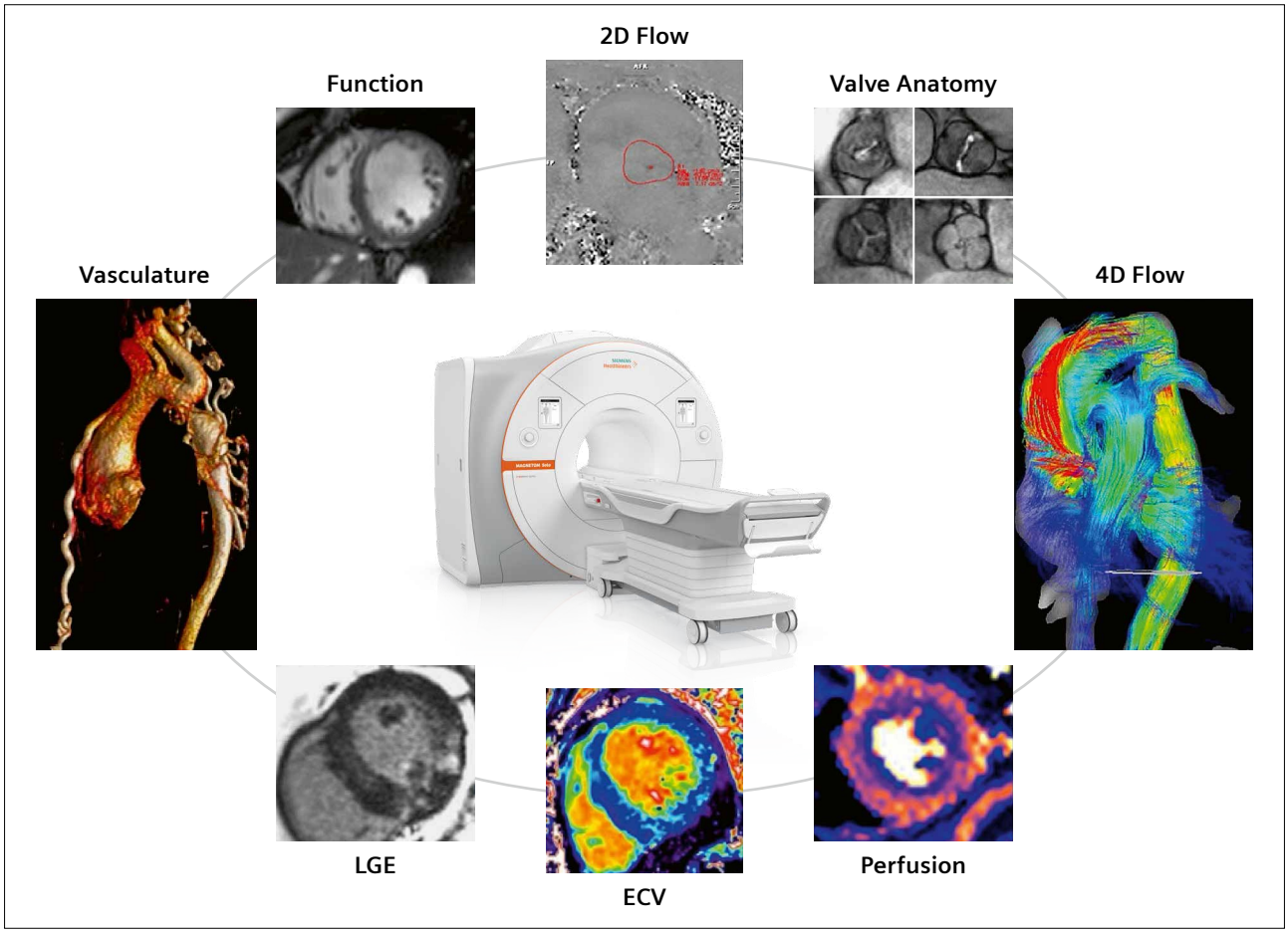

1 Cardiovascular magnetic resonance imaging in valve disease.

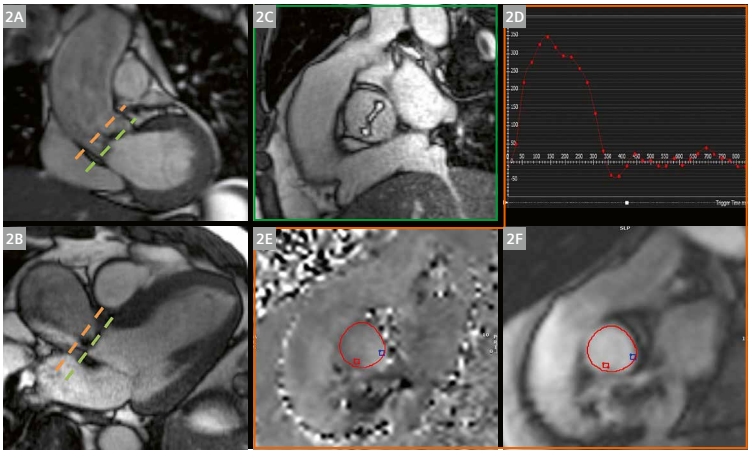

2 *Valve characterization of aortic stenosis.* VLA images of the AoV **(2A, 2B)** are used to plan the aortic valve cine MRI stack to assess valve morphology (green line; **2C** demonstrating bicuspid AS) and through-plane phase contrast velocity mapping (orange line; **2D–2F** demonstrating the velocity flow chart, phase and magnitude images respectively).

			TEE	CT
			++	++
			+	++
			–	+++
			None	Iodine
			-dependent	+++
			++	+++
			+++	+
			++	++*
Valvular flow quantification	+++	++	++	–
Tissue characterization	+++	–	–	+/++**

Table 1: Comparison of cardiac imaging modalities used to assess VHD.
*If functional dataset acquired.
**If late-enhancement images required, or ECV protocol performed.

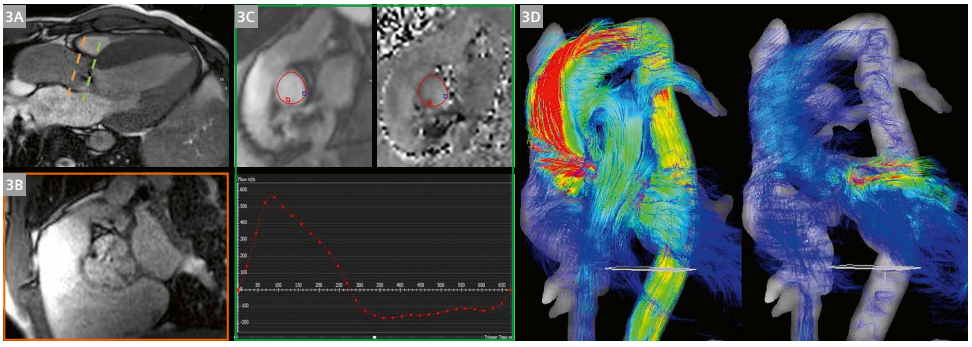

3 *Valve characterization of aortic regurgitation.* VLA images of the AoV **(3A)** are similarly used to plan the aortic valve cine MRI stack for valve morphology (green line, **3B** demonstrating tricuspid AV with central AR); through-plane phase contrast velocity mapping (orange line; **3C** demonstrating severe AR with holodiastolic flow reversal); and **(3D)** 4-dimensional flow to assess complex flow patterns in systole and diastole.

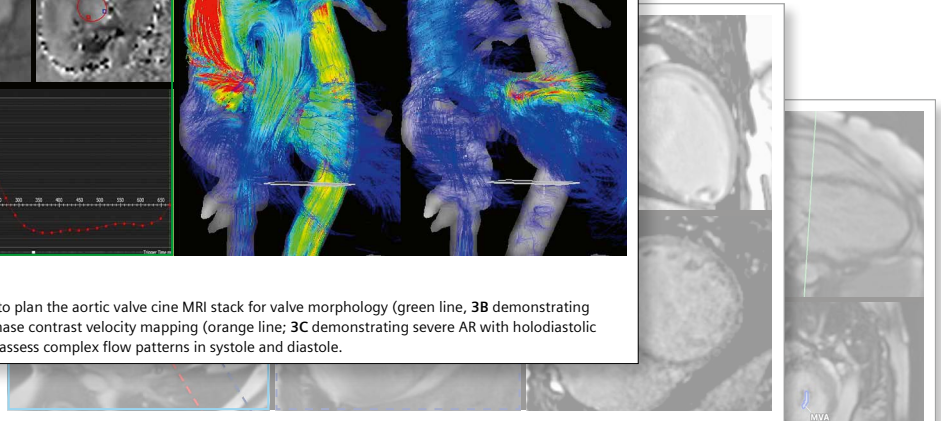

4 *Mitral regurgitation assessment by CMR.* Non-ischemic dilated cardiomyopathy. **(4A)** Dilated LV cavity with severe function regurgitation in to a severely dilated left atrium, **(4B)** Tented mitral valve; **(4C)** Short axis view of the mitral valve showing the regurgitant orifice area; **(4D)** Short axis of the dilated LV and RV; **(4E)** Two-chamber view of the LV early post gadolinium contrast injection showing an apical LV thrombus; **(4F)** Late gadolinium image in the mid short axis demonstrating septal mid-wall enhancement.

to plan a short-axis cine MRI for direct planimetry of the mitral valve **(5D)**, demonstrating severe mitral stenosis with a mitral valve orifice area of 0.8 cm².

Continue reading at:
magnetomworld.siemens-healthineers.com

Cardiovascular Applications of Photon-Counting CT: When Cardiac CT Meets Cardiac MR

Adrien De Minteguiaga, M.D.; Benjamin Longère, M.D., Ph.D.; Christos Gkizas, M.D., Ph.D.; Aimée Rodriguez Musso, M.D.; Mehdi Haidar, M.D.; François Pontana, M.D., Ph.D.

CHU Lille, Department of Cardiothoracic Radiology, Lille, France

Background

Cardiac magnetic resonance imaging (CMR) is now well established as the reference non-invasive modality for the assessment of heart diseases, particularly owing to its ability to characterize the myocardium [1]. Nevertheless, CMR suffers from an extensive acquisition time that may be difficult to handle for patients with cardiac conditions. In clinical routine it typically relies on two-dimensional 5–8 mm thick slices with interslice gaps of up to 20%. Computed tomography (CT) has recently undergone a paradigm shift in detector technology with the advent of photon-counting detectors [2]. With the NAEOTOM Alpha family (Siemens Healthineers, Forchheim, Germany) a photon-counting CT (PCCT) CT generation is made available. Early evaluations of this new generation of detectors have opened the way to PCCT-based myocardial tissue characterization and functional imaging, providing information comparable to that obtained with CMR.

Photon-counting technology

Limitations of energy-integrating detectors

Conventional CT systems are equipped with energy-integrating detectors (EIDs), which indirectly convert X-rays into an electrical signal. In this process, incoming X-rays are first converted into visible light within a scintillator, with light intensity proportional to the X-ray energy. The emitted light is then converted into an electrical signal by a photodiode, with signal intensity proportional to the amount of visible light. To prevent optical crosstalk between adjacent detector elements, blind septa must be interposed, which limits the achievable in-plane spatial resolution and/or reduces the effective surface, especially for very fine pixelations. This indirect detection chain is also prone to increased electronic noise at low X-ray energies, and the resulting electrical signal represents an integrated sum of the entire detected X-ray spectrum over the projection time measurement [3].

Benefits of photon-counting detectors

By contrast, photon-counting detectors (PCDs) directly convert X-ray photons into electrical signals using semiconductor technology. Each incoming photon deposits its energy into the semiconductor, ejecting an electron that is attracted to a pixelated anode under a strong electric field. This generates an electrical pulse, the amplitude of which is proportional to the photon's energy.

Improved spatial resolution: The pixelated anode design eliminates the need for blind septa, thereby enhancing the intrinsic in-plane spatial resolution. Each anode pixel can be subdivided into smaller sub-elements that can be individually processed to achieve ultra-high in-plane resolution. Every photon interaction is individually detected and processed according to its energy, which constitutes the core of the photon-counting principle [4].

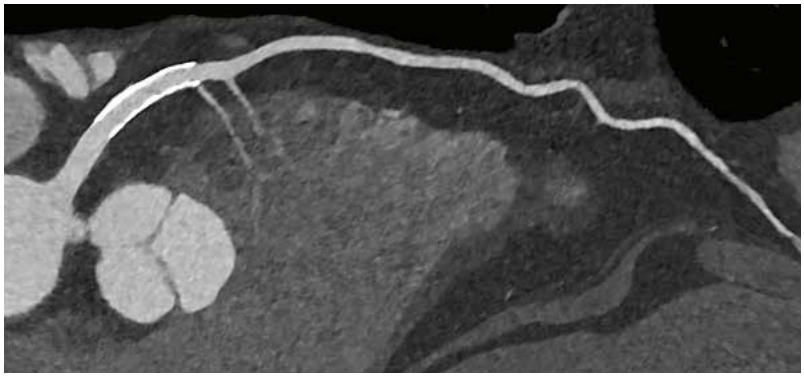

1 Stent patency assessment in a 73-year-old man. Ultra-high-resolution coronary CT angiography ($0.11 \times 0.11 \times 0.2$ mm^3; Bv56 kernel; 768×768 matrix) of the left anterior descending artery. Stent patency is clearly assessed without blooming artifacts. Note the good delineation of two septal branches.

Noise reduction: During signal processing, energy thresholds are applied to exclude electronic noise through a binning process. In contrast to an EID detector system, PCD's can filter out unwarranted/non-event-related signals. This is also one of the reasons why PCCT systems are superior to EID systems in terms of radiation-dose efficiency.

Spectral data without compromising temporal resolution: Additional higher-energy thresholds can be applied to create multiple energy bins, classifying detected photons according to their energy level. For clinical applications, data from higher and lower energies are required. Therefore, during further data management, two bins representing these energy levels are generated and used for further image reconstruction/data analysis. In dual-source dual-energy CT acquisitions, spectral separation is achieved by applying two different mean energies with the spectrum emitted from the X-ray tube (e.g., a tube voltage of 70 kVp and Sn140 kVp), which reduces the in-plane temporal resolution. By contrast, PCCT intrinsically achieves spectral decomposition at the detector level. Consequently, both tube-detector pairs contribute to spectral data acquisition, preserving high temporal resolution without sacrificing spectral information.

Coronary artery disease

Coronary CT angiography is now well established as the first line imaging modality for patients with symptoms suggestive of chronic obstructive coronary artery disease [5]. However, functional testing is generally preferred over anatomical assessment in patients with coronary stents. The ultra-high spatial resolution provided by PCCT enables substantial improvements in diagnostic confidence in assessing coronary stent patency (Fig. 1, Fig. 2) as well as in patients with high calcified plaque burden [6]. PCCT has also shown to reduce beam-hardening artifacts.

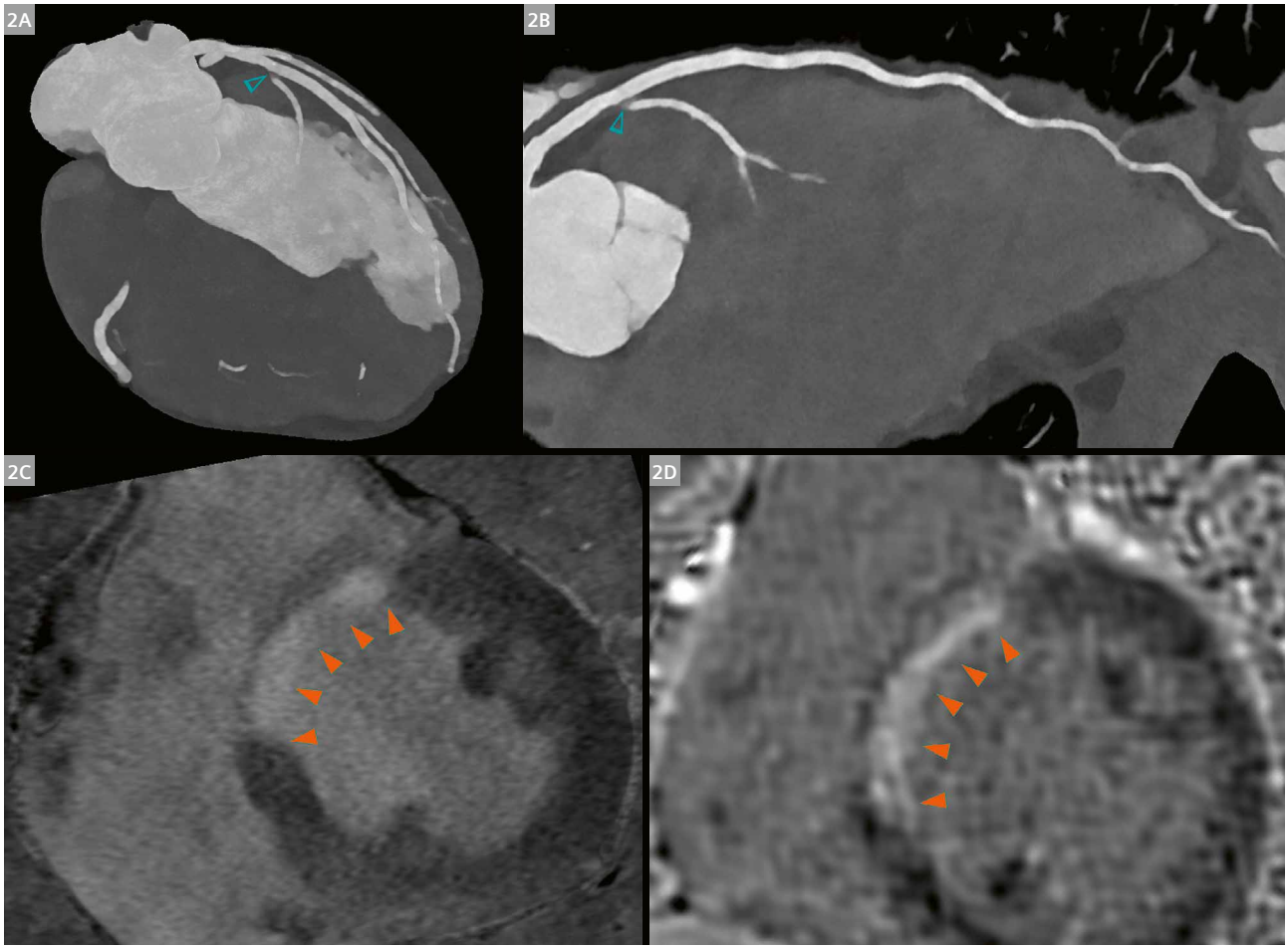

2 34-year-old male patient with a history of drug use, referred for suspected acute myocarditis in the context of viral infection. **(2A, 2B)** Maximum intensity projection reconstructions showing ostial stenosis of the first septal branch arising from the left anterior descending artery (hollow arrowhead), likely related to cocaine-induced vasospasm. **(2C)** Iodine map reconstruction from the photon-counting CT-MDE acquisition and **(2D)** late gadolinium enhancement CMR image showing subendocardial enhancement of the mid-anterior septal wall (solid arrowheads).

Beyond volumetric measurements, the main historical advantage of CMR lies in its ability to detect and quantify myocardial fibrosis through late gadolinium enhancement (LGE), which has demonstrated strong prognostic value in the management of myocardial infarction [7, 8]. The feasibility of CT-based myocardial delayed enhancement (CT-MDE) has also been established using conventional EID systems, with reported radiation doses ranging from 0.5–7 mSv for polychromatic acquisitions, and from 2.2–4.7 mSv for dual-energy acquisitions. However, low-dose polychromatic protocols have shown limited image quality, particularly in larger patients [9]. Using spectral reconstructions such as low-energy monoenergetic imaging or iodine maps, PCCT improves the depiction of myocardial infarction on CT myocardial delayed enhancement (MDE) images (Fig. 2), while achieving approximately 1 mSv for full three-dimensional cardiac coverage [10, 11].

However, the hemodynamic significance of an obstructive coronary artery lesion cannot be determined from anatomical findings alone, as up to half of anatomically obstructive plaques show no lesion-specific ischemia on downstream functional testing [12]. Stress CT myocardial perfusion imaging has been shown to improve the specificity of coronary CT angiography [13]. The feasibility of PCCT-based myocardial perfusion imaging has recently been demonstrated (Fig. 3), with excellent diagnostic accuracy compared with functional reference standards such as stress CMR [14].

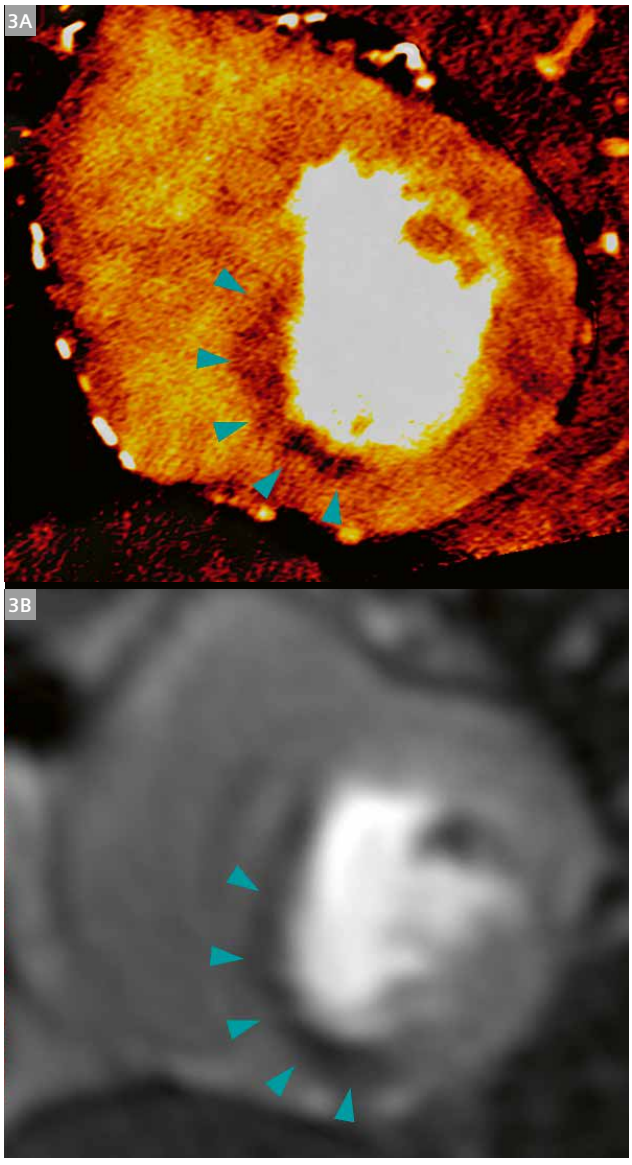

3 55-year-old female patient with a history of coronary artery bypass graft and new-onset exertional chest pain. **(3A)** Stress photon-counting CT myocardial perfusion imaging showing a subendocardial perfusion defect in the mid-inferior septal wall (arrowheads). **(3B)** Corresponding perfusion defect confirmed on stress CMR.

Myocardial characterization

A major strength of CMR lies in its well-established ability to characterize myocardial tissue, particularly through techniques such as parametric mapping and extracellular volume (ECV) quantification [15]. However, CMR-derived ECV requires acquisition of both native and post-contrast T1 maps, typically separated by 20–30 minutes, which may introduce misregistration and consequently bias the ECV calculation [15]. Dual-energy CT can overcome this technical limitation by generating an iodine map from a single scan [10]. Thanks to their dual-source architecture and photon-counting detector technology, the NAEOTOM Alpha.Peak and Pro acquire spectral data with high-temporal resolution. The ECV values derived from CMR and PCCT have been compared in patients with acute myocarditis (Fig. 4) or hypertrophic cardiomyopathies, showing no significant differences between modalities, with mean errors around 0.5% and narrow limits of agreement [16, 17]. Moreover, in patients with hypertrophic cardiomyopathy (Fig. 5), a PCCT-derived ECV cut-off value of 33.4% has been demonstrated to accurately identify patients with LGE ≥ 15% on CMR. This threshold can be considered in the decision-making process for prophylactic placement of an implantable cardioverter-defibrillator[1] [17, 18].

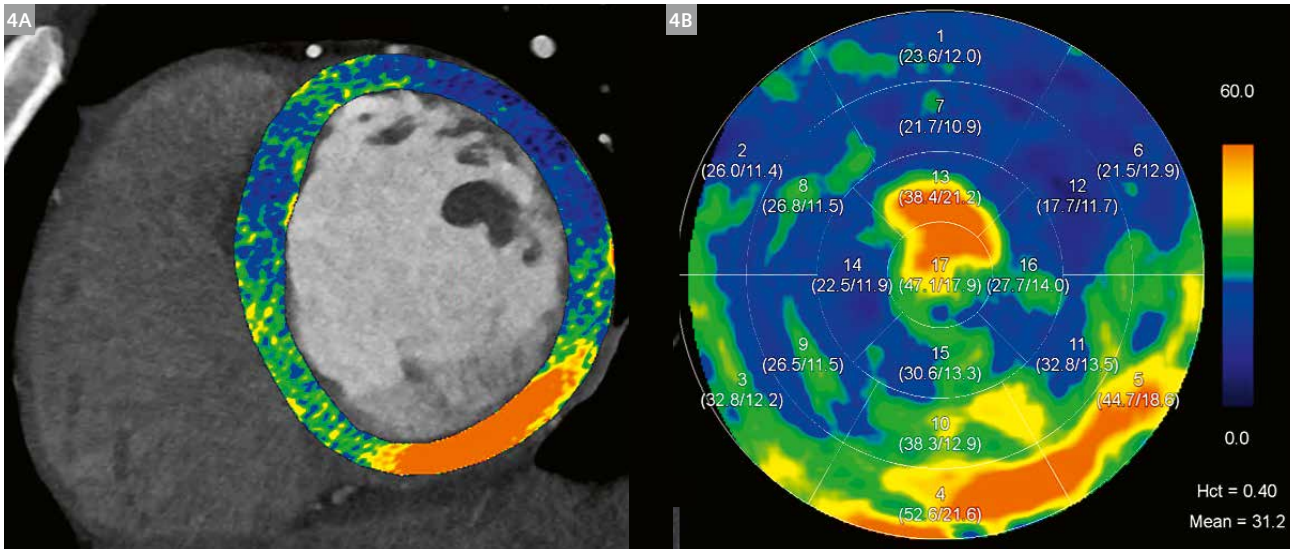

4 18-year-old male patient with acute chest pain in the context of SARS-CoV2 infection. **(4A)** Photon-counting CT-derived extracellular volume map overlay derived from myocardial late enhancement. **(4B)** Extracellular volume polar map derived from photon-counting CT.

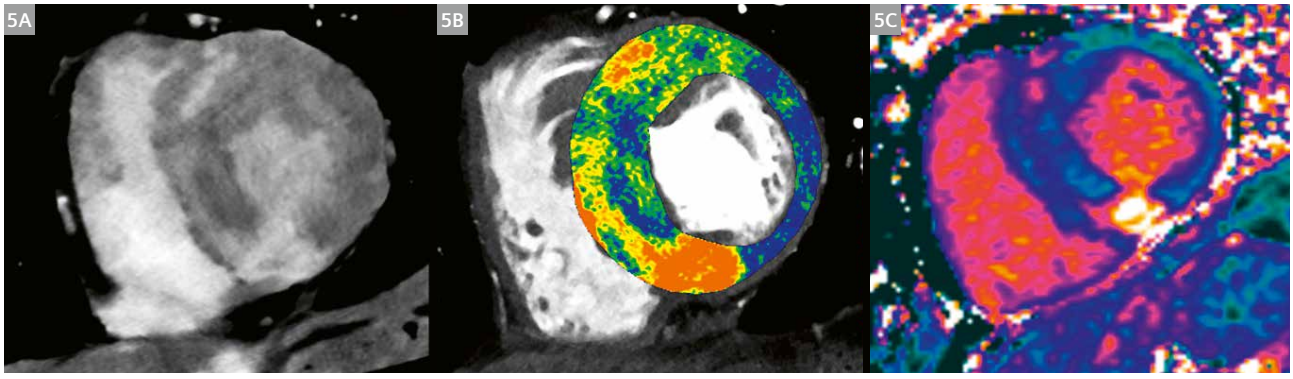

5 69-year-old female patient without history of high blood pressure, referred for evaluation of obstructive coronary heart disease in the context of new-onset dyspnea. **(5A)** Photon-counting CT shows left ventricular hypertrophy with intramyocardial fibrotic lesion on MDE series. **(5B)** Extracellular volume map overlay derived from photon-counting CT. **(5C)** Extracellular volume map calculated from CMR.

[1] *The MRI restrictions (if any) of the metal implant must be considered prior to patient undergoing MRI exam. MR imaging of patients with metallic implants brings specific risks. However, certain implants are approved by the governing regulatory bodies to be MR conditionally safe. For such implants, the previously mentioned warning may not be applicable. Please contact the implant manufacturer for the specific conditional information. The conditions for MR safety are the responsibility of the implant manufacturer, not of Siemens Healthineers.*

Heart valve disease

Advanced imaging modalities such as three-dimensional echocardiography, CMR, and cardiac CT have become central to the assessment of patients with valvular heart disease [19]. In this clinical context, cardiac CT and CMR are highly complementary. Cardiac CT provides a comprehensive assessment of cardiac and vascular anatomy, including evaluation of peripheral arterial calcification, plaque burden, and annular measurements, which are essential for patient eligibility and procedural planning in heart valve interventions. CMR, on the other hand, remains the reference standard for quantifying ventricular volumes and function, as well as regurgitant volumes or myocardial fibrosis. After heart valve intervention, cardiac CT plays a key role in the evaluation of suspected prosthetic valve dysfunction. CMR can quantify perivalvular leaks and assess increases in transvalvular gradients, but metal artifacts often limit visualization of prosthetic leaflets (Fig. 6). The ultra-high-resolution acquisition and preserved contrast at high tube voltage achieved with PCCT allow for a substantial reduction of beam-hardening and blooming artifacts [20]. This facilitates visualization of hypoattenuating structures adjacent to the leaflets or annulus – such as thrombus, pannus, or vegetations.

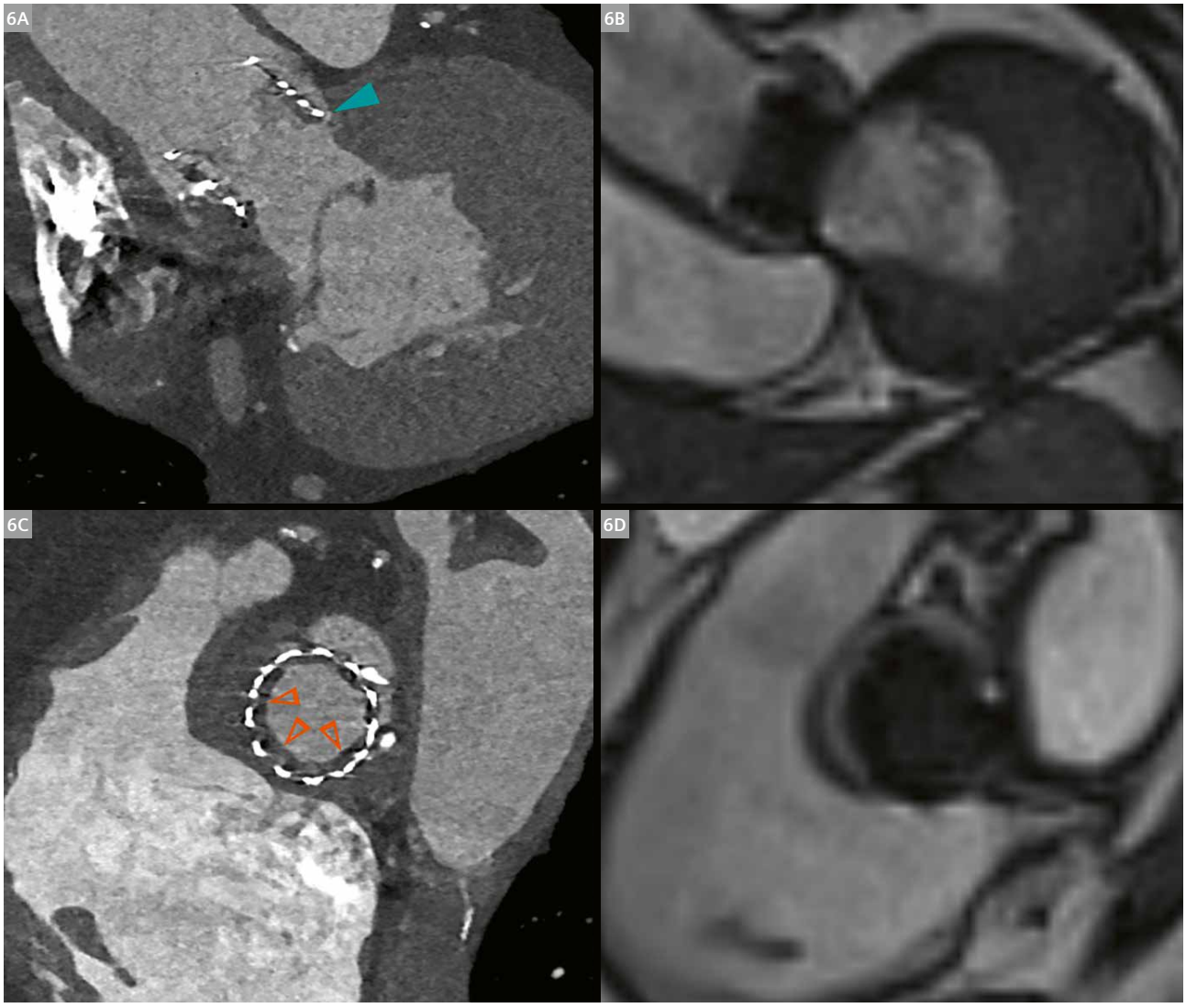

6 78-year-old male patient with a history of transcatheter aortic valve replacement, referred for increased transvalvular gradient detected on transthoracic echocardiography, with suspected periprosthetic regurgitation. **(6A)** Ultra-high-resolution photon-counting CT acquisition demonstrating the paravalvular defect responsible for the regurgitation. **(6B)** CMR accurately quantified the paravalvular leak, but morphological assessment of the prosthetic valve was not feasible due to metal artifacts. **(6C)** Ultra-high-resolution photon-counting CT image showing a circular hypoattenuation within the stent annulus, which could not be assessed on **(6D)** CMR because of susceptibility artifacts.

Flow imaging

Through two-dimensional phase-contrast and four-dimensional flow imaging, CMR is a key modality for evaluating cardiac chamber hemodynamics, especially in patients with poor transthoracic echocardiographic windows [21, 22]. Quantification of regurgitation or intracardiac shunts on CT relies on systolic and diastolic ventricular segmentation, at the cost of increased radiation exposure. An appropriate iodine contrast injection protocol and accurate triggering of the CT acquisition can qualitatively depict intracardiac shunts or leaks. Compared to the materials regularly used in EID systems, the high responsivity of PCDs to low-energy X-ray photons facilitates the visualization of subtle attenuation differences. This is further enhanced by low-keV monoenergetic reconstructions and potentially further improved for the reader by the use of color look-up tables (Fig. 7, Fig. 8) [23].

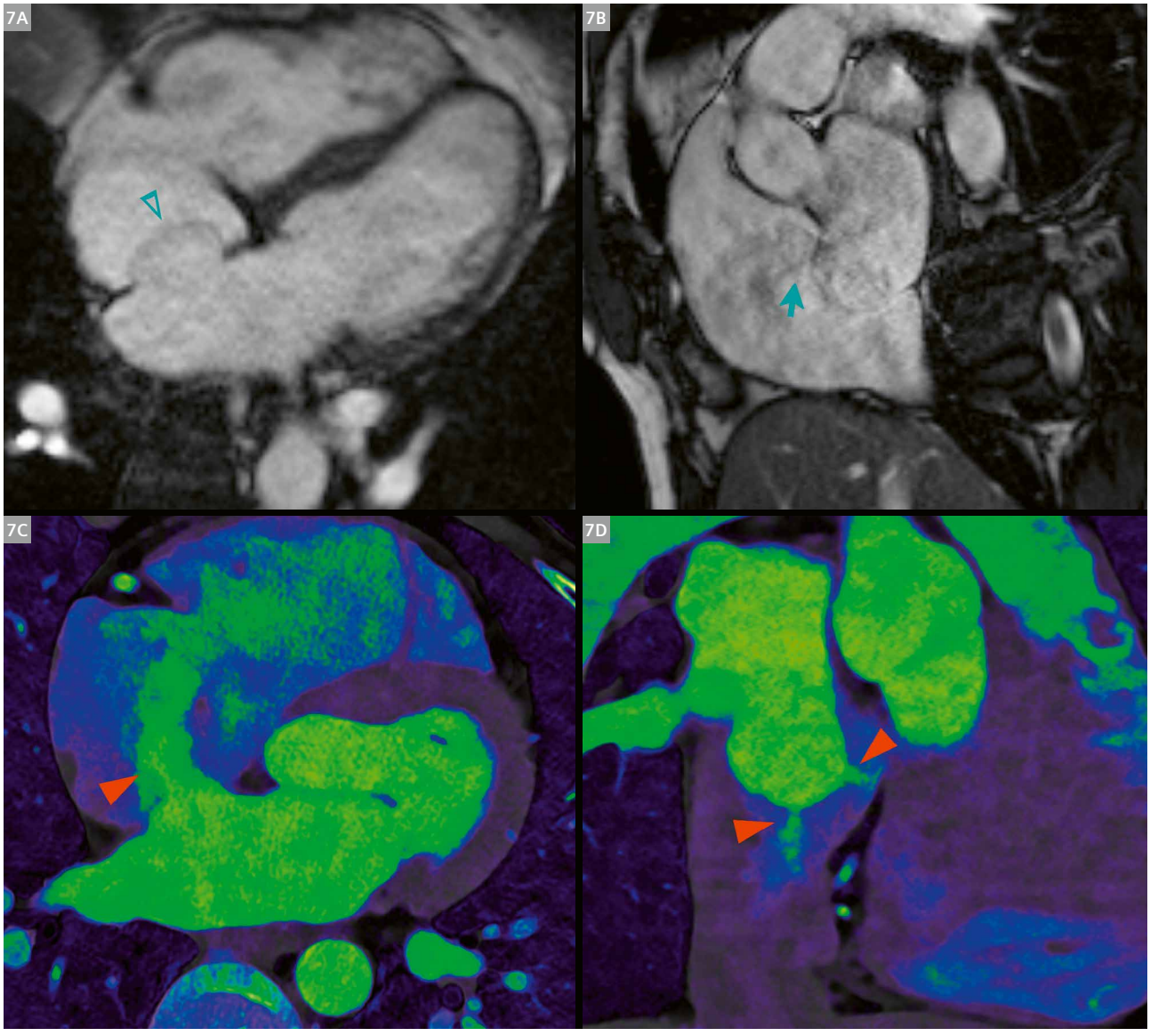

7 39-year-old male patient referred for right-ventricular dilatation. **(7A)** CMR demonstrates an aneurysm of the interatrial septum in the four-chamber view (hollow arrowhead) with **(7B)** interatrial communication visualized as a flow void on the short-axis view (arrow). The Qp/Qs ratio is 1.7. **(7C)** Iodine map derived from photon-counting CT confirms a large interatrial communication on the four-chamber view (arrowhead). **(7D)** Two additional small interatrial communications are identified on the paraseptal right ventricular two-chamber view.

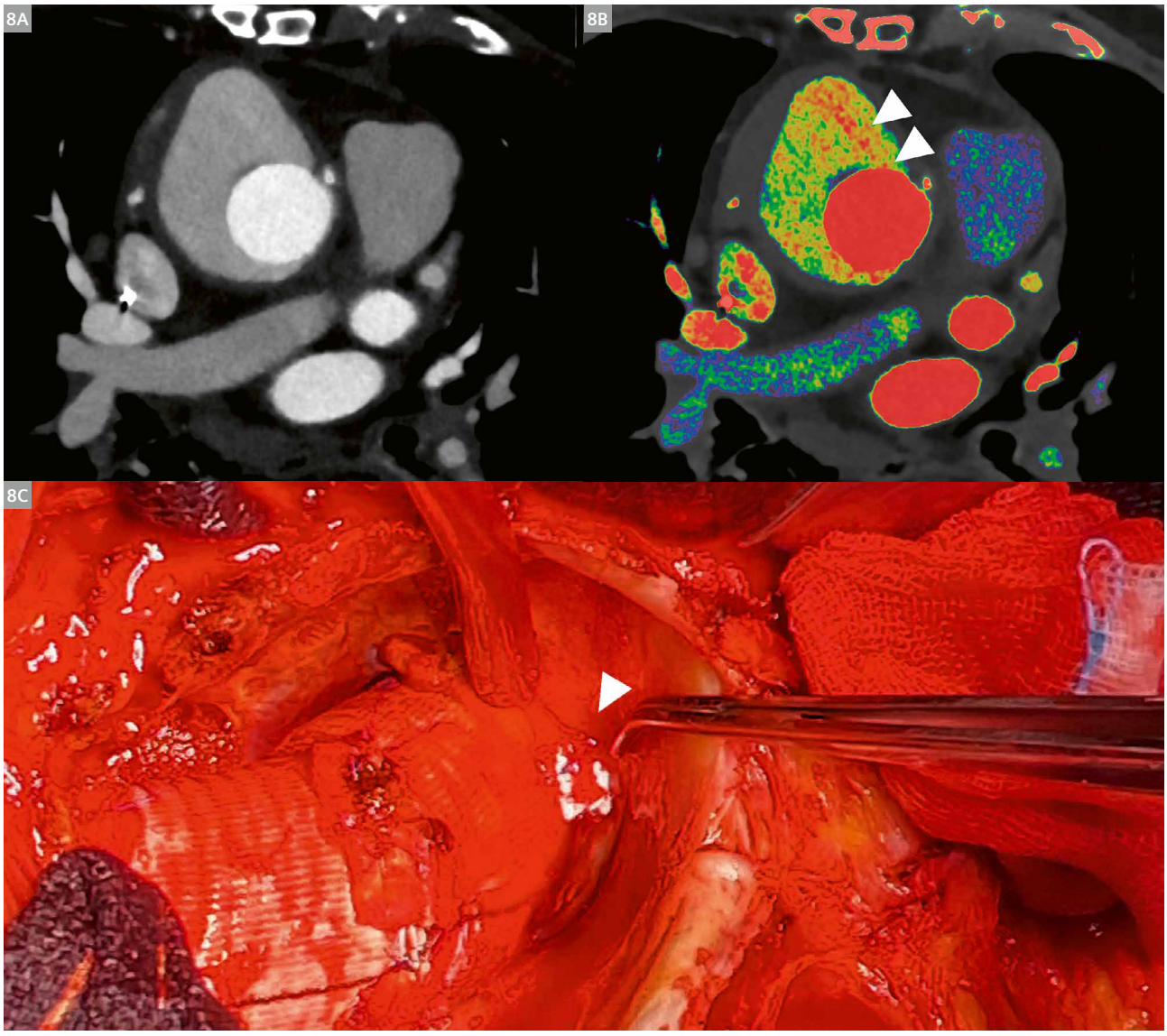

8 88-year-old male patient with a history of ascending aortic replacement, referred for chest pain. (8A) Photon-counting CT angiography of the aorta shows a periaortic hematoma (70 keV monoenergetic reconstruction; 120 kVp conventional-like image). The bleeding source responsible for this hematoma is not confidently identified. (8B) Iodine map overlay using a color look-up table demonstrates the attenuation gradient and precisely locates the bleeding site. (8C) Surgical confirmation of the bleeding origin.
Courtesy of Natacha Rousse, M.D., Heart and Lung Institute, CHU Lille, France.

Conclusion

Photon-counting CT (PCCT) represents a major step toward bridging the historical gap between cardiac CT and CMR. Its ability to provide high-resolution anatomical imaging, quantitative spectral data, and myocardial tissue characterization within a single, time-efficient acquisition brings cardiac CT closer to the comprehensive diagnostic capability traditionally reserved for CMR. However, these modalities should not be seen as competing but as highly complementary. CMR remains the reference standard for advanced tissue characterization, myocardial fibrosis assessment, and complex flow quantification, while PCCT offers unparalleled spatial resolution, reduced acquisition times, and simultaneous evaluation of coronary arteries, myocardium, and valves. Together, PCCT and CMR form a synergistic imaging approach, combining structural and functional insights to refine diagnosis, guide management, and ultimately improve patient care in cardiovascular disease.

References

1 Leiner T, Bogaert J, Friedrich MG, Mohiaddin R, Muthurangu V, Myerson S, et al. SCMR Position Paper (2020) on clinical indications for cardiovascular magnetic resonance. J Cardiovasc Magn Reson. 2020;22(1):76.
2 Willemink MJ, Persson M, Pourmorteza A, Pelc NJ, Fleischmann D. Photon-counting CT: Technical Principles and Clinical Prospects. Radiology. 2018;289:293–312.
3 Flohr T, Schmidt B. Technical Basics and Clinical Benefits of Photon-Counting CT. Invest Radiol. 2023;58(7):441–450.
4 Flohr T, Petersilka M, Henning A, Ulzheimer S, Ferda J, Schmidt B. Photon-counting CT review. Phys Med. 2020;79:126–136.
5 Vrints C, Andreotti F, Koskinas KC, Rossello X, Adamo M, Ainslie J, et al. 2024 ESC Guidelines for the management of chronic coronary syndromes. Eur Heart J. 2024;45(36):3415–3537.
6 Eberhard M, Candreva A, Rajagopal R, Mergen V, Sartoretti T, Stähli BE, et al. Coronary Stenosis Quantification With Ultra-High-Resolution Photon-Counting Detector CT Angiography: Comparison With 3D Quantitative Coronary Angiography. JACC Cardiovasc Imaging. 2024;17(3):342–344.
7 Kim RJ, Fieno DS, Parrish TB, Harris K, Chen EL, Simonetti O, et al. Relationship of MRI delayed contrast enhancement to irreversible injury, infarct age, and contractile function. Circulation. 1999;100(19):1992–2002.
8 Kim RJ, Wu E, Rafael A, Chen EL, Parker MA, Simonetti O, et al. The use of contrast-enhanced magnetic resonance imaging to identify reversible myocardial dysfunction. N Engl J Med. 2000;343(20):1445–53.
9 Rodriguez-Granillo GA. Delayed enhancement cardiac computed tomography for the assessment of myocardial infarction: from bench to bedside. Cardiovasc Diagn Ther. 2017;7(2):159–170.
10 Oyama-Manabe N, Oda S, Ohta Y, Takagi H, Kitagawa K, Jinzaki M. Myocardial late enhancement and extracellular volume with single-energy, dual-energy, and photon-counting computed tomography. J Cardiovasc Comput Tomogr. 2024;18(1):3–10.
11 Mergen V, Sartoretti T, Klotz E, Schmidt B, Jungblut L, Higashigaito K, et al. Extracellular Volume Quantification With Cardiac Late Enhancement Scanning Using Dual-Source Photon-Counting Detector CT. Invest Radiol. 2022;57(6):406–11.
12 Soschynski M, Storelli R, Birkemeyer C, Hagar MT, Faby S, Schwemmer C, et al. CT Myocardial Üerfusion and CT-FFR versus Invasive FFR for Hemodynamic Relevance of Coronary Artery Disease. Radiology. 2024;312(2):e233234.
13 Pontone G, Mushtaq S, Narula J. Dynamic Perfusion with CT Angiography: Adding Another Feather to a Heavily Decorated Cap. J Am Coll Cardiol. 2021;78(20):1950–1953.
14 Longère B, Caseneuve H, Gkizas C, Rodriguez Musso A, Tregubova M, Croisille C, et al. Feasibility of stress myocardial perfusion imaging with photon-counting CT: Initial validation against reference modalities. Diagn Interv Imaging. 2025. Ahead of print. DOI: 10.1016/j.diii.2025.10.005
15 Messroghli DR, Moon JC, Ferreira VM, Grosse-Wortmann L, He T, Kellman P, et al. Clinical recommendations for cardiovascular magnetic resonance mapping of T1, T2, T2* and extracellular volume: A consensus statement by the Society for Cardiovascular Magnetic Resonance (SCMR) endorsed by the European Association for Cardiovascular Imaging (EACVI). J Cardiovasc Magn Reson. 2017;19(1):75.
16 Gkizas C, Longère B, Sliwicka O, Musso AR, Lemesle G, Croisille C, et al. Photon-counting CT-derived extracellular volume in acute myocarditis: Comparison with cardiac MRI. Diagn Interv Imaging. 2025;106(7–8):255–263.
17 Gkizas C, Longère B, Bechrouri S, Ridon H, Musso AR, Haidar M, et al. Photon-counting CT myocardial extracellular volume: A non-invasive biomarker for fibrosis in patients with hypertrophic cardiomyopathy. Diagn Interv Imaging. 2025:S2211–5684(25)00164–0.
18 Arbelo E, Protonotarios A, Gimeno JR, Arbustini E, Barriales-Villa R, Basso C, et al. 2023 ESC Guidelines for the management of cardiomyopathies. Eur Heart J. 2023;44(37):3503–3626.
19 Praz F, Borger MA, Lanz J, Marin-Cuartas M, Abreu A, Adamo M, et al. 2025 ESC/EACTS Guidelines for the management of valvular heart disease. Eur Heart J. 2025:ehaf194.
20 Cademartiri F, Meloni A, Pistoia L, Degiorgi G, Clemente A, Gori CD, et al. Dual-Source Photon-Counting Computed Tomography-Part I: Clinical Overview of Cardiac CT and Coronary CT Angiography Applications. J Clin Med. 2023;12(11):3627.
21 Horowitz MJ, Kupsky DF, El-Said HG, Alshawabkeh L, Kligerman SJ, Hsiao A. 4D Flow MRI Quantification of Congenital Shunts: Comparison to Invasive Catheterization. Radiol Cardiothorac Imaging. 2021;3(2):e200446.
22 Aquaro GD, Barison A, Todiere G, Festa P, Ait-Ali L, Lombardi M, et al. Cardiac magnetic resonance 'virtual catheterization' for the quantification of valvular regurgitations and cardiac shunt. J Cardiovasc Med (Hagerstown). 2015;16(10):663–70.
23 Janin-Manificat A, Sigovan M, Davila E, de Bourguignon C, Si-Mohamed S, Boussel L, et al. Spectral Computed Tomography for the Detection and Characterization of Communications Between the True and the False Lumen in Aortic Dissections. Invest Radiol. 2025. Epub ahead of print.

Professor François Pontana, M.D., Ph.D.
Department of Cardiothoracic Radiology
CHU Lille, Heart and Lung Institute
Boulevard du Professeur Jules Leclercq
59037 Lille Cedex
France
francois.pontana@chu-lille.fr

Contact

Associate Professor Benjamin Longère, M.D., Ph.D.
Department of Cardiothoracic Radiology
CHU Lille, Heart and Lung Institute
Boulevard du Professeur Jules Leclercq
59037 Lille Cedex
France
Benjamin.LONGERE@chu-lille.fr

Contrast-Enhanced iNAV MRA for Whole-Chest, Whole-Heart, and Whole-Aortic Imaging: A Single-Center Experience

Jason Craft[1], Timothy Carter[2], Joshua Y. Cheng[1], Christopher J. Moran[3], Karl P. Kunze[4], Michaela Schmidt[5], Rene M. Botnar[6,7,8], Claudia Prieto[6,7]

[1]DeMatteis Cardiovascular Institute, St. Francis Hospital & Heart Center, Roslyn, NY, USA
[2]Department of Cardiothoracic Surgery, Good Samaritan University Hospital, West Islip, NY, USA
[3]Department of Radiology, Good Samaritan University Hospital, West Islip, NY, USA
[4]MR Research Collaborations, Siemens Healthcare Limited, Camberley, United Kingdom
[5]Research & Clinical Translation, Magnetic Resonance, Siemens Healthineers, Erlangen, Germany
[6]School of Biomedical Engineering and Imaging Sciences, King's College London, London, United Kingdom
[7]School of Engineering, Pontificia Universidad Católica de Chile, Santiago, Chile
[8]Institute for Biological and Medical Engineering, Pontificia Universidad Católica de Chile, Santiago, Chile

Introduction

Undersampled 3D whole-heart inversion recovery (IR) Dixon gradient echo (GRE) accelerated by variable-density spiral-like Cartesian trajectory (VD-CASPR) with image-based navigators (iNAVs) for motion estimation and nonrigid motion-corrected iterative sensitivity-encoding (SENSE) reconstruction with 100% respiratory scan efficiency has the potential for integration into workflows for left atrial and left ventricular delayed enhancement [1]. Our initial aim was to develop an iNAV-compatible method to provide complementary contrast-enhanced (CE) pulmonary vein magnetic resonance angiography (MRA) for registration with delayed enhancement and high-quality left atrial segmentation, while being insensitive to flow and off-resonance artifacts. The need was compounded by the shortage of iohexol and iodixanol intravenous contrast media products for computed tomography angiography (CTA) from May to June 2022. Single-contrast saturation-recovery (SR) and IR GRE have been widely used for this purpose with excellent results [2, 3], although experience is relegated to diaphragmatic navigator prospective motion correction. Widespread clinical adoption has been constrained by commonly recognized limitations to this approach, including an unpredictable scan duration, and residual respiratory motion due to the inaccurately assumed slab tracking ratio. As a solution, we collaborated with our partners at Siemens Healthineers, at Pontificia Universidad Católica de Chile, and at King's College London to configure both SR and IR GRE for iNAV pulmonary vein CE-MRA, later adapting the IR GRE method for whole-chest angiography (iNAV CE-MRA) [4].

For the majority of patients, 3D non-contrast-enhanced T2-prepared balanced steady-state free precession (bSSFP) provides highly diagnostic image quality. However, iNAV CE-MRA has several key advantages that warrant consideration for use. These include a lack of dependency on chemically selective fat saturation preparatory pulses, which may inadvertently saturate the water signal in the aortic arch and proximal descending aorta [5]; and demonstrably superior blood pool signal uniformity, allowing performance consistency of threshold-based anatomical segmentation used to generate centerline semi-automated aortic measurements (CSAMs). iNAV CE-MRA can also be combined with time-resolved angiography with interleaved stochastic trajectories (TWIST) for comprehensive dynamic 4D angiography. Given the rapidly shifting landscape of modern MR imaging, referral patterns, provider needs, and the increase in patient complexity, it is also increasingly important to have techniques that are robust to susceptibility artifacts from sources such as internal cardiac defibrillators (ICDs)/pacemakers[1], thoracic endovascular aortic repairs (TEVAR)[1], and hybrid aortic repairs. That being said, the technical downside to iNAV CE-MRA is variation in image

[1]*The MRI restrictions (if any) of the metal implant must be considered prior to patient undergoing MRI exam. MR imaging of patients with metallic implants brings specific risks. However, certain implants are approved by the governing regulatory bodies to be MR conditionally safe. For such implants, the previously mentioned warning may not be applicable. Please contact the implant manufacturer for the specific conditional information. The conditions for MR safety are the responsibility of the implant manufacturer, not of Siemens Healthineers.*

contrast with irregular rhythms (which can degrade image quality), more elaborate MRA planning, and risk of MR acquisition mistiming in relation to the delivery of gadolinium-based contrast agent (GBCA). To partially alleviate these shortcomings, the artificial intelligence cardiac scan companion (AICSC)[2] WIP and auto resting-phase detection [6] are promising tools to reduce efficiency overhead, and can be used for automated whole-chest slab placement, navigator placement, and alignment of the data window duration. We also favor the use of a simplified injection scheme that is practical for everyday clinical use without contrast dilution, manipulation of extra tubing, syringes, and/or stopcocks. Lastly, it is feasible to monitor GBCA arrival using the low-resolution 2D iNAV images to minimize the possibility of sequence mistiming error.

Protocols

Exams are performed on a MAGNETOM Sola or MAGNETOM Aera 1.5-Tesla scanner (Siemens Healthineers, Erlangen, Germany) with a dedicated 32-channel spine coil and an 18-channel phased array torso coil. In order to minimize confusion and simplify communication across multiple sites where remote scanning is used, a minimal number of core protocols were developed for use regardless of patient complexity.

To date, we have performed over 300 iNAV CE-MRA exams, over 250 of which were whole-chest or whole-aorta imaging. We have three core protocols for whole-chest and whole-aorta MRA imaging:

1) TWIST followed by iNAV CE-MRA: Appropriate for patients with aortic disease limited to the thoracic aorta.
2) First-pass abdominopelvic MRA followed by iNAV CE-MRA: Used in patients with extensive thoracic and abdominal aortic dissection and surgical repair.
3) TWIST followed by iNAV CE-MRA, then first-pass abdominopelvic MRA: Appropriate for patients with extensive thoracic and abdominal aortic dissection, but with TEVAR or hybrid repairs.

Sequence parameters for TWIST and iNAV CE-MRA can be found in Table 1. Before administering GBCA, we test the fidelity of the vectorcardiogram (VCG) gaiting and perform prescan adjustments to be copied to subsequent iNAV scans by running a copy of the sequence for several seconds.

Separate from the test scan, we create identical pairs of iNAV CE-MRA program steps to be run roughly 10 seconds after TWIST completes, which is enough time to give the patient instructions. As our experience matured, we found it was no longer necessary to insert an injector pause between the bolus and continuous GBCA infusion.

[2]Work in progress. The application is currently under development and is not for sale in the U.S. and in other countries. Its future availability cannot be ensured.

MRA sequence	TWIST	iNAV CE-MRA	iNAV CE-MRA$_{Isotropic}$
FOV (coronal)	400 × 300 × 160 mm	380 × 380 × 157 mm	360 × 360 × 153 mm
In-plane spatial resolution	1.13 × 1.62 mm	1.31 × 1.31 mm	1.25 × 1.25 mm
Phase oversampling	50%	30%	30%
Slice thickness	2 mm	1.4–1.5 mm	1.2 mm
Slice resolution	54%	90%	100%
Acceleration factor	GRAPPA 3	3.2*	4.1*
Sampling distribution	Elliptical scanning 15% (region A), 20% (region B)	Elliptical scanning	Elliptical scanning
Bandwidth	676 Hz/px	755 Hx/px	755 Hx/px
Flip angle	23°	18°	18°
Inversion time	N/A	200–290 ms	200–290 ms
TE/TR	.9 ms/2.4 ms	1.1 ms/3.34 ms	1.17 ms/3.44 ms
Data window duration	N/A	130 ms**	130 ms**

Table 1: Imaging parameters for whole-chest TWIST and iNAV CE-MRA.
*Acceleration factor is increased as needed to fit an acquisition duration of ≤ 5 minutes.
**Data window duration is adjusted as needed according to the optimal cardiac rest period.

The first program step is run to completion if continuous infusion peaking is already evident on the low-resolution inline-display 2D images (this makes the second program step unnecessary). Otherwise, the second program step is run to completion and will need to be triggered at the peak of the continuous infusion via the stop-and-continue function on the inline display (Fig. 1).

iNAV CE-MRA can also be acquired without TWIST for single-station whole-chest angiography. It is the experience of others and our own intuition that 0.075 mmol/kg bolus of a 1-molar agent at 1 mL/s, followed by 0.075 mmol/kg at 0.10 mL/s, and 20–30 mL/saline at 0.10 mL/s provides excellent results [3]. In this case, the first program step is used only for testing the VCG gating fidelity, making pre-scan adjustments, and monitoring the passage of contrast with the image navigator. The second program step, which will run to completion, is triggered at the peak of the continuous infusion.

1 **Option 1:** TWIST MRA: 0.05 mmol/kg at 2 ml/s of 1 molar GBCA followed by 30 ml saline **or** **Option 2:** First pass MRA abdomen and pelvis: 0.1 mmol/kg at 2 ml/s of 1 molar GBCA followed by 20–30 ml saline

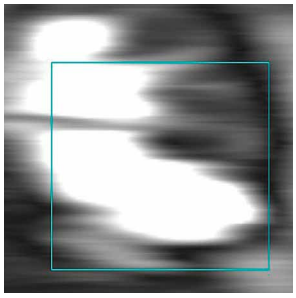

2 Continuous infusion: 0.16 ml/sec GBCA, 20–30 ml saline

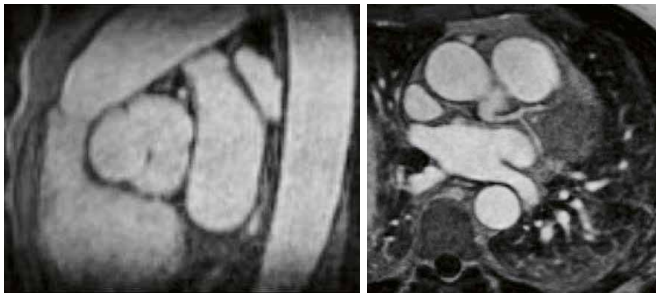

3 iNAV CE-MRA

1 molar GBCA dose: 0.1 mmol/kg

1 Method for whole-chest image-based navigator contrast-enhanced magnetic resonance angiography (iNAV CE-MRA). Two identical 3D whole-chest program steps are created in the workflow. **(1)** Following TWIST (Option 1) or first-pass CE-MRA (Option 2), a continuous infusion of gadolinium-based contrast agent (GBCA) begins **(2)**. The first iNAV program step **(3)** commences afterwards and is run to completion only if the continuous infusion arrival is evident on 2D low-resolution images. Otherwise, the required second program step is triggered as the continuous infusion peaks. If TWIST was performed initially (Option 1), first-pass abdominopelvic MRA can be added after iNAV CE-MRA using 0.05 mmol/kg of 1-molar GBCA.

Use of iNAV CE-MRA in challenging patients

Obesity

From 1990 to 2022, obesity rates more than doubled among women and nearly tripled in men. It is estimated that over 1 billion people worldwide are obese, including 159 million children [7].

In the United States alone, obesity-related healthcare expenditures are estimated to be more than $385 billion in 2024 [8].

High-quality MR imaging in this population poses challenges, such as decreased signal-to-noise ratio (SNR) from reduced radiofrequency penetration, larger acquired voxel dimensions, and increased patient-specific field inhomogeneity as magnetic bore sizes are pushed to the limit. The latter directly contributes to phase incoherency artifacts from T2 and fat saturation preparatory pulses, with large-volume shimming having reduced effectiveness across the whole-chest 3D field of view.

Other modalities are also negatively impacted: Echocardiography with poor acoustic windows and inadequate ultrasound penetration depth, and CT with increased beam attenuation resulting in photon starvation and low SNR.

Although GRE generally has an overall lower SNR in several applications, Tandon et al. demonstrated higher intravascular SNR for gadofosveset-enhanced IR GRE compared to 3D T2-prepared bSSFP [9]. It is yet to be determined if this observation translates to weak albumin-binding GBCAs.

In a single-center study consisting of 65 patients with atrial fibrillation referred for CMRI, mean BMI was 30 ± 6 kg/m^2. However, good or excellent quality pulmonary-vein iNAV CE-MRA was obtained in 95% of exams. Additionally, good or excellent left atrial segmentation was seen in 97% of exams [10].

This helps support the use of MRA in a population that is vulnerable to higher effective radiation doses needed for routine medical imaging [11].

High-quality whole-chest iNAV CE-MRA may also be realized in this patient population. Figure 2 demonstrates two examples where iNAV CE-MRA produced high-quality imaging despite body habitus.

Endografts and implantable cardiac devices[1]

TEVAR is considered first-line therapy for the treatment of complicated Type B aortic dissection (TBAD) and descending thoracic aortic aneurysms [12]. Although the metallic frame structure is readily visible on CT imaging, time-resolved MRA has higher sensitivity for the detection of endoleaks [13]. It is common to encounter intravascular dephasing within the TEVAR using iNAV CE-MRA, but not with TWIST. This signal loss is related to metallic artifact, non-laminar flow, and thus intravoxel velocity heterogeneity. Therefore, TWIST and iNAV CE-MRA are combined for arterial, venous, and delayed phase imaging (Figs. 3, 4). While a TEVAR nitinol exoskeleton composition produces relatively small susceptibility artifacts, the opposite is true regarding ICDs and pacemakers.

Over 200,000 ICDs and 1 million cardiac pacemakers are implanted every year worldwide [14]. Approximately 200,000 cardiac pacemakers are implanted in the United States alone [15], posing a challenge to conventional CMR imaging.

MRA imaging in device patients has historically been an underexplored topic of interest, possibly due to many existing systems containing non-MR-conditional generators or leads. As a consequence, this population may be exposed to recurring doses of ionized radiation (i.e., for annual aortic surveillance).

For these patients, a modified wideband IR pulse with a spectral bandwidth of 2–6 kHz has shown benefit for 3D delayed enhancement, and may have a role in whole-chest angiography [16]. An IR frequency offset may be helpful in shifting artifacts away from pertinent anatomical structures, at the cost of IR efficiency and loss of image contrast. Examples of iNAV CE-MRA with and without wideband IR are found in figures 5, 6, and 7. In contrast, TWIST is more robust due to lack of IR pulse and shorter repetition time, and can provide diagnostic information in areas affected by artifacts on iNAV CE-MRA.

[1] *The MRI restrictions (if any) of the metal implant must be considered prior to patient undergoing MRI exam. MR imaging of patients with metallic implants brings specific risks. However, certain implants are approved by the governing regulatory bodies to be MR conditionally safe. For such implants, the previously mentioned warning may not be applicable. Please contact the implant manufacturer for the specific conditional information. The conditions for MR safety are the responsibility of the implant manufacturer, not of Siemens Healthineers.*

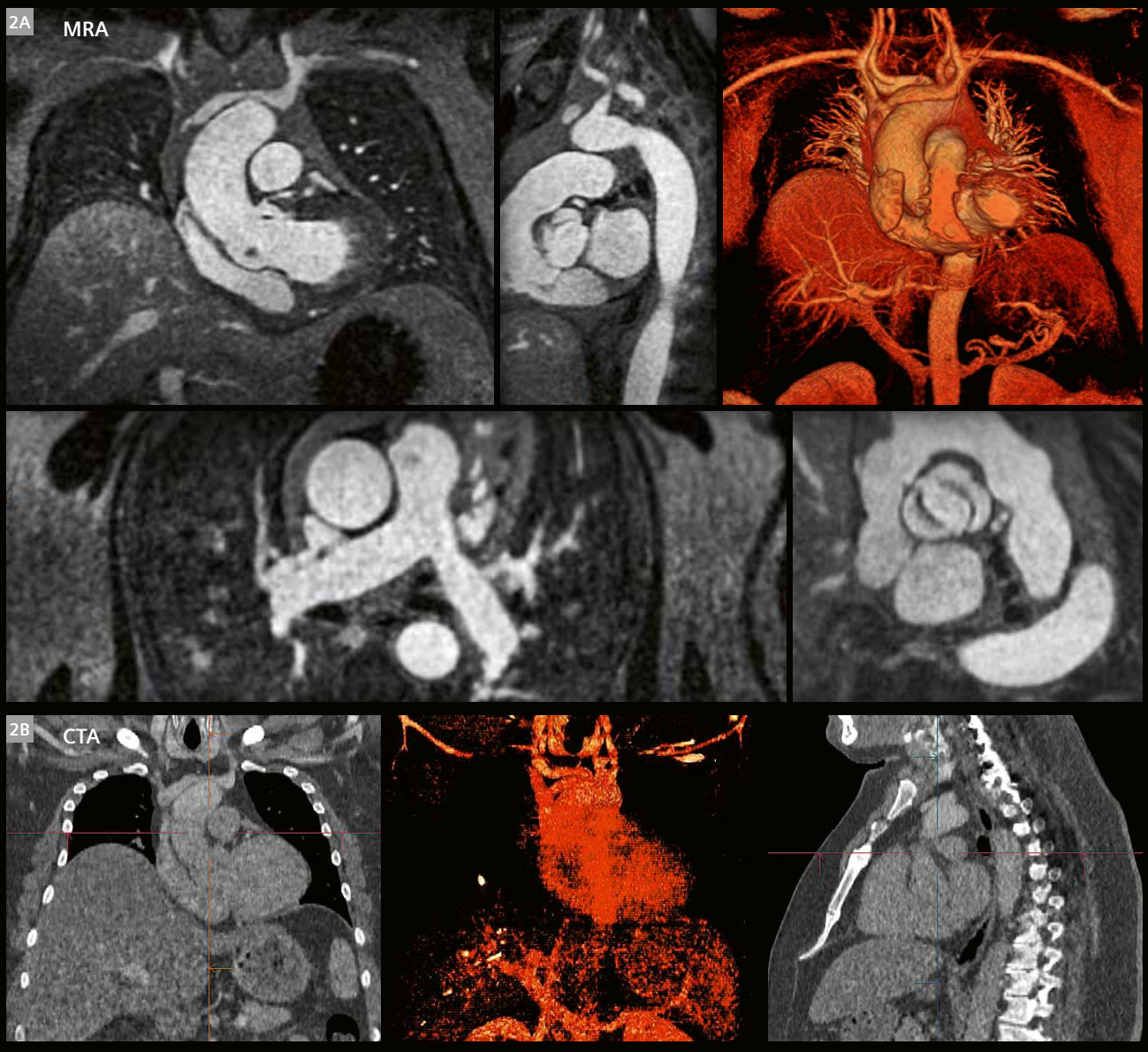

2 Whole-chest iNAV CE-MRA in patients with obesity. **(2A)** Patient 1 with Sievers Type 1 bicuspid aortic valve and thoracic ascending aortic aneurysm, BMI 51 kg/m². **(2B)** CTA images for comparison. **(2C)** Patient 2, status post-thoracic endovascular aortic repair (TEVAR), BMI of 45 kg/m².

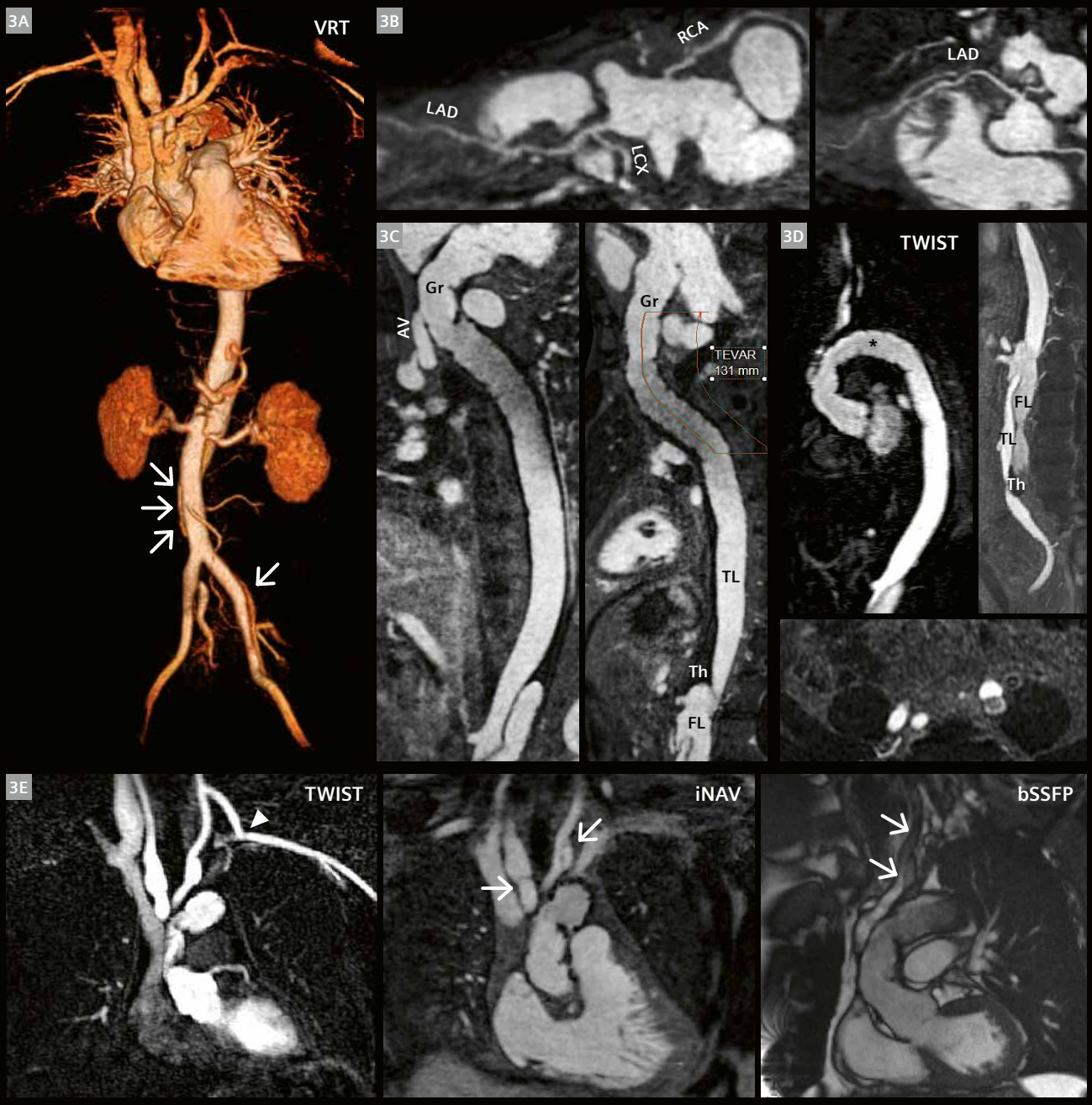

3 A 57-year-old male, Type A aortic dissection, status post-hybrid repair with debranching of the supra-aortic vessels, left common carotid to left subclavian bypass. **(3A)** Composite volume rendering (VRT) of the iNAV and first-pass CE-MRA. **(3B)** The left anterior descending (LAD) artery, right coronary artery (RCA), and left circumflex coronary artery (LCX) are free from dissection. **(3C)** An interposition graft (Gr) is present in the ascending aorta with composite reconstructed arch vessel (AV). The thoracic endovascular aortic repair (TEVAR) graft spanning 131 mm is present in the thoracic descending aorta. Loss of intravascular signal intensity is appreciated within the TEVAR graft. Residual aortic dissection is present in the abdominal aorta, where the true lumen (TL) and false lumen (FL) containing thrombus (Th) can be identified. **(3D)** Compared to iNAV CE-MRA, there is no appreciable signal loss within the TEVAR graft (black asterisk) on arterial phase TWIST. First-pass abdominopelvic CE-MRA redemonstrates the true lumen, false lumen, thrombus, and dissection extension to the level of the common iliac artery. **(3E)** TWIST demonstrates patent left common carotid to left subclavian bypass (white arrowhead). iNAV CE-MRA depicts residual dissection in the brachiocephalic and left common carotid arteries (white arrows). In contrast, balanced steady-state free precession (bSSFP) images are affected by dephasing artifacts in the supra-aortic vessels.

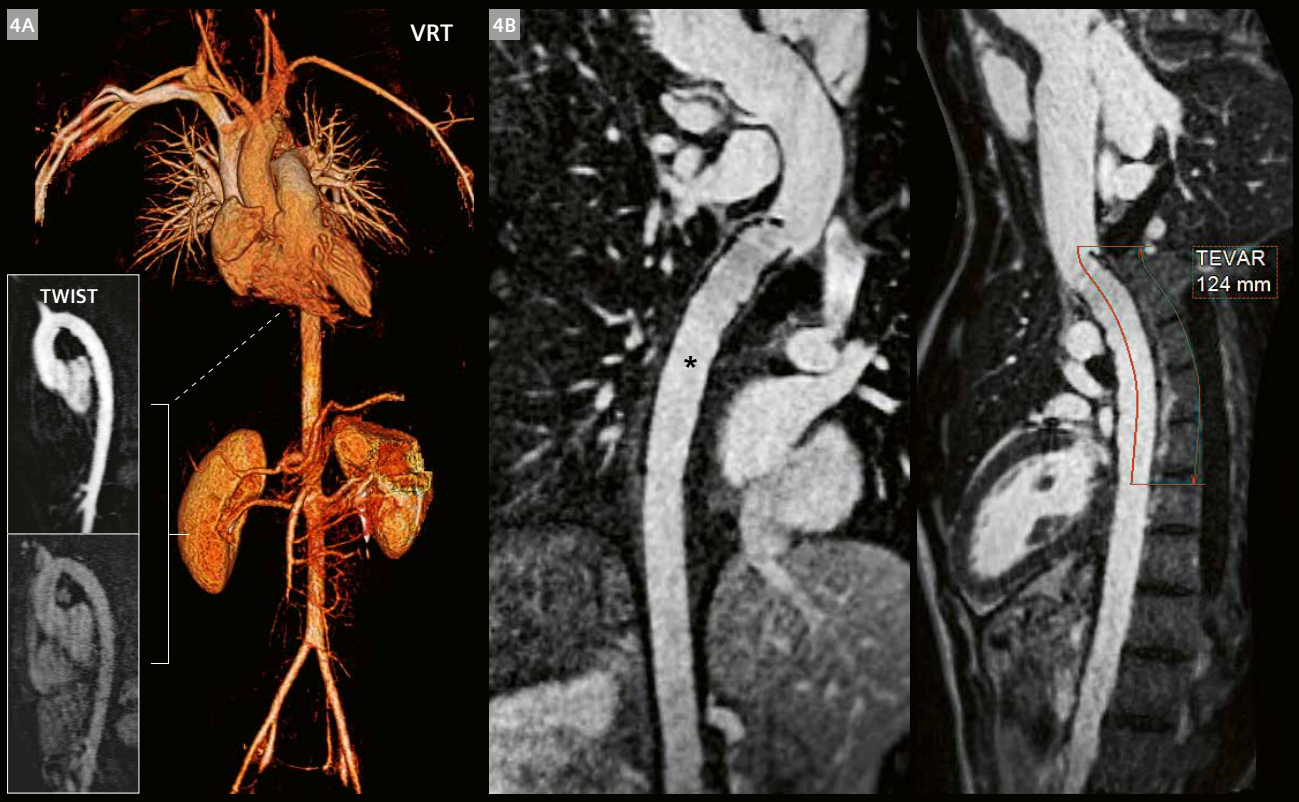

4 iNAV CE-MRA in a patient status post-thoracic endovascular aortic repair (TEVAR). **(4A)** Composite volume rendering (VRT) of iNAV and first-pass abdominopelvic CE-MRA. The inset images demonstrate arterial and venous TWIST phases. There is no evidence of endoleak. **(4B)** Curved multiplanar reconstructions (MPRs) demonstrate the TEVAR graft spanning 124 mm. Minor signal intensity loss is present within the graft (asterisk). **(4C)** Coronal and sagittal maximal intensity projections (MIPs) of the abdominal aorta, which is free from pathology.

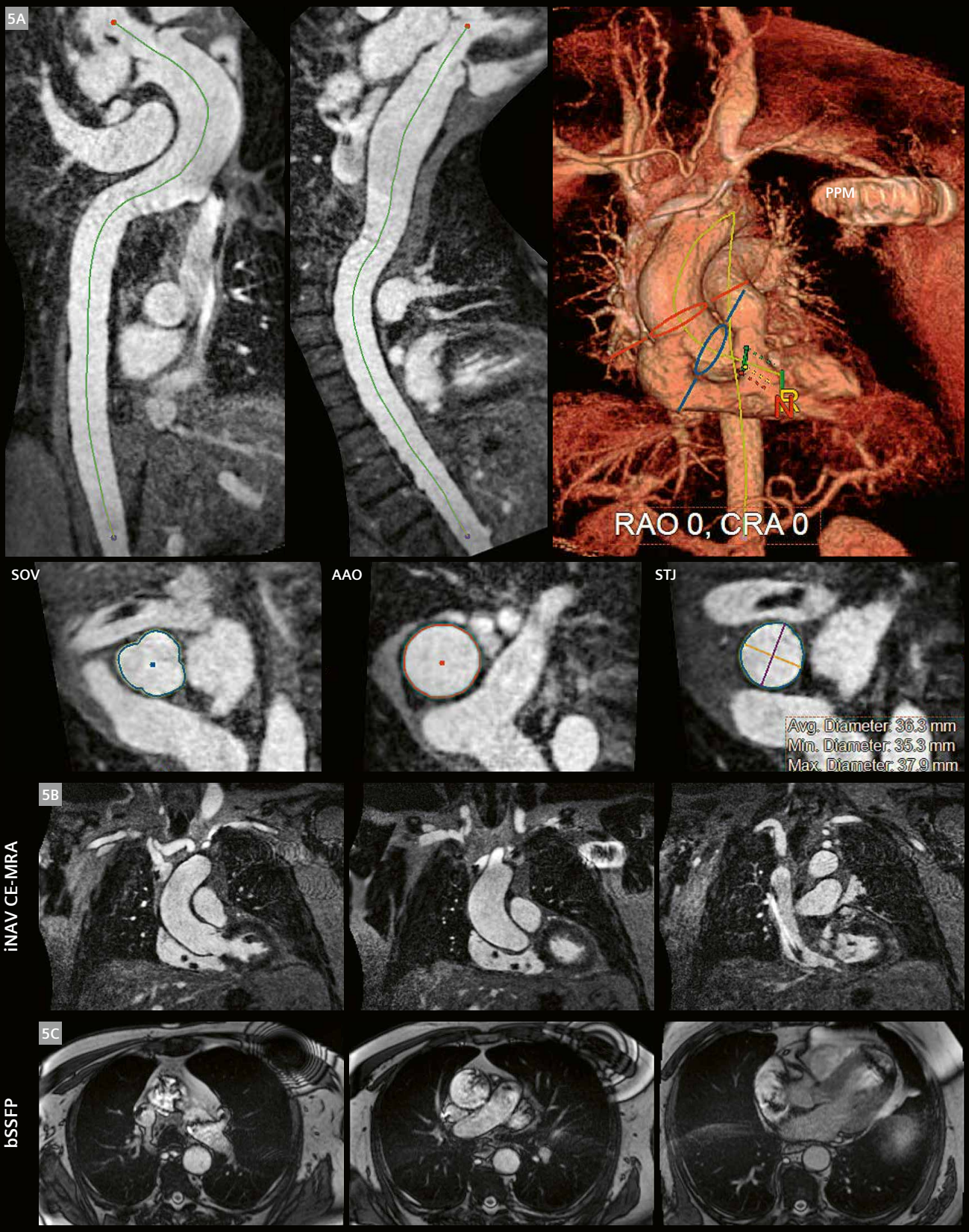

5 **(5A)** iNAV CE-MRA without wideband inversion recovery. Centerline semiautomated aortic measurements (CSAM) in a patient with permanent cardiac pacemaker. **(5B)** iNAV CE-MRA is free from significant artifact in the pertinent anatomical structures compared to balanced steady-state free precession (bSSFP) **(5C).**

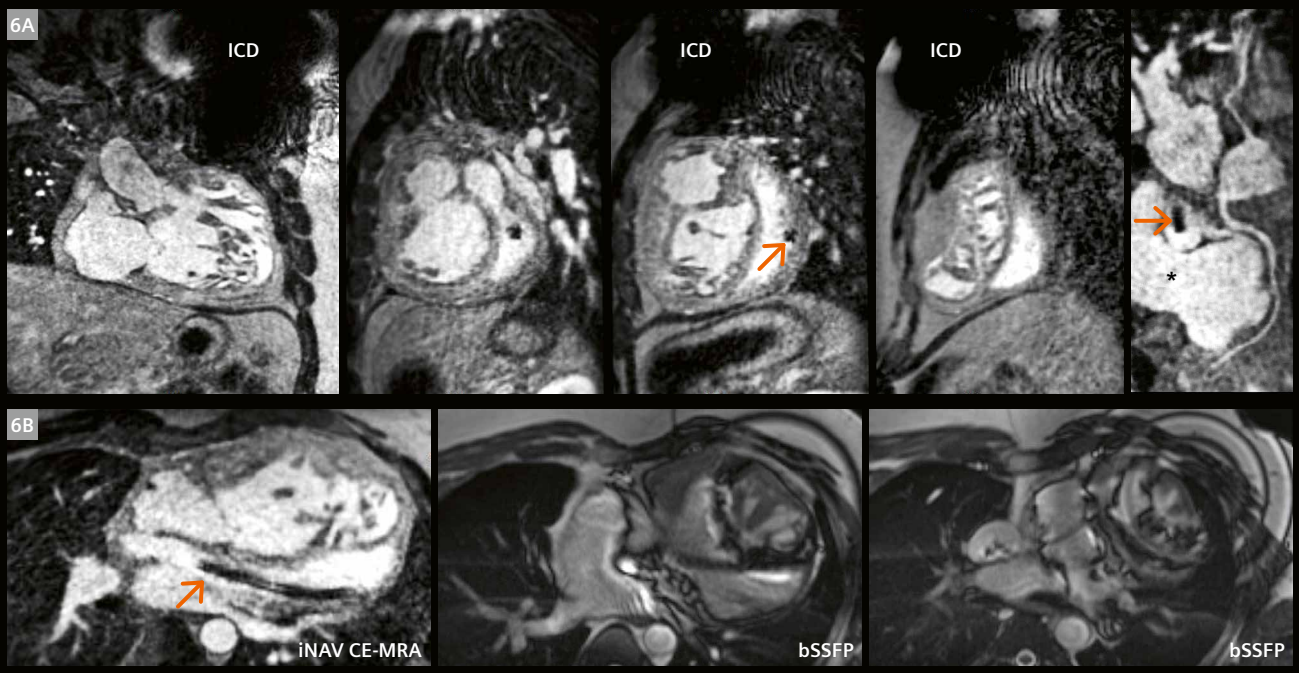

6 A 46-year-old male with a history of D-transposition of the great arteries, status post-atrial switch procedure. Systemic outflow tract **(6A)** and short-axis views demonstrate enlargement of the systemic ventricle and large signal void artifact from the internal cardiac defibrillator (ICD). The coronary artery origins are normal, with demonstration of systemic venous baffle patency and ICD lead within (orange arrows). The pulmonary venous baffle (asterisk) is also widely patent. Extensive artifact is present on balanced steady-state free precession (bSSFP) images compared to wideband iNAV CE-MRA **(6B)**.

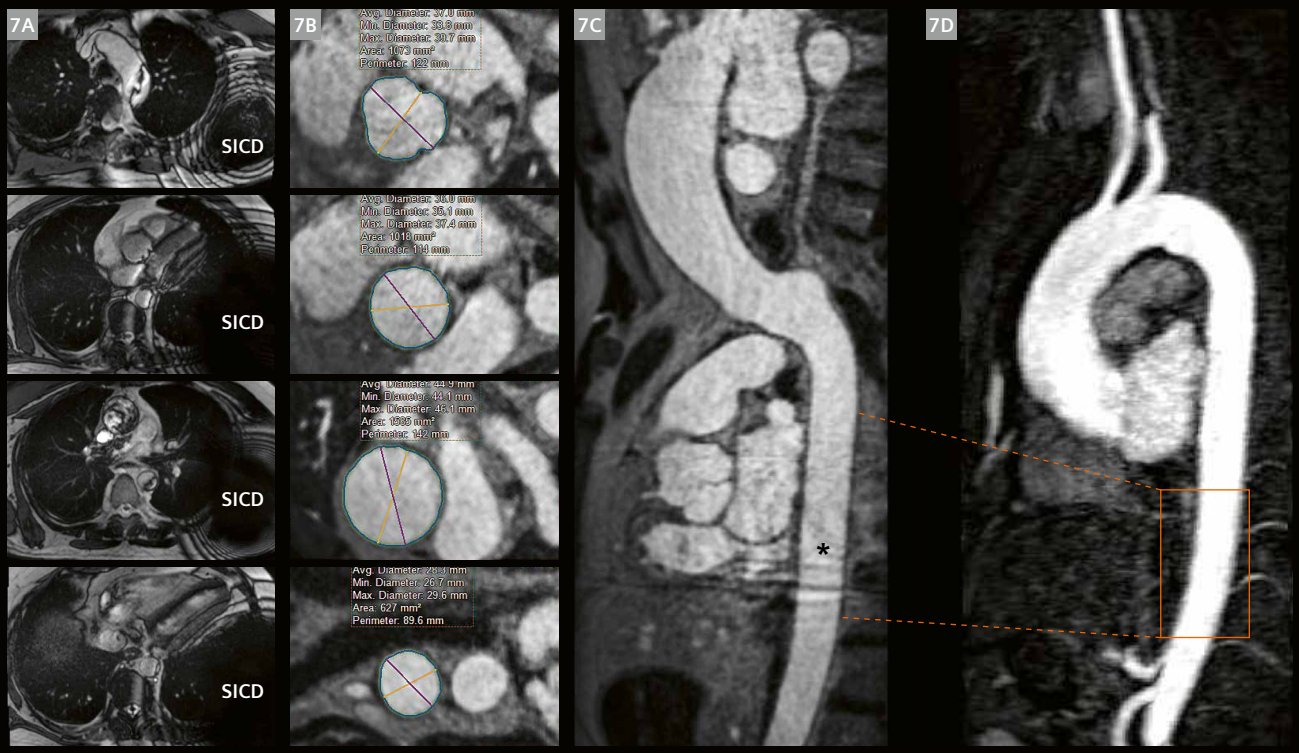

7 A 59-year-old male with subcutaneous internal cardiac defibrillator (SICD). **(7A)** Balanced steady-state free precession (bSSFP) axial images contain extensive artifacts. **(7B)** Centerline semiautomated aortic measurements (CSAM) of the sinus of Valsalva, sinotubular junction, ascending aorta, and arch are still feasible. **(7C)** With use of wideband iNAV CE-MRA, rippling artifacts (asterisks) were still present, overlaying the thoracic descending aorta; however, **(7D)** time-resolved MRA is free from artifacts.

Full aortic imaging

Lifelong aortic surveillance is needed after surgical repair or for medically treated disease. Full-field-of-view coronal imaging is not adequate to capture the entire aorta, arch vessels, and iliofemoral vessels in all patients. Therefore, a combination of acquisitions is often necessary.

Several non-contrast techniques have been used for abdominopelvic MRA. IR inflow techniques are most suitable for small-volume acquisitions. Quiescent-interval single-shot (QISS), with bSSFP, or radial FLASH readout can be acquired with breath-hold or free breathing, respectively, although the former is susceptible to inhomogeneity artifacts. Furthermore, all the above techniques require cardiac gating, which reduces acquisition efficiency. More recent developments include ungated 3D T2-prepared Dixon GRE. However, navigator gating and a comparatively longer repetition time likewise decrease the efficiency of the technique. While large-volume non-contrast techniques require an acquisition duration that spans several minutes, first-pass CE-MRA can be performed in a single breath-hold.

First-pass CE-MRA can be readily combined with iNAV CE-MRA with or without TWIST (Figs. 3, 4, 8, and 9) to provide extended coverage since aortic dissection and manifestations of systemic illnesses may not be isolated to the thoracic region (Fig. 10). Without TWIST, arterial and venous phase high-resolution abdominopelvic CE-MRA images are acquired with Care Bolus, immediately followed by iNAV CE-MRA. Without injector pause, the 0.1 mmol/kg GBCA continuous infusion is administered after the initial contrast/saline bolus combination. Because first-pass MRA is acquired with 0.1 mmol/kg of GBCA, (instead of the standard TWIST dose of 0.05 mmol/kg), the extra intravascular signal is used to acquire iNAV CE-MRA at 1.2 mm isotropic spatial resolution with higher acceleration factor and no overall increase in acquisition duration. Figure 9 is an example of full aortic imaging acquired using first-pass abdominopelvic MRA followed by iNAV CE-MRA at 1.2 mm isotropic spatial resolution.

For TEVAR hybrid repairs, TWIST is important for evaluation of the endograft. For this protocol, we start with the standard TWIST using 0.05 mmol/kg of 1-molar contrast agent with 30 mL saline, followed by 0.1 mmol/kg GBCA infusion for iNAV CE-MRA without delay. This is followed by Care Bolus and first-pass CE-MRA of the abdomen and pelvis with the remaining 0.05 mmol/kg GBCA.

Combined iNAV CE-MRA and LGE imaging

Many conditions, such as hypertension, vasculitis, and atherosclerotic disease, affect the thoracic vasculature and have downstream effects on the myocardium. Depending on the indication or clinical question, both thoracic MRA and cardiac MRI may be required within the same exam (Fig. 11). Tissue characterization with delayed enhancement imaging and extracellular volume fraction provide highly desirable information; therefore, it may be preferable to acquire gated MRA using GBCA. iNAV CE-MRA is compatible with the typical workhorses of the CMR imaging suite, such as bSSFP cine, post-contrast T1 parametric mapping, and late gadolinium enhancement.

Assessing intracardiac anatomy

4D flow has proven effective in quantifying hemodynamic properties across a large volume of anatomical coverage, given the ability to retrospectively prescribe any slice plane for analysis. Characterization of relatively low intracardiac velocities is most impacted by limited velocity-to-noise ratio (VNR) without GBCA at 1.5T. Technical adjustments may be required to increase acquired voxel size and to lower the acceleration factor and/or the receiver bandwidth as compensation. The proposition of highly undersampled *k*-space acquisition with Compressed-Sensing reconstruction is especially attractive, given the significantly shorter acquisition time. Compared to conventional 4D flow, there is significant underestimation of mitral-valve forward and net volumes, early-to-active left ventricular filling velocity ratio [17], aortic-valve forward volume, peak aortic systolic velocity [18], and higher noise values with increasing acceleration factors [19]. As a contrast-enhanced technique, iNAV CE-MRA provides the secondary benefit of boosting 4D flow SNR by up to 1.8× [19], which can be traded for higher spatiotemporal fidelity. Additionally, a key advantage of gated iNAV CE-MRA is the assessment of intracardiac structure and anatomical defects. These include atrial and ventricular septal defects, and arteriovenous connections. The high-resolution anatomic information is complementary to phase-contrast MRI quantitative flow data (Fig. 12).

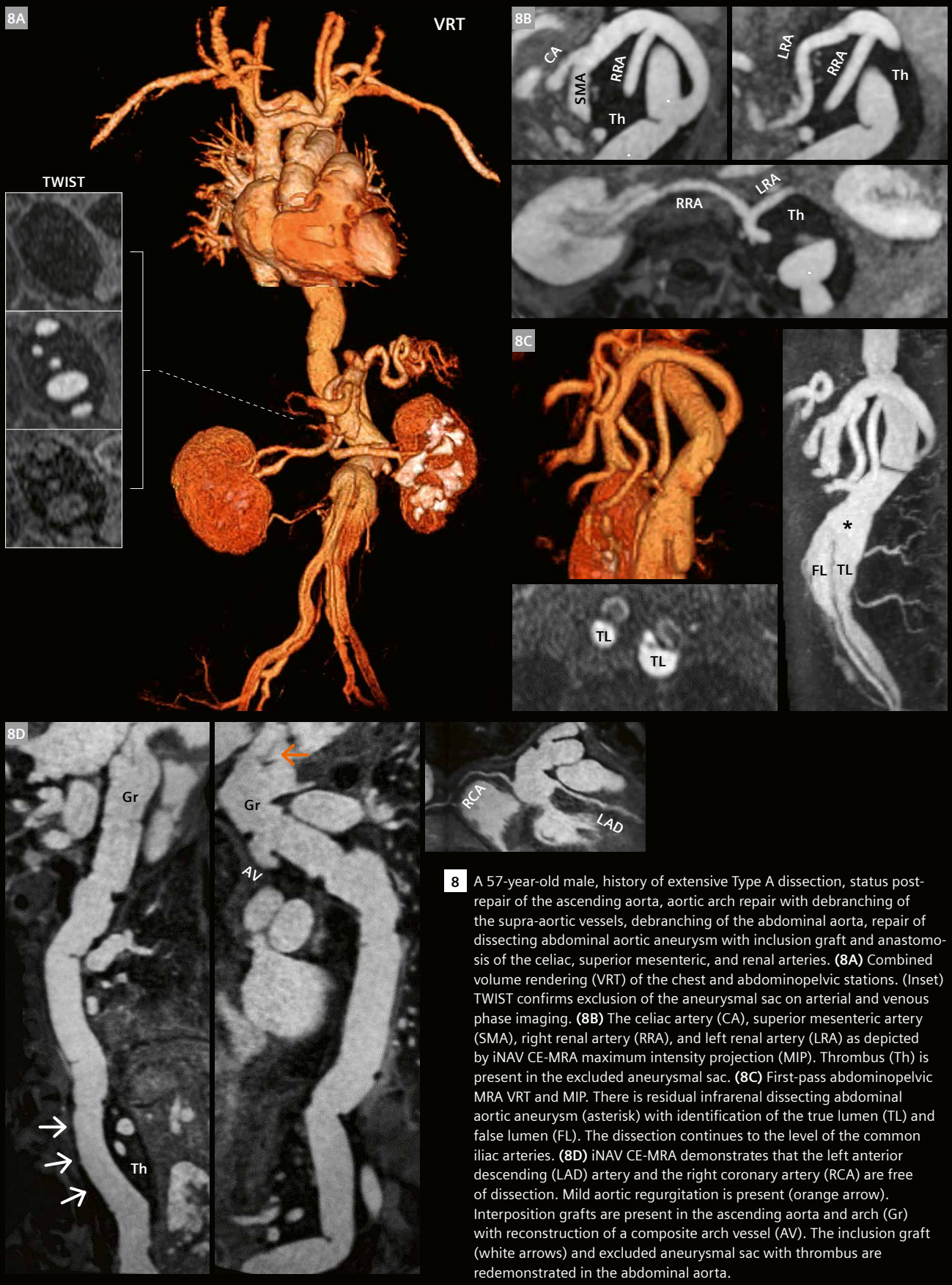

8 A 57-year-old male, history of extensive Type A dissection, status post-repair of the ascending aorta, aortic arch repair with debranching of the supra-aortic vessels, debranching of the abdominal aorta, repair of dissecting abdominal aortic aneurysm with inclusion graft and anastomosis of the celiac, superior mesenteric, and renal arteries. **(8A)** Combined volume rendering (VRT) of the chest and abdominopelvic stations. (Inset) TWIST confirms exclusion of the aneurysmal sac on arterial and venous phase imaging. **(8B)** The celiac artery (CA), superior mesenteric artery (SMA), right renal artery (RRA), and left renal artery (LRA) as depicted by iNAV CE-MRA maximum intensity projection (MIP). Thrombus (Th) is present in the excluded aneurysmal sac. **(8C)** First-pass abdominopelvic MRA VRT and MIP. There is residual infrarenal dissecting abdominal aortic aneurysm (asterisk) with identification of the true lumen (TL) and false lumen (FL). The dissection continues to the level of the common iliac arteries. **(8D)** iNAV CE-MRA demonstrates that the left anterior descending (LAD) artery and the right coronary artery (RCA) are free of dissection. Mild aortic regurgitation is present (orange arrow). Interposition grafts are present in the ascending aorta and arch (Gr) with reconstruction of a composite arch vessel (AV). The inclusion graft (white arrows) and excluded aneurysmal sac with thrombus are redemonstrated in the abdominal aorta.

9 A 58-year-old male with a history of Type A aortic dissection, status post-repair. Whole-chest acquisition duration was 4.84 minutes with 1.2 mm isotropic acquired spatial resolution. **(9A)** Volume rendering (VRT) of the combined iNAV and first-pass CE-MRA with coverage to the level of the femoral vessels. Residual aortic dissection extending to the right common iliac artery and infrarenal aortic aneurysm is visible (white arrows). **(9B)** Complex to-and-fro flow patterns across the dissection flap (white asterisk) result in dephasing artifacts on balanced steady-state free precession (bSSFP) images. Susceptibility artifacts from sternal wires also encroach into the aortic arch intravascular space (white arrows). **(9C)** The right coronary artery (RCA), left anterior descending (LAD) artery, and left circumflex (LCX) artery are free from dissection. **(9D)** In comparison to bSSFP, iNAV CE-MRA curved multiplanar reconstructions (MPRs) are free from significant artifacts. Distal to the ascending aortic graft (Gr) insertion, the dissection flap (black asterisk), false lumen (FL), and true lumen (TL) can be visualized. **(9E)** Maximal intensity projection (MIP) of first-pass abdominopelvic MRA demonstrates continuation of aortic dissection of true lumen (TL) and false lumen (FL) to the abdominal aorta.

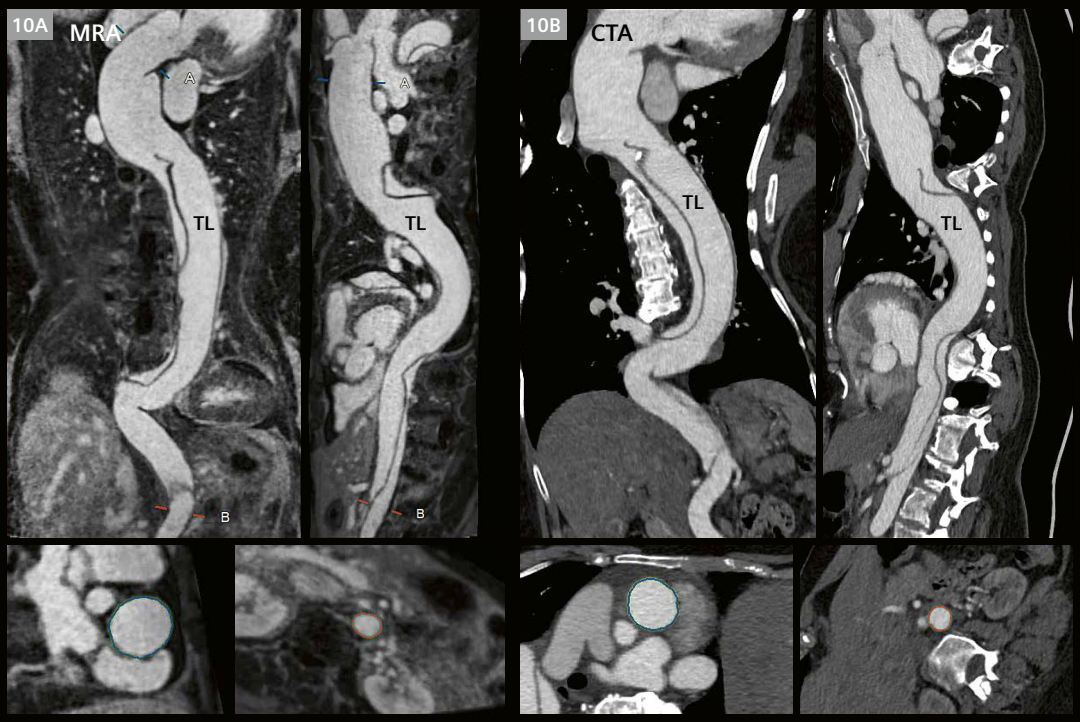

10 Comparison of iNAV CE-MRA **(10A)** and CTA **(10B)** curved multiplanar reconstruction (MPR) images in a patient with Type A aortic dissection extending beyond the thoracic station.

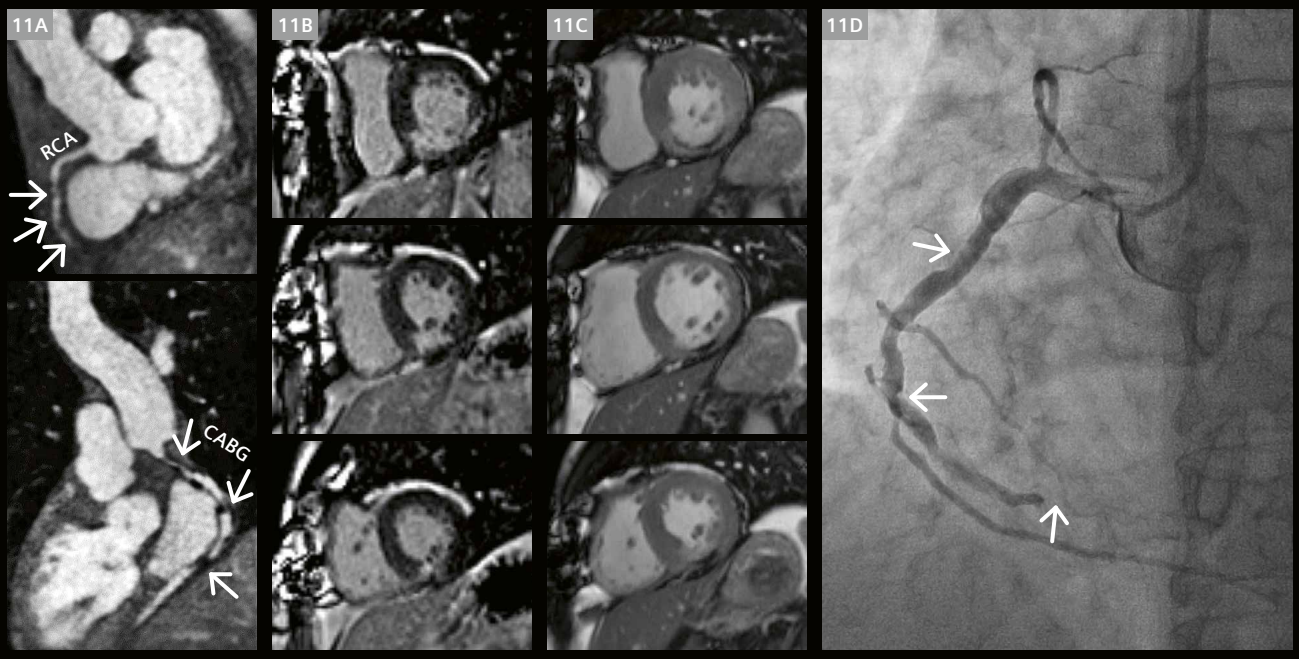

11 A 62-year-old male with a history of coronary artery disease and coronary artery bypass grafts. **(11A)** Multifocal stenosis and midvessel occlusion (white arrows) are present in the right coronary artery (RCA), with severe disease of the coronary artery bypass graft (CABG) to posterior descending artery (white arrows). **(11B, 11C)** Late gadolinium enhancement and cine images respectively demonstrate inferior wall myocardial infarction. **(11D)** Invasive coronary angiogram in the same patient with corresponding stenosis and occlusion of the mid-RCA (white arrows).

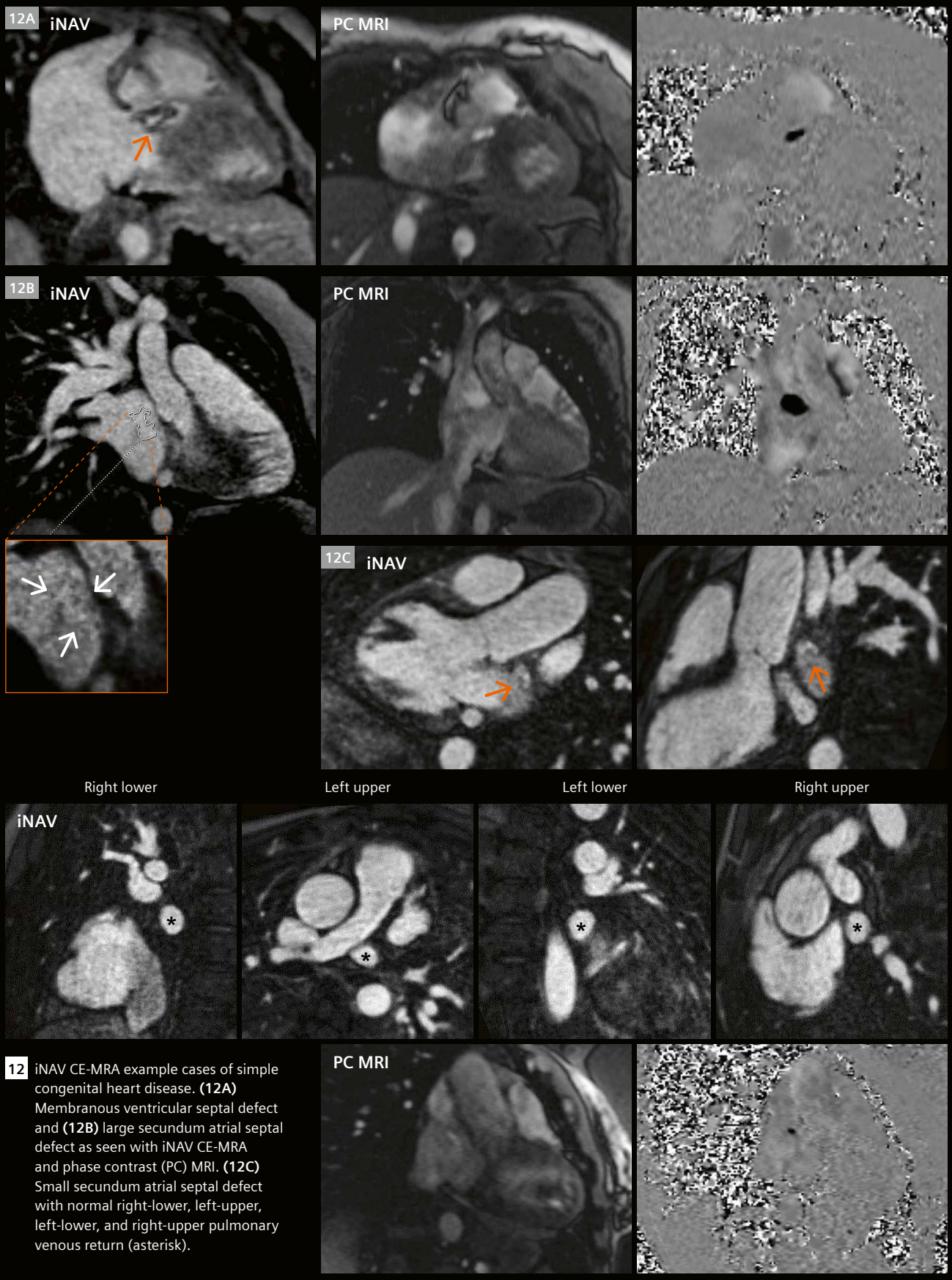

12 iNAV CE-MRA example cases of simple congenital heart disease. **(12A)** Membranous ventricular septal defect and **(12B)** large secundum atrial septal defect as seen with iNAV CE-MRA and phase contrast (PC) MRI. **(12C)** Small secundum atrial septal defect with normal right-lower, left-upper, left-lower, and right-upper pulmonary venous return (asterisk).

In summary, with the iNAV/VD-CASPR framework gated MRA can be performed with 100% respiratory efficiency and thus with a predictable acquisition duration. Both non-contrast and contrast-enhanced techniques have been used, each with its own distinct advantages and disadvantages. iNAV CE-MRA can be combined with TWIST and abdominopelvic first-pass CE-MRA for dynamic information and/or extended coverage, respectively. Based on our single-center experience, this allows for versatile and efficient imaging that shows promise in complex patients with extensive aortic repairs, obesity, and implantable cardiac devices and is robust to magnetic field inhomogeneity and local susceptibility artifacts.

References

1 Munoz C, Bustin A, Neji R, Kunze KP, Forman C, Schmidt M, et al. Motion-corrected 3D whole-heart water-fat high-resolution late gadolinium enhancement cardiovascular magnetic resonance imaging. J Cardiovasc Magn Reson. 2020;22(1):53.
2 Groarke JD, Waller AH, Vita TS, Michaud GF, Di Carli MF, Blankstein R, et al. Feasibility study of electrocardiographic and respiratory gated, gadolinium enhanced magnetic resonance angiography of pulmonary veins and the impact of heart rate and rhythm on study quality. J Cardiovasc Magn Reson. 2014;16(1):43.
3 Siebermair J, Kholmovski EG, Sheffer D, Schroeder J, Jensen L, Kheirkhahan M, et al. Saturation recovery-prepared magnetic resonance angiography for assessment of left atrial and esophageal anatomy. Br J Radiol. 2021;94(1123):20210048.
4 Craft J, Parikh R, Cheng JY, Diaz N, Kunze KP, Schmidt M, et al. Isotropic, high-resolution, whole-chest inversion recovery contrast-enhanced magnetic resonance angiography in under 4.5 min using image-based navigator fluoro trigger. Front Cardiovasc Med. 2025;12:1549275.
5 Bley TA, Wieben O, François CJ, Brittain JH, Reeder SB. Fat and water magnetic resonance imaging. J Magn Reson Imaging. 2010;31(1):4–18.
6 Wood G, Pedersen AU, Kunze KP, Neji R, Hajhosseiny R, Wetzl J, et al. Automated detection of cardiac rest period for trigger delay calculation for image-based navigator coronary magnetic resonance angiography. J Cardiovasc Magn Reson. 2023;25(1):52.
7 NCD Risk Factor Collaboration (NCD-RisC). Worldwide trends in underweight and obesity from 1990 to 2022: a pooled analysis of 3663 population-representative studies with 222 million children, adolescents, and adults. Lancet. 2024;403(10431):1027–1050.
8 Thorpe KE, Joski PJ. Estimated Reduction in Health Care Spending Associated With Weight Loss in Adults. JAMA Netw Open. 2024;7(12):e2449200.
9 Tandon A, Hashemi S, Parks WJ, Kelleman MS, Sallee D, Slesnick TC. Improved high-resolution pediatric vascular cardiovascular magnetic resonance with gadofosveset-enhanced 3D respiratory navigated, inversion recovery prepared gradient echo readout imaging compared to 3D balanced steady-state free precession readout imaging. J Cardiovasc Magn Reson. 2016;18(1):74.
10 Craft J, Weber J, Li Y, Cheng JY, Diaz N, Kunze KP, et al. Inversion recovery and saturation recovery pulmonary vein MR angiography using an image based navigator fluoro trigger and variable-density 3D cartesian sampling with spiral-like order. Int J Cardiovasc Imaging. 2024;40(6):1363–1376.
11 Sperry BW, Vamenta MS, Gunta SP, Thompson RC, Einstein AJ, Castillo M, et al. Influence of Body Mass Index on Radiation Exposure Across Imaging Modalities in the Evaluation of Chest Pain. J Am Heart Assoc. 2024;13(8):e033566.
12 Mazzolai L, Teixido-Tura G, Lanzi S, Boc V, Bossone E, Brodmann M, et al. 2024 ESC Guidelines for the management of peripheral arterial and aortic diseases. Eur Heart J. 2024;45(36):3538–3700.
13 Habets J, Zandvoort HJ, Reitsma JB, Bartels LW, Moll FL, Leiner T, et al. Magnetic resonance imaging is more sensitive than computed tomography angiography for the detection of endoleaks after endovascular abdominal aortic aneurysm repair: a systematic review. Eur J Vasc Endovasc Surg. 2013;45(4):340–50.
14 Ammannaya GKK. Implantable cardioverter defibrillators – the past, present and future. Arch Med Sci Atheroscler Dis. 2020;5:e163–e170.
15 Bhatia N, El-Chami M. Leadless pacemakers: a contemporary review. J Geriatr Cardiol. 2018;15(4):249–253.
16 Ibrahim EH, Runge M, Stojanovska J, Agarwal P, Ghadimi-Mahani M, Attili A, et al. Optimized cardiac magnetic resonance imaging inversion recovery sequence for metal artifact reduction and accurate myocardial scar assessment in patients with cardiac implantable electronic devices. World J Radiol. 2018;10(9):100–107.
17 Varga-Szemes A, Halfmann M, Schoepf UJ, Jin N, Kilburg A, Dargis DM, et al. Highly Accelerated Compressed-Sensing 4D Flow for Intracardiac Flow Assessment. J Magn Reson Imaging. 2023;58(2):496–507.
18 Neuhaus E, Weiss K, Bastkowski R, Koopmann J, Maintz D, Giese D. Accelerated aortic 4D flow cardiovascular magnetic resonance using compressed sensing: applicability, validation and clinical integration. J Cardiovasc Magn Reson. 2019;21(1):65.
19 Hess AT, Bissell MM, Ntusi NA, Lewis AJ, Tunnicliffe EM, Greiser A, et al. Aortic 4D flow: quantification of signal-to-noise ratio as a function of field strength and contrast enhancement for 1.5T, 3T, and 7T. Magn Reson Med. 2015;73(5):1864–71.

Contact

Jason Craft, M.D.
Director, Cardiac MRI
Good Samarian University Hospital
West Islip, NY, USA

Associate Director, Cardiac MRI
St Francis Hospital & Heart Center
100 Port Washington Blvd
Roslyn, NY 11576
USA
Jason.craft@chsli.org

From Diagnosis to Lifelong Care: Cardiac Magnetic Resonance in Adult Congenital Heart Disease

Fabienne Dirbach[1]; Marco Müller[2]; Christopher W. Roy[2]; Paolo Garelli[1]; Jürg Schwitter[1,3]; Matthias Stuber[2,4]; Tobias Rutz[1,3]

[1]Service of Cardiology, Lausanne University Hospital and University of Lausanne, Switzerland
[2]Department of Diagnostic and Interventional Radiology, Lausanne University Hospital and University of Lausanne, Switzerland
[3]Centre de résonance magnétique cardiaque (CRMC) du CHUV, Lausanne University Hospital, Lausanne, Switzerland
[4]Center for Biomedical Imaging (CIBM), Lausanne, Switzerland.
[5]Swiss Innovation Hub, Siemens Healthineers International AG, Lausanne, Switzerland

The cornerstone of imaging in adult congenital heart disease

Survival of patients with congenital heart disease (CHD) has dramatically improved over the last 30 years. Over 97% of patients now reach adulthood and due to increased survival, the number of adult patients has outgrown the pediatric population [1, 2]. However, despite their improved survival, CHD patients cannot be considered as cured. The increased life expectancy exposes them to potential complications such as arrhythmias, stroke, heart failure, valvular heart lesions, and pulmonary arterial hypertension (PAH) [3–10].

Due to their high risk of complications, patients with CHD need life-long specialized follow-up [11]. Imaging plays a central role in diagnosis and surveillance, particularly for valvular lesions, shunt quantification and assessment of cardiac volumes, and function [12]. While transthoracic echocardiography (TTE) remains the first-line modality, it has several limitations in CHD, particularly in the assessment of right-heart lesions, which are frequently encountered in the CHD population [12, 13]. Cardiac magnetic resonance (CMR) overcomes these limitations and is considered the gold standard for non-invasive evaluation of ventricular volumes, myocardial structure, and flow evaluation [14–17]. The latter is particularly important in assessing shunt lesions or valvular pathologies.

A glimpse of our institution

The Centre Hospitalier Universitaire Vaudois (CHUV), in Lausanne in Switzerland is a tertiary referral center for CHD, providing highly specialized care for this growing patient population. Due to the improved survival rate, our clinical activity is increasing by 10% per year. CMR is fully integrated into our clinical practice, with close collabora-

	Localizer, TRUFI	bSSFP cine (4, 3, 2 chamber and lax RV, +/- RVOT)	T1 map	Angiography	3D whole heart	LGE	2D phase contrast	4D/5D flow	5D (free running for anatomy, function, and flow)
Standard CMR for CHD	+	+	+	+	+	+	+	+	
Accelerated protocol	+	+	+		+		+	+/-	
Future/ideal protocol	+		+			+			+

Table 1: Abbreviations: CHD = congenital heart disease, CMR = cardiac magnetic resonance, TRUFI = true fast imaging, bSSFP = balanced steady-state free precession, lax = long axis, RV = right ventricle, RVOT = right ventricular outflow tract, LGE = late gadolinium enhancement

tion between CHD specialists, MRI clinicians, as well as researchers, engineers, and data scientists. Interdisciplinary meetings allow clinicians to articulate clinical needs, enable researchers to promptly address practical challenges in the implementation of novel imaging sequences, and facilitate rapid translation of technical advances into clinical practice. This unique multidisciplinary approach allows to continuously push technical boundaries, refine imaging sequences, and enhance diagnostic accuracy. Ongoing innovation in MRI technology enables improvement in image quality, optimization of follow-up measurements, and implementation of faster, more efficient protocols aiming to meet the increasing demand for high-quality CMR in this complex patient population.

Evolving workflows in congenital cardiac MRI

Since the number of adult CHD patients and consequently the demand for congenital CMR is steadily increasing, rapid access to CMR has become increasingly challenging due to long waiting times. To address this issue and expand the number of examinations performed per week, our center introduced a "short CMR" strategy in 2024. In this approach, selected patients undergo an accelerated protocol tailored to the clinical indication and the need for contrast administration.

A standard protocol, typically lasting around 60 minutes, includes the following: localizers; *syngo* NATIVE (true fast imaging with steady-state free precession; TRUFI, SSFP); in axial, coronal, and sagittal planes; long- and short-axis compressed sensing cine SSFP; 3D self-navigated whole-heart imaging; T1 mapping; and 2D as well as 4D or 5D flow acquisitions [18, 19]. When injection of contrast agent is required, contrast-enhanced angiography and late gadolinium enhancement sequences are added. By comparison, the short CMR protocol currently requires approximately 40 minutes and typically does not involve the administration of contrast agent.

To further improve efficiency, facilitate CMR, and reduce examination duration, novel techniques are under active development at our center. Free-running techniques are a promising approach as they are fully free-breathing sequences that require neither ECG triggering nor respiratory gating and allow visualization of anatomy, evaluation of cardiac structures throughout the cardiac cycle, and flow quantification. Such an approach could significantly enhance efficiency while simultaneously improving patient comfort. The ultimate goal is an integrated 5D sequence capable of providing comprehensive anatomical, functional, and flow information within a single acquisition.

Table 1 illustrates the workflows of the current standard CMR protocol, the accelerated protocol, and a proposed future 5D protocol.

CMR image acquisition and reconstruction

At our institution, CMR for adult CHD patients is usually performed on a 1.5T clinical MR scanner (MAGNETOM Sola, Siemens Healthineers, Erlangen, Germany) with an 18-channel surface coil.

The *Respiratory Self-Navigated Whole-Heart and Coronary Imaging*[1] research sequence enables free-breathing 3D radial CMR imaging with simple planning and efficient scans. It provides high-resolution assessment of cardiac anatomy and facilitates fast, straightforward whole-heart coronary angiography without the need for a respiratory navigator. Motion-robust radial 3D acquisitions with superior-inferior (SI) respiratory compensation ensure good image quality, while self-navigation reduces scan time and achieves exam duration predictability from the subject's cardiac frequency. The inline reconstruction automatically selects coil elements with the highest heart signal for optimal self-navigation and integrates 1D and iterative respiratory self-navigation with online motion correction. It performs rapid 3D gridding and reconstruction of isotropic radial datasets within 30–60 seconds. All 3D acquisitions are acquired during a prospectively chosen mid-diastolic resting phase.

The *Advanced Flow Imaging*[1] research sequence introduces symmetric velocity encoding, where flow encoding is distributed across all acquisitions, reducing echo times, minimizing intra-voxel dephasing, and enabling shared velocity reconstruction compared to conventional asymmetric encoding. It also integrates compressed sensing (CS) and Respiratory-Controlled Adaptive *k*-space Reordering (ReCAR) to allow efficient 2D/4D flow imaging with reduced respiratory motion artifacts by synchronizing *k*-space acquisition with respiratory phases. Reconstruction is performed using a graphics-processing-unit-accelerated nonlinear iterative algorithm with coil sensitivity mapping. This enables high-quality online results without reference scans and with reconstruction times under five minutes for an aorta 4D flow protocol.

The free-running *Fast-Interrupted Steady-State (FISS) sequence*[1] is used to acquire trigger-free fat-suppressed cardiac and respiratory-resolved 5D images in CHD patients [20]. The acquisition is reconstructed offline into 5D cardiac and respiratory motion-resolved images using a fully self-gated compressed sensing reconstruction available as C2P developed by CHUV [21–24].

[1] *Work in progress. The sequence is still under development and not commercially available. Its future availability cannot be ensured.*

Clinical application of highly efficient MR sequences from Siemens Healthineers in daily practice

Case 1: Aortic root dilation in a patient with Turner syndrome

This is a female patient with Turner syndrome, known for a bicuspid aortic valve, dilation of the aortic root, and an anomalous pulmonary venous return of the right superior pulmonary vein. CMR was indicated for follow-up assessment of aortic root dimensions and shunt quantification. The patient was selected for a short CMR protocol (40 minutes) without planned contrast administration.

Standard imaging was acquired, including localizers, TRUFI, and cine bSSFP images, followed by native T1 mapping, 3D whole-heart, and FISS for evaluation of the aortic valve during the cardiac cycle.

Aortic root diameters were measured on the 3D whole-heart sequence, a self-navigated acquisition obtained in diastole. Maximal diameters from cusp to cusp were 32 × 33 × 36 mm, corresponding to a significant dilation for a patient with Turner syndrome (22.5 mm/m^2, z-score 3.46) and fulfilling the criteria for aortic root surgery (Fig. 1).

Measurements obtained with the free-running 5D FISS sequence were identical (32 × 33 × 36 mm, Figs. 1 and 2). As proposed by the current European Society of Cardiology (ESC) guidelines, a cardiac CT was performed for validation, yielding comparable values (31 x 34 x 37 mm), well within the accepted ± 2 mm variability (Fig. 1) [25].

This case illustrates the clinical utility of the 3D whole-heart sequence for accurate assessment and follow-up of great vessel dimensions. Acquisition requires only approximately six minutes, allows immediate reconstruction, and provides measurements comparable to cardiac CT, all without contrast administration. The free-running 5D FISS sequence, while currently offering slightly lower spatial resolution and longer reconstruction times, also yielded consistent aortic root measurements, highlighting its potential as a promising non-contrast technique for future clinical applications (Figs. 1 and 2).

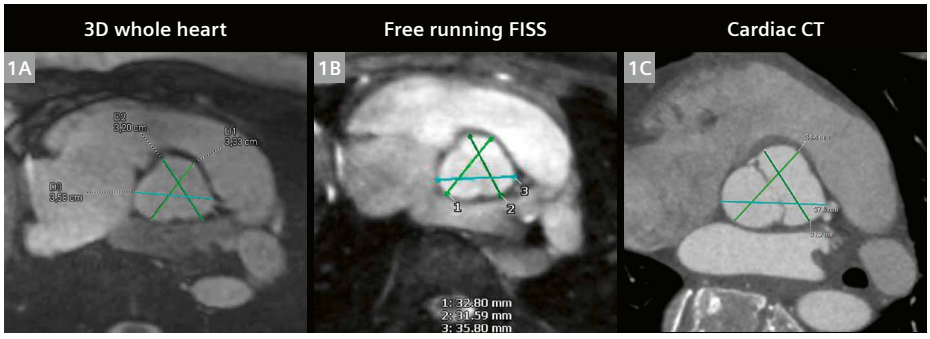

1 **(1A)** 3D whole-heart, self-navigated diastolic sequence, aortic root measurements cusp-cusp: 32 × 33 × 36 mm. **(1B)** Free-running FISP, self-navigated, diastolic, and free-breathing, aortic root measurements cusp-cusp: 32 × 33 × 36 mm. **(1C)** Cardiac CT, aortic root measurements cusp-cusp: 31 × 34 × 37 mm.

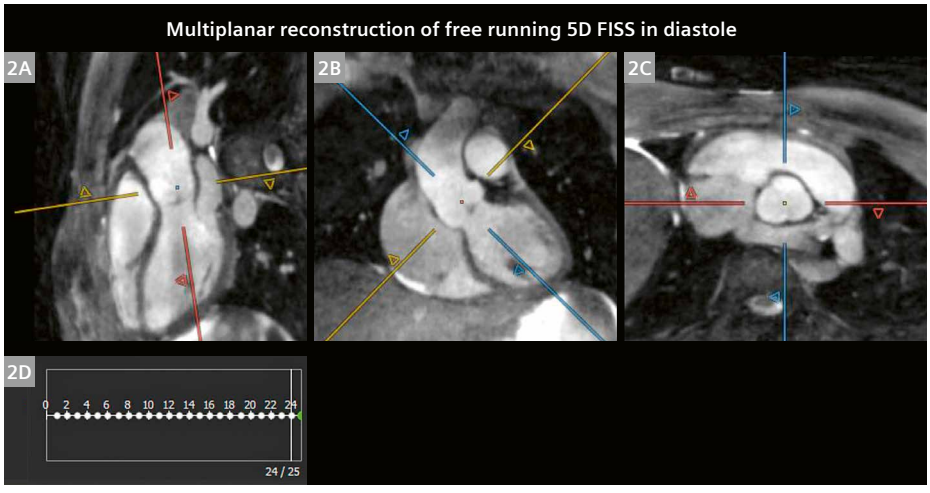

2 **(2A–2C)** Multiplanar reconstruction in three planes, helping to correctly align onto the aortic root. **(2D)** Cardiac cycle showing acquisition of the multiplanar reconstruction at end-diastole.

Case 2:
Functional and anatomical assessment of d-transposition using 3D and flow imaging

This is a patient with dextro-transposition of the great arteries, surgically corrected in infancy by an arterial switch operation (ASO) with Lecompte maneuver. The patient was known for moderate pulmonary insufficiency, and CMR was indicated for follow-up assessment of biventricular function, great vessel dimensions, pulmonary valve regurgitation, and screening for stenoses in the pulmonary arterial circulation.

The patient underwent a standard CMR protocol (60 minutes). Standard imaging included localizers, TRUFI, and cine bSSFP sequences, followed by 3D whole-heart imaging, T1 mapping, flow measurements (2D phase-contrast and 4D flow), and 5D FISS imaging.

Following an arterial switch operation, patients are at risk of developing stenosis of the pulmonary branch arteries. 5D FISS imaging helped to exclude the presence of an anatomical stenosis of the pulmonary arteries throughout the cardiac cycle. Figure 3 shows the typical image after a Lecompte maneuver, with the pulmonary trunk positioned anteriorly and the pulmonary branch arteries running to the right and left of the ascending aorta. 4D flow imaging permitted visualization of flow through the pulmonary and systemic circulation using path- and streamlines. Flow quantification using the Circle cvi42 software (Circle Cardiovascular Imaging Inc., Calgary, AB, Canada) calculated an equal distribution of pulmonary flow between the right and left pulmonary branch arteries, thus confirming the absence of a relevant stenosis.

This case demonstrates the utility of advanced CMR sequences – including 3D whole-heart imaging, 4D flow, and free-running 5D FISS – for providing comprehensive anatomical and functional assessment in complex post-surgical CHD patients.

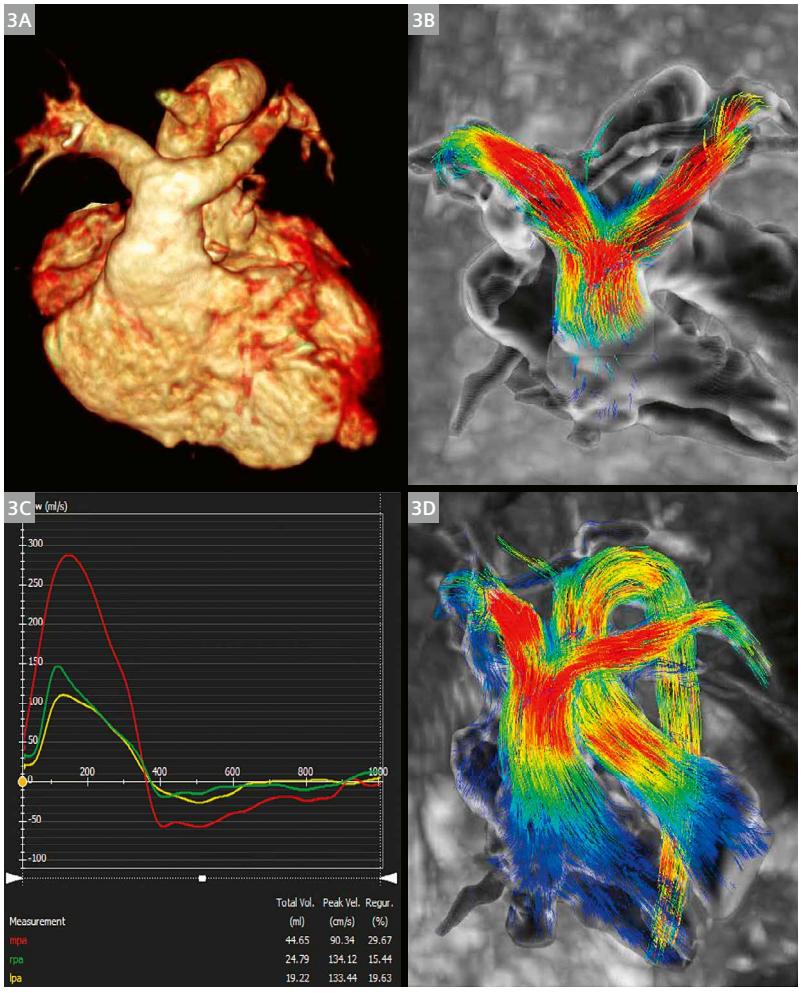

3 **(3A)** 3D reconstruction of the FISS showing the transposition of the great arteries. **(3B)** 4D flow showing flow in the pulmonary circulation. **(3C)** 4D flow measures in the main (mpa), right (rpa), and left (lpa) pulmonary artery. **(3D)** 4D flow image showing flow streamlines during systole.

Case 3: Complex aortic coarctation with extracardiac bypass

This patient with a history of aortic coarctation underwent surgical resection in childhood, followed by stenting for recoarctation. Due to persistently low descending aortic flow, she later underwent aortic bypass surgery, with implantation of a 14 mm Gore-Tex graft from the ascending to the descending aorta. CMR was indicated for follow-up assessment of biventricular function, aortic dimensions, and flow assessment within the thoracic aorta.

The patient underwent a standard CMR protocol (60 minutes), including localizers, TRUFI, and cine bSSFP sequences, followed by contrast-enhanced angiography. Additional acquisitions included 5D FISS, T1 mapping, and 2D phase-contrast flow and 4D flow measurements.

The free-running FISS sequence allowed precise measurement of aortic diameters along the entire aorta and the extracardiac conduit (Fig. 4), facilitating surveillance of the dilation in the descending aorta distal to the ascendens-descendens graft anastomosis. 4D flow imaging provided additional insights, enabling comprehensive flow evaluation of the ascendens-descendens graft and the thoracic aorta (Fig. 5). Flow quantification showed that the graft flow represented 28% of the total systemic output and provided 48% of the cardiac output to the inferior body half.

The 4D flow assessment allowed three-dimensional visualization of the entire aortic circuit and identification of turbulent flow at the distal anastomosis (Fig. 5). The latter is critical as it is a risk factor for future development of dilatation in this region, which requires a dedicated follow-up.

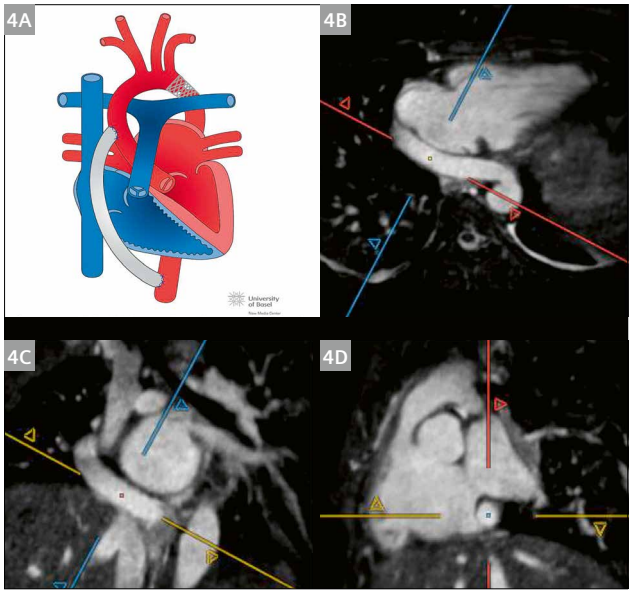

4 **(4A)** Model of aortic coarctation after repair by implantation of an ascendens-descendens graft. **(4B–4D)** Multiplanar reconstruction of FISS showing the ascendens-descendens graft.

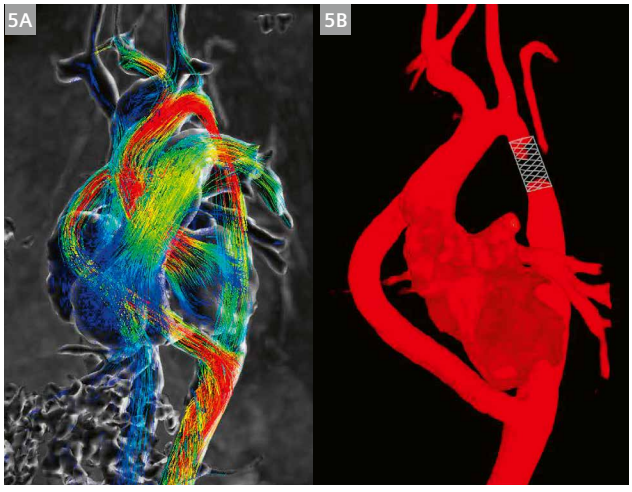

5 **(5A)** 4D flow showing flow through the ascending, descending aorta and through the graft. **(5B)** 3D reconstruction of the angiography showing the aorta, the ascendens-descendens graft, and the stent in the region of the coarctation.

Outlook and conclusions

As outlined above, the rapidly growing population of adults with CHD has led to an increasing demand for CMR examinations. To meet this demand and ensure high-quality care for diagnosis and follow-up, there is an urgent need for faster and more efficient CMR protocols that maintain diagnostic accuracy while also improving patient comfort and accessibility.

At our center, novel techniques are being actively developed to address these challenges. Free-running sequences that require neither contrast administration, ECG triggering, respiratory gating, breath holding, nor sophisticated plan-scanning are particularly promising approaches.

Early results from implementing these free-breathing techniques at our institution are encouraging, and the sequences are gradually being introduced into clinical practice. However, further refinement is still required. Importantly, validation in larger patient cohorts remains essential, and a prospective multicenter study is currently planned.

The ultimate goal would be to develop an integrated 5D sequence capable of providing comprehensive anatomical, functional, and flow information within a single acquisition [26]. Such methods have the potential to markedly shorten examination times, thereby increasing efficiency while maintaining image quality, diagnostic accuracy, and reproducibility. In future, these images could be acquired in a local center and then analyzed remotely by a specialist. This could improve accessibility to CMR, particularly in regions with less direct access to cardiologists or radiologists specialized in congenital CMR.

In conclusion, we rely on further technical advances and interdisciplinary collaborations to ensure that CMR continues to provide precise, patient-centered imaging while becoming faster and more efficient, thereby securing optimal care for patients with CHD.

Abbreviations:

ASO: Arterial Switch Operation
bSSFP: Balanced steady-state free precession
CHD: Congenital heart disease
CMR: Cardiac magnetic resonance
CT: Computed tomography
ECG: Electrocardiogram
FISS: Fast interrupted steady-state
LGE: Late gadolinium enhancement
lax: Long axis
PAH: Pulmonary arterial hypertension
RV: Right ventricle
RVOT: Right ventricular outflow tract
SSFP: Steady-state free precession
TRUFI: True fast imaging with steady-state free precession
TTE: Transthoracic echocardiography
VENC: Velocity encoding

References

1 Marelli AJ, Ionescu-Ittu R, Mackie AS, Guo L, Dendukuri N, Kaouache M. Lifetime prevalence of congenital heart disease in the general population from 2000 to 2010. Circulation. 2014;130(9):749–56.
2 Mandalenakis Z, Giang KW, Eriksson P, Liden H, Synnergren M, Wahlander H, et al. Survival in Children With Congenital Heart Disease: Have We Reached a Peak at 97%? J Am Heart Assoc. 2020;9(22):e017704.
3 Bouchardy J, Therrien J, Pilote L, Ionescu-Ittu R, Martucci G, Bottega N, et al. Atrial arrhythmias in adults with congenital heart disease. Circulation. 2009;120(17):1679–86.
4 Verheugt CL, Uiterwaal CS, van der Velde ET, Meijboom FJ, Pieper PG, van Dijk AP, et al. Mortality in adult congenital heart disease. Eur Heart J. 2010;31(10):1220–9.
5 Lowe BS, Therrien J, Ionescu-Ittu R, Pilote L, Martucci G, Marelli AJ. Diagnosis of pulmonary hypertension in the congenital heart disease adult population impact on outcomes. J Am Coll Cardiol. 2011;58(5):538–46.
6 Marelli A. Trajectories of care in congenital heart disease – the long arm of disease in the womb. J Intern Med. 2020;288(4):390–399.
7 Kuijpers JM, Vaartjes I, Bokma JP, van Melle JP, Sieswerda GT, Konings TC, et al. Risk of coronary artery disease in adults with congenital heart disease: A comparison with the general population. Int J Cardiol. 2020;304:39–42.
8 Lanz J, Brophy JM, Therrien J, Kaouache M, Guo L, Marelli AJ. Stroke in Adults With Congenital Heart Disease: Incidence, Cumulative Risk, and Predictors. Circulation. 2015;132(25):2385–94.
9 Arnaert S, De Meester P, Troost E, Droogne W, Van Aelst L, Van Cleemput J, et al. Heart failure related to adult congenital heart disease: prevalence, outcome and risk factors. ESC Heart Fail. 2021;8(4):2940–2950.
10 Muller MJ, Norozi K, Caroline J, Sedlak N, Bock J, Paul T, et al. Morbidity and mortality in adults with congenital heart defects in the third and fourth life decade. Clin Res Cardiol. 2022;111(8):900–911.
11 Baumgartner H, De Backer J, Babu-Narayan SV, Budts W, Chessa M, Diller GP, et al. 2020 ESC Guidelines for the management of adult congenital heart disease. Eur Heart J. 2021;42(6):563–645.

12 Burchill LJ, Huang J, Tretter JT, Khan AM, Crean AM, Veldtman GR, et al. Noninvasive Imaging in Adult Congenital Heart Disease. Circ Res. 2017;120(6):995–1014.
13 Mathew RC, Löffler AI, Salerno M. Role of Cardiac Magnetic Resonance Imaging in Valvular Heart Disease: Diagnosis, Assessment, and Management. Curr Cardiol Rep. 2018;20(11):119.
14 Grothues F, Smith GC, Moon JC, Bellenger NG, Collins P, Klein HU, et al. Comparison of interstudy reproducibility of cardiovascular magnetic resonance with two-dimensional echocardiography in normal subjects and in patients with heart failure or left ventricular hypertrophy. Am J Cardiol. 2002;90(1):29–34.
15 Maceira AM, Prasad SK, Khan M, Pennell DJ. Reference right ventricular systolic and diastolic function normalized to age, gender and body surface area from steady-state free precession cardiovascular magnetic resonance. Eur Heart J. 2006;27(23):2879–88.
16 Gordon B, González-Fernández V, Dos-Subirà L. Myocardial fibrosis in congenital heart disease. Front Pediatr. 2022;10:965204.
17 Moscatelli S, Leo I, Lisignoli V, Boyle S, Bucciarelli-Ducci C, Secinaro A, et al. Cardiovascular Magnetic Resonance from Fetal to Adult Life-Indications and Challenges: A State-of-the-Art Review. Children (Basel). 2023;10(5):763.
18 Rutz T, Wustmann K, Prsa M, Vallée J-P, Donner B, Bremerich J, et al. Cardiac magnetic resonance imaging in congenital heart disease. Cardiovascular Medicine. 2016;19:176–184.
19 Fratz S, Chung T, Greil GF, Samyn MM, Taylor AM, Valsangiacomo Buechel ER, et al. Guidelines and protocols for cardiovascular magnetic resonance in children and adults with congenital heart disease: SCMR expert consensus group on congenital heart disease. J Cardiovasc Magn Reson. 2013;15(1):51.
20 Bastiaansen JAM, Piccini D, Di Sopra L, Roy CW, Heerfordt J, Edelman RR, et al. Natively fat-suppressed 5D whole-heart MRI with a radial free-running fast-interrupted steady-state (FISS) sequence at 1.5T and 3T. Magn Reson Med. 2020;83(1):45–55.
21 Di Sopra L, Piccini D, Coppo S, Stuber M, Yerly J. An automated approach to fully self-gated free-running cardiac and respiratory motion-resolved 5D whole-heart MRI. Magn Reson Med. 2019;82(6):2118–2132.
22 Ogier AC, Monton Quesada I, Sieber X, Calarnou P, Ledoux JB, Milani B, et al. Free-running 5D whole-heart MRI for isotropic cardiac function measurements at 3T without contrast agents. Magn Reson Med. 2025;93(6):2386–2400.
23 Roy CW, Milani B, Yerly J, Si-Mohamed S, Romanin L, Bustin A, et al. Intra-bin correction and inter-bin compensation of respiratory motion in free-running five-dimensional whole-heart magnetic resonance imaging. J Cardiovasc Magn Reson. 2024;26(1):101037.
24 Yerly J, Roy CW, Milani B, Eyre K, Raifee MJ, Stuber M. High on sparsity: Interbin compensation of cardiac motion for improved assessment of left-ventricular function using 5D whole-heart MRI. Magn Reson Med. 2025;93(3):975–992.
25 Mazzolai L, Teixido-Tura G, Lanzi S, Boc V, Bossone E, Brodmann M, et al. 2024 ESC Guidelines for the management of peripheral arterial and aortic diseases. Eur Heart J. 2024;45(36):3538–3700.
26 Falcão MBL, Mackowiak ALC, Rossi GMC, Prša M, Tenisch E, Rumac S, et al. Combined free-running four-dimensional anatomical and flow magnetic resonance imaging with native contrast using Synchronization of Neighboring Acquisitions by Physiological Signals. J Cardiovasc Magn Reson. 2024;26(1):101006.

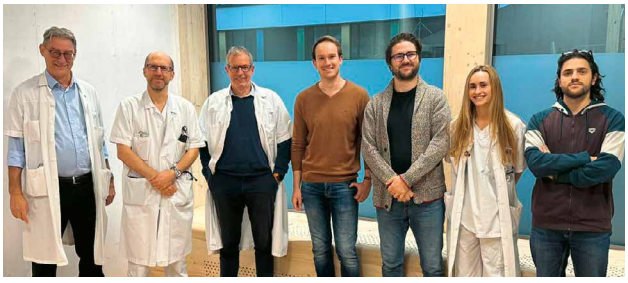

Contact

Tobias Rutz, M.D.
Centre de résonance magnétique cardiaque (CRMC)
CHUV, Lausanne University Hospital
Rue du Bugnon 44/46 BU44/07
CH-1011 Lausanne
Switzerland
Tel.: +41 21 314 48 00
tobias.rutz@chuv.ch

Ebstein's Anomaly: Current Evaluation with CMR

Sergio Patrón, M.D.; Aloha Meave, M.D.

Instituto Nacional de Cardiología Ignacio Chávez, México City, México

Introduction

Ebstein's anomaly (EA) is the most frequent anomaly of the tricuspid valve. Some authors consider it a myopathy of the right ventricle. Its clinical and anatomical features are heterogeneous. Given this variability in its presentation (Fig. 1), a multimodal approach is mandatory [1].

Cardiac magnetic resonance (CMR) imaging plays a key role in evaluating the anatomical features, and is also the gold standard for evaluating right ventricular (RV) systolic function and flow. One of the advantages of CMR over an echocardiogram is the multiplanar approach, especially when evaluating the posterior valve and the rotation degree of the anterior valve (Fig. 2) [2–4].

CMR protocol for Ebstein's anomaly

The current CMR evaluation of EA includes steady-state free precession (SSFP) cine (retrospective ECG gating; in-plane resolution 1.5–2 mm; slice thickness 6 mm; interslice gap 4 mm; breath-holding) in 4-chamber view (for measuring adherence of the septal leaflet), 2-chamber view of the RV (for measuring adherence of the posterior leaflet), and short-axis and transaxial views (for evaluating the biventricular systolic function). It also includes contrast-enhanced angiography using gadolinium-based contrast agents: inversion recovery late gadolinium enhancement (LGE) after contrast injection (especially for evaluating left ventricle fibrosis), and flow evaluation for tricuspid regurgitation using 2D phase contrast and more recent sequences, such as 4D Flow (Fig. 3).

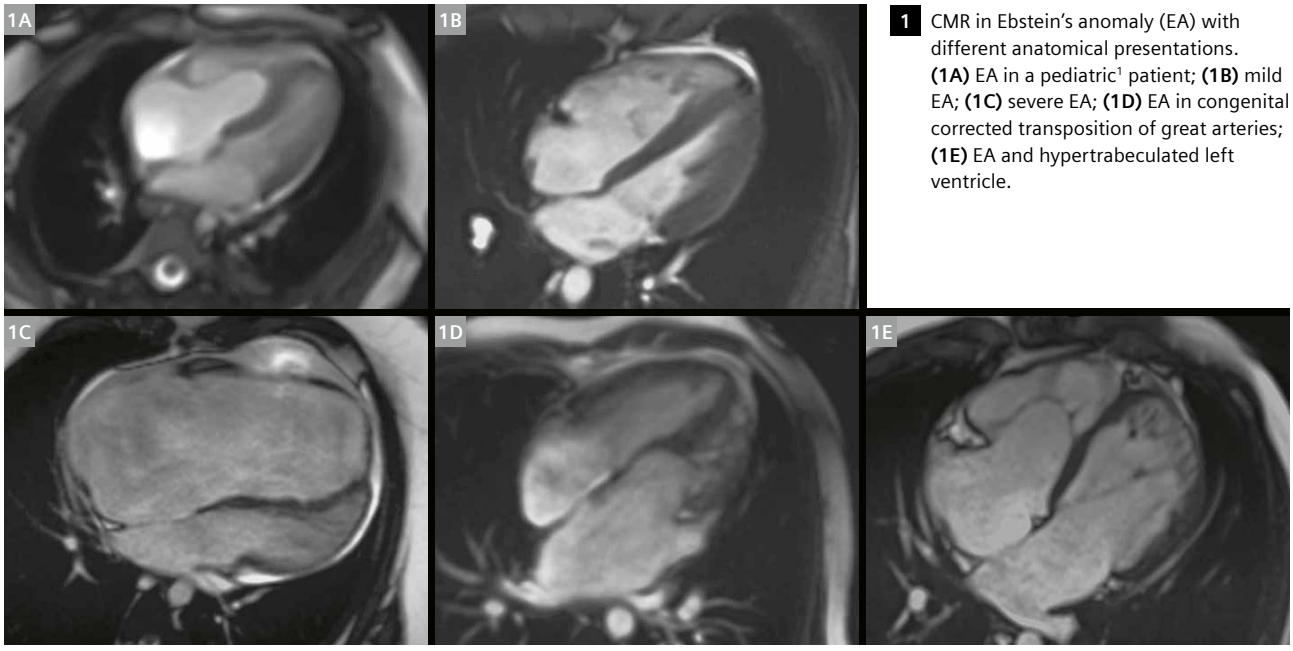

1 CMR in Ebstein's anomaly (EA) with different anatomical presentations. **(1A)** EA in a pediatric[1] patient; **(1B)** mild EA; **(1C)** severe EA; **(1D)** EA in congenital corrected transposition of great arteries; **(1E)** EA and hypertrabeculated left ventricle.

[1] *MR scanning has not been established as safe for imaging fetuses and infants less than two years of age. The responsible physician must evaluate the benefits of the MR examination compared to those of other imaging procedures.*

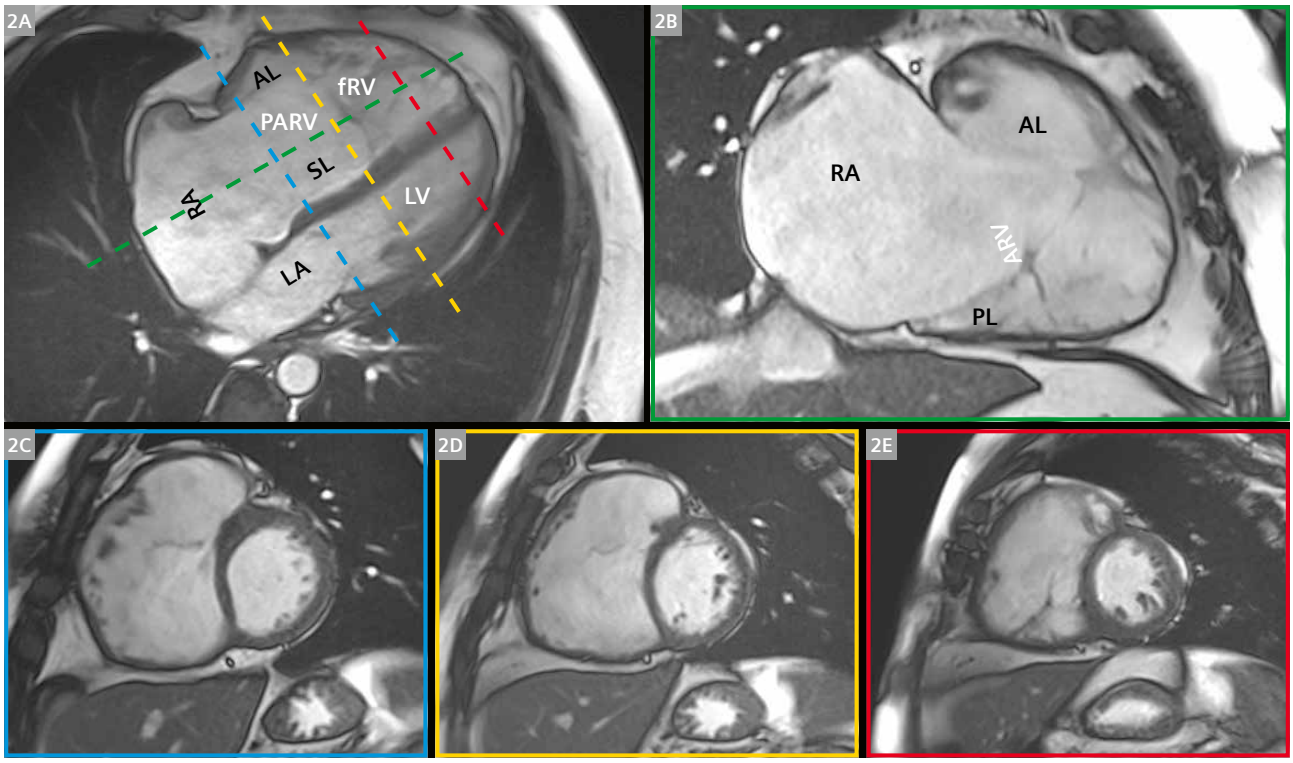

2 MR in Ebstein's anomaly: Anatomical evaluation. **(2A)** 4-chamber view for evaluation of anterior and septal leaflets. **(2B)** 2-chamber view of the RV for the evaluation of anterior and posterior leaflets. **(2C–2E)** Short axis showing the anatomical disposition of the three leaflets. RA = right atrium; RV = right ventricle; LA = left atrium; LV = left ventricle; ARV = atrialized right ventricle; fRV = functional right ventricle; AL = anterior leaflet; SL = septal leaflet; PL = posterior leaflet

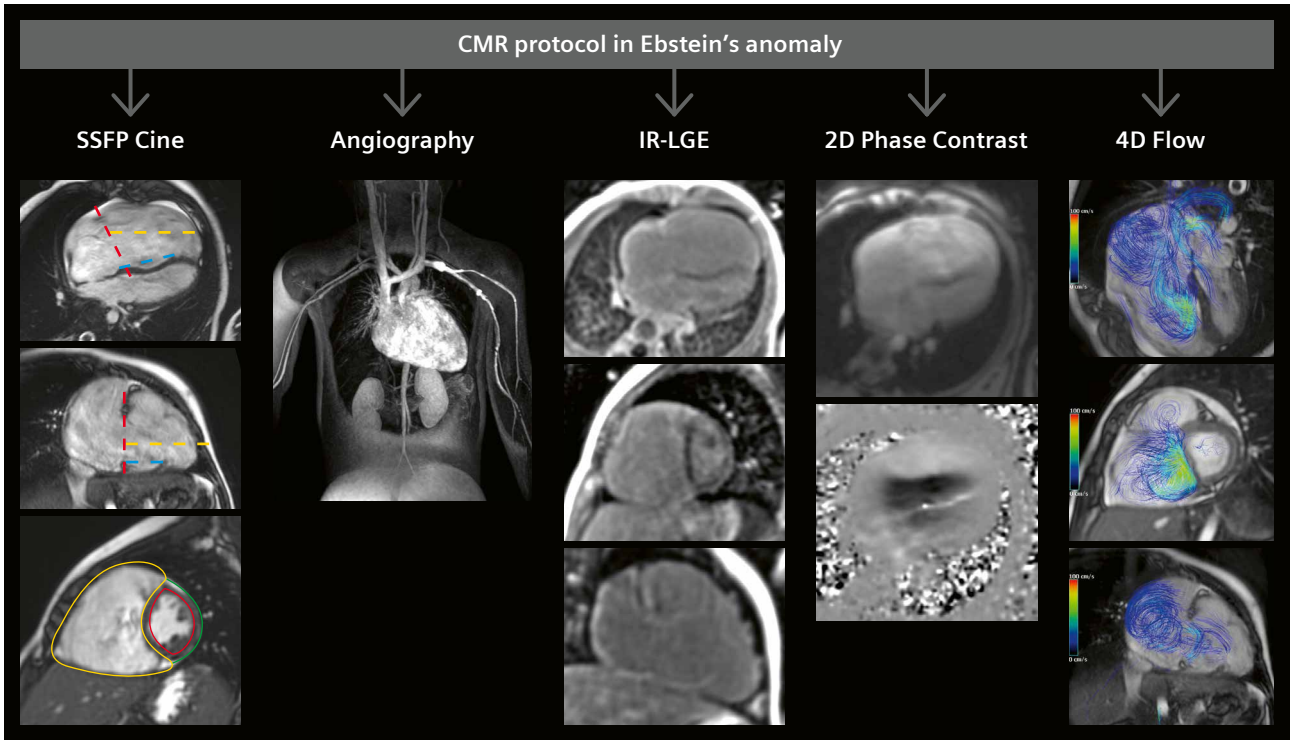

3 CMR protocol in Ebstein's anomaly.

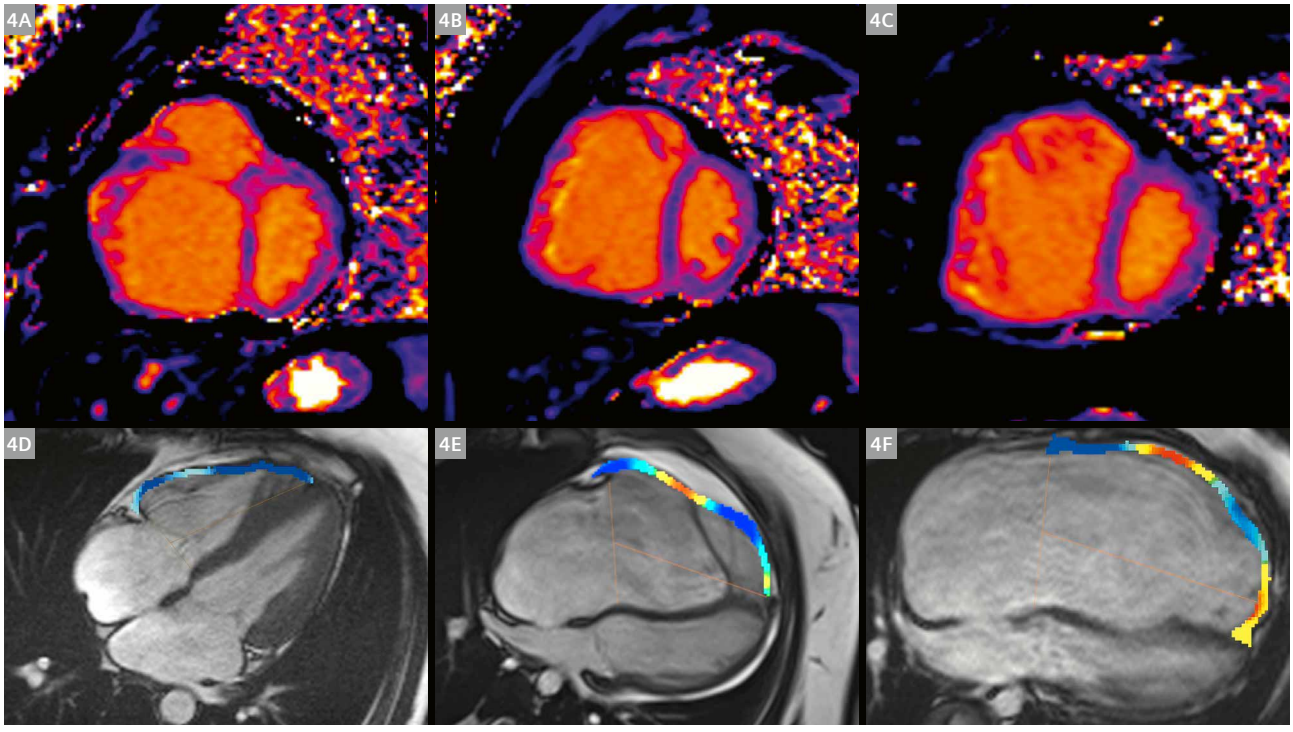

4 Additional evaluation in Ebstein's anomaly: Upper panel **(4A–4C)** T1 mapping in short-axis view for evaluation of biventricular fibrosis. Lower panel **(4D–4F)** SSFP cine with feature tracking for evaluation of free wall deformation in different stages of EA (from mild to severe).

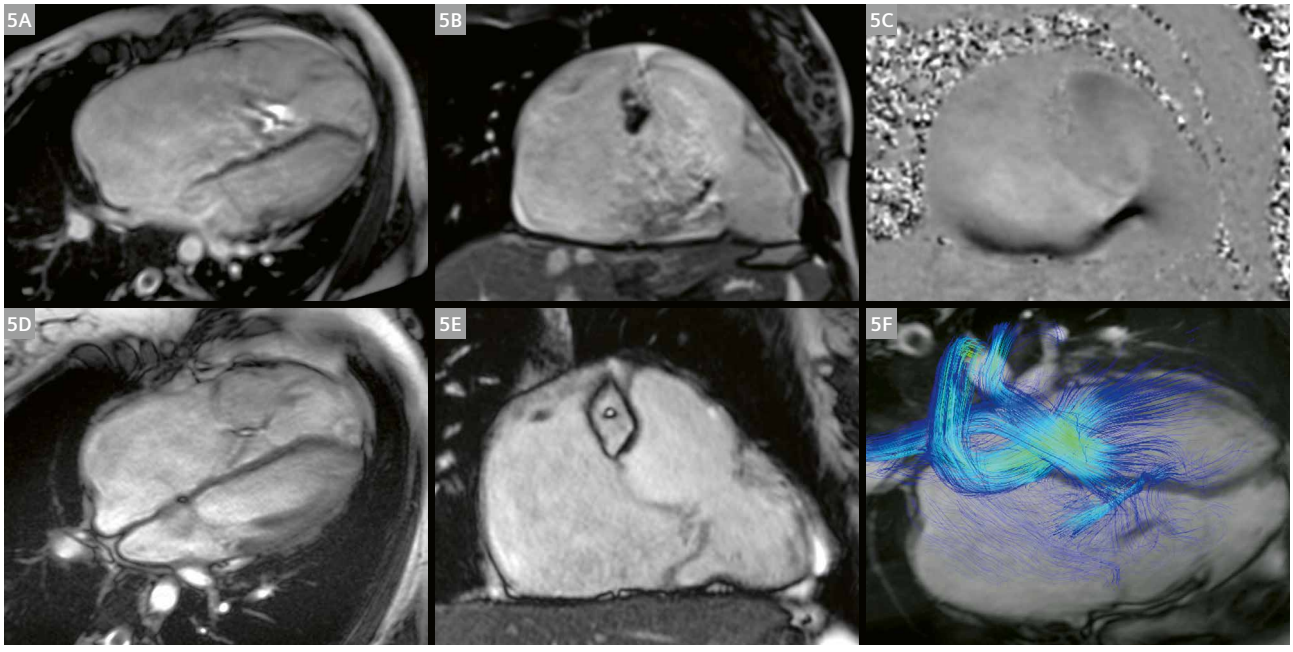

5 CMR in the pre- and postsurgical evaluation of cone repair. Top row: Evaluation in 4 chambers **(5A)** and 2 chambers of the RV **(5B)** of the anatomical features of the anterior leaflet. **(5C)** 2D phase contrast for imaging tricuspid regurgitation. Bottom row: **(5D, 5E)** anatomical evaluation of the anterior leaflet after surgical intervention. **(5F)** 4D Flow evaluation for residual tricuspid regurgitation.

Additional sequences such as T1 mapping have proven to be very useful, especially in establishing the prognosis during follow-up of patients with EA (Fig. 4) [5].

Feature tracking using SSFP for evaluating right and left ventricular myocardial deformation can also be added as a standard postprocessing measurement. In EA, determination of this parameter is suitable for early diagnosis of dysfunction (Fig. 4) [6, 7].

CMR protocol in pediatric Ebstein's anomaly

All of these tools can also be used in pediatric patients. Sometimes, however, sedation is necessary. Children younger than 6 years old[1] and those who have cognitive difficulties typically require some form of sedation. In addition to the general acquisition parameters, the pediatric protocol involves retrospective ECG gating; in-plane resolution 1–2 mm; slice thickness 6 mm; interslice gap 0–2 mm; free breathing; and a significant increase in the number of signal averages to three [8].

CMR in the follow-up after surgical intervention

As well as assessing EA, the CMR evaluation is also very important after surgical repair, especially after the cone procedure (Fig. 5). Sequences such as 4D Flow can be helpful in the assessment of residual tricuspid regurgitation [9].

Conclusion

CMR is a powerful tool for evaluating all forms of presentation of Ebstein's anomaly. Currently, CMR measurements include anatomical evaluation for complex cases, subclinical ventricular dysfunction in patients who require surgical intervention, and predictors in pre- and postsurgical evaluation.

References

1 Holst KA, Connolly HM, Dearani JA. Ebstein's Anomaly. Methodist Debakey Cardiovasc J. 2019;15(2):138–144.
2 Attenhofer Jost CH, Edmister WD, Julsrud PR, Dearani JA, Savas Tepe M, Warnes CA, et al. Prospective comparison of echocardiography versus cardiac magnetic resonance imaging in patients with Ebstein's anomaly. Int J Cardiovasc Imaging. 2012;28(5):1147–59.
3 Pasqualin G, Boccellino A, Chessa M, Ciconte G, Marcolin C, Micaglio E, et al. Ebstein's anomaly in children and adults: multidisciplinary insights into imaging and therapy. Heart. 2024;110(4):235–244.
4 Hughes ML, Bonello B, Choudhary P, Marek J, Tsang V. A simple measure of the extent of Ebstein valve rotation with cardiovascular magnetic resonance gives a practical guide to feasibility of surgical cone reconstruction. J Cardiovasc Magn Reson. 2019;21(1):34.
5 Aly S, Seed M, Yoo SJ, Lam C, Grosse-Wortmann L. Myocardial Fibrosis in Pediatric Patients With Ebstein's Anomaly. Circ Cardiovasc Imaging. 2021;14(3):e011136.
6 Baessato F, Furtmüller C, Shehu N, Ferrari I, Reich B, Nagdyman N, et al. Detection of early signs of right ventricular systolic impairment in unoperated Ebstein's anomaly by cardiac magnetic resonance feature tracking. Cardiovasc Diagn Ther. 2022;12(3):278–288.
7 Motevalli M, Allameh A, Tefagh G, Pouraliakbar H, Rabiei P, Asadian S, et al. The Use of Feature Tracking Technique for the Quantification of Ventricular Strain Pattern in Patients with Ebstein's Anomaly: A Case-Control Study. Iran J Med Sci. 2022;47(4):314–319.
8 Fratz S, Chung T, Greil GF, Samyn MM, Taylor AM, Valsangiacomo Buechel ER, et al. Guidelines and protocols for cardiovascular magnetic resonance in children and adults with congenital heart disease: SCMR expert consensus group on congenital heart disease. J Cardiovasc Magn Reson. 2013;15(1):51.
9 Alsaied T, Castrillon CD, Christopher A, Da Silva J, Morell VO, Lanford L, et al. Cardiac MRI predictors of right ventricular dysfunction after the Da Silva cone operation for Ebstein's anomaly. Int J Cardiol Congenit Heart Dis. 2022;7:100342.

Aloha Meave, M.D.

Sergio Patrón, M.D.

Contact

Sergio Patrón, M.D.
Instituto Nacional de Cardiología Ignacio Chávez
Juan Badiano 1, sección XVI, Tlalpan
México City
México
drsergiopatron@gmail.com

Cardiac Magnetic Resonance Imaging of Congenital Heart Disease under Sedation: Balancing Efficiency and Image Quality

Gabriela Nicolini Carvalho[1], Jacqueline Kioko Nishimura Matsumoto[1], Suzane Silva Lima[1], João Victor Santana Muslera[2], Rafael Donoso Scoppetta Filho[1], Dayana Cristina Assunção Yamasaki[1], João Luiz Piccioni[1], Claudia Castelo Branco[1], Michael Silva[2], Cesar Higa Nomura[1]

[1]Department of Diagnostic Imaging, Heart Institute (InCor), Hospital das Clínicas, University of São Paulo Medical School, São Paulo, Brazil
[2]Siemens Healthineers, São Paulo, Brazil

Abstract

Cardiac magnetic resonance (CMR) is a cornerstone imaging modality for the assessment of congenital heart disease (CHD), providing detailed anatomic and functional information without ionizing radiation. In pediatric[1] patients or those unable to remain still, CMR must often be performed under general anesthesia, which introduces additional complexity and requires meticulous coordination among multidisciplinary teams. This article outlines the workflow and technical strategies adopted at the Heart Institute (InCor), Latin America's leading cardiovascular center, to optimize image quality and procedural efficiency in CMR of CHD performed under sedation. The discussion integrates anesthesia management, nursing preparation, protocol selection, sequence optimization, and emerging technological perspectives. In doing so, it highlights the synergistic role of all professionals involved in achieving diagnostic excellence and patient safety.

Introduction

The Heart Institute (InCor) is one of Latin America's most advanced centers for cardiovascular and pulmonary care, performing approximately 400 magnetic resonance imaging (MRI) studies each month, including about 10 examinations under anesthesia. As a tertiary referral center, InCor manages a wide variety of complex cardiac and pulmonary conditions, particularly congenital heart disease (CHD) – structural abnormalities that alter cardiac morphology and physiology. Early and accurate diagnosis of CHD is essential to guide appropriate therapeutic interventions and improve long-term outcomes.

In pediatric and uncooperative patients, cardiac magnetic resonance (CMR) is typically performed under general anesthesia, with continuous monitoring by a specialized team to ensure ventilation control and procedural safety. CMR is regarded as the gold standard for

[1]*MR scanning has not been established as safe for imaging fetuses and infants less than two years of age. The responsible physician must evaluate the benefits of the MR examination compared to those of other imaging procedures.*

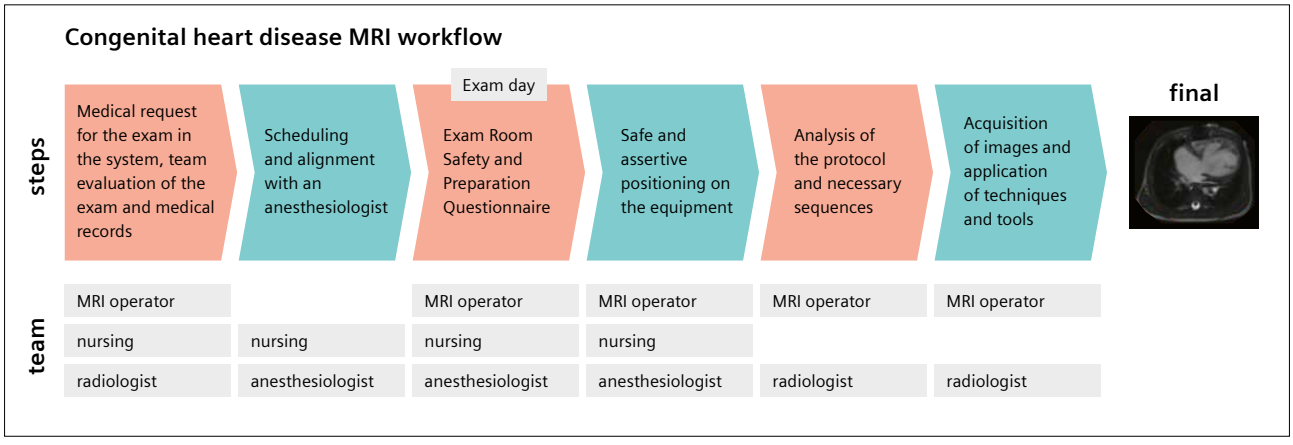

1 Workflow for CMR in congenital heart disease.

comprehensive evaluation of CHD, offering unmatched insights into cardiac anatomy, ventricular function, flow quantification, myocardial tissue characterization, and coronary anatomy. Its value extends beyond diagnosis to include longitudinal follow-up, surgical planning, and postoperative assessment.

This study describes the clinical workflow and technical considerations implemented in pediatric CMR under anesthesia, focusing on strategies to optimize image quality, minimize artifacts, and ensure procedural efficiency. The discussion also emphasizes the critical role of multidisciplinary collaboration across anesthesia, nursing, and imaging teams.

Workflow overview

Upon receipt of the physician's request, the imaging team initiates examination planning. The MRI technologist and the multidisciplinary staff play a pivotal role in ensuring safety, efficiency, and diagnostic quality throughout the process. Each step – from pre-examination preparation to post-processing – requires synchronized communication among all professionals involved.

Anesthesia management

Pediatric CMR under general anesthesia is conducted with a supervising anesthesiologist who is responsible for induction and for maintaining controlled ventilation during image acquisition. Patients arrive in the MRI suite already intubated. The anesthesiologist's primary objective is to maintain hemodynamic stability, avoiding apnea and other complications inherent to complex CHD. Sedation depth is individualized, and neuromuscular blockers may be administered to minimize involuntary movements or spasms that could degrade image quality.

Given the structural and hemodynamic variability in CHD, anesthetic management requires heightened vigilance and individualized dosing. Continuous monitoring of ECG, blood pressure, and pulse oximetry is mandatory, as physiological parameters can fluctuate rapidly. Balanced administration of anesthetic agents and precise real-time monitoring are essential to procedural safety. Collaboration between anesthesia, nursing, and biomedical teams ensures both clinical stability and imaging quality.

Nursing preparation

Nursing plays a decisive role in balancing procedural efficiency and image quality. From scheduling to recovery, the team verifies all clinical and logistical requirements – fasting status, allergy history, venous access, and implant[2] safety. On the examination day, nursing staff complete the safety checklist, reinforce instructions to families, monitor vital signs, and ensure correct patient positioning to prevent complications and delays. The nursing contribution combines technical rigor with effective communication and compassionate care, enhancing both workflow fluency and patient experience.

Patient positioning and monitoring

Patients are positioned supine and head-first within the scanner bore. Ventilation tubing and anesthesia lines are secured to prevent accidental displacement during table movement. ECG leads are applied using standardized placement with gauze insulation to prevent skin burns. Monitoring includes MR-compatible ECG, pulse oximetry, capnography, and a pneumatic respiratory cushion to track diaphragmatic motion.

The UltraFlex 18-channel coil is the preferred configuration for pediatric cardiac imaging due to its optimal balance between coverage and signal-to-noise ratio (SNR). Cotton sheets or pads are used to prevent direct coil-skin contact. In infants, additional padding is placed between the coil and chest to reduce pressure. Metallic cuffs or devices near the thorax are isolated with medical tape and positioned outside the imaging field to avoid artifacts.

Throughout the examination, continuous observation of the anesthetized patient is essential, as physiological

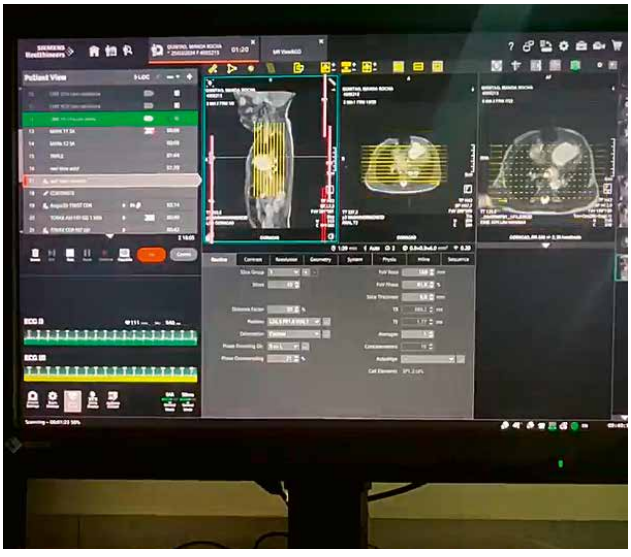

2 CMR acquisition for CHD using our 1.5T MAGNETOM Altea system.

[2]*The MRI restrictions (if any) of the metal implant must be considered prior to patient undergoing MRI exam. MR imaging of patients with metallic implants brings specific risks. However, certain implants are approved by the governing regulatory bodies to be MR conditionally safe. For such implants, the previously mentioned warning may not be applicable. Please contact the implant manufacturer for the specific conditional information. The conditions for MR safety are the responsibility of the implant manufacturer, not of Siemens Healthineers.*

changes can occur abruptly. Specific absorption rate (SAR), body temperature, and vital signs are monitored in real time, in constant communication with the anesthesia team. Short pauses between acquisitions are recommended, even during free-breathing scans, to limit radiofrequency (RF) energy deposition.

Protocol design and image acquisition

After reviewing the medical request and defining objectives, the technologist registers the patient and organizes the imaging sequences. The standard CMR protocol for CHD includes cine imaging, T1 mapping, time-resolved angiography with interleaved stochastic trajectories (TWIST angiography), late gadolinium enhancement (LGE) imaging, and phase-contrast sequence for flow quantification in major vessels and intracardiac shunts. Protocol customization is guided by the anatomic and functional complexity of each case. The axial T2-weighted sequence is acquired first to delineate cardiac chambers, great vessels, and structural variations, informing subsequent angulations. This approach is particularly relevant in transposition of the great arteries and hypoplastic left heart syndrome, where major morphological deviations require tailored slice planning.

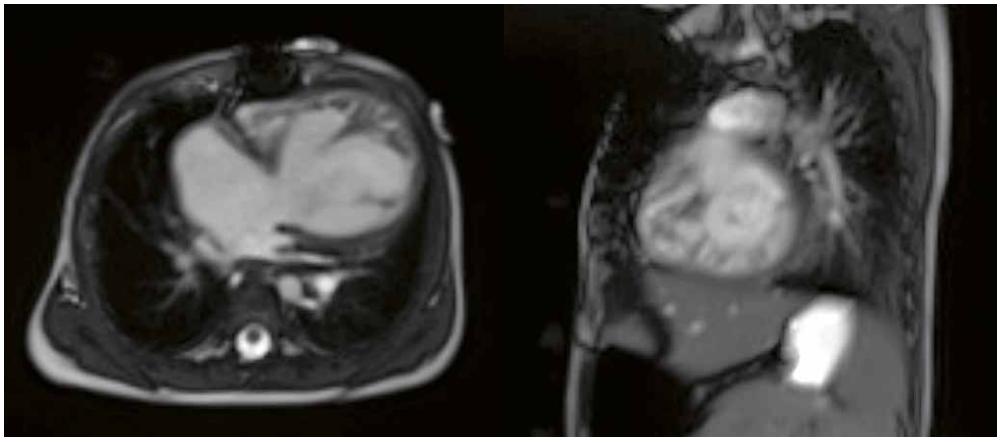

3 Patient with hypoplastic left heart syndrome at 10 months, demonstrating complex CHD anatomy in TRUFI cine sequences (4-chamber and short-axis views).

Reducing cine flow artifact by adapting volume shim and using manual adjustments.

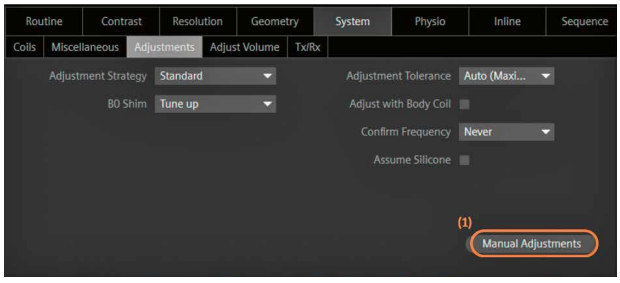

1. In the System tab and the Adjustment subfolder, select this item (1) to adjust the calibration manually. It is important that the adjustment volume (green box) is adjusted to the heart (Example 1).

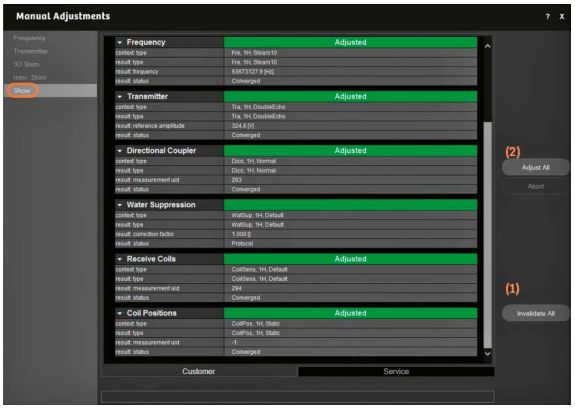

2. Open the Show tab. Make sure there are no sequences in scan. Invalidate all (1) and then adjust all (2). This generates new calibrations for the region, which reduce the artifact (Example 2).

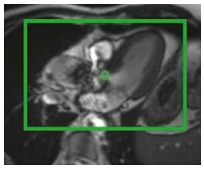

Example 1
Before

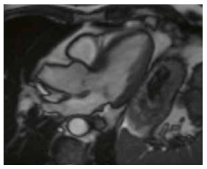

Example 2
After

4 Example of flow artifact correction using manual adjustments and adjustment volume.

Parameter optimization

In pediatric imaging, a reduced field of view (FOV ≈ 260 mm) is typically required. To compensate for SNR loss, parameters such as phase resolution, bandwidth, and matrix size are optimized. Respiratory motion, inevitable under anesthesia, is mitigated by increasing averages – commonly four averages – which improves SNR and overall image quality. A slice thickness of 6 mm and a 20% gap are used to achieve detailed anatomic visualization.

In cases of stenosis or coarctation, high-velocity flow can cause artifacts that affect adjacent structures. Magnetic field homogeneity is improved using manual adjustments and the adjustment volume, especially in cine sequences, to minimize distortions.

Advanced techniques

The TWIST sequence plays a pivotal role in CHD assessment by enabling time-resolved contrast angiography, which guides the planning of phase-contrast flow studies (Fig. 5). Slice angulations are optimized using maximum intensity projection (MIP) reconstructions and 2D snapshots for accurate alignment with target vessels.

Phase-contrast series programming using TWIST

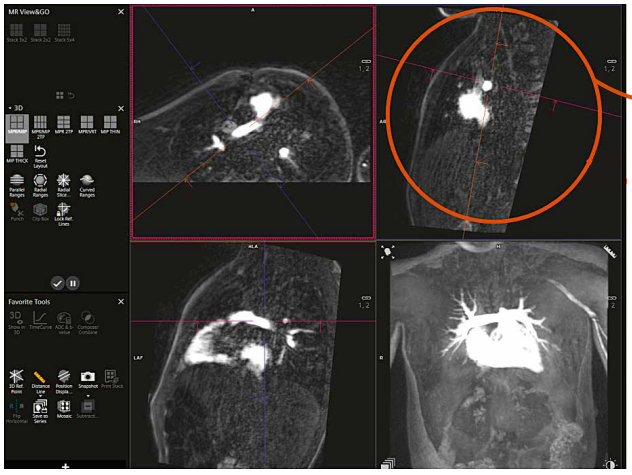

1. Acquisition of TWIST: Choose between the best phase, where the main contrast-filled pathways are observed. Use MR View&GO (Siemens Healthineers, Erlangen, Germany) in the 3D tab to angle with the anatomic structure. In the example above, the angulation is based on the right pulmonary artery.

2. Use the Snapshot tool in the ideal plane to angulate the phase-contrast series. The software allows you to use the MR View&GO results as an image to align on the acquisition screen.

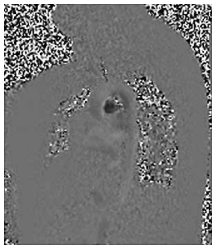

Final result of phase-contrast

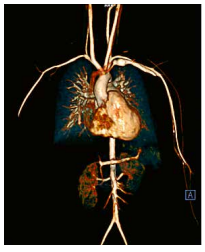

Final result of TWIST angiography

5 Coronal TWIST angiography illustrating angulation planning for flow quantification.

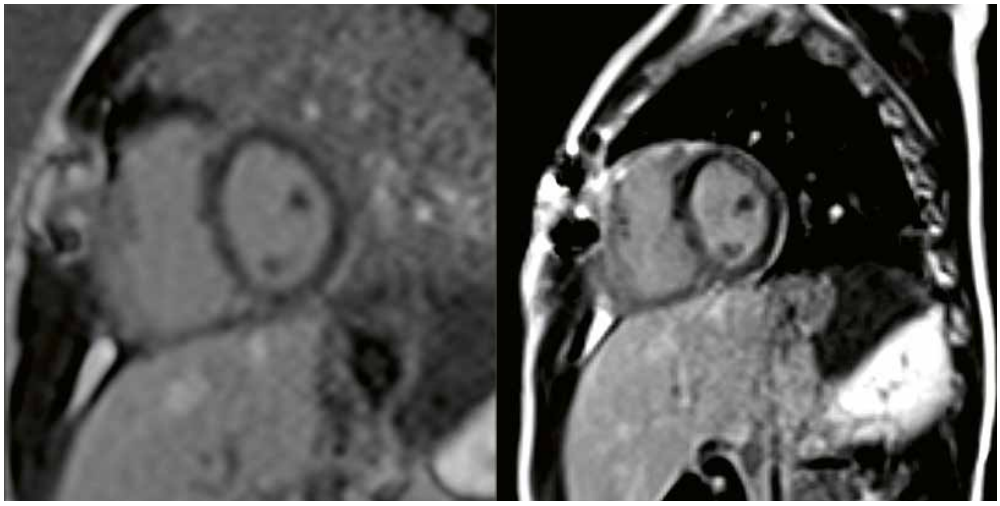

6 Short-axis late enhancement in a 6-year-old patient

For LGE imaging, free-breathing phase-sensitive inversion recovery (PSIR) or single-shot sequences are recommended at least five minutes after contrast administration. Although their spatial resolution is lower than high-resolution breath-hold PSIR, they minimize motion artifacts and provide diagnostically adequate images in sedated pediatric patients with variable respiratory stability.

Medical imaging specialists' perspective

High-quality CMR in CHD requires seamless collaboration among anesthesiologists, nurses, technologists, and medical imaging specialists. Each professional contributes uniquely to patient safety and diagnostic precision – from pre-examination preparation and sedation management to image acquisition and interpretation. The integration of clinical and technical expertise ensures a balance between efficiency, image quality, and procedural safety.

The medical imaging specialist role extends beyond image interpretation, encompassing an active partnership with technologists and physicians to ensure appropriate protocol selection and parameter optimization for each specific case.

Customizing acquisition strategies has a decisive impact on image clarity and diagnostic confidence. Modern MRI platforms now provide real-time optimization tools, including arrhythmia detection, dynamic averaging, phase resolution, and adaptive bandwidth, enabling immediate compensation for rhythm irregularities or respiratory motion.

Conclusion

Looking ahead, several technological innovations are beginning to emerge, although they have not yet been integrated into routine clinical practice. Among them, 4D flow MRI stands out for its potential to provide comprehensive and detailed hemodynamic information in patients with congenital heart disease. Soon, artificial intelligence is expected to play a pivotal role in real-time adaptation of CMR examinations – automatically recognizing respiratory patterns in anesthetized patients, integrating anthropometric data, and dynamically adjusting parameters such as averages and field of view. These advances have the potential to increase acquisition efficiency, significantly shorten total scan time, and consequently reduce the duration of sedation.

Reflecting on the practical experience at InCor, it becomes clear that the role of the MRI operator extends far beyond technical execution. It requires a multidirectional and critical perspective – one that considers the patient's physiological variables, clinical stability, and the specific technical challenges inherent to each case. This integrated mindset is essential to ensure diagnostic quality, procedural safety, and excellence in patient care.

In this context, CMR in congenital heart disease transcends its technical boundaries, representing a synthesis of precision, adaptability, and collaboration. When technology and clinical reasoning converge with purpose, CMR becomes not only a diagnostic tool but a true instrument of care, reaffirming its vital role in advancing cardiovascular medicine.

References

1 Sreedhar CM, Ram MS, Alam A, Indrajit IK. Cardiac MRI in Congenital Heart Disease - Our Experience. Med J Armed Forces India. 2005;61(1):57–62.
2 Siemens Healthineers. User Manual: Siemens Altea – *syngo* MR XA51. Erlangen, Germany: Siemens AG; 2023.

Contact

Gabriela Nicolini Carvalho
Imaging Biomedical Scientist
Instituto do Coração – HCFMUSP
Avenida Dr. Enéas de Carvalho Aguiar, 44
Cerqueira César
São Paulo – SP
CEP 05403-000
Brazil
gabriela.nicolini@hc.fm.usp.br

João Victor Santana Muslera
MRI Clinical Application Specialist
Siemens Healthineers LAM
joaovictorsantana.muslera@siemens-healthineers.com

Bringing Together Cardiovascular MR Imaging and Echocardiography with *syngo* Dynamics: How We Report it

Michael Silberbach, M.D.[1] and Brian Fonseca, M.D.[2]

[1]Oregon Health & Science University, Portland, OR, USA
[2]Children's Hospital Colorado, Aurora, CA, USA

The *syngo* Dynamics team, Circle Cardiovascular Imaging, and the Society for Cardiac Magnetic Resonance (SCMR) are planning to integrate MRI and cardiac ultrasound by creating structured clinical reports that take advantage of the powerful tools of semantic interoperability. More than four years of hard work and dedication between *syngo* Dynamics and the SCMR's Congenital Heart Structured Report Group (CHSRG) have resulted in a reporting template that captures the complex anatomy of congenital heart malformations, cardiac function, strain, 2D and 4D cardiovascular flow, and contrast-enhanced assessments of cardiac fibrosis. This step forward has been a long time coming.

The historic bifurcation of cardiovascular MR and echocardiography: getting back to collaboration and efficiency

The late David J. Sahn, a pioneering echocardiographer, told this apocryphal story: Fifty years ago, the largest medical imaging companies gathered the leaders of clinical radiology and cardiology. Radiologists, unimpressed with the prospects for echo, chose to follow MRI into the future while cardiologists committed themselves to echo research and its clinical applications. This created a bifurcation that resulted in MRI training for both technologists and clinicians becoming centered in radiology, whereas schools for echo technologists developed independently of MRI and other radiology programs. University cardiology programs that collaborated with industry discovered clinical modalities such as intravascular ultrasound, 2D echo, color flow Doppler, and 3D echo.

Echo and cardiovascular MR (CMR) capabilities are in fact complementary. Researchers, clinicians, and patients have much to gain from the cross-fertilization of these two powerful imaging tools. CMR reveals cardiovascular structure, flow, metabolism, and function using exquisite cross-sectional, 3- or 4-dimensional formats. Yet it will be a long time before CMR can mimic the frame rates, portability, and convenient patient interface of echocardiography.

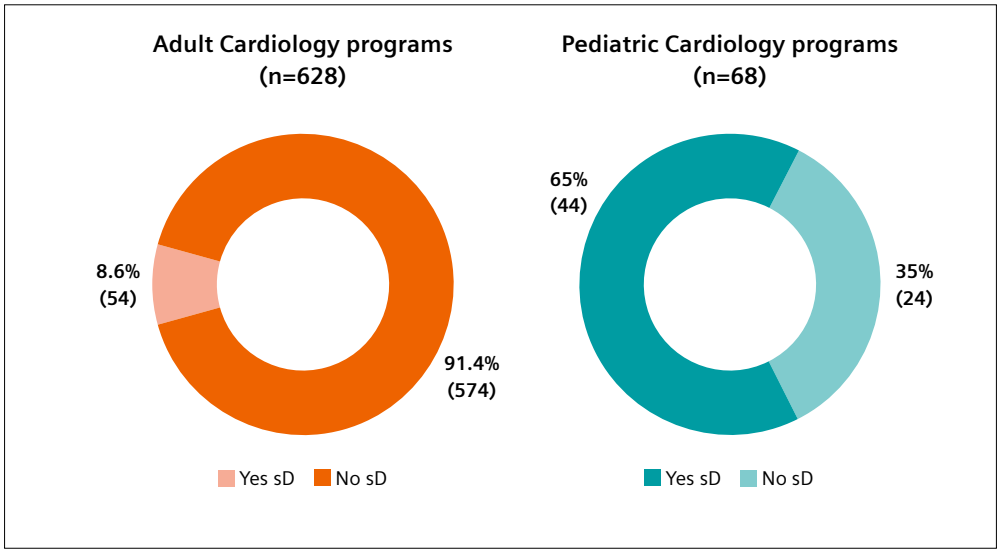

1 Use of *syngo* Dynamics. Survey of SCMR member adult and pediatric cardiology programs.

There are important questions that can only be answered by bringing echo and CMR clinical care together.

An unanticipated and unfortunate outcome of this bifurcation was that CMR and echo practitioners found themselves in competition. This had a chilling effect on research collaborations and efficiency. Our new *syngo* Dynamics CMR congenital heart reporting solution is designed to eliminate wasted effort from image acquisition through to post-processing, report generation, and collaboration, all with the overarching goal of serving our patients.

The SCMR and *syngo* Dynamics collaboration

For many years the *syngo* Dynamics echocardiography report has been the mainstay for congenital heart disease reporting in the U.S. As *syngo* Dynamics' interest in CMR reporting grew, and knowing that 65% of the SCMR pediatric institutional membership use the solution for echocardiography (Fig. 1), the team reached out to the SCMR Pediatrics group to explore their interest in developing a structured reporting template for congenital heart disease cases.

For their part, the members of the SCMR Pediatrics group recognized the value of a platform that mirrors the *syngo* Dynamics echo template, its simple interface, logical algorithm, and visual elegance. They seized upon an opportunity to create a CMR structured report that could facilitate multicenter collaborative studies. Figure 2 compares the similar appearance of *syngo* Dynamics' CMR and echo reports.

SCMR's Congenital Heart Structured Report Group, the CHSRG (Brian Fonseca, Lars Grosse-Wortmann, Josh Robinson, Animesh Tandon, Andrew Powell, and Michael Silberbach), also knew that the greatest obstacle was not the report format itself. Rather, two issues needed to be addressed: First, consensus on how to manage the labyrinthine complexity of cardiac malformation nomenclature. All agreed that following the nomenclature of the International Paediatric and Congenital Cardia Code (IPCCC) was the way to go [1]. The *syngo* Dynamics team had already created an MRI report for the adult cardiology group at the Cleveland Clinic that contained 506 data elements. Building on the foundation of the adult CMR report, the CHSRG has now constructed a congenital heart report that includes 1,554 data elements. Second, there needed to be a report architecture that facilitates multicenter studies that readily communicate with the National Institutes of Health, academic institutions around the world, industry partners, and other entrepreneurs and collaborators in the private sector. In other words, the new report needed to incorporate semantic interoperability, which is the modern-day sine qua none of all large information systems.

Circle Cardiovascular Imaging joins the project with cvi42

As luck would have it, efforts had begun to tackle the interoperability problem during the Cleveland Clinic project when the *syngo* Dynamics team established a fruitful collaboration with the industry leader in CMR post-processing: Circle. Together, Circle and *syngo* Dynamics established an integration between their two solutions that

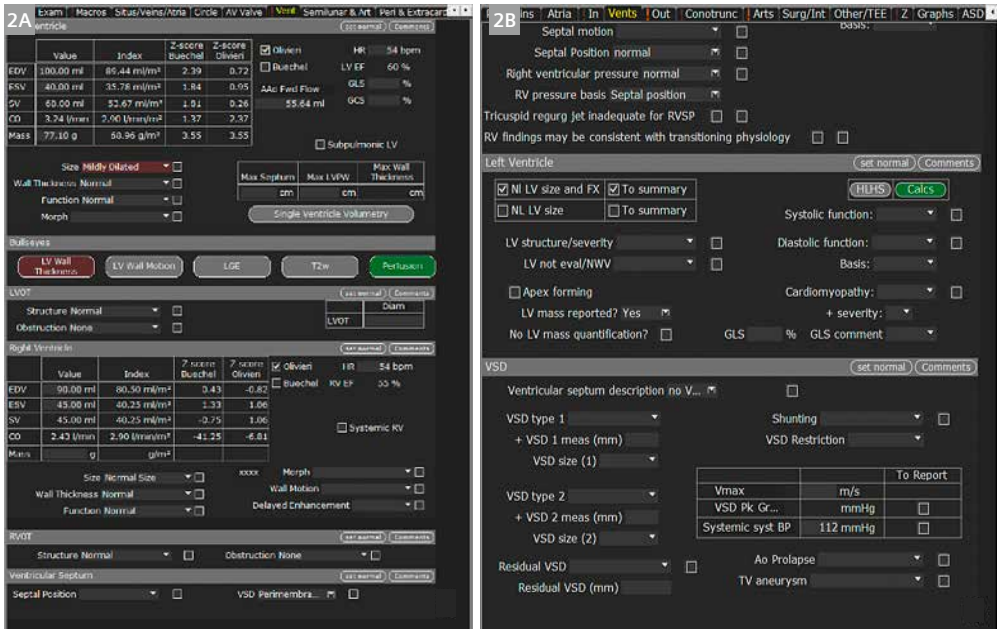

2 Comparison between CMR and echocardiographic reporting in *syngo* Dynamics. **(2A)** shows the ventricular tab in the CMR reporting template, which is structurally very similar to the corresponding ventricular tab in the echocardiographic report template in **(2B)**.

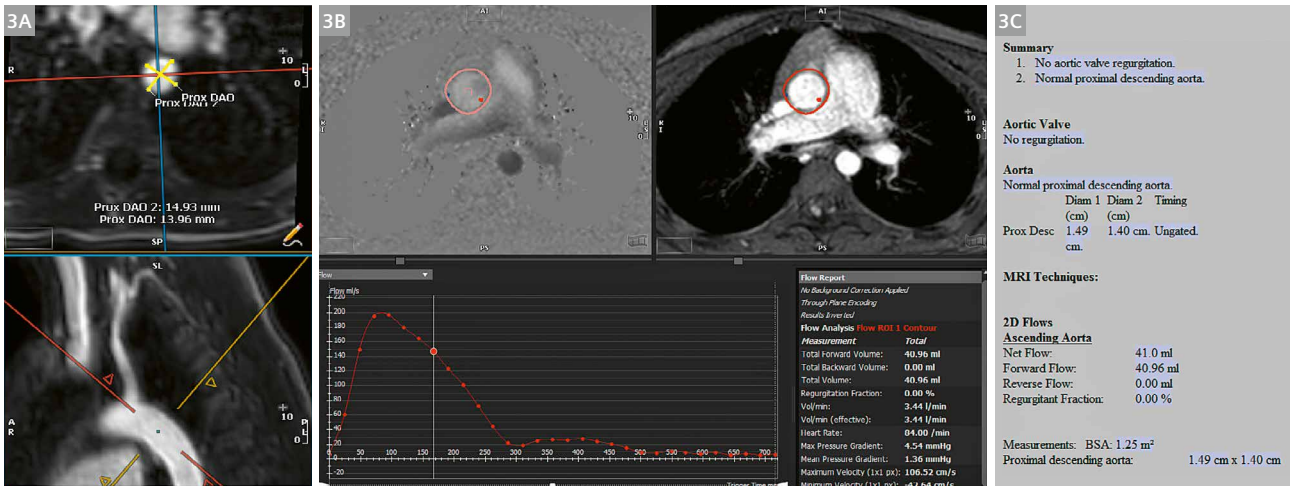

3 *syngo* Dynamics congenital CMR reporting data flow. Linear measurements **(3A)** and flow measurements **(3B)** are imported directly into the *syngo* Dynamics report. Measurements and flow data are displayed in the measurement section of the report and can be used to guide qualitative assessments in the body and summary **(3C)**.

instantaneously populates important quantitative data from cvi42, such as ventricular function, and parametric mapping values to the *syngo* Dynamics CMR report. The new *syngo* Dynamics congenital heart report expands this transfer to include flow and linear measurements specific to congenital CMR reporting (Fig. 3). The group is excited to be working alongside Circle's new CEO, Erkan Akyuz, an industry leader in designing and launching interoperability platforms between disparate healthcare systems.

The future looks bright

The CHSRG will be initiating multicenter studies involving the SCMR's 62 institutional members that already use both *syngo* Dynamics and cvi42. Moving forward, as the American Society of Echocardiography (ASE) group establishes a *syngo* Dynamics structured report employing the same IPCCC nomenclature, key ASE-SCMR collaborative efforts will unfold. For example: studying the relative strengths of echo vs. CMR; determining distinguishing characteristics of the two modalities and emphasizing information gaps; evaluating outcomes; and conducting multicenter studies. Even as these projects emerge, our priority is to write a comprehensive whitepaper that will encourage others in the industry to create compatible reports that enable collaborations across platforms throughout the U.S. and the world. We envision successes that emulate the remarkable advancements in cancer therapy achieved by the multicenter Children's Oncology Group [2].

References

1 Jacobs JP, Franklin RCG, Beland MJ, Spicer DE, Colan SD, Walters HL, et al. Nomenclature for Pediatric and Congenital Cardiac Care: Unification of Clinical and Administrative Nomenclature - The 2021 International Paediatric and Congenital Cardiac Code (IPCCC) and the Eleventh Revision of the International Classification of Diseases (ICD-11). Cardiol Young. 2021;31(7):1057–1188.

2 O'Leary M, Krailo M, Anderson JR, Reaman GH, Children's Oncology Group. Progress in childhood cancer: 50 years of research collaboration, a report from the Children's Oncology Group. Semin Oncol. 2008;35(5):484–93.

Contact

Michael Silberbach, M.D.
Emeritus Professor of Pediatrics and Radiology
Oregon Health & Science University
OHSU Doernbecher Children's Hospital
7th Floor
700 SW Campus Dr
Portland, OR 97239
USA
Tel.: +1 503-418-5750
silberbm@ohsu.edu

Brian Fonseca, M.D.
Professor of Pediatric Cardiology
Children's Hospital Colorado
13123 E 16th Ave # B100
Aurora, CO 80045
USA
Tel.: +1 720-777-1234
Brian.fonseca@childrenscolorado.org

From Acquisition to Analysis: How AI is Revolutionizing Cardiac MRI

Solenn Toupin, Ph.D.; Théo Pezel, M.D., Ph.D.

Lariboisière Hospital, MIRACL.ai platform, AP-HP, Paris, France

Introduction

Artificial intelligence (AI) is emerging as a powerful ally in cardiac MRI, addressing many of the challenges that previously limited its efficiency and accessibility. By automating and optimizing steps from protocol planning and image acquisition to reconstruction, analysis, and integration with clinical data, AI can make cardiac MRI faster, more consistent, and more widely available. Far from replacing clinicians, AI supports them by reducing repetitive tasks, improving reproducibility, and enabling the extraction of advanced diagnostic and prognostic information.

An important aspect of this evolution is the integration of cardiac MRI into a multimodality framework where it is combined with other imaging techniques such as echocardiography or CT, and with clinical, biological, and electrophysiological data. This approach paves the way for advanced concepts like the digital twin – a virtual model of the patient's heart that can guide diagnosis and therapy planning, further enhancing precision and personalization in cardiovascular care.

In this article, we will explore how AI is transforming our cardiac MRI practice in four main domains (Fig. 1):

1. **Planning and acquisition:** including automated plane prescription and parameter optimization
2. **Image reconstruction:** accelerating acquisitions and improving image quality
3. **Image analysis and post-processing:** enabling rapid and consistent quantification
4. **Development of diagnostic and prognostic tools:** integrating imaging with multisource and multimodal patient data

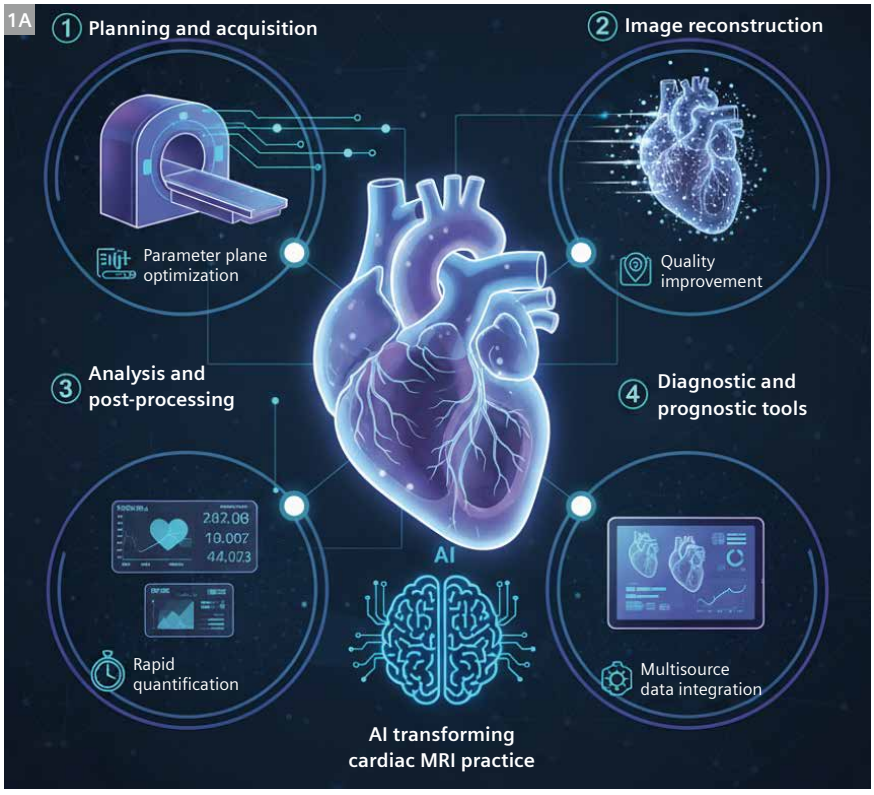

1 **(1A)** Artificial intelligence is transforming cardiac MRI by enhancing image acquisition, reconstruction, post-processing, and diagnosis.

Through these advances, AI is enhancing both the efficiency and the diagnostic power of cardiac MRI, ultimately contributing to better patient outcomes.

AI-assisted planning and acquisition

One of the most visible improvements is AI-assisted slice positioning for cardiac MRI exams. Traditionally, slice positioning relied heavily on operator expertise, with variability due to operator experience and patient anatomy. Now, AI automatically detects cardiac landmarks from the localizer images and proposes standard short- and long-axis views with high precision, allowing quick confirmation or adjustment. This ensures more consistent orientation between patients and in follow-up scans of the same patient. Such reproducibility is essential for both quality patient care and data consistency in longitudinal studies.

AI algorithms also assist in adapting imaging parameters to the patient's individual anatomy and clinical indication. A notable example is automatic inversion time (TI) estimation for late gadolinium enhancement. Unlike manual interpretation of the TI scout, which sometimes requires repeated acquisitions, AI calculates the optimal value directly from the scout images. The technologist still retains the ability to review and adjust the suggested TI value if needed, which ensures flexibility and clinical oversight. This reduces scan time, minimizes breath-hold repetitions for the patient, and improves image consistency across patients.

These AI tools are particularly valuable in our environment at Lariboisière Hospital. We are a tertiary referral center with strong expertise in cardiac imaging, and as a university hospital we routinely manage patients with complex and severe pathologies. Our technologists work across all imaging modalities and organ systems. Our scanners are shared between multiple specialties, which means that dedicated cardiac MRI technologists are not always available. AI solutions that simplify acquisition and standardize quality therefore benefit everyone by ensuring consistently high-quality images regardless of the operator's primary area of expertise. They also shorten examination times, reduce repeated sequences, and bring greater standard-

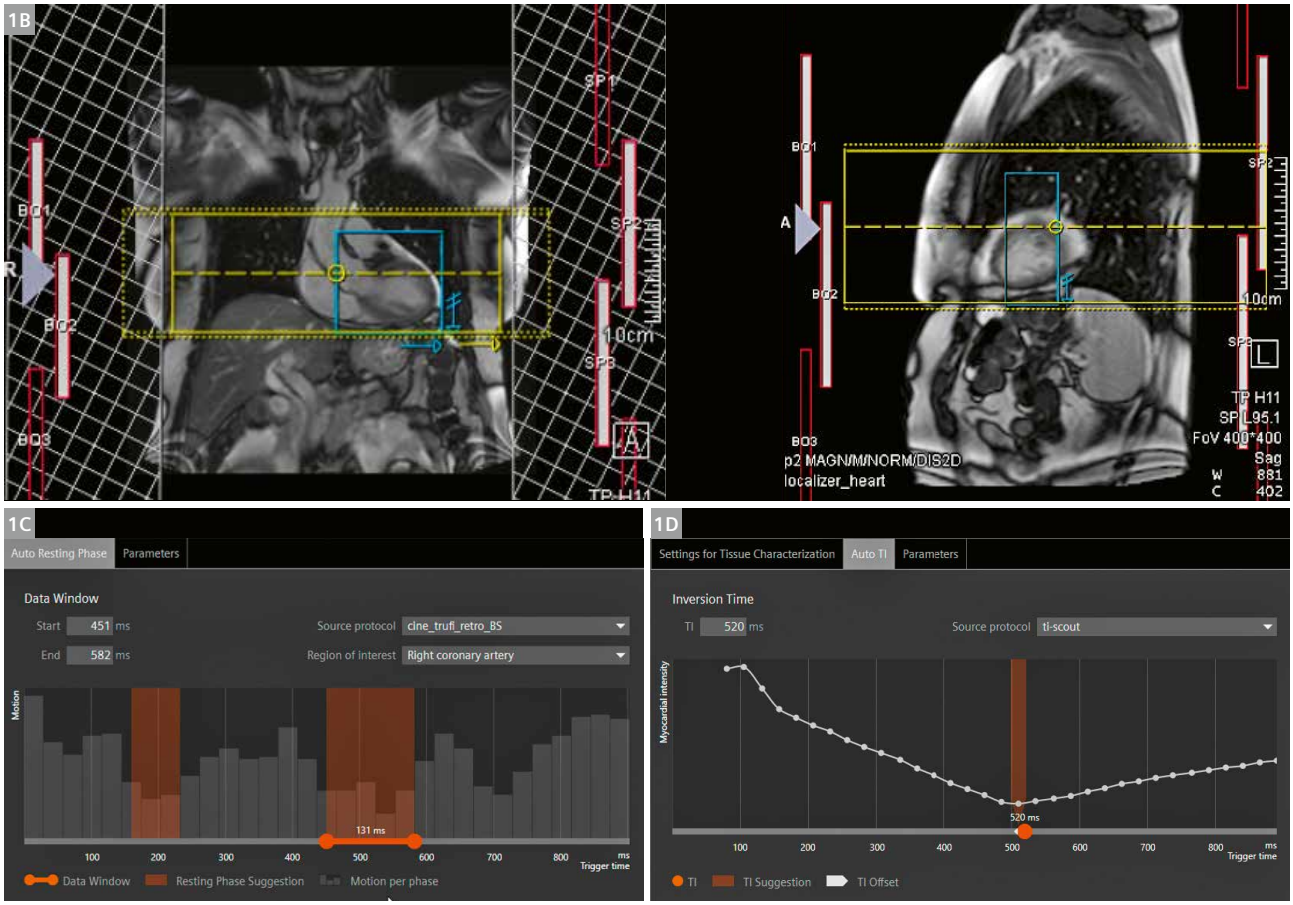

1 **(1B)** AutoPositioning automatically places the heart in the isocenter and plans slices, volumes, navigators, and saturation bands. **(1C)** AutoRestingPhase detects the optimal data acquisition window during the cardiac resting phase. **(1D)** AutoTI proposes the optimal inversion time for delayed enhancement measurement.

ization, which is especially valuable in research involving large patient cohorts and multiple operators. These capabilities allow our technologists to spend less time on manual adjustments and more on patient comfort, while clinicians gain more reliable datasets for reconstruction, analysis, and integration with other modalities.

Looking ahead, smart prescan guidance systems could take this further by analyzing patient-specific data such as heart rate, ventricular morphology, or implanted devices even before the patient enters the scanner room. This would allow AI to propose optimized protocols, minimize unnecessary sequences, and ensure all essential information is acquired, improving efficiency and reproducibility in both high-volume clinical practice and multicenter research.

AI-powered reconstruction for consistent, high-quality cardiac MRI

AI-based image reconstruction has become one of the most impactful applications of artificial intelligence in medical imaging. By learning from large datasets of high-quality images, deep learning algorithms can remove noise, reduce artifacts, and even predict missing data, allowing significant acceleration of acquisition without compromising diagnostic quality. These methods are now integrated into clinical scanners, such as the 1.5T MAGNETOM Sola, to improve workflow efficiency, enable shorter breath-holds, and enhance image sharpness. Beyond saving time, AI reconstruction also ensures more consistent image quality between patients and operators, which is critical for longitudinal follow-up and multicenter research studies. Importantly, these algorithms are always validated against raw *k*-space data to guarantee authenticity and preserve diagnostic reliability.

One pertinent example in the cardiovascular MRI offering from Siemens Healthineers is an AI-based reconstruction tool for T2 STIR sequences, which are essential for detecting myocardial edema. In clinical practice, and especially in the assessment of acute myocarditis, T2 STIR is interpreted together with T2 mapping to confirm and quantify edema. In our tertiary referral setting at Lariboisière Hospital, patients often present with severe or complex cardiovascular conditions, including myocarditis with arrhythmia or limited breath-holding capacity. These factors can compromise conventional T2 STIR image quality. The AI-enhanced reconstruction denoises the images, improves the myocardium–blood contrast, and reduces motion artifacts, resulting in clearer visualization of areas of edema. This translates into greater diagnostic confidence for clinicians, more reliable detection of subtle lesions, and improved consistency across patient populations and imaging operators.

From acquisition to insights: AI in post-processing for cardiac MRI

Artificial intelligence now plays a central role in post-processing for cardiac MRI, transforming tasks that were once manual and time-consuming into fast, reproducible, and operator-independent steps. Automated segmentation of the ventricles, atria, and myocardium allows direct quantification of volumes, function, mass, and tissue characteristics within seconds. This reduces variability between operators and ensures consistent measurements, even in complex cases with significant anatomical or pathological changes. Inline processing at the MRI console is also an important evolution that enables several analyses to be performed automatically before the patient even leaves the scanner room. These analyses include auto-

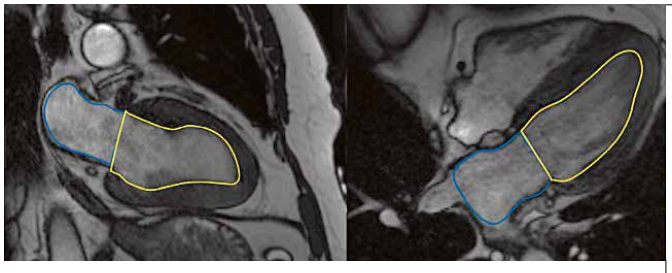

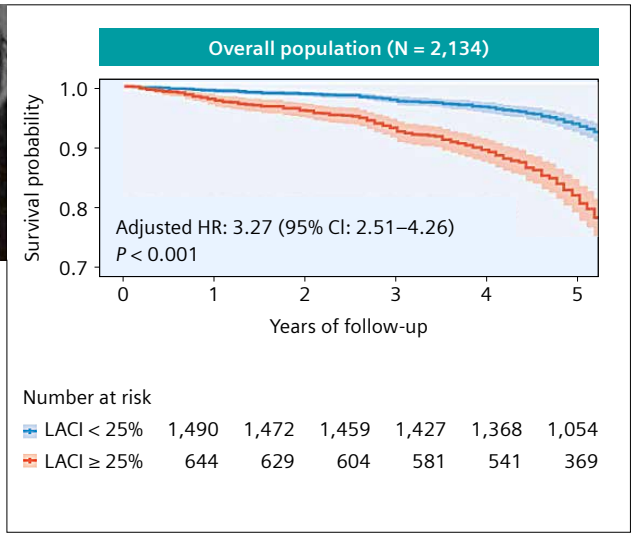

2 Example of a fully automated AI analysis to calculate the left atrioventricular coupling index (LACI). The AI algorithm automatically delineates the left atrial (yellow contour) and left ventricular (blue contour) volumes at end-diastole and computes their ratio. In more than 2,000 patients undergoing stress cardiac MRI, an elevated LACI (≥ 25%) identified by AI was strongly associated with a higher risk of hospitalization for heart failure or cardiovascular death during follow-up (Kaplan-Meier survival curves, adjusted HR 3.27, 95% CI 2.51–4.26, p < 0.001).

mated calculation of ventricular function from cine sequences, inline T1 and T2 mapping quantification, and strain analysis from feature tracking.

One of the current challenges lies in the automatic segmentation of late gadolinium enhancement (LGE). The wide variety of enhancement patterns across different pathologies, and variations between imaging sequences, make it difficult for algorithms to deliver consistently accurate results in every case. Even when advanced image analysis can identify highly relevant diagnostic and prognostic markers – such the left atrial coupling index (LACI) [1] – their use in clinical routine is often limited by the time required for manual measurements. This highlights the strong potential of fully automated algorithms that can perform these complex segmentations and calculations under the supervision of physicians, ensuring both speed and reliability while preserving clinical oversight (Fig. 2).

The impact on efficiency is considerable: Physicians spend less time on repetitive and manual processing steps and can focus more on interpretation and clinical decision-making while benefiting from standardized, high-quality outputs that facilitate reporting. In addition, the availability of structured and machine-readable quantitative data supports downstream applications such as multimodality integration, phenomapping, and prognostic modeling. AI in image analysis is therefore not only a time-saver but also a cornerstone for building robust diagnostic and prognostic tools for patient care.

AI-driven diagnostic and prognostic tools in multimodality cardiac imaging

Artificial intelligence has opened up new possibilities for creating powerful diagnostic and prognostic tools in cardiac MRI, enabling a shift from purely descriptive imaging towards predictive and decision-support systems. The first step in this process is the identification of relevant variables – a task at which AI algorithms such as the random forest excel. By processing hundreds of clinical, biological, and imaging parameters, these algorithms can rank features according to their importance for predicting patient outcomes, while avoiding redundancy from highly correlated variables. Once the most informative parameters are selected, a second step involves building a prognostic model. Advanced machine learning methods, such as multiple fractional polynomial modelling, combine and transform these variables into a predictive score that can outperform traditional risk models like the Framingham or ESC scores.

Beyond single-event prediction, AI can be applied to phenomapping, a form of unsupervised learning that groups patients into homogeneous clusters based on multimodal data. In cardiac MRI, this approach has proven valuable in heterogeneous conditions such as heart failure with preserved ejection fraction, pulmonary hypertension, and dilated cardiomyopathy. By revealing subgroups with distinct prognoses, phenomapping can guide both follow-up strategies and therapeutic decisions. Moreover, integrating cardiac MRI data with other modalities – such as echocardiography, CT, biomarkers, and even genetic information – moves us closer to the concept of the digital twin, a virtual replica of the patient's heart used to simulate disease evolution and test interventions before they are applied in real life.

A recent example from our team illustrates the potential of this approach [2]. In a large multicenter study of over 2,000 patients with newly diagnosed coronary artery disease, we developed a machine learning model that combined stress cardiac MRI and coronary CT angiography parameters, alongside clinical and electrocardiographic variables, to predict major adverse cardiovascular events. Using automated feature selection (least absolute shrinkage and selection operator) and an XGBoost algorithm, the model significantly outperformed existing prognostic scores and single-modality approaches, both in internal validation and in two independent external datasets (Fig. 3). This work demonstrates how AI can integrate complementary information from different imaging modalities to deliver more accurate and personalized risk stratification.

Random forest is a machine-learning method designed to classify or predict binary events (such as the presence or absence of disease). It builds a large number of decision trees, each trained on a random subset of the data and variables. The final prediction is obtained by majority vote across all trees, which reduces overfitting and improves accuracy compared to a single tree. Random forest can also rank variables according to their contribution to the prediction, helping to identify the most important risk factors.

A **digital twin for cardiac MRI** is a virtual model of the patient's heart. It combines imaging data with computational simulations to replicate actual cardiac structure and function. The digital twin can be used to produce patient-specific analyses and predictions, and test different treatment options before involving the patient.

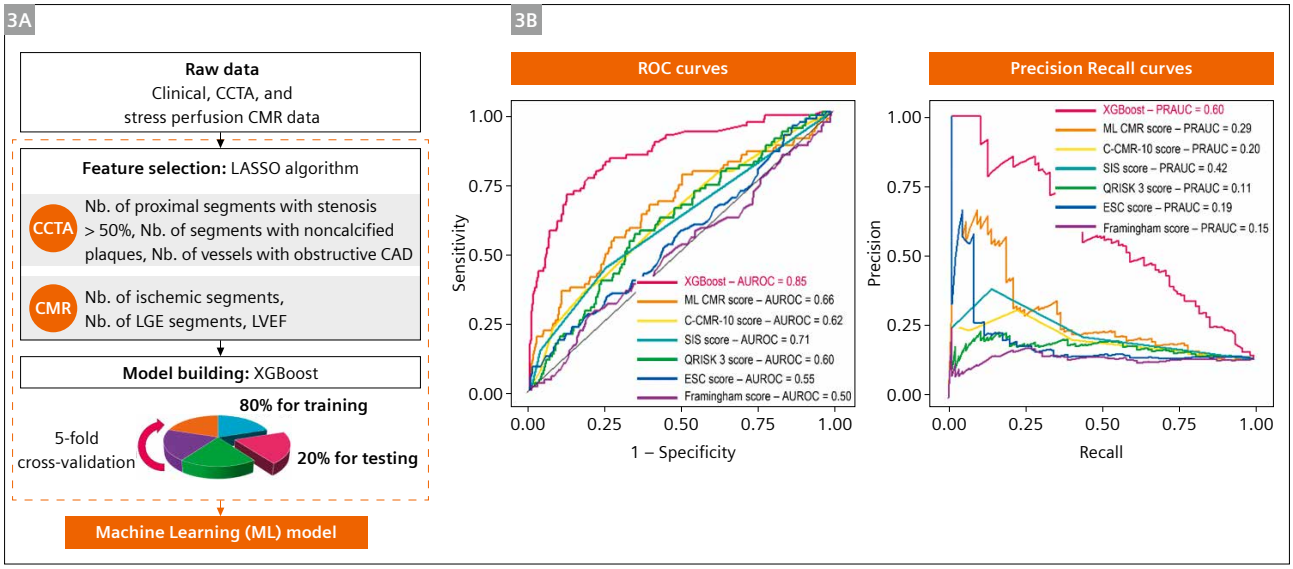

3 Machine-learning model using coronary CT angiography (CCTA) and stress CMRI to predict major adverse cardiovascular events.
(3A) The machine-learning-model method involved automated feature selection by least absolute shrinkage and selection operator (LASSO; three CCTA variables in the blue box and three CMRI variables in the green box), model building with an XGBoost algorithm, and five repetitions of 10-fold stratified cross-validation for the entire process.
(3B) Area under the receiver-operating characteristic curve (AUROC) and the precision recall curve (PRAUC) for the prediction of major adverse cardiovascular events (MACEs). The ML model had significantly higher AUROC and PRAUC for MACE prediction than all other risk scores ($p < 0.001$).

The ultimate goal of these AI-powered diagnostic and prognostic tools is to provide clinicians with accurate, reproducible, and actionable insights, enabling earlier interventions, more personalized treatment strategies, and improved outcomes for patients with cardiovascular disease.

Conclusion

Artificial intelligence is now a key driver in the evolution of cardiac MRI, with tangible benefits across all stages of the workflow from acquisition planning to reconstruction, image analysis, and advanced prognostic modeling. Current tools already reduce operator dependency, shorten examination times and improve reproducibility while paving the way for the extraction of new diagnostic and prognostic biomarkers.

The next step will be the seamless integration of multimodal data combining cardiac MRI with other imaging modalities and clinical and biological information to build comprehensive digital twins and decision-support systems. These advances will not replace clinicians; they will empower them, allowing more time for critical thinking and patient-centered decision making.

As we stand at the frontier of this transformation, our role as physicians is to ensure that these technologies are developed, validated, and implemented with the highest standards of scientific rigor, clinical relevance, and patient safety. In doing so, we can fully harness the potential of AI to deliver earlier, more precise, and more personalized care to our patients.

Contact

Solenn Toupin, Ph.D.
Département de Cardiologie et Radiologie
Hôpital Lariboisière, AP-HP Nord
2 Rue Ambroise Paré
75475 Paris Cedex 10
France
Solenn.toupin@gmail.com

Théo Pezel, M.D., Ph.D., FESC
Département de Cardiologie et Radiologie
Hôpital Lariboisière, AP-HP Nord
2 Rue Ambroise Paré
75475 Paris Cedex 10
France
Theo.pezel@aphp.fr

References

1 Pezel T, Garot P, Toupin S, Sanguineti F, Hovasse T, Unterseeh T, et al. AI-Based Fully Automated Left Atrioventricular Coupling Index as a Prognostic Marker in Patients Undergoing Stress CMR. JACC Cardiovasc Imaging. 2023;16(10):1288–1302.
2 Pezel T, Toupin S, Bousson V, Hamzi K, Hovasse T, Lefevre T, et al. A Machine Learning Model Using Cardiac CT and MRI Data Predicts Cardiovascular Events in Obstructive Coronary Artery Disease. Radiology. 2025;314(1):e233030.

A New Era in Cardiovascular MRI: The Advent of Full Free-Breathing Mode

Wenli Zhou[1], Kai Yang[1], Gang Yin[1], Jing An[2], Xinling Yang[1], Xiaoming Bi[3], Jianing Pang[3], Kelvin Chow[4], Minjie Lu[1,5]

[1]Department of Radiology, Fuwai Hospital, State Key Laboratory of Cardiovascular Disease, National Center for Cardiovascular Diseases, Beijing, China
[2]Siemens Shenzhen Magnetic Resonance Ltd., Shenzhen, China
[3]Siemens Medical Solutions USA Inc., Chicago, IL, USA
[4]Siemens Healthcare Ltd. Calgary, AB, Canada
[5]Key Laboratory of Cardiovascular Imaging (Cultivation), Chinese Academy of Medical Sciences, Beijing, China

Current status of CMR in China

Cardiovascular magnetic resonance (CMR) is a noninvasive, high-resolution imaging modality that enables comprehensive, one-stop evaluation of cardiac morphology, function, perfusion, and tissue characteristics [1]. Unlike other imaging techniques, CMR does not rely on ionizing radiation and can simultaneously provide multiple parameters with superior tissue contrast. It is particularly valuable in detecting myocardial edema, fibrosis, ischemia, and scar formation, and has become an indispensable diagnostic and prognostic tool in myocarditis, cardiomyopathies, coronary artery disease, heart failure, and various cardiovascular diseases (CVD) [2–4].

With the growing recognition of its clinical utility, CMR adoption in China has expanded rapidly since 2015, especially in eastern and southern regions [5]. Our center performs more than 20,000 CMR cases every year. These figures reflect the rising demand for CMR in clinical practice. Despite this progress, the problem of markedly uneven development remains. Prolonged examination time is one of the principal causes of this limitation – a single examination often requires 40 to 60 minutes, hindering throughput and worsening the patient experience. The complex workflow of conventional CMR demands repeated breath-holding interspersed with resting periods, leading to prolonged scan times. For vulnerable groups such as children, elderly patients, or individuals with heart failure who cannot adequately cooperate, image quality is often compromised, and in some cases examinations fail entirely, necessitating invasive alternatives that increase patient burden.

Technological breakthrough: Free-breathing CMR exams

To overcome the challenges of prolonged scan duration and dependence on breath-holding, various free-breathing techniques have been developed over the past decade, including respiratory navigator gating, self-gating, motion correction, compressed sensing, and AI-assisted sequence optimization [6, 7]. However, these approaches were generally limited to specific sequences and they failed to systematically transform the workflow. Fuwai Hospital, as the national cardiovascular center of China, plays a leading role in advancing cardiovascular care and imaging

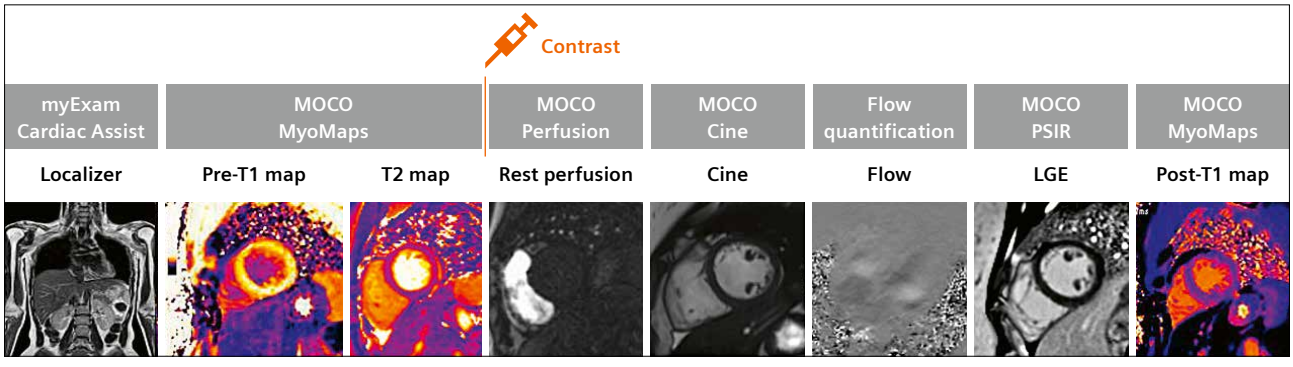

1 Full free-breathing CMR protocol.

research. In close partnership with Siemens Healthineers, our center has fostered intensive collaborations among clinicians, imaging scientists, and engineers, creating a fertile environment for the joint development and clinical translation of novel imaging technologies. Through this collaboration, we have pioneered the world's first fully integrated free-breathing CMR protocol, enabling intelligent and rapid examinations without the need for breath-holding. This breakthrough, patented in China, represents a milestone achievement of international significance.

Compressed Sensing (CS) and motion correction (MOCO) are core techniques implemented in the full free-breathing CMR protocol. Conceptually, CS leverages the inherent sparsity of CMR data to enable accurate image reconstruction from undersampled *k*-space, thereby substantially reducing acquisition time without compromising diagnostic fidelity [6]. Motion correction utilizes advanced retrospective algorithms to compensate for respiratory and cardiac motion, effectively reducing motion-related artifacts and maintaining image quality [8, 9]. The core innovation of our work lies in the deep integration of these two methodologies across several critical CMR sequences, leading to a qualitative leap in acquisition efficiency and diagnostic robustness.

Full free-breathing CMR examinations are performed on a 3T scanner (MAGNETOM Vida, Siemens Healthineers, Erlangen, Germany) using an 18-channel body coil. The detailed protocol (Fig. 1) included:

1. cardiac cine imaging: a prototype sequence with balanced steady-state free precession (bSSFP) readout, CS acceleration, and respiratory MOCO for left ventricular (LV) two-chamber, four-chamber, outflow tract, and multi-slice short-axis cine images[1];
2. T1 mapping: a modified Look-Locker inversion recovery (MOLLI) sequence was applied to acquire short-axis images at three different levels of the left ventricle;
3. T2 mapping: A T2-prepared sequence was implemented with identical acquisition levels as those used for T1 mapping;
4. flow imaging: a phase-contrast sequence with three averages was employed for acquiring images in four-chamber and outflow tract orientations;
5. rest perfusion: gadolinium-DTPA (Bayer AG, Leverkusen, Germany) was intravenously administered, followed by dynamic acquisition of 80 cardiac phases;
6. LGE imaging: following intravenous injection of gadolinium-DTPA at a dose of 0.2 mmol/kg and an infusion rate of 2 mL/s, imaging was performed 10 minutes later using a phase-sensitive inversion recovery (PSIR) sequence.

Clinical value of a full CMR exam in free-breathing

To evaluate the efficiency and feasibility of a full CMR exam in free-breathing in real-world clinical practice, our center has conducted several prospective validation studies, including the assessment of cine and LGE sequences in 250 patients and the validation of the entire protocol in a cohort of 605 subjects. We present the clinical feasibility of the full free-breathing CMR protocol by evaluating results from three perspectives: examination time, image quality, and the consistency of CMR-derived parameters.

Our recently published data in the Journal of Cardiovascular Magnetic Resonance showed that a full free-breathing CMR exam reduces the total examination time from 40 minutes to approximately 20 minutes (22.6 ± 3.7 min) while maintaining comprehensive diagnostic coverage [10]. Regarding image quality, all free-breathing sequences achieved image quality above the diagnostic threshold (≥ 3 points). The median image quality score for free-breathing short-axis cine imaging was 4 points (IQR: 4–4), and the image quality score for short-axis breath-holding cine was 5 points (IQR: 4–5), which was statistically higher than that of the free-breathing short-axis cine imaging ($P < 0.001$). However, unpublished data from another validation study showed that LGE imaging demonstrated superior quality compared with conventional breath-hold acquisition (5 vs. 4 points, $P < 0.001$), while the remaining sequences showed non-inferior performance. Importantly, in patients unable to cooperate with breath-holding, the full free-breathing scan significantly improved image quality and enhanced diagnostic reliability.

Furthermore, comparative data demonstrated that the end-diastolic volume (EDV), end-systolic volume (ESV), EDV index, and ESV index measured by free-breathing CMR were slightly higher than those measured under breath-holding (all $P < 0.05$), whereas the left ventricular ejection fraction and left ventricular mass were slightly lower (both $P < 0.05$). Native T1 values were slightly higher in the free-breathing scans compared with the breath-holding scans (1303.64 ± 74.44 ms vs. 1291.50 ± 77.32 ms, $P = 0.001$). Similarly, LGE mass was marginally greater in the free-breathing acquisitions than in the breath-holding acquisitions (10.49 ± 18.35 g vs. 9.41 ± 16.62 g, $P = 0.001$). Although some values showed minor differences, these were mainly attributable to physiological factors such as changes in intrathoracic pressure between free-breathing and breath-holding conditions, and they do not affect diagnostic performance or carry clinical significance. In addition, all parameters demonstrated

[1] *Work in progress. The application is currently under development and is not for sale in the U.S. and in other countries. Its future availability cannot be ensured.*

strong correlations between the two approaches (r = 0.92 – 0.99), with intraclass correlation coefficients (ICC) consistently above 0.91, indicating excellent measurement consistency and equivalent diagnostic accuracy. Overall, this complete workflow ensures that clinicians receive all necessary diagnostic information while patients benefit from a shorter, more comfortable examination (Figs. 2–4).

Future perspectives: Clinical and societal impact

The implementation of free-breathing CMR signals a paradigm shift toward more accessible and convenient cardiovascular imaging. In late 2024, the Ministry of Industry and Information Technology and the National Health Commission in China jointly approved the project "Development and Promotion of Full Free-Breathing CMR Examination," designating it a national key initiative.

The adoption of free-breathing protocols at Fuwai Hospital is expected to yield multiple benefits:

1. Expand patient eligibility by enabling reliable non-invasive imaging for vulnerable populations.
2. Enhance efficiency through reduced waiting times and increased scanner throughput.
3. Standardize image quality to ensure consistency across diverse clinical scenarios.
4. Democratize access by facilitating the dissemination of advanced CMR techniques from tertiary centers to regional and community institutions.

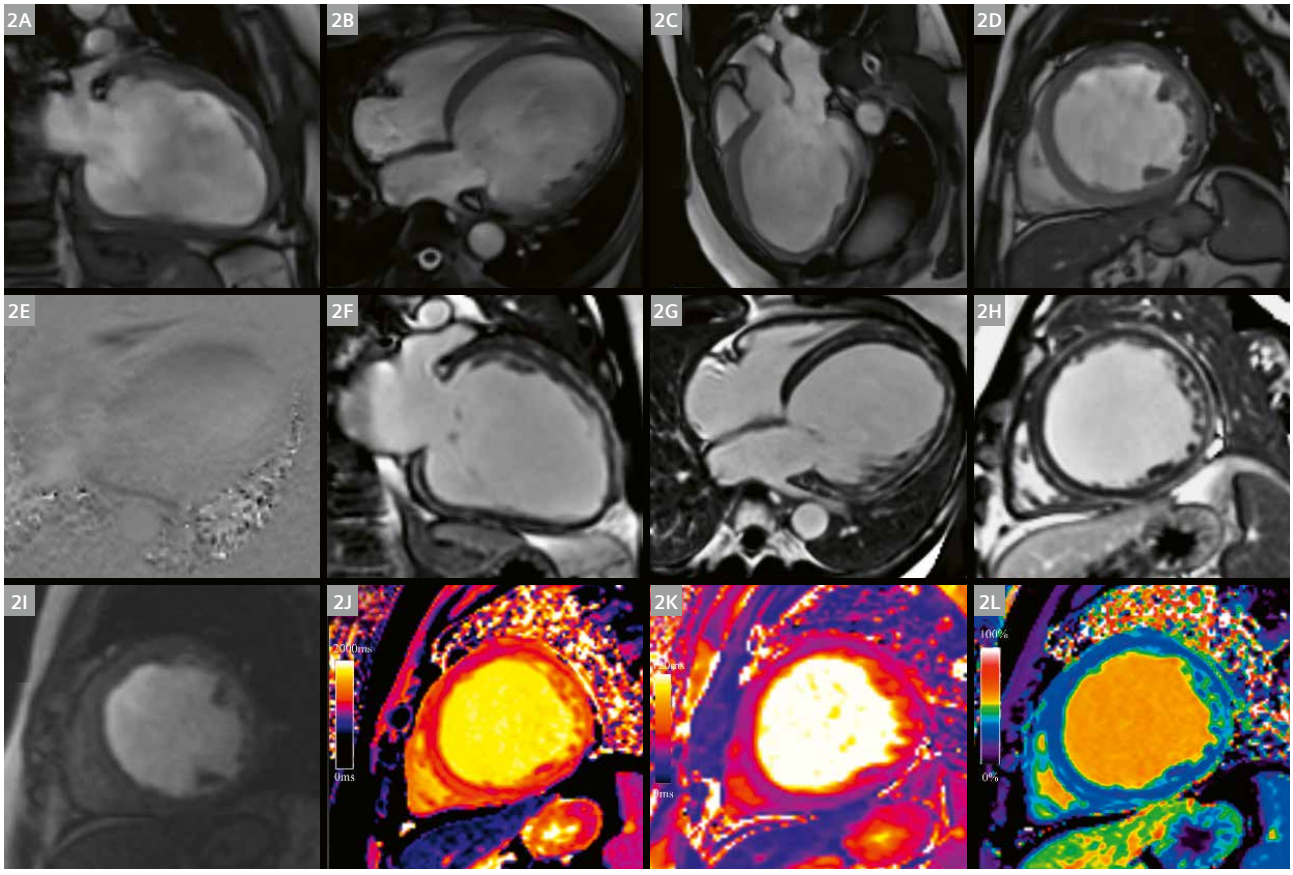

2 Full free-breathing CMR acquisitions of a 46-year-old patient with DCM and heart failure, with excellent image performance.
(2A) two-chamber view of cine; **(2B)** four-chamber view of cine; **(2C)** three-chamber view of cine; **(2D)** short-axis view of cine; **(2E)** flow; **(2F)** two-chamber view of LGE; **(2G)** four-chamber view of LGE; **(2H)** short-axis view of LGE; **(2I)** rest perfusion; **(2J)** pre-T1 map; **(2K)** T2 map; **(2L)** ECV.
CMR = cardiac magnetic resonance; DCM = dilated cardiomyopathy; LGE = late gadolinium enhancement; ECV = extracellular volume

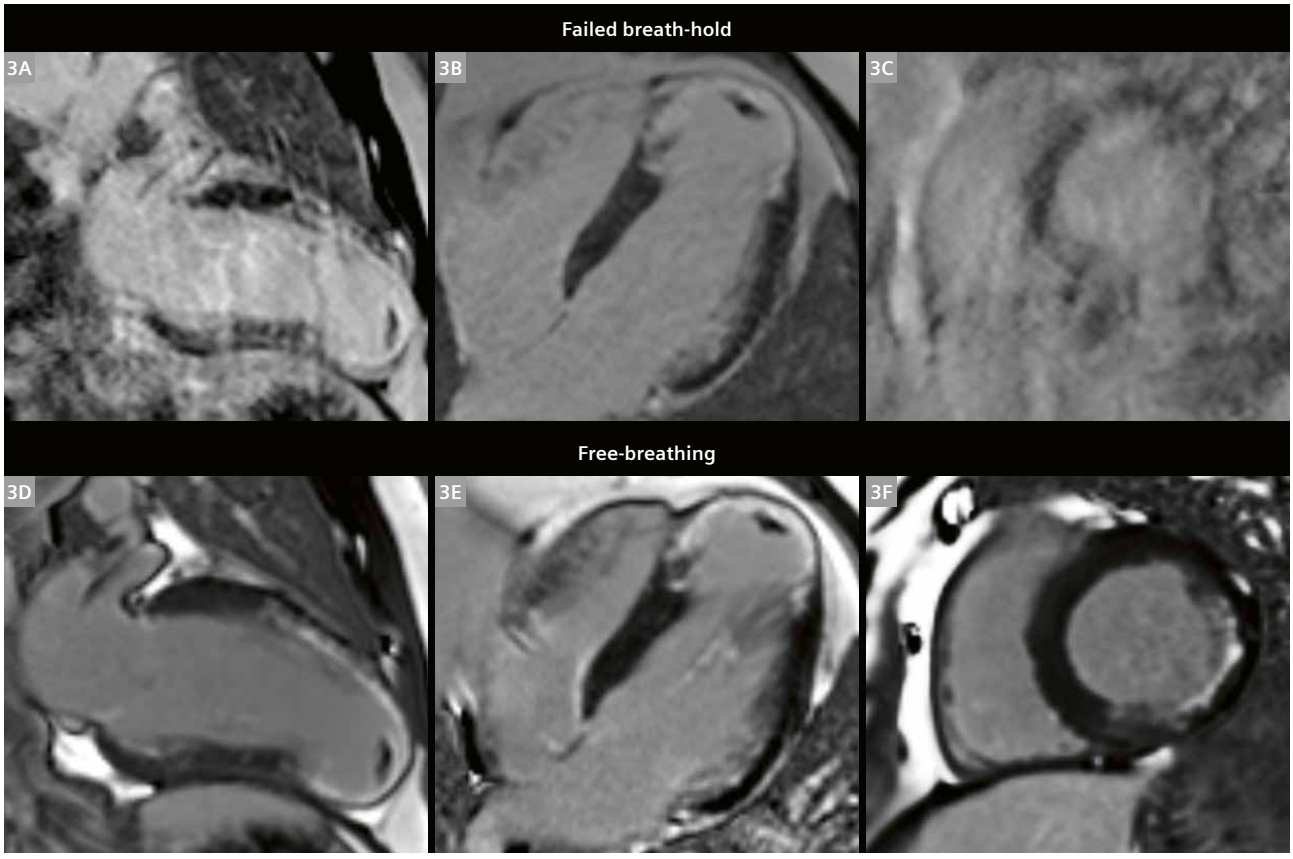

3 A 43-year-old male reported intermittent chest tightness for three years. Coronary CT angiography found triple vessel disease. The patient could not hold his breath during the CMR exam (score 1; **3A–C**). Free-breathing LGE scans substantially improved image quality (score 5; **3D–F**), revealing subendocardial enhancement in the anterior septum and lateral mid-ventricular wall, as well as transmural enhancement in the mid-distal septum, anterior wall, and apex.
CMR = cardiac magnetic resonance; CT = computed tomography; LGE = late gadolinium enhancement

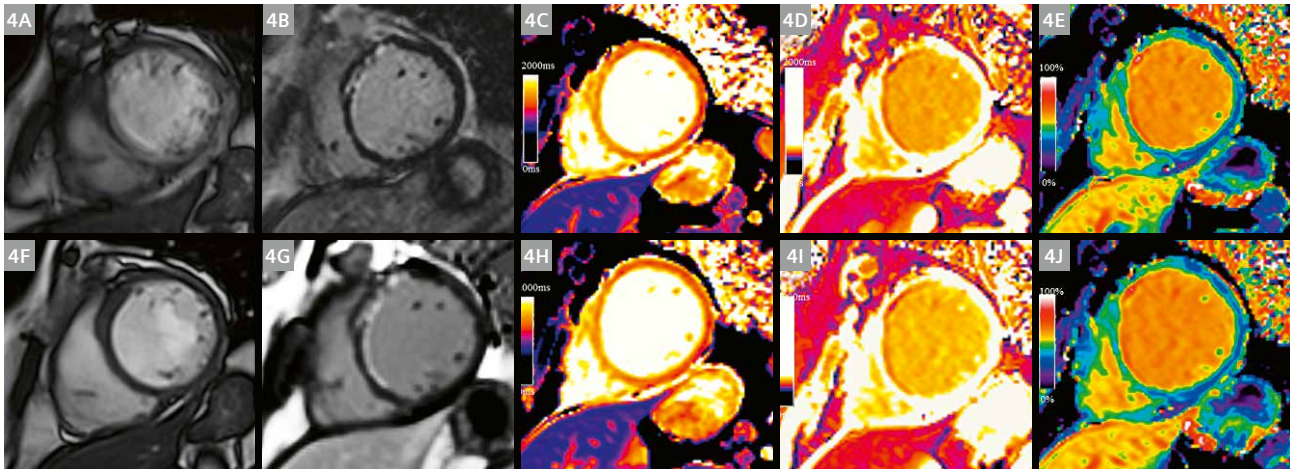

4 A 56-year-old female was diagnosed with CAD with chronic myocardial infarction. During a breath-holding CMR examination, the patient was unable to cooperate with breath-holding, resulting in significant artifacts in the cine images **(4A)**. A full free-breathing scan improved image quality **(4F)**. LGE showed subendocardial enhancement of the interventricular septum under breath-holding **(4B)** and free-breathing **(4G)**. No differences were observed between the three sequences in terms of image quality. **(4C, 4H)** BH vs. FB pre-T1 map; **(4D, 4I)** BH vs. FB post-T1 map; **(4E, 4J)** BH vs. FB ECV.
CAD = coronary artery disease; CMR = cardiac magnetic resonance; BH = breath-holding; FB = free-breathing; LGE = late gadolinium enhancement; ECV = extracellular volume

Ongoing work is focusing on more robust motion correction and conducting large-scale multicenter validations. Collaboration with equipment manufacturers will further improve adaptability and facilitate widespread clinical adoption.

Conclusion

Free-breathing CMR is not only a technological innovation, but also a milestone in making advanced cardiovascular imaging more equitable and patient-centered. By eliminating reliance on breath-holding, this approach delivers faster, smarter, and more widely accessible diagnostic services. With the scale of implementation at Fuwai Hospital and its national-level endorsement, free-breathing CMR is poised to become a cornerstone of precision cardiovascular medicine, bridging the gap between feasibility and accessibility, and between technological advancement and universal benefit.

References

1 Leiner T, Bogaert J, Friedrich MG, Mohiaddin R, Muthurangu V, Myerson S, et al. SCMR Position Paper (2020) on clinical indications for cardiovascular magnetic resonance. J Cardiovasc Magn Reson. 2020;22(1):76.

2 Lu M, Zhu L, Prasad SK, Zhao S. Magnetic resonance imaging mimicking pathology detects myocardial fibrosis: a door to hope for improving the whole course management. Sci Bull (Beijing). 2023;68(9):864–867.

3 Wang J, Yang S, Ma X, Zhao K, Yang K, Yu S, et al. Assessment of late gadolinium enhancement in hypertrophic cardiomyopathy improves risk stratification based on current guidelines. Eur Heart J. 2023;44(45):4781–4792.

4 Li S, Wang Y, Yang W, Zhou D, Zhuang B, Xu J, et al. Cardiac MRI Risk Stratification for Dilated Cardiomyopathy with Left Ventricular Ejection Fraction of 35% or Higher. Radiology. 2023;306(3):e213059.

5 Zhang H, Jiang M, Yang W, Zhou D, Wang Y, Zhu L, et al. Status of cardiovascular magnetic resonance in clinical application and scientific research: a national survey in China. J Cardiovasc Magn Reson. 2025;27(1):101877.

6 Bustin A, Fuin N, Botnar RM, Prieto C. From Compressed-Sensing to Artificial Intelligence-Based Cardiac MRI Reconstruction. Front Cardiovasc Med. 2020;7:17.

7 Ledesma-Carbayo MJ, Kellman P, Hsu LY, Arai AE, McVeigh ER. Motion corrected free-breathing delayed-enhancement imaging of myocardial infarction using nonrigid registration. J Magn Reson Imaging. 2007;26(1):184–90.

8 Piehler KM, Wong TC, Puntil KS, Zareba KM, Lin K, Harris DM, et al. Free-breathing, motion-corrected late gadolinium enhancement is robust and extends risk stratification to vulnerable patients. Circ Cardiovasc Imaging. 2013;6(3):423–32.

9 Fan H, Li S, Lu M, Yin G, Yang X, Lan T, et al. Myocardial late gadolinium enhancement: a head-to-head comparison of motion-corrected balanced steady-state free precession with segmented turbo fast low angle shot. Clin Radiol. 2018;73(6):593.e1–593.e9.

10 Yang K, Cui C, Teng F, Yin G, An J, Yang X, et al. Full Free-Breathing Cardiac MRI: Enhancing Efficiency and Image Quality in Clinical Practice. J Cardiovasc Magn Reson. 2025:101955.

Contact

Professor Minjie Lu, M.D., Ph.D.
Department of Magnetic Resonance Imaging, Fuwai Hospital
National Center for Cardiovascular Diseases
Chinese Academy of Medical Sciences & Peking Union Medical College
No. 167 Beilishi Road, Xicheng District
Beijing, 100037
China
Tel.: +010 68314466
coolcan@163.com

Transforming the Cardiac MRI Workflow with myExam Cardiac Assist

Thamara Carvalho Morais[1], Michael Silva[2], Kleber Schuler[1]

[1]Hospital Sirio-Libanês, Sao Paulo, Brazil
[2]Siemens Healthcare Diagnósticos Ltda., Sao Paulo, Brazil

Introduction

myExam Cardiac Assist represents a significant advancement in cardiovascular magnetic resonance (CMR) exams. Its features include automatic planning of cardiac views, calculation of the ideal number of slices to cover all short-axis views (preventing loss of slices at the base or apex of the heart, which is essential for accurate ejection fraction calculations), and calculation of the maximum number of slices based on the patient's breath hold capacity. Moreover, it provides clear step-by-step guidance throughout the examination process. It is an intuitive and quick-to-implement solution that requires minimal steps for application.

Impressive automation technology

One of the most impressive aspects of myExam Cardiac Assist is the fact that it is powered by artificial intelligence. The AutoAlign algorithm, for instance, automatically plans all cardiac views, ensuring exams are standardized and reproducible. This reduces the potential for error and delivers more reliable cardiac chamber volumes and ejection fraction measurements. Additionally, the step-by-step guides are extremely helpful, especially for teams with varied experience levels. Whether you're an experienced CMR operator or new to this area, the guides provide the right level of support to streamline the process.

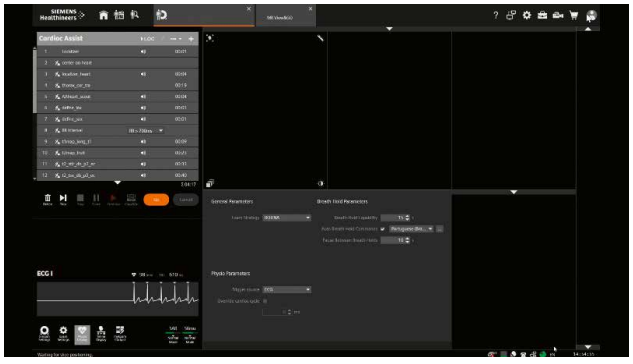

1 The intuitive home screen enables adjustments to settings such as the breath hold time to enhance the patient experience.

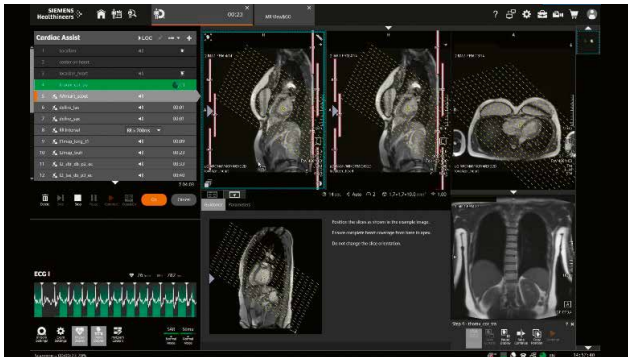

2 AutoAlign Heart Scout.

Physician's perspective: The positive impact of automation in CMR imaging

myExam Cardiac Assist has truly impressed me with how it simplifies and enhances CMR exams. The automated planning of cardiac views is fast and precise. The tool can also safely reorganize the acquisition order of basic CMR sequences, prioritizing late gadolinium enhancement (LGE) sequences, which can be easily acquired before cine imaging, for example.

Additionally, it ensures consistency in the alignment and number of slices across different sequence types, such as dark-blood sequences, mapping, cine MRI, and LGE. All these improvements significantly reduce scanner time, enhancing both workflow efficiency and the overall patient experience.

One thing I particularly like is the option to easily make manual adjustments. If I don't agree with the automated planning, manual intervention is simple and efficient, giving me full control without complicating the overall workflow. It's the best of both worlds.

Radiographer's perspective: The impact of myExam Cardiac Assist implementation

The myExam Cardiac Assist software has significantly enhanced the efficiency and accuracy of CMR imaging by automating the exam planning process. This minimizes the need for manual adjustments during slice acquisition and planning, enabling faster execution of standardized examinations.

Initial experience

Our initial experience spans six months of using myExam Cardiac Assist on our 1.5T MAGNETOM Aera (software version *syngo* MR XA60). This period yielded remarkable results. The automation reduces the number of manual interactions ("clicks"), allowing MRI radiographers to focus more on patient monitoring. It also enhances the ability to precisely verify the quality of the acquired sequences, optimizes workflow organization, and enables more meticulous review of the images. The automation of planning processes has substantially reduced exam duration, thereby increasing overall productivity.

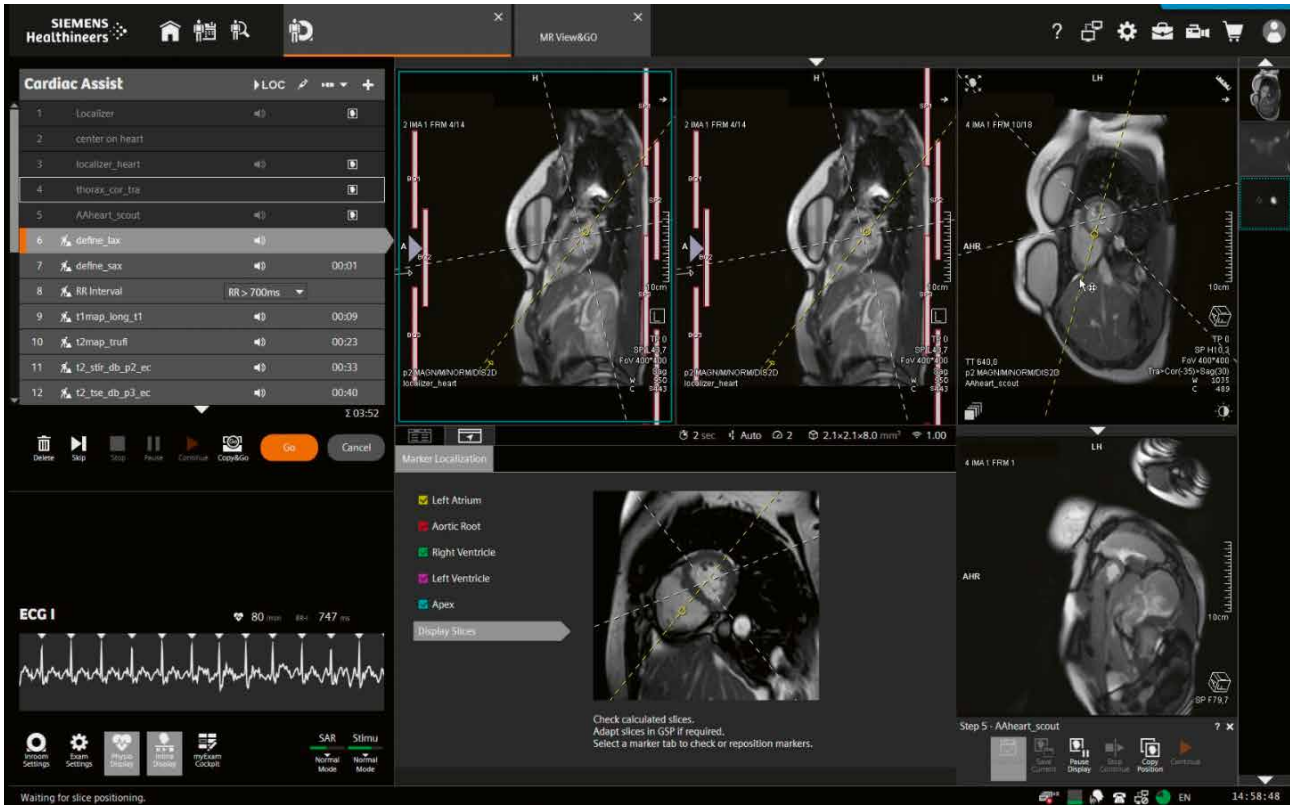

3 In addition to automation, the system offers a reference base image, which is essential for guiding less experienced operators through the planning process.

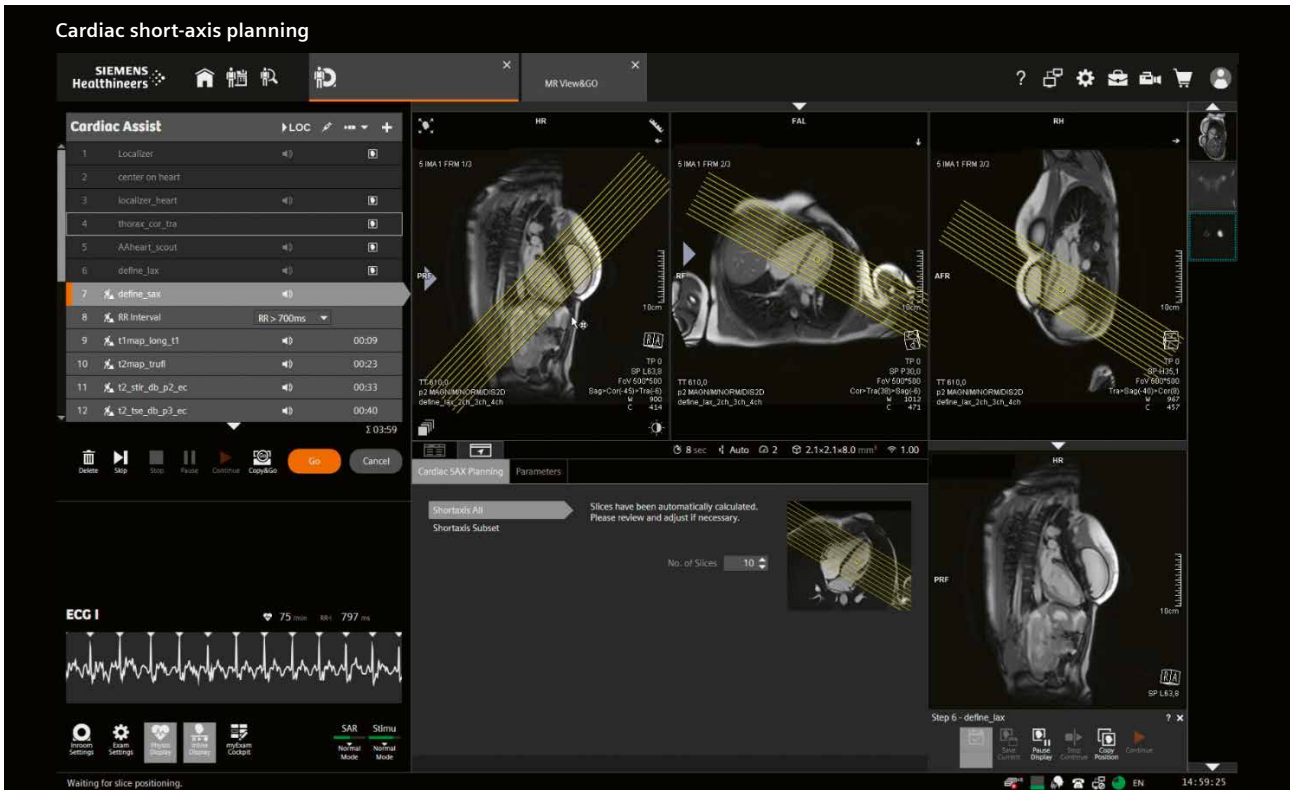

4 Planning Shortaxis All.

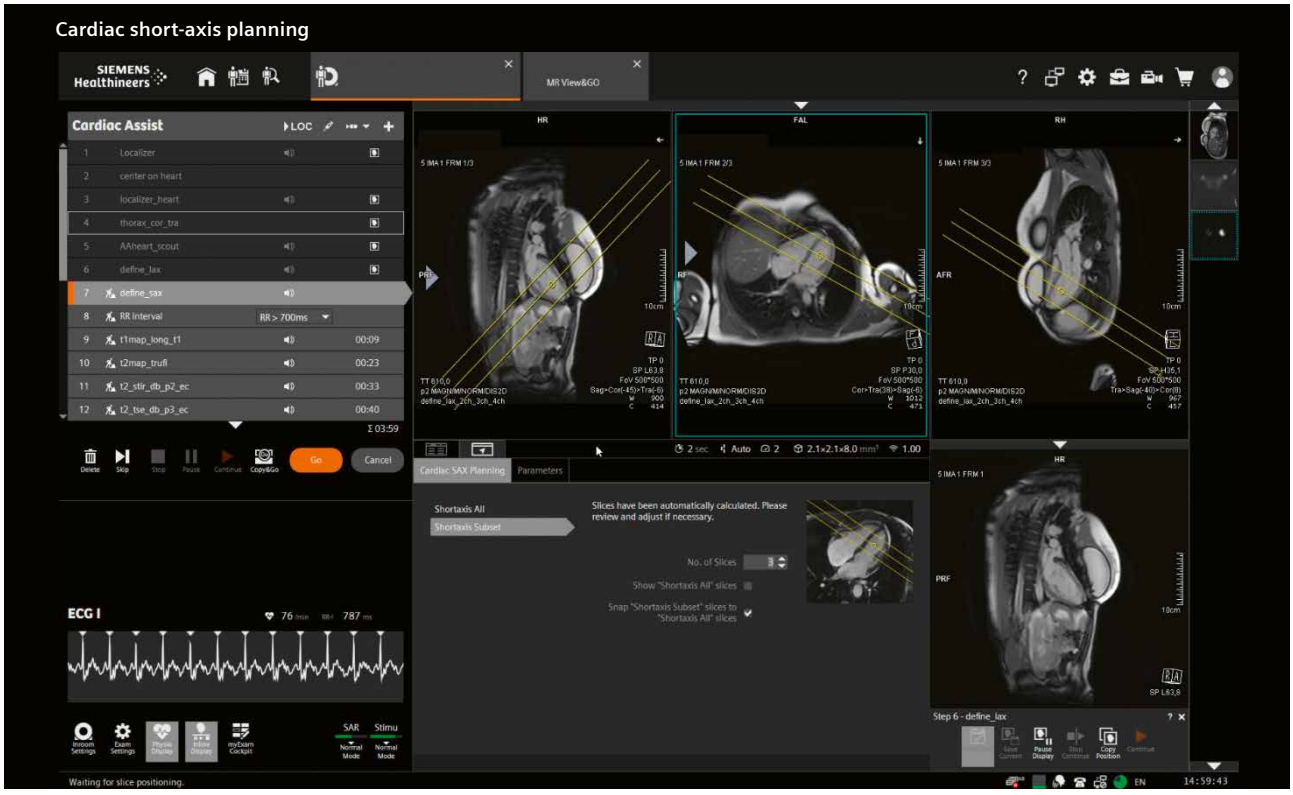

5 Planning Shortaxis Subset.

6 During cardiac planning, the reference lines allow users to verify the alignment of all cardiac views in just a few clicks.

Advantages observed

myExam Cardiac Assist incorporates several advantages as listed above. These benefit both MRI radiographers and patients by reducing scanner time and enhancing the patient experience.

From my perspective, myExam Cardiac Assist is a groundbreaking innovation that simplifies complex CMR imaging. It is important to note that effective use of this tool still requires a comprehensive understanding of cardiac anatomy and technical proficiency to accurately assess the quality of the acquired sequences.

Conclusion

myExam Cardiac Assist is a game-changer. It exemplifies how technology can streamline the workflow for health-care professionals while improving patient satisfaction with faster examinations. Its ability to organize protocols for a variety of clinical conditions – myocarditis, arrhythmias, cardiomyopathies, and more – while minimizing planning and execution errors is invaluable. For us, this tool is not just a time-saver; it is a meaningful step forward in how we approach CMR exams.

Contact

Thamara Carvalho Morais, M.D.
Department of Radiology
Hospital Sírio-libanês
Rua Adma Jafet, 91, Sao Paulo,
SP 01308-050, Brazil.
thamara.cmorais@hsl.org.br

Kleber Shiratori Schuler
MRI Biomedical Professional
Department of Radiology
Hospital Sírio-libanês
Rua Adma Jafet, 91, Sao Paulo,
SP 01308-050, Brazil.
kleber.schuler@hsl.org.br

BioMatrix Beat Sensor: Initial Clinical Experience with a MAGNETOM Flow. System

Siderlei Lemes[1], Clanir Dias[2], Michael Silva[2], Tatiana Velez[2]

[1]Hospital Beneficência Portuguesa, Bauru, SP, Brazil
[2]Siemens Healthineers LAM, Rio de Janeiro, Brazil

Introduction

The BioMatrix Beat Sensor is a technological advancement in the field of cardiac magnetic resonance imaging (CMR), offering an effective and simplified alternative to the traditional electrocardiogram (ECG) method [1, 2]. Cardiac synchronization is essential for CMR, but ECG accuracy can be significantly affected by artifacts related to gradient pulses, the magnetohydrodynamic effect, and the patient's physical characteristics and conditions such as body size, chest hair, and arrhythmias [1, 3].

The BioMatrix Beat Sensor is a cardiac triggering system that is independent of the MR image acquisition and represents the cardiac application of the general pilot tone (PT) motion detection technology [3]. The PT technology is based on the principle that a constant continuous wave (CW) RF signal transmitted by a small loop antenna, typically integrated into a body coil, is modulated by physiological motion, among them cardiac movement. The signal captured by the receiving coils, after being modulated by the movement of conductive tissues, corresponds to the cardiac volume curve which used as a trigger signal source [1, 2, 4].

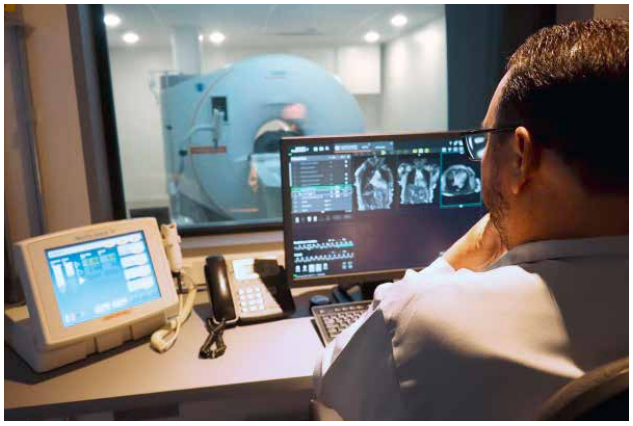

1 MRI examination using the BioMatrix Beat Sensor on a MAGNETOM Flow. scanner at Hospital Beneficência Portuguesa.

We used Beat Sensor on the first 1.5T MAGNETOM Flow. installed in Brazil. The MAGNETOM Flow. Platform features 1.5T MRI systems with DryCool technology. With just 0.7 liters of liquid helium, the sealed-for-life magnet design removes the need to refill the system with liquid helium [5]. The system features three body coils (Contour Small, Medium, and Large) for use with patients of different sizes and all coils provide Beat Sensor functionality.

Initial clinical experience

In our work routine the main benefits of using of the BioMatrix Beat Sensor are the gain in practicality and time savings in patient positioning. We observed a reduction of approximately 10 to 15 minutes in patient preparation time, not to mention the time spent repositioning electrodes in cases of failures in the capture of ECG data. Another very important benefit is the patient's experience and comfort, as we can reduce patient exposure compared to electrodes, for which it is necessary to partially open the clothing at the top.

BioMatrix Beat Sensor in routine heart exams

The BioMatrix Beat Sensor training scan must be executed once. It is a crucial preparatory step that aims to calibrate PT signal processing for robust acquisition of cardiac and respiratory data during CMR imaging.

Protocol optimization

To ensure good practice and better reproducibility when using the BioMatrix Beat Sensor, we follow a number of procedures. They include keeping the patient relaxed during the training scan, and ensuring correct positioning of the coil (in case of doubt, we use the guidance on the Touch Patient Data Display). After the training stage, we check the signal quality before starting the scan. Then we apply the protocol strategy that we defined with the use of the Beat Sensor.

2 The BioMatrix Beat Sensor interface for a cardiac MRI scan.

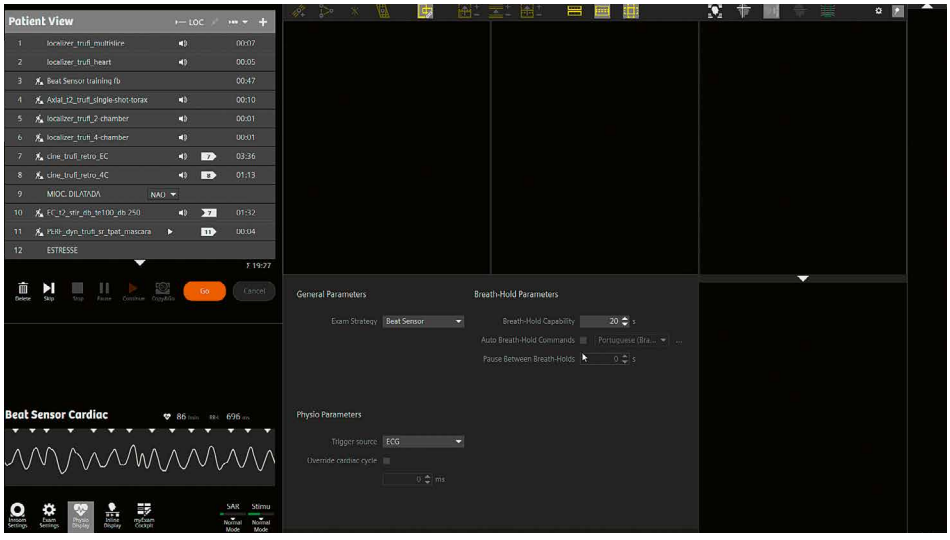

3 Defining the exam strategy using the BioMatrix Beat Sensor.

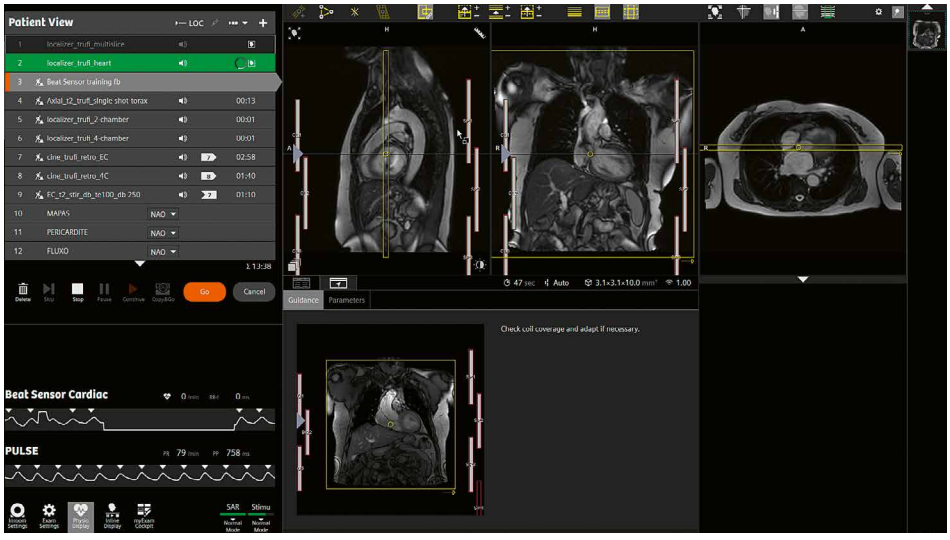

4 BioMatrix Beat Sensor training.

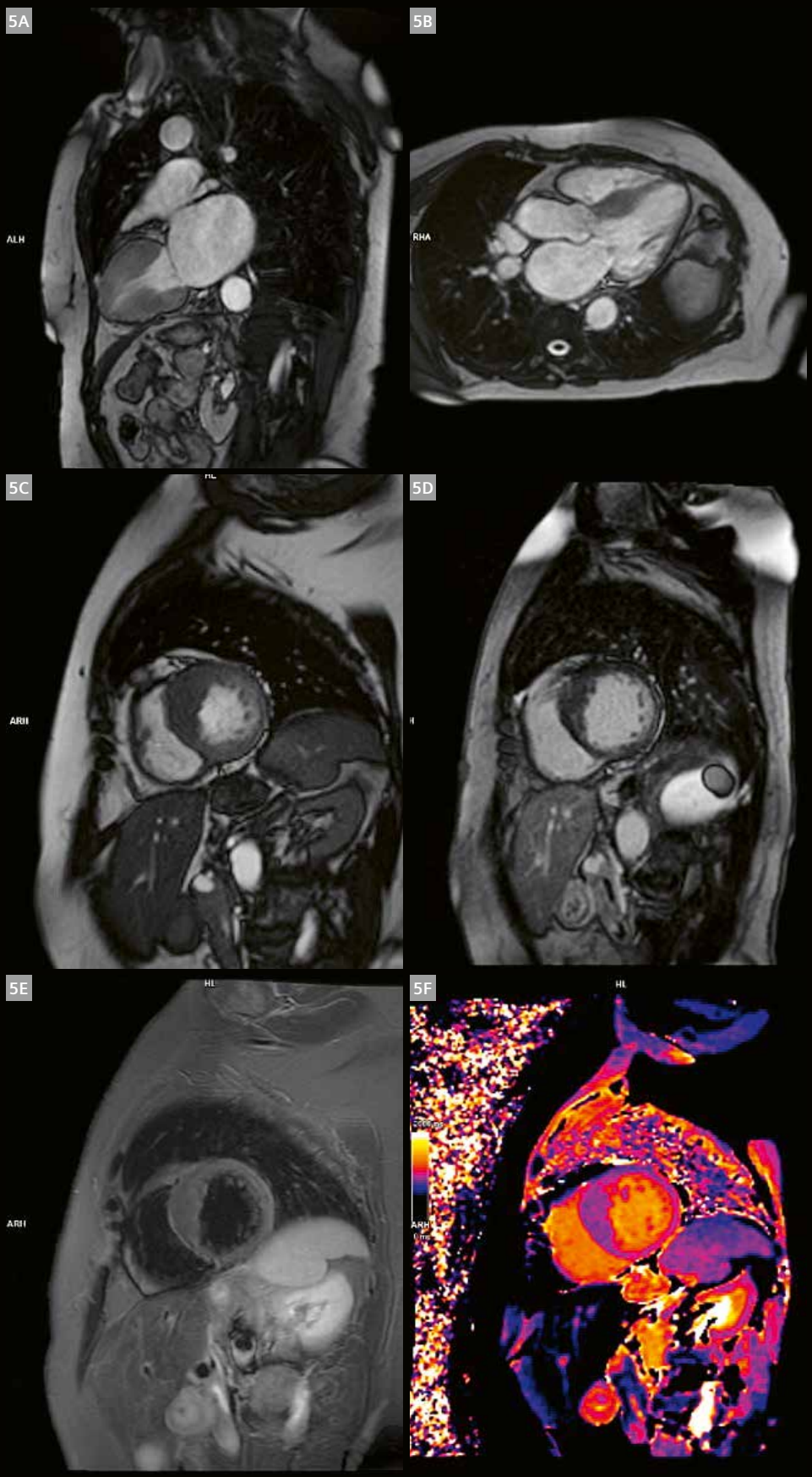

5 Example images acquired using MAGNETOM Flow. with the BioMatrix Beat Sensor. **(5A)** 2-chamber view, cine TRUFI; **(5B)** 3-chamber view, cine TRUFI; **(5C)** SAX cine TRUFI; **(5D)** LGE TRUFI,high-resolution PSIR; **(5E)** SAX STIR; **(5F)** T1 map long axis. TRUFI = true fast imaging with steady-state free precession; SAX = short axis; LGE = late gadolinium enhancement; PSIR = phase-sensitive inversion recocvery; STIR = short tau inversion recovery.

Conclusion

In addition to the benefits for optimizing the patient preparation time, we have also been able to verify the versatility of the Beat Sensor technology on the new 1.5T MAGNETOM Flow. Platform.

Using the BioMatrix Beat Sensor provides us with agility and practicality in the execution of exams. It improves the patient's experience during the exam, avoids time lost from repositioning electrodes, and reduces the costs associated with consumables such as carbon electrodes, material for cleaning and preparing the skin, and hair removal devices. In the context of "Cardiac Assist" workflows the trigger signal (ECG or Beat Sensor) is selected centrally at the beginning of the exam. Thus, besides the additional training step for Beat Sensor, exam follows same standard flow of slice planning and acquisition, including cardiac synchronization.

References

1 Mizuno N, Otaki Y, Manabe A, Iguchi N. Clinical Experience with the BioMatrix Beat Sensor: Cardiac MRI Exams Without ECG Leads. MAGNETOM Flash. 2024;86(1):54–59. ↗ https://marketing.webassets.siemens-healthineers.com/f487581014332bd3/afca4a63f593/siemens-healthineers-mizuno_Beat_Sensor_SCMR_2024.pdf

2 Goela A, Cesarin D. BioMatrix Beat Sensor: Initial Clinical Experience at a Regional Cardiac MR Center. MAGNETOM Flash. 2025;90(1):17–21. ↗ https://marketing.webassets.siemens-healthineers.com/279ef4ae5278b76d/5383101c1ff4/siemens-healthineers_Goela_Cesarin_BeatSensor_SCMR_2025.pdf

3 Speier P, Bacher M. Skip the Electrodes, But Not A Beat: The Engineering Behind the Beat Sensor. MAGNETOM Flash. 2023;84(2):106–117. ↗ https://marketing.webassets.siemens-healthineers.com/fc1d12f654808347/cd2adb8da170/siemens-healthineers_magnetom-world_Speier_BeatSensor_SCMR_2023_KORR.pdf

4 Falcão MBL, Di Sopra L, Ma L, Bacher M, Yerly J, Speier P, et al. Pilot tone navigation for respiratory and cardiac motion-resolved free-running 5D flow MRI. Magn Reson Med. 2022;87(2):718–732.

5 Siemens Healthineers. MAGNETOM Flow. Platform [Internet]. Erlangen, Germany: Siemens Healthineers. AG; 2025 [cited 2025 Oct 10]. Available from: ↗ https://www.siemens-healthineers.com/magnetic-resonance-imaging/0-35-to-1-5t-mri-scanner/magnetom-flow

Contact

Siderlei Reginaldo Lemes
Radiology Coordinator Technologist
Hospital Beneficência Portuguesa
Rua Rio Branco, 13-83, Centro
Bauru, SP, 17015-311
Brazil
Sider_lemes@hotmail.com

Clanir Dias
Senior MR Application Specialist
Siemens Healthineers LAM
SHS AM LAM CS EDU&BD BRA
clanir.dias@siemens-healthineers.com

Wideband Black-Blood Cardiac Magnetic Resonance in Patients with Implantable Cardiac Devices

Pauline Gut, M.Sc.[1,2,3]; Hubert Cochet, Ph.D.[1,4]; Matthias Stuber, Ph.D.[1,2,5]; Aurélien Bustin, Ph.D.[1,2,4]

[1]IHU LIRYC, Heart Rhythm Disease Institute, Université de Bordeaux – INSERM U1045, Pessac, France
[2]Department of Diagnostic and Interventional Radiology, Lausanne University Hospital and University of Lausanne, Switzerland
[3]Faculty of Biology and Medicine, University of Lausanne, Switzerland
[4]Department of Cardiovascular Imaging, Hôpital Cardiologique du Haut-Lévêque, CHU de Bordeaux, Pessac, France
[5]CIBM Center for Biomedical Imaging, Lausanne, Switzerland

Introduction

The use of implantable cardiac devices (ICDs), such as implantable cardioverter defibrillators and pacemakers, is the most effective treatment for ventricular tachycardia, for heart failure, and for preventing sudden cardiac death [1, 2]. Use of these devices has been increasing over the past decades [3, 4], with approximately 1.4 million implantations occurring worldwide each year [5]. Cardiovascular magnetic resonance imaging (MRI) has become an essential diagnostic tool, due to its ability to generate high-resolution images of soft tissues without ionizing radiation. With the development of modern MR-compatible ICDs [6], the prevalence of patients with ICDs undergoing cardiovascular MRI has increased in recent decades. About 50%–70% of these patients will require follow-up MRI scans during their lifetime [7].

Bright-blood late gadolinium enhancement (LGE) imaging, such as phase-sensitive inversion recovery (PSIR) [8], is clinically routinely applied in patients for myocardial scar assessment, as it provides an excellent scar-myocardium contrast. However, the poor scar-blood contrast can challenge the detection and assessment of subendocardial, small, or focal scars. This scar-blood contrast can be improved using black-blood LGE imaging [9], which simultaneously darkens healthy myocardium and blood signals while enhancing scar signal using an appropriate inversion time (TI).

Thanks to technological advances, most implantable devices such as ICDs are now designed to be MR compatible[1], enabling wider clinical use of cardiac MRI in this patient population. However, the presence of ferromagnetic materials in the generator of these devices creates strong field inhomogeneities around the device. This results in bright-blood LGE images and black-blood LGE images that are heavily impacted by signal loss, hyperintensity artifacts, and image distortion, often resulting in non-diagnostic images [10]. In this article, we present the "wideband" MRI technique for reducing ICD-related artifacts, and its application to black-blood LGE imaging.

Theory

The inversion recovery pulse used in the PSIR and black-blood sequences and discussed in this article is an adiabatic hyperbolic secant radiofrequency (RF) pulse. An adiabatic hyperbolic secant pulse of duration T_p, amplitude modulation A(t), phase modulation ϕ(t), and frequency modulation ω(t) is described by the following equations:

$$B_1(t) = A(t)\, e^{-i\phi(t)}$$

$$A(t) = A_0\, sech(\beta t)$$

$$\phi(t) = \mu\, ln(sech(\beta t))$$

$$\omega(t) = \frac{d\phi(t)}{dt} = -\mu\beta\, tanh(\beta t)$$

with $-T_p/2 \le t \le T_p/2$ (seconds), A_0 the maximum B_1 field amplitude (micro tesla), β the frequency modulation parameter (radians per second), and μ the degree of phase modulation (dimensionless). The RF spectral bandwidth Δf of an adiabatic hyperbolic secant is determined by:

$$\Delta f = \frac{\mu\beta}{\pi}$$

[1]*The MRI restrictions (if any) of the metal implant must be considered prior to patient undergoing MRI exam. MR imaging of patients with metallic implants brings specific risks. However, certain implants are approved by the governing regulatory bodies to be MR conditionally safe. For such implants, the previously mentioned warning may not be applicable. Please contact the implant manufacturer for the specific conditional information. The conditions for MR safety are the responsibility of the implant manufacturer, not of Siemens Healthineers.*

Finally, to fulfil the adiabatic passage, the maximum B_1 field amplitude must satisfy the following condition:

$$A_0 \geq \frac{\mu\sqrt{\beta}}{\gamma}$$

with γ being the gyromagnetic ratio in Hz/Gauss. A smaller increase in μ and a larger increase in β can achieve a certain RF spectral bandwidth without a dramatic increase in the B_1 amplitude A_0.

ICD-related artifacts on LGE images

Implantable cardiac devices have ferromagnetic components with positive magnetic susceptibility. When placed in a magnetic field environment, the field lines are distorted around the cardiac device. This generates local field inhomogeneities, resulting in off-resonant spins (≠ Larmor frequency) with a frequency shift of 2 to 6 kHz of tissues located at 5 to 10 cm from the device generator [11]. When applying a bright-blood LGE sequence such as PSIR, the inversion recovery pulse used in the sequence will correctly invert spins at the Larmor frequency, but not off-resonant spins, as the frequency shift caused by the device may exceed the spectral bandwidth of the inversion pulse, typically around 0.8–1.1 kHz. This incorrect inversion results in a region of high signal intensity (bright region) caused by the mismapping of a disproportionate number of spins (MR signal) to this location during image reconstruction (Fig. 1). This abnormally bright region is known as a hyperintensity artifact, which often obscures the myocardium and compromises image quality and diagnosis. In addition, dephasing of protons on either side of the device generator boundary results in signal loss (dark region) (Fig. 1).

Banding artifacts can also be seen on PSIR LGE images in the presence of an ICD, and are associated with balanced steady-state free-precession (bSSFP) readout (Fig. 1A). The bSSFP readout relies on steady-state magnetization, which is achieved by rapidly repeating RF pulses with very short repetition times (TRs). The signal in bSSFP is a function of off-resonance frequency and varies periodically with off-resonance with a period of 1/TR. Field inhomogeneities (B0) cause phase accumulation between RF pulses. When the accumulation is a multiple of π, the signal nulls and dark bands appear [12]. A gradient recalled echo (GRE) readout can be used instead to avoid the banding artifacts when a cardiac implant is present (Fig. 1B). The GRE readout is much less sensitive to off-resonance since its signal does not periodically null with frequency offsets.

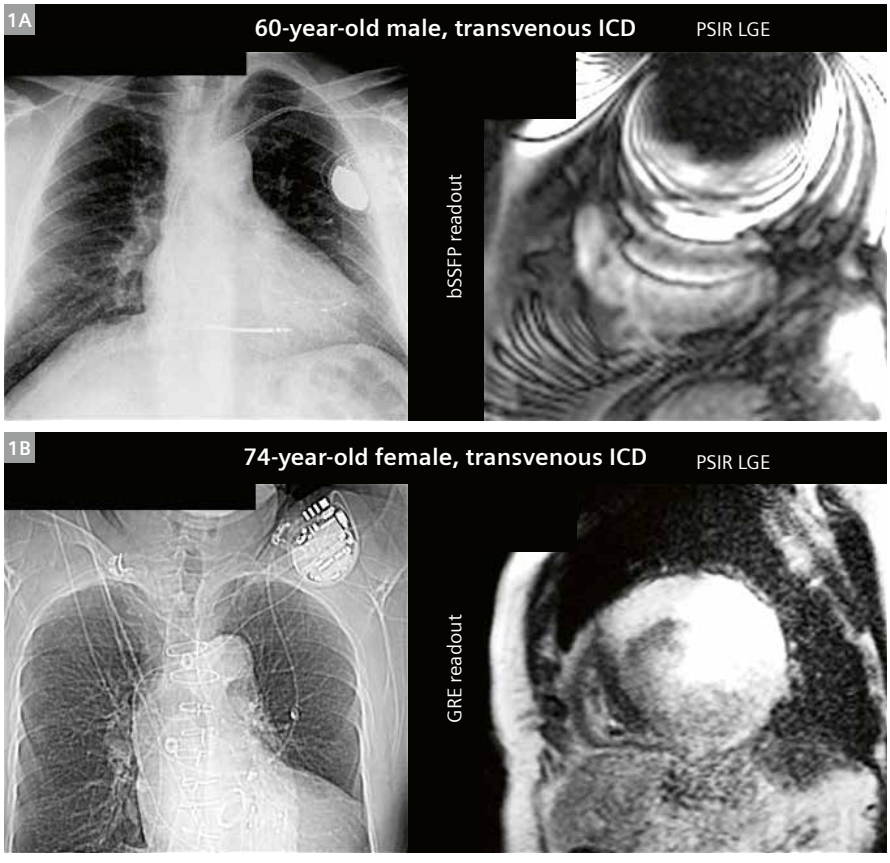

1 ICD-related artifacts on PSIR LGE images. **(1A)** Hyperintensity, signal loss, and bSSFP-associated banding artifacts. **(1B)** Hyperintensity and signal-loss artifacts, no banding artifacts with gradient echo readout.

Wideband bright-blood LGE

In 2014, Rashid et al. [11] introduced the concept of wideband PSIR LGE. They showed in their study a frequency shift of 2 to 6 kHz of tissues located at 5 to 10 cm from the device generator, which is well outside the standard spectral bandwidth of the 1.1 kHz inversion pulse. They therefore proposed to broaden the RF spectral bandwidth of the inversion pulse in the PSIR sequence from 1.1 to 3.8 kHz (μ = 16, β = 750 rad/s) (Figs. 2A, 2B). They showed that this RF spectral bandwidth broadening, known as wideband, enables the correct inversion of off-resonant spins, reducing or even eliminating hyperintensity artifacts that obscure the myocardium (Figs. 2C, 2D).

Wideband black-blood LGE

A black-blood LGE sequence can be achieved using inversion recovery followed by T2 preparation [13–15]. In this article, we present a 2D GRE black-blood sequence with inversion recovery (pulse duration = 10.24 ms) and T2 preparation (duration = 27 ms) (Fig. 3). The T2 preparation used is B1-insensitive and adiabatic, and consists of a 90°

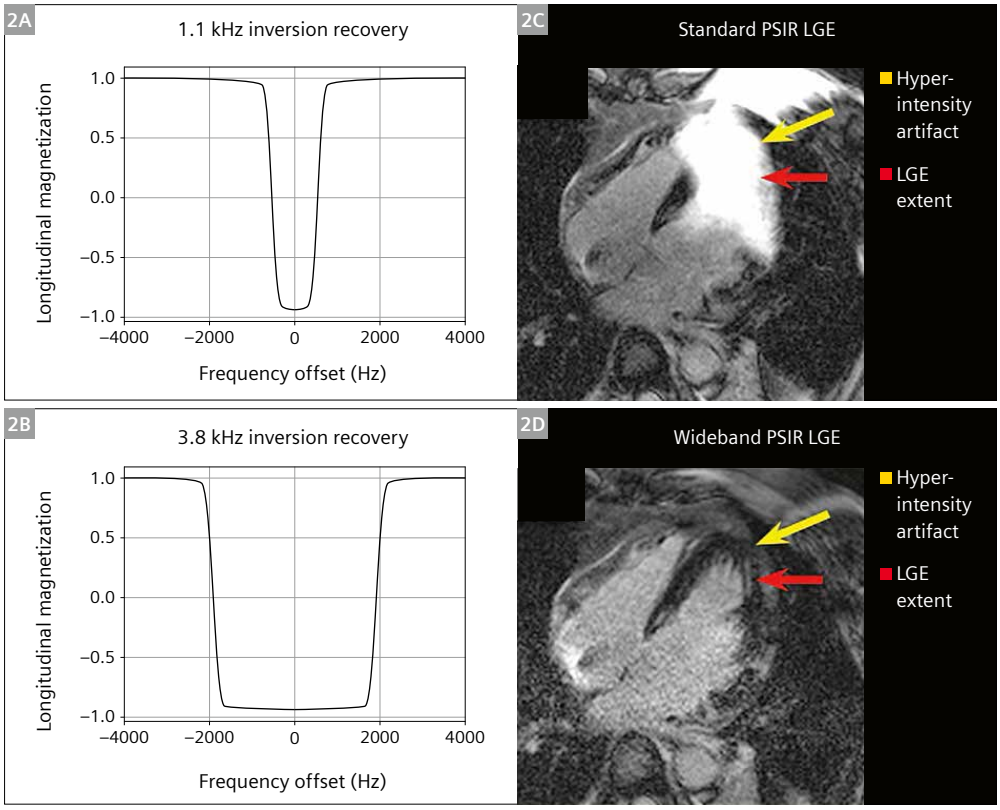

2 **(2A)** Standard spectral bandwidth of 1.1 kHz and **(2B)** wideband spectral bandwidth of 3.8 kHz of the inversion recovery pulse in the PSIR sequence, providing **(2C)** images with severe ICD-related hyperintensity artifacts and **(2D)** images with a net reduction in hyperintensity artifacts.

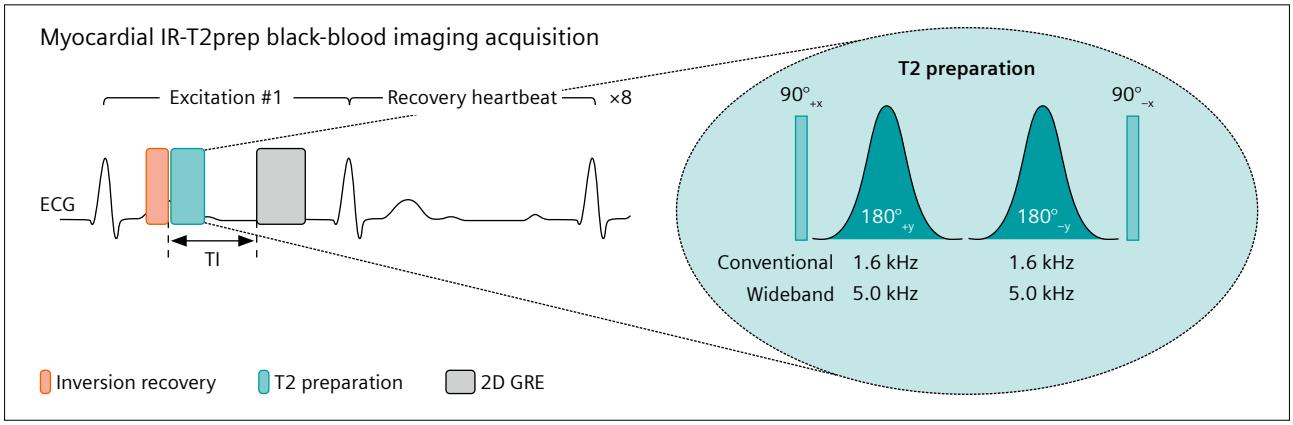

3 Myocardial IR-T2prep black-blood imaging framework, inversion recovery (IR) and T2 preparation pulses employed. Abbreviations: TI = inversion time; ECG = electrocardiogram; GRE = gradient echo.

tip-down RF pulse, two hyperbolic secant 180° refocusing RF pulses, and a 90° tip-up RF pulse [16] (Fig. 3). A spoiling gradient is then applied to suppress any residual transverse magnetization.

Similarly to PSIR, the spectral bandwidths used in the inversion recovery pulse (0.8 kHz), and the T2 preparation refocusing pulses (1.6 kHz) in the standard black-blood sequence are too narrow to properly prepare the magnetization in the presence of cardiac implants, resulting in LGE images with hyperintensities, signal loss, and image distortion (Figs. 4, 5). In 2024, wideband RF pulses were integrated into this black-blood LGE imaging to allow better LGE detection with reduced hyperintensity artifacts that obscure the myocardium in ICD patients [17] (Figs. 4, 5). It was proposed to broaden the spectral bandwidth of the inversion recovery from 0.8 to 3.8 kHz ($\mu = 16$, $\beta = 750$ rad/s, $A_0 = 19$ µT), as proposed for wideband PSIR, and to broaden the spectral bandwidth of the T2 preparation refocusing pulses from 1.6 to 5.0 kHz ($\mu = 25$, $\beta = 785$ rad/s, $A_0 = 30$ µT).

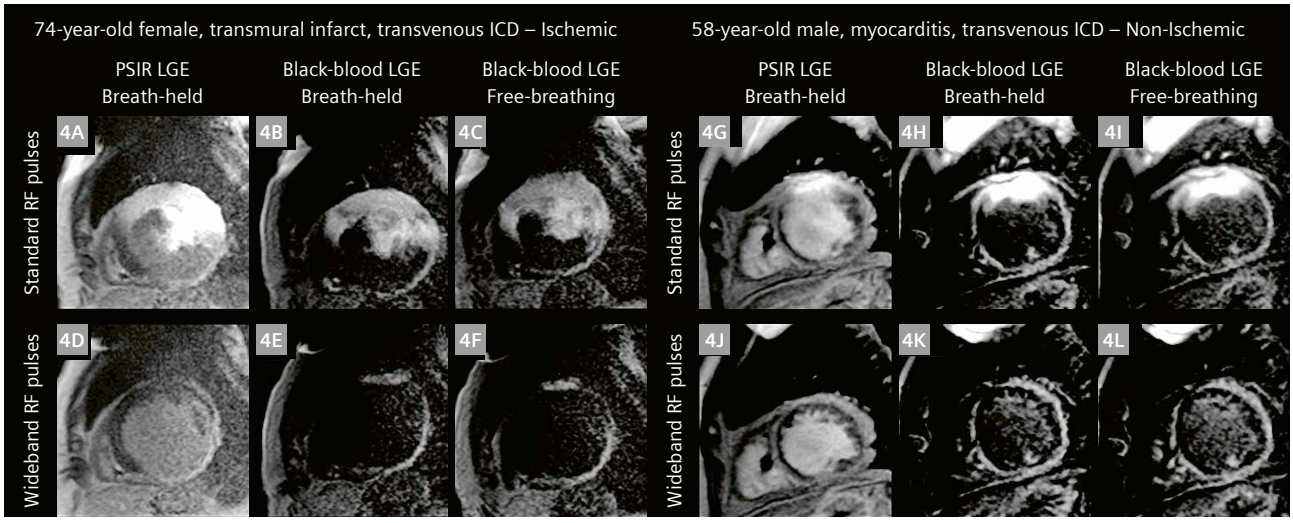

4 Cases 1 and 2. One female patient with ischemic infarct and one male patient with dilated cardiomyopathy with heart failure and reduced ejection fraction on probable myocarditis scar imaged at CHUV Lausanne University Hospital on a 1.5T MAGNETOM Sola system. Severe hyperintensities obscure the myocardium using standard PSIR LGE **(4A, 4G)** and standard black-blood LGE **(4BC, 4HI)**. These are suppressed using wideband PSIR LGE **(4D, 4J)** and wideband black-blood LGE **(4EF, 4KL)**.

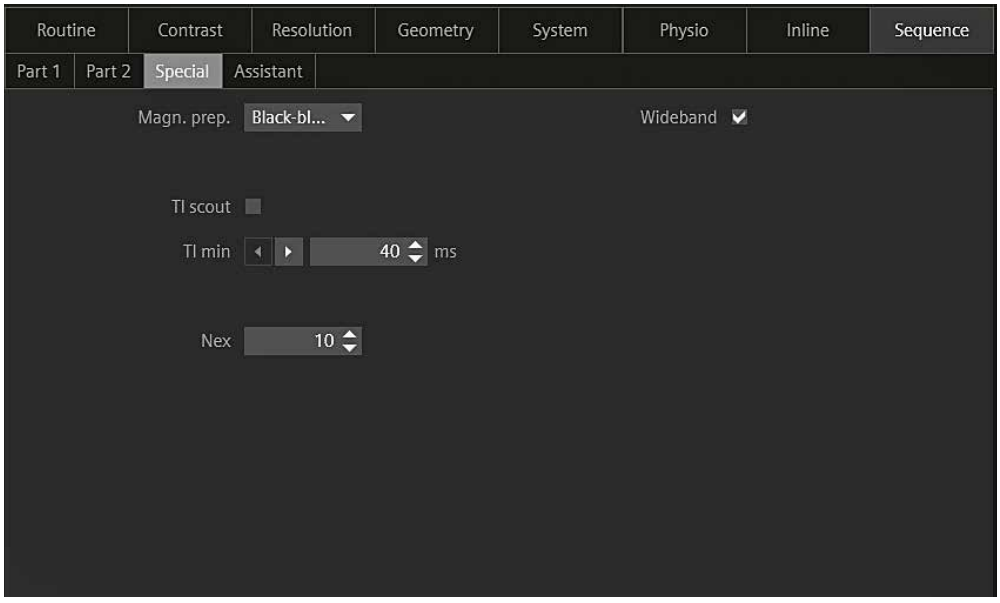

5 The Special card of the wideband black-blood sequence on a 1.5T MAGNETOM Sola system. Either PSIR or black-blood imaging can be chosen under "Magn. prep," not under "Contrast." Wideband RF pulses can be selected if the patient has an ICD. A TI scout can be performed for PSIR and black blood with or without wideband RF pulses. The number of excitations (Nex) is manually set and corresponds to the number of collected images for each slice position.

Tips and tricks for successful black-blood LGE imaging

Since its introduction, the 2D wideband black-blood GRE LGE sequence has been applied in a breath-hold study [17] and in a free-breathing study [18] with nonrigid motion correction at 1.5T (MAGNETOM Aera and MAGNETOM Sola, Siemens Healthineers, Erlangen, Germany). The protocol used is described in Table 1. It employs an electrocardiogram-triggered pulse to capture multiple single-shot images for each slice location during mid-diastole. In the special card of the protocol of the sequence at the MRI machine, PSIR or black-blood imaging can be chosen and wideband RF pulses can be activated or deactivated.

A dedicated TI scout can be performed with or without wideband RF pulses for both PSIR and black-blood LGE imaging. The optimal TI is then set to cancel to tissue of interest: black healthy myocardium for PSIR, and both black myocardium and black blood for black-blood imaging. The number of excitations (Nex) per slice location is determined manually (Fig. 5). A single short-axis slice is acquired within a single breath-hold or in free breathing with advanced non-rigid motion correction (Fig. 6), producing Nex images per slice position. The Nex images are then averaged, after motion correction if acquired in free breathing, into one high-quality image. A one-heartbeat gap between acquisitions allows for magnetization recovery. Below are some protocol recommendations:

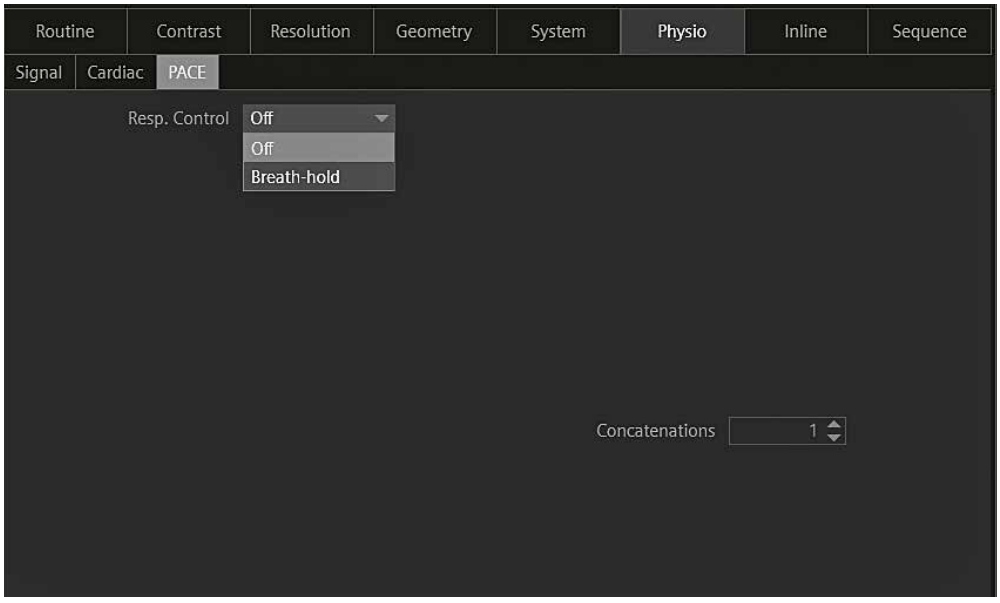

6 The Physio-PACE card of the black-blood imaging sequence on a 1.5T MAGNETOM Sola system. Images can be collected either during breath-hold or free breathing ("Resp. Control: Off"). In the case of free breathing, images will be delivered with motion correction (embedded in the reconstruction of the sequence).

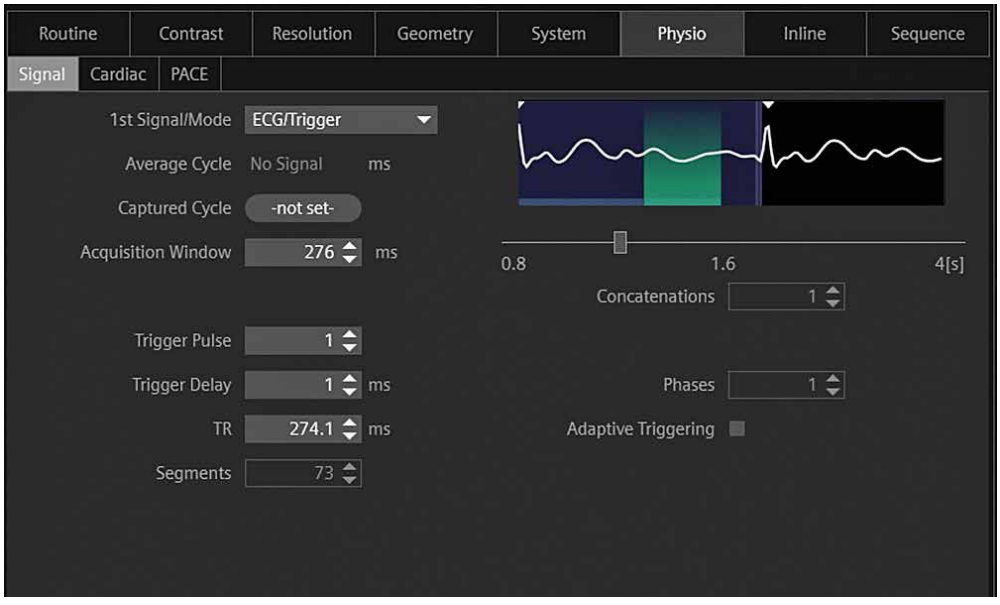

7 The Physio-Signal card of the black-blood imaging sequence on a 1.5T MAGNETOM Sola system. Images are collected during mid-diastole, and repetition time (TR) is set to the minimum.

1) We recommend collecting the images in mid-diastole (Fig. 7).
2) To achieve simultaneous darkening of healthy myocardium and blood signals, the correct TI needs to be determined with a dedicated wideband black-blood TI scout sequence (Fig. 5).
3) Regularly review the image contrast during acquisition (single-shot images are reconstructed and sent back to the operator on a beat-to-beat basis) and adjust the TI if necessary. Monitor the heart rate and adjust the trigger delay if necessary. Check for ghosting artifacts if performed in breath-hold, and check for wrapping artifacts.
4) Check for residual ICD-related hyperintensity artifacts obscuring the myocardium. If they are not completely suppressed, we recommend acquiring images with breath-hold during full inspiration to increase the heart-ICD distance. If this is not sufficient, the distance can be further increased by raising the patient's left arm and placing it next to their head.

MRI safety considerations

Before the 2000s, MRI was contraindicated in patients with any kind of cardiac implants (pacemaker, ICD, etc.). With the development of modern, smaller cardiac implants [6] with fewer magnetic components and improved electromagnetic interference safety, cardiac MRI has been shown to be safe at 1.5T with both MR-conditional and nonconditional cardiac implants [19–21] when following specific protocols and intraprocedural programming of the device [22–24]. The presence of fractured, abandoned, or epicardial leads still remains a contraindication to MRI.

Another aspect that has to be considered is the specific absorption rate (SAR). Wideband black-blood imaging is more SAR intensive than standard black-blood imaging, due to the increased B_1 amplitude in the inversion recovery and T2 preparation refocusing pulses. Wideband black-blood imaging is also more SAR intensive than wideband PSIR, due to the four additional RF pulses of the T2 preparation. For this prototype wideband black-blood imaging sequence at 1.5T, the proposed parameters (see Table 1) remained below the acceptable limit of 2 W/kg for clinical application, although SAR values were around 24 times higher than those of wideband PSIR. Nevertheless, a reassessment of the SAR deposit will be necessary for 3D applications.

Clinical applications

All images shown in this article were acquired by the Lausanne University Hospital on a 1.5T MAGNETOM Sola (software version *syngo* MR XA31 and XA51, Siemens Healthineers, Erlangen, Germany) and the University Hospital of Bordeaux on a 1.5T MAGNETOM Aera (software version *syngo* MR E11C) using a 32-channel spine coil and an 18-channel body coil.

Sequence setting	Parameter range
Acquisition	2D single-shot GRE
Cardiac control	ECG triggering
Respiratory control	Breath-holding
Spatial resolution	1.4 × 1.4 mm^2
Slice thickness	8 mm
Acquisition window	170–200 ms
Receiver bandwidth	751 Hz/pixel
Flip angle	15°
Paralell imaging	GRAPPA 2 with 36 reference lines
Phase FOV	75%
Phase resolution	76%
Partial Fourier	6/8
Asymmetric echo	Weak or Strong
Dummy heartbeats	0
k-space encoding	Linear
IR duration	10.24 ms
IR bandwidth	Conventional: 0.8 kHz; Wideband: 3.8 kHz
T2prep module	$90_x - 180_y - 180_{-y} - 90_{-x}$
T2prep duration	27 ms
T2prep refoc. bandwidth	Conventional: 1.6 kHz; Wideband: 5.0 kHz
Nex	5–10
Scan time	Nex * 2 heartbeats

Table 1: Wideband black-blood imaging sequence parameters. Abbreviations: ECG, electrocardiogram; FOV, field of view; GRAPPA, generalized autocalibrating partially parallel acquisitions; GRE, gradient recalled echo; Nex, number of excitations.

Findings in ischemic patients

In individuals with subendocardial or transmural infarct, wideband black-blood could improve LGE detection by 58% compared to wideband PSIR. This is explained by the contrast improvement at the scar-blood interface with the simultaneous darkening of healthy myocardium and blood. The improved scar detection was associated with an improvement in image quality of 5% [17, 18]. ICD-related hyperintensity artifacts were suppressed as well as with wideband PSIR, revealing LGE areas that may have been obscured.

Case 1: A 74-year-old female patient presenting with reduced left ventricular ejection fraction (20%), preserved right ventricular ejection fraction (48%), and a transvenous ICD. Severe hyperintensity artifacts hide half of the myocardium when using standard PSIR (Fig. 4A) and standard black-blood (Figs. 4B, 4C) LGE imaging, potentially masking the scar. Wideband sequences (Figs. 4D–4F) drastically reduced these artifacts, revealing all scarred segments with the presence of LGE in the inferior and inferolateral segments. The transmural LGE could be better manually segmented using wideband black-blood imaging than wideband PSIR. The application of nonrigid motion correction to black-blood LGE images obtained during free breathing resulted in sharp images (Fig. 4F).

Findings in non-ischemic patients

Dilated cardiomyopathy, hypertrophic cardiomyopathy, myocarditis, calmodulinopathy, and unknown-origin cardiomyopathy have been inspected with wideband black-blood LGE imaging, with midwall and subepicardial LGE findings. Overall, wideband black-blood LGE improved scar detection by 31%, with the same efficacy as wideband PSIR in suppressing ICD-associated hyperintensity artifacts. However, image quality was decreased by 8% compared to wideband PSIR, due to the lack of anatomical information [17, 18]. Scar localization with respect to the myocardial wall is challenged in black-blood imaging, due to the black healthy myocardium and blood signal. Therefore, especially for non-ischemic patients, bright-blood imaging remains essential to localize the LGE segments, whereas black-blood imaging is essential to detect the LGE segments. It is worth mentioning that these two acquisitions can be combined into a single sequence that provides coregistered bright- and black-blood LGE images.

Case 2: A 58-year-old male patient presenting with dilated cardiomyopathy with heart failure and reduced left and right ventricular ejection fraction (26% and 38%, respectively) on probable myocarditis scar. The patient was implanted with a transvenous ICD. Standard PSIR (Fig. 4G) and standard black-blood (Figs. 4H, 4I) LGE imaging revealed hyperintensity artifacts in the anteroseptal, anterior, and anterolateral segments. Wideband sequences (Figs. 4J–4L) were able to remove hyperintensity artifacts that masked the myocardium and LGE. Scar depiction was challenging with wideband PSIR, but improved markedly with wideband black-blood LGE imaging. The latter suggested strong evidence of subepicardial LGE in all segments. As in Case 1, the application of nonrigid motion correction to black-blood LGE images obtained during free breathing resulted in sharp images without ghosting artifacts (Figs. 4K, 4L).

What does the future look like?

Black-blood LGE imaging offers a significant advantage by improving LGE detection. However, as previously mentioned, accurate scar localization is essential for differentiating between ischemic and nonischemic cardiomyopathy, as well as for comprehensive pathological assessment. Bright-blood LGE plays a critical role in providing this spatial context but is acquired independently from black-blood LGE. A promising future direction involves combining these two techniques into a single integrated bright- and black-blood LGE sequence that enables coregistered imaging [25–27], as well as its 3D application.

Beyond distinguishing acute from chronic myocardial injuries with LGE, risk stratification in various myocardial diseases is vital for enhancing diagnostic and prognostic capabilities in structural heart disease. Cardiac parametric mapping, particularly T1 and T2 mapping, shows considerable promise in refining risk stratification in patients being evaluated for ICD therapy. These techniques may also enable longitudinal monitoring of myocardium post-ICD implantation, offering valuable insights into arrhythmic risk progression and supporting the tailoring of adjunctive therapies. The integration of parametric mapping with wideband RF pulses could be pivotal for quantitative cardiac MRI in ICD patients. Wideband T1 mapping has been proposed as a solution to the limitations of conventional T1 mapping in the presence of ICDs, though further clinical validation is needed [28, 29]. The feasibility of wideband T2 mapping in ICD patients has also been recently introduced but remains at an early stage of investigation [30]. Future preclinical and clinical studies are required to assess its sensitivity and specificity for detecting myocardial edema, acute inflammation, myocarditis, and takotsubo cardiomyopathy.

Conclusion

Magnetic resonance myocardial black-blood LGE imaging with wideband RF pulses holds significant promise for better LGE identification and characterization in ICD patients. The release of this C2P sequence could contribute to better LGE assessment in myocardial disorders in ICD patients and offer better access to cardiac MRI for this population.

Sequence availability

Our C2P sequence is currently available for sharing in *syngo* MR E11C, XA20, XA30, XA31, XA51, XA60, and XA61 on the C2P platform. The .exar1 protocol for the 1.5T MAGNETOM Sola (software version *syngo* MR XA61) is available to download on the MAGNETOM World website.

Acknowledgments

This research was supported by funding from the French National Research Agency under grant agreements Equipex MUSIC ANR-11-EQPX-0030, ANR-22-CPJ2-0009-01, and Programme d'Investissements d'Avenir ANR-10-IA-HU04-LIRYC, and by funding from the European Research Council (ERC) under the European Union's Horizon Europe research and innovation program (Grant Agreement No. 101076351).

References

1 Priori SG, Blomstrom-Lundqvist C, Mazzanti A, Blom N, Borggrefe M, Camm J, et al. 2015 ESC Guidelines for the management of patients with ventricular arrhythmias and the prevention of sudden cardiac death: The Task Force for the Management of Patients with Ventricular Arrhythmias and the Prevention of Sudden Cardiac Death of the European Society of Cardiology (ESC). Endorsed by: Association for European Paediatric and Congenital Cardiology (AEPC). Eur Heart J. 2015;36(41):2793–2867.

2 Ponikowski P, Voors AA, Anker SD, Bueno H, Cleland JGF, Coats AJS, et al. 2016 ESC Guidelines for the diagnosis and treatment of acute and chronic heart failure: The Task Force for the diagnosis and treatment of acute and chronic heart failure of the European Society of Cardiology (ESC)Developed with the special contribution of the Heart Failure Association (HFA) of the ESC. Eur Heart J. 2016;37(27):2129–2200.

3 Vaidya VR, Asirvatham R, Kowlgi GN, Dai MY, Cochuyt JJ, Hodge DO, et al. Trends in Cardiovascular Implantable Electronic Device Insertion Between 1988 and 2018 in Olmsted County. JACC Clin Electrophysiol. 2022;8(1):88–100.

4 Patel NJ, Edla S, Deshmukh A, Nalluri N, Patel N, Agnihotri K, et al. Gender, Racial, and Health Insurance Differences in the Trend of Implantable Cardioverter-Defibrillator (ICD) Utilization: A United States Experience Over the Last Decade. Clin Cardiol. 2016;39(2):63–71.

5 Kusumoto FM, Schoenfeld MH, Wilkoff BL, Berul CI, Birgersdotter-Green UM, Carrillo R, et al. 2017 HRS expert consensus statement on cardiovascular implantable electronic device lead management and extraction. Heart Rhythm. 2017;14(12):e503–e551.

6 Roguin A, Zviman MM, Meininger GR, Rodrigues ER, Dickfeld TM, Bluemke DA, et al. Modern pacemaker and implantable cardioverter/defibrillator systems can be magnetic resonance imaging safe: In vitro and in vivo assessment of safety and function at 1.5 T. Circulation. 2004;110(5):475–82.

7 Kalin R, Stanton MS. Current clinical issues for MRI scanning of pacemaker and defibrillator patients. Pacing Clin Electrophysiol. 2005;28(4):326–8.

8 Kellman P, Arai AE, McVeigh ER, Aletras AH. Phase-sensitive inversion recovery for detecting myocardial infarction using gadolinium-delayed hyperenhancement. Magn Reson Med. 2002;47(2):372–83.

9 Sridi S, Nuñez-Garcia M, Sermesant M, Maillot A, Hamrani DE, Magat J, et al. Improved myocardial scar visualization with fast free-breathing motion-compensated black-blood T1-rho-prepared late gadolinium enhancement MRI. Diagn Interv Imaging. 2022;103(12):607–617.

10 Gut P, Cochet H, Stuber M, Bustin A. Magnetic Resonance Myocardial Imaging in Patients With Implantable Cardiac Devices: Challenges, Techniques, and Clinical Applications. Echocardiography. 2024;41(11):e70012.

11 Rashid S, Rapacchi S, Vaseghi M, Tung R, Shivkumar K, Finn JP, et al. Improved late gadolinium enhancement MR imaging for patients with implanted cardiac devices. Radiology. 2014;270(1):269–74.

12 Bieri O, Scheffler K. SSFP signal with finite RF pulses. Magn Reson Med. 2009;62(5):1232–41.

13 Basha T, Roujol S, Kissinger KV, Goddu B, Manning WJ, Nezafat R. Black blood late gadolinium enhancement using combined T2 magnetization preparation and inversion recovery. J Cardiovasc Magn Reson. 2015;17(Suppl 1):O14.

14 Kellman P, Xue H, Olivieri LJ, Cross RR, Grant EK, Fontana M, et al. Dark blood late enhancement imaging. J Cardiovasc Magn Reson. 2016;18(1):77.

15 Basha TA, Tang MC, Tsao C, Tschabrunn CM, Anter E, Manning WJ, et al. Improved dark blood late gadolinium enhancement (DB-LGE) imaging using an optimized joint inversion preparation and T2 magnetization preparation. Magn Reson Med. 2018;79(1):351–360.

16 Nezafat R, Ouwerkerk R, Derbyshire AJ, Stuber M, McVeigh ER. Spectrally selective B1-insensitive T2 magnetization preparation sequence. Magn Reson Med. 2009;61(6):1326–35.

17 Gut P, Cochet H, Caluori G, El-Hamrani D, Constantin M, Vlachos K, et al. Wideband black-blood late gadolinium enhancement imaging for improved myocardial scar assessment in patients with cardiac implantable electronic devices. Magn Reson Med. 2024;92(5):1851–1866.

18 Gut P, Cochet H, Antiochos P, Caluori G, Durand B, Constantin M, et al. Improved myocardial scar visualization using free-breathing motion-corrected wideband black-blood late gadolinium enhancement imaging in patients with implantable cardiac devices. Diagn Interv Imaging. 2025;106(5):169–182. Epub 2024 Dec 12.

19 Nazarian S, Hansford R, Rahsepar AA, Weltin V, McVeigh D, Gucuk Ipek E, et al. Safety of Magnetic Resonance Imaging in Patients with Cardiac Devices. N Engl J Med. 2017;377(26):2555–2564.

20 Kim D, Collins JD, White JA, Hanneman K, Lee DC, Patel AR, et al. SCMR expert consensus statement for cardiovascular magnetic resonance of patients with a cardiac implantable electronic device. J Cardiovasc Magn Reson. 2024;26(1):100995.
21 Indik JH, Gimbel JR, Abe H, Alkmim-Teixeira R, Birgersdotter-Green U, Clarke GD, et al. 2017 HRS expert consensus statement on magnetic resonance imaging and radiation exposure in patients with cardiovascular implantable electronic devices. Heart Rhythm. 2017;14(7):e97–e153.
22 Nazarian S, Roguin A, Zviman MM, Lardo AC, Dickfeld TL, Calkins H, et al. Clinical utility and safety of a protocol for noncardiac and cardiac magnetic resonance Imaging of patients with permanent pacemakers and implantable-cardioverter defibrillators at 1.5 tesla. Circulation. 2006;114(12):1277–84.
23 Nazarian S, Halperin HR. How to perform magnetic resonance imaging on patients with implantable cardiac arrhythmia devices. Heart Rhythm. 2009;6(1):138–43.

Contact

Aurélien Bustin, Ph.D.
IHU LIRYC, Heart Rhythm Disease Institute
Avenue du Haut Lévêque
33000, Bordeaux
France
aurelien.bustin@ihu-liryc.fr

24 Nazarian S, Hansford R, Roguin A, Goldsher D, Zviman MM, Lardo AC, et al. A prospective evaluation of a protocol for magnetic resonance imaging of patients with implanted cardiac devices. Ann Intern Med. 2011;155(7):415–24.
25 Bustin A, Sridi S, Kamakura T, Jais P, Stuber M, Cochet H. Free-breathing joint bright- and black-blood cardiovascular magnetic resonance imaging for the improved visualization of ablation-related radiofrequency lesions in the left ventricle. EP Europace. 2022;24(Supplement_1).
26 de Villedon de Naide V, Maes JD, Villegas-Martinez M, Ribal I, Maillot A, Ozenne V, et al. Fully automated contrast selection of joint bright- and black-blood late gadolinium enhancement imaging for robust myocardial scar assessment. Magn Reson Imaging. 2024;109:256–263.
27 Richard T, de Villedon de Naide V, Nogues V, Génisson T, Narceau K, He K, et al. Improved and Automated Detection of Papillary Muscle Infarction Using Joint Bright- and Black-Blood Late Gadolinium Enhancement MRI. J Magn Reson Imaging. 2025. Online ahead of print.
28 Shao J, Rashid S, Renella P, Nguyen KL, Hu P. Myocardial T1 mapping for patients with implanted cardiac devices using wideband inversion recovery spoiled gradient echo readout. Magn Reson Med. 2017;77(4):1495–1504.
29 Hong K, Jeong EK, Wall TS, Drakos SG, Kim D. Wideband arrhythmia-Insensitive-rapid (AIR) pulse sequence for cardiac T1 mapping without image artifacts induced by an implantable-cardioverter-defibrillator. Magn Reson Med. 2015;74(2):336–45.
30 Gut P, Kim D, Cochet H, Sacher F, Jaïs P, Stuber M, et al. Wideband myocardial T2 mapping with implantable cardiac device: A preliminary evaluation in healthy volunteers at 1.5T. J Cardiovasc Magn Reson. 2025;27(Supplement 1):101276.

Try them on your system

Trial licenses for many of the applications featured in this issue of MAGNETOM Flash are available as a trial license free of charge for a period of 90 days.

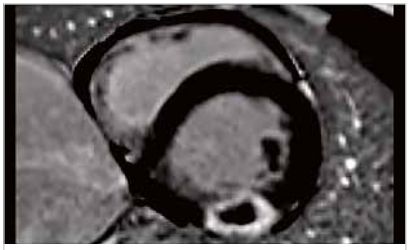

PSIR HeartFreeze

Late Gadolinium Enhancement (LGE) imaging in free-breathing.

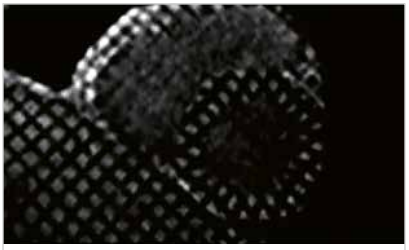

Advanced Cardiac

Special sequences and protocols for advanced cardiac imaging.

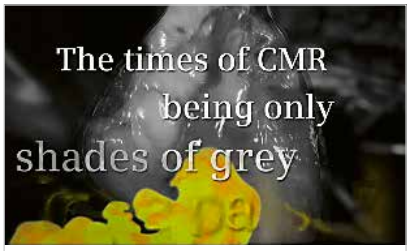

MyoMaps

The next step in quantitative cardiac assessment.

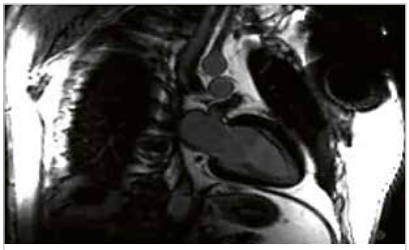

High Bandwidth Inversion Recovery

Cardiac inversion recovery for patients prone to susceptibility artefacts.

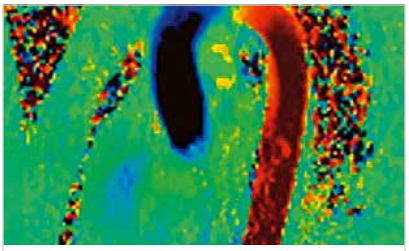

Flow Quantification

Special sequences (only AWP) for quantitative flow determination studies, measuring blood/CSF flow non-invasively.

Compressed Sensing Cardiac Cine

Beyond speed.
Beyond breathholds.

Additional technical prerequisites may apply. Upon receiving your request, your local Siemens Healthineers representative will clarify whether your system meets the requirements.

For further details, product overviews, image galleries and general requirements please visit us at:

www.siemens-healthineers.com/magnetic-resonance-imaging/options-and-upgrades/clinical-applications

Enabling Cardiac MRI at 0.55T: Early Results from MAGNETOM Free.XL

Daniel Giese, Manuela Rick, Oskar Isay, Axel Joachim Krafft, Michaela Schmidt

Siemens Healthineers, Erlangen, Germany

Cardiac magnetic resonance imaging (CMR) is crucial in the diagnosis and management of many cardiovascular diseases. The newly released 2025 ESC Guidelines for the management of myocarditis and pericarditis now include Class 1 recommendations for the use of CMR as a first-line diagnostic tool [1]. However, the availability of CMR remains limited, mainly due to cost, siting requirements, and lack of experienced personnel [2].

With the advancement of technical innovations such as minimal helium inventory, strong gradients, improved receiver coils, and deep learning-based image reconstruction algorithms, a renewed interest in lower field strengths is emerging in the MRI community [3]. Following the launch of the first 0.55T system – MAGNETOM Free.Max – in 2020, the worldwide CMR community immediately put it to the CMR test. Although the system was not released for cardiac applications, several research sites have highlighted its great potential for nearly all CMR contrasts and acquisitions [4, 5]. The large 80 cm bore has additionally allowed imaging in challenging cases, such as obese or claustrophobic patients who would not have had access to CMR [6]. A study using an animal model has even demonstrated the feasibility of using this system in an interventional CMR setting [7] Yet two limitations of the MAGNETOM Free.Max configuration for CMR, namely the limited gradient performance and the lack of a physiological triggering unit for ECG synchronization, were still to be overcome.

With the arrival of the newest 0.55T system from Siemens Healthineers, MAGNETOM Free.XL[1] (Fig. 1), comprehensive CMR exams can now be performed at 0.55T. Thanks to the integrated physiological monitoring unit and stronger gradient performance, users will be able to take full advantage of the benefits of scanning at 0.55T. Shorter echo times can reduce B_0 artifacts around devices[2]. Furthermore, the stronger gradients allow shorter acquisition times of single-shot-based CMR images, such as myocardial mapping, real-time cine, and myocardial perfusion imaging. The system will be presented to the CMR community at SCMR 2026 in Rio de Janeiro, Brazil. With its 100 cm flared opening, MAGNETOM Free.XL is also designed to support the workflow of interventional procedures. Its widespread application in diagnostic CMR has been eagerly awaited, especially due to the stronger gradient performance compared to MAGNETOM Free.Max.

1 MAGNETOM Free.XL has a 100 cm flared opening and is fully equipped to allow unprecedented CMR imaging at 0.55T.

Field strength	0.55T
Bore size	> 100 cm flared opening with 80 cm bore
Max. amplitude per axis	34 mT/m
Max. slew rate per axis	160 T/m/s
Spine coil (table-integrated)	18 elements
Body surface coil M	12 elements
Body surface coil L	6 elements

Table 1: MAGNETOM Free.XL is equipped with hardware that allows users to take advantage of the physics at 0.55T.

[1]Work in progress. The application / the system is currently under development and is not for sale in the U.S. and in other countries. Its future availability cannot be ensured.
[2]The MRI restrictions (if any) of the metal implant must be considered prior to patient undergoing MRI exam. MR imaging of patients with metallic implants brings specific risks. However, certain implants are approved by the governing regulatory bodies to be MR conditionally safe. For such implants, the previously mentioned warning may not be applicable. Please contact the implant manufacturer for the specific conditional information. The conditions for MR safety are the responsibility of the implant manufacturer, not of Siemens Healthineers.

The hardware specifications of MAGNETOM Free.XL are listed in Table 1.

In this article, we present our initial experience of performing CMR scans in volunteers at 0.55T without contrast administration using a MAGNETOM Free.Max system and a MAGNETOM Free.XL system with its stronger gradients.

Due to the system's lower field strength and corresponding **reduced magnetohydrodynamic effect**, ECG synchronization is greatly simplified, as the ECG curve shows fewer artifacts. This can be seen in Figure 2, which shows an ECG signal outside the magnet, in a 3T system, in a 1.5T system, and in the 0.55T MAGNETOM Free.XL magnet.

The reduced main magnetic field and subsequent **reduction in B_0 distortions** can now be exploited with stronger gradient performance. In Figure 3, we show example images of three devices: a pacemaker[2], a transcatheter aortic valve replacement device[2], and a left atrial appendage closure implant[2], all acquired on a MAGNETOM Avanto Fit (1.5T), a MAGNETOM Free.Max (0.55T) and a MAGNETOM Free.XL (0.55T). Acquisitions were performed using a balanced steady-state free precession (bSSFP) contrast, as typically used for cine functional CMR assessment. Especially for the pacemaker, the banding artifacts (dark rim around the device) are reduced with the MAGNETOM Free.XL system.

The gradient performance and its influence on several CMR protocols can be seen in Table 2, which compares MAGNETOM Free.Max to MAGNETOM Free.XL.

2 The native ECG signal (top row), is barely distorted at 0.55T, whereas distortions become stronger with increasing magnetic field strengths (1.5T and 3T).

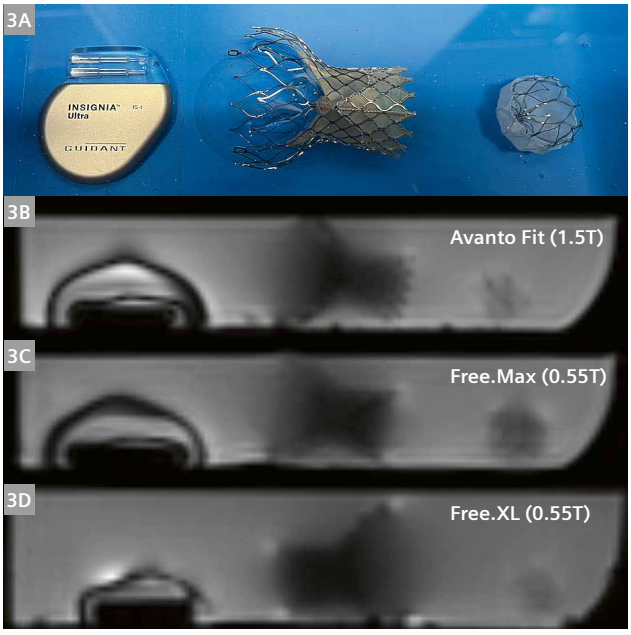

3 **(3A)** from left to right: pacemaker, transcatheter aortic valve replacement device, and a left atrial appendage closure implant. **(3B)** 1.5T MAGNETOM Avanto Fit; **(3C)** 0.55T MAGNETOM Free.Max; **(3D)** 0.55T MAGNETOM Free.XL.
The pacemaker exhibits fewer banding artifacts on MAGNETOM Free.XL, due to the combination of lower field strength and stronger gradient performance.

		MAGNETOM Free.Max	MAGNETOM Free.XL
Segmented cine	TE	1.7 ms	1.05 ms
	TR	4.2 ms	2.6 ms
	Breath-hold duration	9 s	5.2 s
Dynamic perfusion (3 slices)	TE	1.78 ms	1.1 ms
	Frame duration	252 ms	157 ms
	Maximum heart rate	79 bpm	125 bpm
3D bSSFP	Segments	28	39
	Acquisition duration	6.6 min	5.6 min
Interactive real-time cine	Frame duration	221 ms	132 ms
	Frame rate	4 fr/s	7 fr/s

Table 2: A comparison of several acquisition parameters achievable on the MAGNETOM Free.XL and MAGNETOM Free.Max systems. The 3D bSSFP is a T2-prepared 3D morphological acquisition with fat saturation, as typically used for coronary MR angiography (MRA). The interactive real-time cine is used for interventional imaging and allows real-time acquisition and inline reconstruction.

For all imaging protocols, the stronger gradients allow a **reduction in the echo times** (TE) and therefore in the echo spacing (TR). This time-reduction can be used for **shorter acquisition times** in the case of segmented cine or 3D bSSFP, or for **higher frame rates** for single-shot applications such as real-time cine or perfusion imaging. In the case of perfusion imaging, the stronger gradients allow the acquisition of three slices per heartbeat, even in situations of high (< 125 bpm) heart rates.

MAGNETOM Free.XL comes with the full portfolio of **planning and workflow features** from Siemens Healthineers. These include automatic cardiac view planning using myExam Cardiac Assist as shown in Figure 4.

Similarly, the resting phase is automatically detected based on a 4-chamber cine as part of the AutoMate Cardiac functionality. This is shown in Figure 5 for the automatic parametrization of a 3D iNAV-based acquisition on MAGNETOM Free.XL.

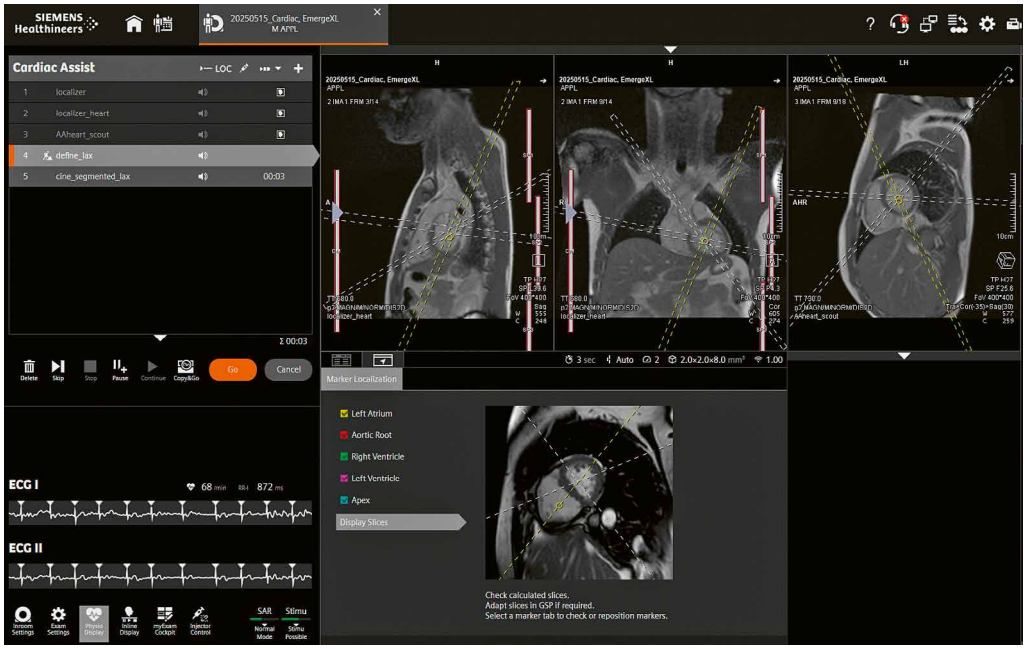

4 Scout images and planning results in a healthy volunteer. Landmarks and planes are automatically found using myExam Cardiac Assist.

5 Example of AutoRestingPhase detection in the AutoMate Cardiac feature of MAGNETOM Free.XL.

Figure 6 shows morphological short-axis dark-blood images using a TSE-based sequence with Deep Resolve (upper row: T2; lower row: turbo inversion recovery magnitude, TIRM) on MAGNETOM Free.XL.

Figure 7 shows functional cardiac assessment, including the automatic inline segmentation and ventricular function calculation on bSSFP cine imaging.

A direct comparison of cine images, acquired in the same volunteer on MAGNETOM Free.XL and MAGNETOM Free.Max, is shown in Figure 8. The images depict a single time frame of two segmented acquisitions with bSSFP contrast in the same volunteer. The images demonstrate that the stronger gradient performance allows the **reduction of flow-related dark-band artifacts** due to shortened echo spacing.

Figure 9 shows real-time cine images acquired on both systems. In real-time cine applications, where interactive slice modifications and inline reconstruction and visualization are needed, the improved gradient performance of MAGNETOM Free.XL helps to achieve substantially **higher frame rates**. For example, with the protocol settings for real-time cine with an in-plane resolution of 2.4 × 2.4 mm

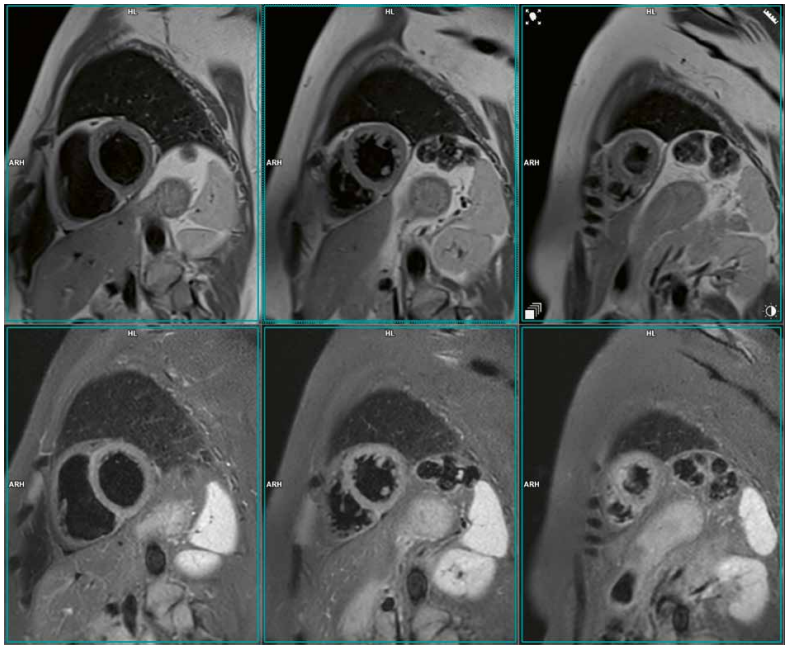

6 T2 TSE (top row) and TIRM (bottom row) acquisition with Deep Resolve on MAGNETOM Free.XL.

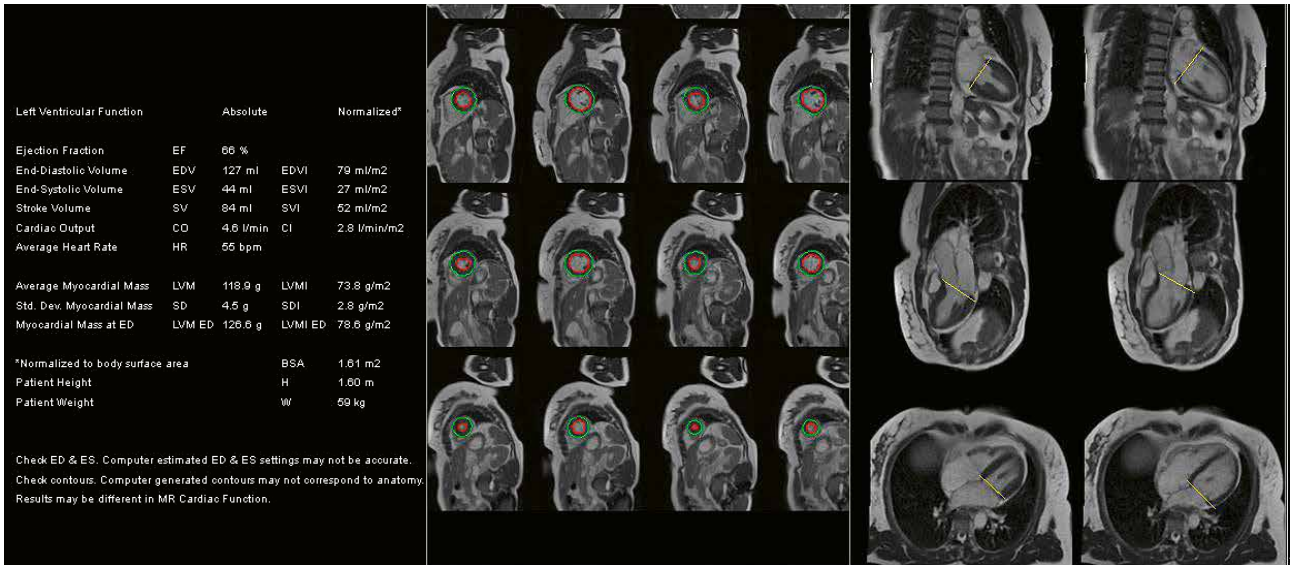

7 Results of the inline ventricular function assessment with automatic generation of a report (left) and visualization of the segmentation results (middle and right).

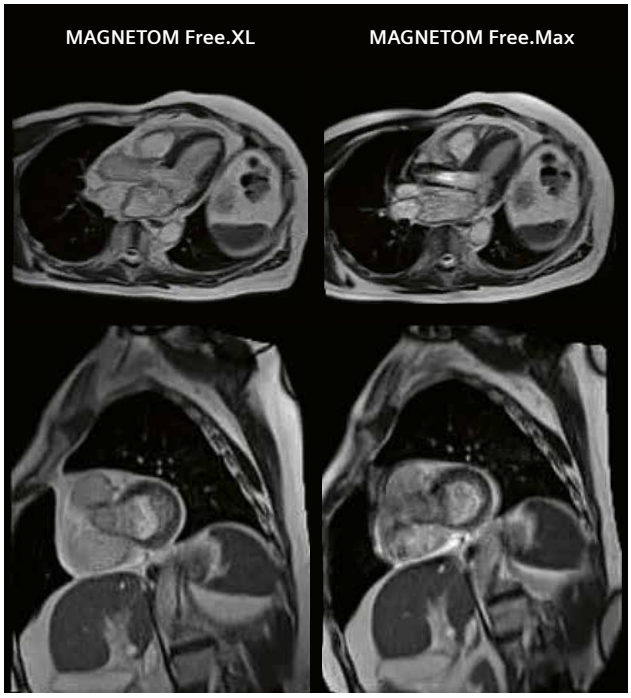

8 A single time frame of segmented bSSFP images in a 3-chamber view (top) and basal short-axis view (bottom) acquired in the same volunteer on MAGNETOM Free.XL and MAGNETOM Free.Max. The reduction in flow artifacts is visible on the MAGNETOM Free.XL images, due to decreased echo spacings.

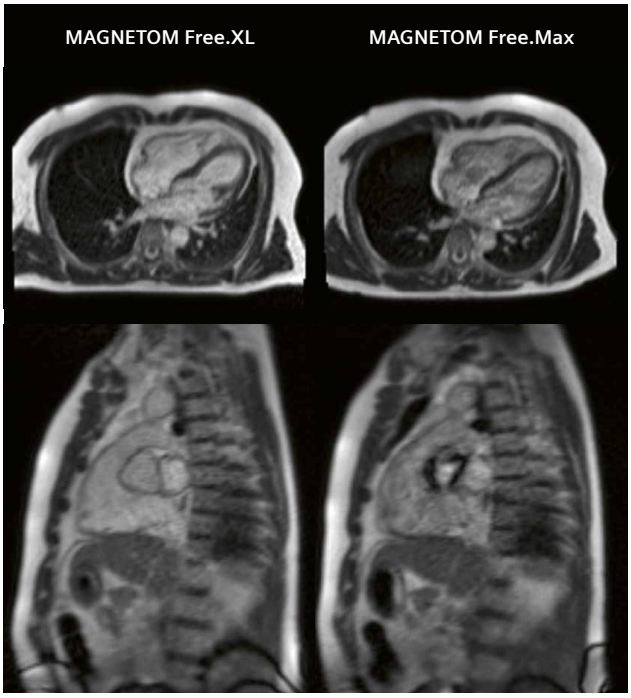

9 Single time-frame bSSFP images (in-plane: 2.4 × 2.4 mm, slice thickness: 7 mm) in 4-chamber view (top) and right ventricular outflow tract (bottom) in the same volunteer on MAGNETOM Free.XL (left) and MAGNETOM Free.Max (right). This demonstrates the improvement in image quality, e.g., reduced flow artifacts, obtained with the shorter acquisition times (132 ms with MAGNETOM Free.XL vs. 221 ms with MAGNETOM Free.Max).

and a slice thickness of 7 mm, the acquisition time of a single frame was reduced from 221 ms on MAGNETOM Free.Max to 132 ms with MAGNETOM Free.XL.

The ability to acquire **real-time cine at high frames rates** is an important step toward achieving applications that go beyond purely diagnostic examinations, e.g., interventional cardiac procedures such as right heart catheterizations. These applications require visualization of the device and the surrounding anatomy at high frame rates for safe navigation and procedural success. Together with the advantages of the lower field strength for device safety (e.g., reduced radiofrequency (RF)-induced heating), and improved patient access from the larger bore opening, this might pave the way for using MAGNETOM Free.XL as a versatile diagnostic and interventional[3] platform.

The combination of **Deep Resolve with Compressed Sensing** for cine bSSFP imaging on MAGNETOM Free.XL can be appreciated in Figure 10, which demonstrates a clear improvement in sharpness and reduced level of noise.

Multiparametric mapping using MyoMaps is also fully supported on MAGNETOM Free.XL. Due to the reduced T1 values at 0.55T, the acquisition scheme on

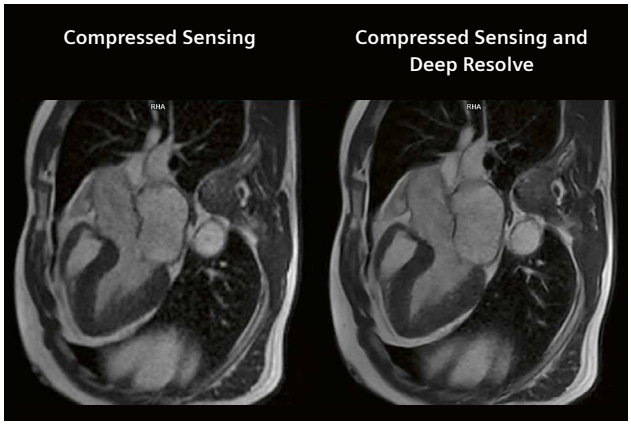

10 While Compressed Sensing allows the acceleration of cine acquisitions, the addition of Deep Resolve increases sharpness and reduces noise.

MAGNETOM Free.XL for native T1 mapping is currently set to 4-3-2-2 (as compared to 5-(3)-3 at 1.5T and 3T). Figure 11 shows example T1 and T2 images and maps acquired on MAGNETOM Free.XL.

[3]*Work in progress. The system is currently nor released for cardiac interventions.*

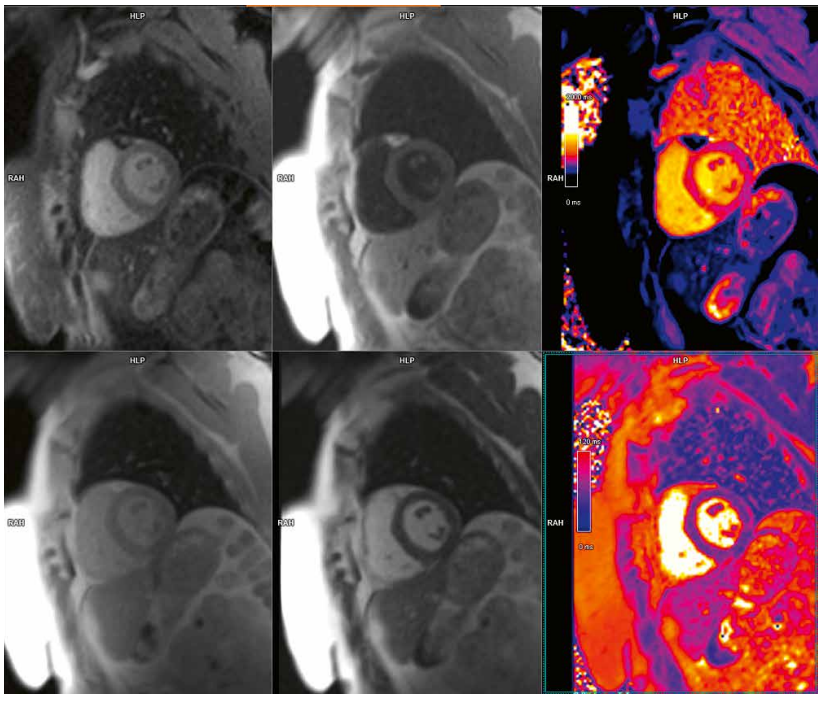

11 T1 and T2 mapping on MAGNETOM Free.XL is feasible. Nevertheless, reference values still need to be collected at 0.55T and this is a prerequisite for clinical use of MyoMaps.

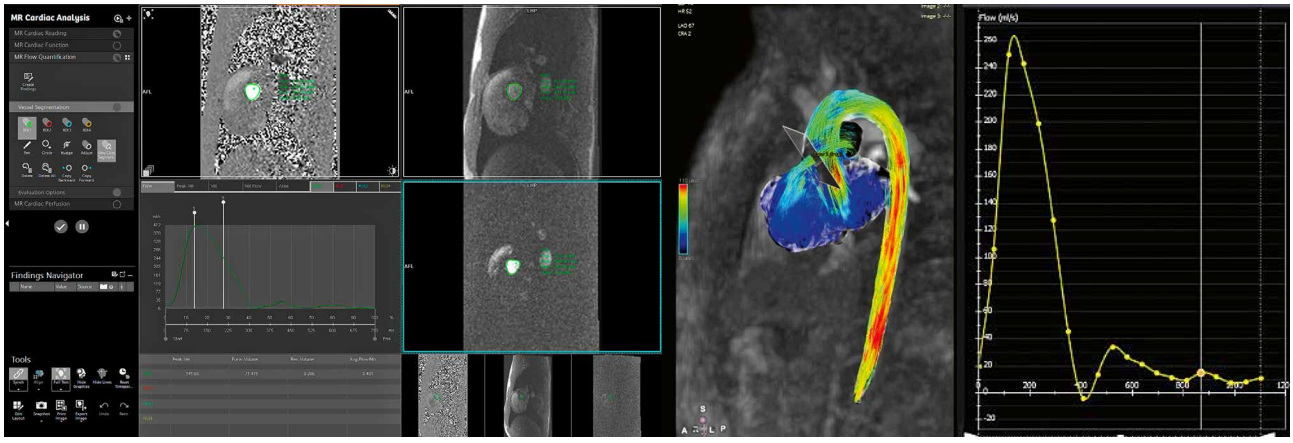

12 Phase-contrast imaging on MAGNETOM Free.XL. Although signal-to-noise ratio (SNR) is reduced at 0.55T compared to 1.5T and 3T, the values for 2D Flow and 4D Flow match, and advanced visualization on 4D Flow (here using cvi42) is feasible.

Although phase-contrast imaging is known to benefit from higher field strengths, Figure 12 demonstrates that classical **2D Flow** imaging is possible on MAGNETOM Free.XL, as is **4D Flow**, which was processed using cvi42 (Circle Cardiovascular Imaging, Calgary, Canada) in this case.

Finally, an image-based navigated 3D bSSFP with fat saturation using the **WholeHeart Pro** sequence is shown in Figure 13. This demonstrates high resolution, a large homogeneous signal, and good fat saturation.

In conclusion, MAGNETOM Free.XL showed consistent performance across all relevant CMR applications that we could test natively (imaging with contrast media is not permitted in volunteer scans at Siemens Healthineers). Not only was the image quality stable and met expectations throughout the image contrasts, but all AI-based workflow-support applications are also available and were shown to work successfully. These can be integrated into the examination, if needed. Workflow automation includes user support in planning the cardiac views, adapting protocols to the patient's physiology, and assuring a comparable, robust, and excellent image quality independent of the user. The AutoMate Cardiac AutoPositioning feature further supports users with automatic positioning of the heart in the isocenter and with planning of additional protocol parameters and geometries such as saturation bands, navigators, and coronal or transversal 2D or 3D slices or slabs. Additionally, AutoTI (which we are yet to test on the 0.55T system in patients after contrast agent

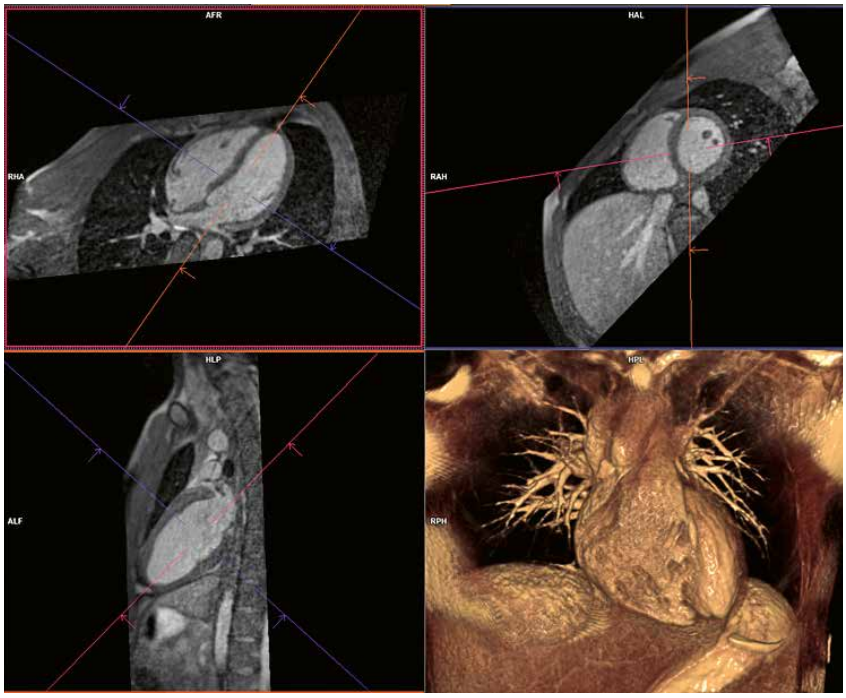

13 Acquisition of the 3D WholeHeart Pro sequence on MAGNETOM Free.XL exhibits excellent contrast and good fat saturation using 3D bSSFP.

administration) suggests an optimal inversion time (TI) for maximum signal intensity differentiation between healthy myocardium and scar. Finally, the AutoRestingPhase detection feature automatically detects the quiescent cardiac phase to enable optimized motion-free image acquisition. AI-based Deep Resolve Sharp is now also available in several CMR applications, including cine and black-blood imaging. This achieves improved sharpness and reduced noise, which is especially useful at 0.55T. Compared to 0.55T MAGNETOM Free.Max, the improved gradient performance of MAGNETOM Free.XL can improve speed, reduce artifacts, and enable all typical CMR acquisitions.

With its combination of the inherent advantages of low-field imaging, enhanced gradient performance, and advanced AI-driven automation and reconstruction, the MAGNETOM Free.XL system is well positioned for clinical adoption in cardiac MRI.

Contact

Daniel Giese, Ph.D.
Siemens Healthineers
SHS DI MR RCT CLS CARD
Research & Clinical Translation,
Magnetic Resonance
Allee am Roethelheimpark 2
91052 Erlangen
Germany
giese.daniel@siemens-healthineers.com

References

1 Schulz-Menger J, Collini V, Gröschel J, Adler Y, Brucato A, Christian V, et al. 2025 ESC Guidelines for the management of myocarditis and pericarditis. Eur Heart J. 2025;46(40):3952–4041.
2 Qin C, Murali S, Lee E, Supramaniam V, Hausenloy DJ, Obungoloch J, et al. Sustainable low-field cardiovascular magnetic resonance in changing healthcare systems. Eur Heart J Cardiovasc Imaging. 2022;23(6):e246–e260.
3 MAGNETOM Flash. MAGNETOM Free.Max special issue. RSNA Edition 2020. Available from: ↗ https://marketing.webassets.siemens-healthineers.com/90472072ae6f7648/3230ad37f3ce/MAGNETOM_Flash_Free-Max_Edition_RSNA_Edition.pdf?ste_sid=ebd817edf840e277fb20f2e1e0b1c4aa
4 Varghese J, Jin N, Giese D, Chen C, Liu Y, Pan Y, et al. Building a comprehensive cardiovascular magnetic resonance exam on a commercial 0.55 T system: A pictorial essay on potential applications. Front Cardiovasc Med. 2023;10:1120982.
5 Campbell-Washburn AE, Varghese J, Nayak KS, Ramasawmy R, Simonetti OP. Cardiac MRI at Low Field Strengths. J Magn Reson Imaging. 2024;59(2):412–430.
6 Kaushal A, Crawley R, Jeljeli S, Sequeiros T, Valapil R, Bolla R, et al. Use of a 0.55T 80cm-wide Bore Scanner for Cardiac Imaging in Bariatric and Claustrophobic Patients: A Preliminary Single Centre Experience. J Cardiovasc Magn Reson. 2024;26(1):101017.
7 Armstrong AK, Liu Y, Kelly JM, Krishnamurthy R, Swinning J, Liu Y, et al. Feasibility of magnetic resonance imaging-guided cardiac catheterization, angioplasty, and stenting in a commercial wide-bore 0.55T scanner. J Cardiovasc Magn Reson. 2025;27(1):101858.

Meet Siemens Healthineers

Siemens Healthineers: Our brand name embodies the pioneering spirit and engineering expertise that is unique in the healthcare industry. The people working for Siemens Healthineers are totally committed to the company they work for, and are passionate about their technology. In this section we introduce you to colleagues from all over the world – people who put their hearts into what they do.

Michael da Silva

Michael da Silva has turned a childhood fascination with biology, anatomy, and physiology into a career. His interest in the human body led him to study radiology at university and complete an internship in MRI. After graduating, he continued his education, earning a postgraduate degree in biomedical engineering and an MBA in business intelligence. Michael went on to work in various technical and educational roles, including as a magnetic resonance technologist, a university professor, and an application specialist. He also worked in a number of administrative roles, including as a reference technician and a radiological protection supervisor. Michael joined Siemens Healthineers in 2021, starting out as an MR application specialist. Three years later, he moved into his current role as an MR collaboration specialist for Latin America.

Rio de Janeiro, Brazil

How did you first come into contact with MRI?
My first contact with magnetic resonance imaging was in a book that I received as a gift at the beginning of my studies. My first real contact was as an intern during my degree. The internship gave me the opportunity to learn about the processes of executing, programming, and documenting exams on various systems from 0.5T to 3T.

What do you find motivating about your job?
It's really motivating to be part of a multidisciplinary area, where anatomy, physics, and physiology come together and there is always something new to explore. As a collaboration specialist, my main motivation is to be able to support customers in using the equipment to carry out clinical research, and to guide them on optimizing protocols and sequences. In addition, I enjoy providing solutions to customers' requests. I'm always seeking out different ways to ensure the success of their research.

What are the biggest challenges in your job?
One of the biggest challenges in my work is also the greatest privilege: the ability to learn every day. As I am a collaboration specialist in MR, I provide support that covers a wide range of topics, ranging from adapting a protocol or a sequence for clinical research to supporting projects, identifying the requester's needs, and providing guidance so that they can start their project.

What are the most important developments in healthcare?
I believe that developments in automation and the use of artificial intelligence are intertwined with developments in healthcare. I would like to mention as an example myExam Cardiac Assist, which is a fully automated system that facilitates the execution of the exam and promotes assertiveness in planning. When I started working in the MRI area about 20 years ago, performing a cardiac exam was extremely complex. Today, we have yet another tool that facilitates the performance of the exam through automation, which is amazing: The Beat Sensor recognizes the heartbeat without the need to use the electrodes. This supports the service workflow and improves the patient experience.

What would you do if you could spend a month doing whatever you wanted?
Professionally, I would like to spend a month working in and learning about product development in MR – from the conceptual phase to the final phase, and even how ideas for new products and solutions are born.
On a personal level, I would spend a month with my family and cook for my wife and daughter, as one of my hobbies is gastronomy. I love to invent things in the kitchen.

Luis Arley Evangelista Peña

I grew up in Tumbes, a very modest town in the north of Peru. At 16, like many teenagers, I wasn't sure what I wanted to do with my life. I couldn't decide between becoming a doctor, an engineer, or a physicist. Then I saw a cranial MRI study for the first time in my life. I remember consulting with my friends, and they told me that to do those studies, you had to know a lot about medicine, physics, and a little bit of engineering. I thought, "That combines everything I'm interested in!" And so began my insatiable desire to understand more about this field.

In college, I was never the best at physics, but I was definitely the one who asked the most questions. And it led to success. During my studies, I heard about a great company that was always at the forefront of technology. At that moment, I knew where I wanted to work. After a decade of working in magnetic resonance imaging, I had the opportunity to join Siemens Healthineers. The role brought me to Bogotá, Colombia, a wonderful place that I quickly fell in love with.

How did you first come into contact with MRI?
The first time I came into contact with magnetic resonance imaging was during my pre-professional training at university. That was when I discovered the wonderful spin-echo T1 sequence in the brain. It was the first time I had seen the brain with real contrasts showing the anatomy.

What do you find motivating about your job?
Three things motivate me: First, the infinite unknowns of this wonderful world; second, serving patients, who depend on a correct diagnosis, good follow-up, and effective treatment; and third, my family, who are partners in all my projects and support me through all my challenges.

What do you think are the most important developments in MRI?
I believe the most important advance in magnetic resonance imaging is the ability to perform procedures within the MRI scanner. This type of interventional radiology is enabling huge leaps forward: Think about MRI-guided breast biopsies, or tumor treatments inside the machine guided by phase maps that allow to control temperature with pinpoint accuracy. Today, we can even work with hybrid rooms or intraoperative MRI systems. It's also very exciting to think about what we will achieve in the coming years.

If you could do anything you wanted for a month what would it be?
I would focus on my two great passions: magnetic resonance imaging and cooking. For MRI, I would work on designing and optimizing cardiovascular sequences, which often pose a great challenge for our clients. The rest of the time I would spend cooking for my loved ones. I really enjoy sharing a barbecue with good friends, for instance, with lots of laughter and good music. That would be a wonderful month.

Get to know us

Find more portraits of our colleagues around the world!

www.magnetomworld.siemens-healthineers.com/meet-siemens-healthineers

The entire editorial staff at Heart Institute (InCor), University of São Paulo Medical School, Brazil and at Siemens Healthineers extends their appreciation to all the radiologists, technologists, physicists, experts, and scholars who donate their time and energy – without payment – in order to share their expertise with the readers of MAGNETOM Flash.

MAGNETOM Flash – Imprint

Publisher:
Siemens Healthineers AG
Magnetic Resonance,
Karl-Schall-Str. 6, D-91052 Erlangen, Germany

Editor-in-chief:
Antje Hellwich
antje.hellwich@siemens-healthineers.com

Guest Editor:
Carlos E. Rochitte, M.D., Ph.D., FSCMR
Associate Professor of Cardiology
University of São Paulo Medical School
InCor – Instituto do Coração
Av. Dr. Enéas Carvalho de Aguiar, 44
Cerqueira César
São Paulo – SP 05403-000
Brazil

Editorial Board:
André Fischer, Ph.D.; Kera Westphal, Ph.D.;
Kathrin El Nemer, M.D.; Wellesley Were;
Katie Grant, Ph.D.; Christian Geppert, Ph.D.

Review Board:
Gaia Banks, Ph.D.; Carmel Hayes, Ph.D.;
Manuela Rick; Michaela Schmidt;
Christian Schuster, Ph.D.; Peter Speier, Ph.D.

Copy Editing:
Sheila Regan, Jen Metcalf, UNIWORKS,
www.uni-works.org
(with special thanks to Kylie Martin)

Layout:
Agentur Baumgärtner,
Friedrichstr. 4, D-90762 Fürth, Germany,
www.agentur-baumgaertner.com

PrePress and Image Editing, Production:
Clemens Ulrich, Paul Linssen,
Siemens Healthineers AG

Printer:
Schmidl & Rotaplan Druck GmbH,
Hofer Str. 1, D-93057 Regensburg, Germany

MAGNETOM Flash includes reports in the English language on magnetic resonance: diagnostic and therapeutic methods and their application as well as results and experience gained with corresponding systems and solutions. It introduces from case to case new principles and procedures and discusses their clinical potential. The statements and views of the authors in the individual contributions do not necessarily reflect the opinion of the publisher.

The information presented in these articles and case reports is for illustration only and is not intended to be relied upon by the reader for instruction as to the practice of medicine. Any health care practitioner reading this information is reminded that they must use their own learning, training and expertise in dealing with their individual patients. This material does not substitute for that duty and is not intended by Siemens Healthcare to be used for any purpose in that regard. The drugs and doses mentioned herein are consistent with the approval labeling for uses and/or indications of the drug. The treating physician bears the sole responsibility for the diagnosis and treatment of patients, including drugs and doses prescribed in connection with such use. The Operating Instructions must always be strictly followed when operating the MR system. The sources for the technical data are the corresponding data sheets. Results may vary.

We welcome your questions and comments about the editorial content of MAGNETOM Flash. Please contact us at magnetomworld.team@siemens-healthineers.com

Manuscripts as well as suggestions, proposals and information are always welcome; they are carefully examined and submitted to the editorial board for attention. MAGNETOM Flash is not responsible for loss, damage, or any other injury to unsolicited manuscripts or other materials. We reserve the right to edit for clarity, accuracy, and space. Include your name, address, and phone number and send to the editors, address above.

MAGNETOM Flash is also available online:
www.magnetomworld.siemens-healthineers.com

Not for distribution in the US

On account of certain regional limitations of sales rights and service availability, we cannot guarantee that all products included in this brochure are available through the Siemens Healthineers sales organization worldwide. Availability and packaging may vary by country and is subject to change without prior notice. Some/All of the features and products described herein may not be available in the USA.

The information in this document contains general technical descriptions of specifications and options as well as standard and optional features which do not always have to be present in individual cases, and which may not be commercially available in all countries. Due to regulatory reasons their future availability cannot be guaranteed. Please contact your local Siemens Healthineers organization for further details.

Siemens Healthineers reserves the right to modify the design, packaging, specifications, and options described herein without prior notice. Please contact your local Siemens Healthineers sales representative for the most current information.

Note: Any technical data contained in this document may vary within defined tolerances. Original images always lose a certain amount of detail when reproduced.

Siemens Healthineers Headquarters
Siemens Healthineers AG
Siemensstr. 3
91301 Forchheim, Germany
Phone: +49 9191 180
siemens-healthineers.com

Published by Siemens Healthineers AG · Order No. A91MR-1000-180M-7600 · Printed in Germany · 17492 0126 ·